Title
Postmodern Electronic Structure Theory

Author
Lee, Joonho

Publication Date
2019

Peer reviewed|Thesis/dissertation

Postmodern Electronic Structure Theory

by

Joonho Lee

A dissertation submitted in partial satisfaction of the

requirements for the degree of

Doctor of Philosophy

in

Chemistry

in the

Graduate Division

of the

University of California, Berkeley

Committee in charge:

Professor Martin P. Head-Gordon, Chair
Professor Eran Rabani
Professor Lin Lin

Summer 2019

Postmodern Electronic Structure Theory

Abstract

Postmodern Electronic Structure Theory

by

Joonho Lee

Doctor of Philosophy in Chemistry

University of California, Berkeley

Professor Martin P. Head-Gordon, Chair

This dissertation is concerned with the development and applications of approaches to the electron correlation problem. We start with an introduction that summarizes modern approaches to the electron correlation problem. In our view, there are two remaining challenges that modern density functional theory cannot satisfactorily solve. The first challenge is due to self-interaction error and the second is due to strong correlation. We discuss two methods developed by the author that attempt to make progress to address the second challenge.

The first approach is useful in distinguishing strong and weak correlation in a computationally economical way. It is based on orbital optimization in the presence of regularized second-order Møller-Plesset perturbation theory (κ-OOMP2), which is an approximate method to obtain Brückner orbitals. κ-OOMP2 includes weak correlation while attenuating strong correlation. As such, it distinguishes artificial and essential symmetry breaking which occur at the Hartree-Fock (HF) level. Artificial symmetry breaking appears due to the lack of weak correlation, not due to the lack of strong correlation. Therefore, the common wisdom in quantum chemistry, which equates symmetry breaking at the HF level and strong correlation, can result in a wrong understanding of the system. Essential symmetry breaking, on the other hand, signals strong correlation that is beyond the scope of simple perturbation theory. κ-OOMP2 has been shown to reliably distinguish these two: symmetry breaking in the κ-OOMP2 orbitals is essential. This has been applied to a recent controversy about whether C_{60} is strongly correlated. Starting from a broken-symmetry HF solution, κ-OOMP2 restores every symmetry. As such, C_{60} is not strongly correlated. Moreover, κ-OOMP2 successfully predicts strong correlation for a known biradicaloid, C_{36}, by showing essential symmetry breaking in its orbitals. We also exploited essential symmetry breaking in singlet biradicaloids using κ-OOMP2 and

showed quantitative accuracy in obtaining singlet-triplet gaps of various molecules. This new approach should be helpful for redefining the common wisdom in quantum chemistry.

The second method is an exact, spin-pure, polynomial-scaling way to describe strong spin-correlation (SSC). SSC is present when there are many spatially separate open-shell electrons with small spin-flip energy cost. Describing SSC exactly requires the inclusion of all essential spin-couplings. The number of such spin-couplings scales exponentially with the number of electrons. Because of this, SSC was thought to require an exponential number of wavefunction parameters in general. However, new development suggests that there is an efficient way to obtain all these spin-couplings with only a quadratic number of wavefunction parameters, which is called the coupled-cluster valence-bond (CCVB) method. We discuss different challenges in CCVB: (1) its non-black-box nature and (2) its inability to describe SSC in spin-frustrated systems. We present two improved CCVB approaches that address these two challenges. These approaches were applied to describe emergent strong correlation in oligoacenes and SSC in spin-frustrated systems such as single molecular magnets and metalloenzymes. The remaining challenges in CCVB are the inclusion of ionic excitations which are not relevant for SSC, but crucial for obtaining quantitative accuracy.

To my wife Soojin

Acknowledgments

The first to thank is my advisor, Prof. Martin Head-Gordon. The best academic decision I made so far was to move from Caltech to Berkeley to work with Martin. The transfer was very difficult and the intellectual stimuli provided by Martin were the only things that I could hold on to in the beginning. I am proud of having learned and contributed to his scientific philosophy and legacy. Among many things, I would like to thank Martin for having taught me how to critically assess not only other people's work but also my own work. Most importantly, I thank Martin for giving me intellectual freedom for the last 4 years. Without this freedom, I would not have become the scientist that I am now. I also thank Martin for proofreading every chapter of this dissertation carefully. Any remaining errors are my own.

I would like to thank everyone with whom I interacted during my time in Berkeley. I must thank Prof. Eran Rabani and Prof. Lin Lin for giving me career advice and being approachable whenever I needed their help. I must thank Dr. Dave Small for teaching me everything I know about coupled-cluster theory. The second best thing that happened to me during my time in Berkeley was to work with Dave early on. I must thank Dr. Evgeny Epifanovsky for encouraging me to reimplement anything that interests me in Q-Chem. Without his encouragement, I would not have learned as much about scientific programming as I know now. I must thank Luke Bertels, Srimukh Prasad, and Matthias Loipersberger for being best friends, always standing by me, and working with me on projects that have taught me a lot. I spent more time with you guys than with my wife Soojin during Ph.D. and I am grateful for the quality time we had together. I must thank Evgeny once more, Dr. Jerome Gonthier, and Dr. Eloy Ramos for sharing the courage I had about periodic boundary conditions and following me down the path of endless implementations of missing features when no publication was guaranteed. Lastly, I thank other people with whom I interacted through Martin's group including Eric Sundstrom, Paul Horn, Narbe Mardirossian, Jonathan Thirman, Yuezhi Mao, Jon Witte, Alec White, Jon Weisberg, Brad Ganoe, Leo Cunha, Dr. Shane Yost, Dr. Udi Tsivion, Dr. Roberto Pevrati, Dr. Xintian Feng, Dr. Cameron Mackie, Dr. Tim Stauch, and Dr. Christopher Stein for being good co-workers. I must thank Eric once again for convincing me to transfer to Berkeley when I was unhappy about my scientific development. I thank Jessie Woodcock for making sure that I get paid on time.

Outside the Head-Gordon group, I have many individuals to thank. First, I thank Prof. Eric Neuscamman, Luning Zhao, Brett Van Der Goetz, Sergio Flores, Dr. Peter Walters, and Leon Otis for welcoming me to the Neuscamman group's meetings and teaching me some aspects of variational Monte Carlo. I thank Luning once more for good friendship and always giving me good scientific arguments. I thank Lin again,

Jiefu Zhang, Leo Zepeda, Michael Lindsey, and others in the Lin group for warm hospitality when I joined their meetings at Evans and teaching me useful applied math tricks from time to time. I thank Prof. Birgit Whaley and Donghyun Lee for welcoming me back to Berkeley and helping me finish my undergraduate project with them. I thank Donghyun again for sharing his dissertation template which saved me weeks when writing this dissertation. I must thank Birgit again and Bill Huggins for teaching me many things (mostly things that are not yet possible!) about quantum computing. I thank Dr. Miguel Morales and Fionn Malone for teaching me almost everything I know about quantum Monte Carlo (QMC). I thank Fionn once more for being patient with me when I ask millions of questions about QMC.

I would also like to thank people from my Caltech time who helped me prepare for my Ph.D. journey at Berkeley. I thank Prof. Fred Manby for teaching me tricks in density functional theory and joys of working on quantum chemistry early on. I thank Mike Webb, Michiel Niesen, Dr. Pengfei Huo, Mark Fornace, and Kevin Shen for being good colleagues with me.

I would like to thank Luke, Srimukh, and Fionn for proofreading the abstract, introduction, and conclusions of this dissertation.

Finally, I am truly grateful to my family for all their support and patience. Thank you Soojin for your love, patience, understanding, encouragement, and everything else. I look forward to building our new home together (briefly in Berkeley and) in New York City and our future afterwards. Thank you my dad Hyungkeun, my mom Jungsook, and my sister Eunkyung for consistent support throughout my academic journey.

Contents

List of Figures

List of Tables

Note on Previously Published work

The following chapters are adaptions of published papers:

- Chapter 2:
  Joonho Lee and Martin Head-Gordon. "Regularized Orbital-Optimized Second-Order Møller-Plesset Perturbation Theory: A Reliable Fifth-Order Scaling Electron Correlation Model with Orbital Energy Dependent Regularizers". J. Chem. Theory Comput. 2018, 14, 5203–5219.

- Chapter 3:
  Joonho Lee and Martin Head-Gordon. "Distinguishing artificial and essential symmetry breaking in a single determinant: approach and application to the C_{60}, C_{36}, and C_{20} fullerenes". Phys. Chem. Chem. Phys. 2019, 21, 4763–4778.

- Chapter 4:
  Joonho Lee and Martin Head-Gordon. "Two Single-Reference Approaches to Biradicaloid Problems: Complex, Restricted Orbitals and Approximate Spin-Projection Combined With Regularized Orbital-Optimized Møller-Plesset Perturbation Theory". Accepted in J. Chem. Phys.

- Chapter 5:
  Joonho Lee, David W. Small, Evgeny Epifanovsky, and Martin Head-Gordon. "Coupled-Cluster Valence-Bond Singles and Doubles for Strongly Correlated Systems: Block-Tensor Based Implementation and Application to Oligoacenes". J. Chem. Theory Comput. 2017, 13, 602–615.

- Chapter 6:
  Joonho Lee, David W. Small, and Martin Head-Gordon. "Open-Shell Coupled-Cluster Valence-Bond Theory Augmented with an Independent Amplitude

Approximation for Three-Pair Correlations: Application to a Model Oxygen-Evolving Complex and Single Molecular Magnet". J. Chem. Phys. 2018, 149, 244121.

Chapter 1

Introduction

"My definition of an expert in any field is a person who knows enough about what's really going on to be scared."
– PJ Plauger

Quantum chemistry is a discipline that aims to provide chemically useful information by solving the Schrödinger equation. In particular, for the purpose of this dissertation we shall focus on the time-independent version of the Schrödinger equation (TISE) [1]. The TISE reads

$$\hat{H}|\Psi\rangle = E|\Psi\rangle \tag{1.1}$$

where $\hat{H}$ is the Hamiltonian which depends on problems of our interest and E is the energy of the ground state $|\Psi\rangle$. In particular, the Hamiltonian that is most widely used in quantum chemistry is the system-dependent *ab-initio* electronic Hamiltonian within the Born-Oppenheimer approximation (i.e., nuclei are fixed and behave like point charges) [2]. That is,

$$\hat{H}_{\text{el}} = -\frac{1}{2}\sum_{i}\nabla_i^2 - \sum_{iA}\frac{Z_{iA}}{|\mathbf{r}-\mathbf{R}_A|} + \frac{1}{2}\sum_{i\neq j}\frac{1}{|\mathbf{r}_i-\mathbf{r}_j|} + E_{\text{nuc}} \tag{1.2}$$

where

$$E_{\text{nuc}} = \frac{1}{2}\sum_{A\neq B}\frac{Z_A Z_B}{|\mathbf{R}_A-\mathbf{R}_B|} \tag{1.3}$$

This Hamiltonian includes the kinetic energy operator for each electron (the first term), the Coulomb attraction between electrons and nuclei (the second term), the

Coulomb repulsion between electrons (the third term), and the Coulomb repulsion between nuclei (the last term). Representing $\hat{H}_{\text{el}}$ in a practically feasible way requires the use of a finite basis set at the expense of introducing "discretization errors". We note that it is possible to work directly at the infinite basis set limit (or complete basis set limit) in some stochastic approaches such as quantum Monte Carlo (QMC) [3].

Most quantum chemistry research focuses on deterministic (non-stochastic) algorithms and therefore we shall assume that a finite basis set is used. For a given basis set, one may solve Eq. (1.1) exactly for $\hat{H}_{\text{el}}$ of Eq. (1.2) represented in the many-electron Hilbert space spanned by the basis, which is known as full configuration interaction (FCI) or exact diagonalization (ED). FCI is a useful approach due to its exactness for a given basis set whenever it is possible to run it. The major issue with FCI is that, due to its exponential size-scaling, it is only feasible to run on a very small number of electrons (roughly about 15–16 electrons). This is usually considered too small for most chemical applications. As such, modern quantum chemistry research has focused on approximating FCI with as a little loss of accuracy as possible while increasing the computational feasibility as much as possible.

1.1 Modern Quantum Chemistry

Pople's Model Chemistries

The requirements of model chemistries were first proposed by John Pople, one of the two 1998 Chemistry Nobel laureates, in 1973 [4]. It has set the standard in the modern era of quantum chemistry and we will briefly review each of the Pople's original principles along with those presented in his Nobel lecture [5] in this section. According to Pople, a successful model chemistry should be:

1. simple enough to be applied to a wide range of chemical systems so that realistic simulations can be performed. This sets our preference on approaches that scale polynomially with system size over those that scale exponentially.

2. able to obtain energies with an error less than 1 kcal/mol (chemical accuracy).

3. defined uniquely and continuously throughout potential energy surfaces.

4. systematically compared with experimental data. Such a benchmark is necessary for one to understand the limitation of a given model chemistry.

5. size-consistent. That is, if one runs a calculation on a system A and a well-separated system B, the resulting energy must be the sum of the energy of A and B. This is the only technical requirement that Pople had in his original article.

6. implemented in a black-box fashion such that anyone can easily perform a calculation with only an input geometry, charge, spin, and a choice of discretization (basis set).

At the time of writing this dissertation, no single method satisfies all these criteria and most research has focused on trade-off between 1 (cost) and 2 (accuracy). For instance, the exact approach, FCI, is not really a successful model chemistry due to its highly limited applicability. Therefore, a useful model chemistry must be approximate by nature. Initial developments of approximate quantum chemistry methods by Pople were mostly based on methods that satisfy 3, 4, 5, and 6 while establishing a whole hierarchy of models with trade-offs between 1 and 2. Pople and co-workers carefully assessed individual approaches in order to understand whether both 1 and 2 can be met in some class of chemical applications. These approaches include Møller-Plesset (MP) perturbation theory [6–11], quadratic configuration interaction (QCI) [12], coupled cluster (CC) theory [13–15], and density functional theory (DFT) [16–21]. This philosophy was shared by others in the field and therefore was deemed as the standard in modern quantum chemistry.

Remaning Challenges

In this section, we review the remaining challenges in modern quantum chemistry. These challenges are currently those problems to which the most widely used approach, DFT, cannot yet offer solutions [22]. The first challenge is due to the self-interaction error (SIE) of electrons posed by the use of an approximate exchange-correlation (XC) functional. In DFT, the difficult 2-electron term in Eq. (1.2) is replaced by a classical Coulomb term and a 1-electron term called an XC functional. Namely, this corresponds to

$$\langle\Psi|\frac{1}{2}\sum_{i\neq j}\frac{1}{|\mathbf{r}_i-\mathbf{r}_j|}|\Psi\rangle=\frac{1}{2}\int_{\mathbf{r}_1}\int_{\mathbf{r}_2}\frac{\rho(\mathbf{r}_1)\rho(\mathbf{r}_2)}{|\mathbf{r}_1-\mathbf{r}_2|}+E_{\mathrm{xc}}[\rho(\mathbf{r})] \tag{1.4}$$

where $|\Psi\rangle$ is the exact ground state, the first term corresponds to the classical Coulomb energy, the second term is the XC energy, and $\rho(\mathbf{r})$ is a one-electron reduced density defined as

$$\rho(\mathbf{r})=\int_{\mathbf{r}_2,\mathbf{r}_3,\cdots,\mathbf{r}_N}|\Psi(\mathbf{r},\mathbf{r}_2,\mathbf{r}_3,\cdots,\mathbf{r}_N)|^2 \tag{1.5}$$

This is an exact expression as the definition of $E_{\text{xc}}[\rho(\mathbf{r})]$ is given by this equation. In passing, we note that in the most usual form of DFT (i.e., Kohn-Sham (KS-) DFT) some additional subtleties arise due to the kinetic energy term in Eq. (1.2). As a result, $E_{\text{xc}}[\rho(\mathbf{r})]$ is typically thought to also include the correlation effect in the kinetic energy of an exact wavefunction.

Looking at Eq. (1.4), the origin of SIE is now evident. When there is only a single electron, the energy in Eq. (1.4) should be exactly zero because an electron should not interact with itself. However, approximate treatments to E_{xc} do not exactly cancel the classical Coulomb energy and thus lead to SIE. This SIE has been shown to play a crucial role in DFT errors for many electron systems [23–27]. Although there are some existing approaches in DFT to help reduce SIE [23], a perfect way to avoid any potential SIEs is simply to use wavefunction based approaches such as MP and CC.

The second challenge is due to the inadequacy of DFT in describing strong correlation (SC). Like in the case of SIE, this inadequacy of DFT is due to the limitations of existing approximate XC functionals. As the exact XC functional is currently unavailable, SC remains to be a challenge. We define SC based on the applicability of low-order MP perturbation theory (PT). When low-order MPPT is quantitatively accurate, it is safe to assume that the system is only "weakly" correlated. Unfortunately, such distinction between strong and weak correlation cannot be uniquely achieved and therefore their definitions are also vague to some extent. More intuitively, strongly correlated systems carry many open-shell (OS) electrons whereas weakly correlated systems carry only almost exclusively spin-paired closed-shell (CS) electrons. Therefore, weakly correlated systems can be well described by a simple perturbation expansion around a perfectly closed-shell single determinant (i.e., no electron-correlation) state.

Often, the SC problem requires a non-local form of the XC functional and thus currently available XC functionals are inadequate to yield accurate energies even with accurate densities. There are other approaches in KS-DFT that attempt to incorporate SC [28–33] but all of them encounter formal challenges such as double counting of correlation or unsatisfying separation of correlation. Furthermore, even with wavefunction approaches, SC remains unsolved because the exact description for SC in general scales exponentially with system size.

For the purpose of this dissertation, we will focus on the second challenge (i.e., strong correlation) using wavefunction approaches which do not suffer from SIE.

1.2 Author's Views on Pople's Criteria

Ideally, satisfying all of Pople's requirements is desirable. In lieu of modern development in the electron correlation approaches, we review this very desirable goal. In recent development, much focus has be spent on achieving 1 and 2 at the expense of other requirements. This is not necessarily a negative trend for quantum chemistry, but rather it is necessary to make changes to solve problems that are already in the reach of existing tools. We will revisit some of Pople's criteria and mention some recent electronic structure methods that do not satisfy these criteria but yet proved to be valuable.

Lack of Universal Applicability is Tolerable

A model chemistry lacking universal applicability is often well received in the community if the scope of the model is clearly understood. In such cases, one can pick a class of problems that are well suited for a chosen model chemistry. This is not necessarily a bad practice of quantum chemistry. Rather it motivates development of new approaches only when there is a physical problem that cannot be answered by currently available tools.

For instance, the density matrix renormalization group (DMRG) approach is the *de facto* approach for simulating one-dimensional (1D) quantum lattice problems [34]. It can be used to obtain near-exact energies at a polynomial cost for 1D problems and therefore this must be a choice of method for 1D. However, its scaling becomes exponential with system size and it scope becomes more limited as one goes to higher dimensional systems. We further note that despite its exponential scaling for higher dimensional systems DMRG has been applied with much caution to solve 2D lattice models [35, 36] and more general 3D chemistry problems [37–41].

The same can be said for many conventional single-reference approaches such as CC and MP methods since their performance typically degrades for strongly correlated systems. Of course, their scope is well understood and therefore they remain widely accepted as useful tools for simulating weakly correlated systems.

Physical Accuracy is More Important Than Chemical Accuracy

As mentioned earlier, achieving chemical accuracy (1 kcal/mol) while maintaining universal applicability (i.e., polynomial scaling) is too difficult. We shall focus on achieving "physical accuracy". Physical accuracy is about qualitative accuracy rather than quantitative accuracy. However, this does not mean that we do not need

quantitative accuracy for physical accuracy. Some qualitative answers still require accurate energies and properties. They just do not have to be within 1 kcal/mol and are not as strict as chemical accuracy. Questions that require physical accuracy include (1) stability of a molecule in a specific geometry, (2) the spin state of the electronic ground state of a molecule, (3) whether a given molecule is strongly correlated and etc.

In this dissertation, we answer a question of physical accuracy which is about what reference wavefunction to use for simulating weakly or strongly correlated systems. By reference wavefunction, we mean that this wavefunction is used for subsequent higher level correlation calculations such as CI, CC or PT. It can be a single Slater determinant such as a HF state or a linear combination of multiple Slater determinants as in the complete active space self-consistent field (CASSCF) method. For weakly correlated systems, a HF state may be a suitable starting point except that sometimes it may suffer from artificial symmetry breaking (see below). For strongly correlated systems, a CASSCF state is the *de facto* reference state despite its exponential size-scaling. It is then natural to ask what is the best reference state for strongly correlated systems that scales polynomially in system size.

Condensed-Phase Applications Are Now Necessary

With the development of modern high-performance computing, it is no longer just quantum chemists' dream to simulate systems with thousands of atoms to probe bulk properties. Size-consistency is absolutely necessary for simulating bulk materials and therefore it is still a required property in model chemistries. Furthermore, polynomial scaling is more desirable than before. It is possible to simulate correlated solids in a very small unit cell with brute-force approaches such as FCI quantum Monte Carlo (FCIQMC) [42]. Such materials with a very small unit cell are far from what is required to compare with experiments. CC methods stand out uniquely as they are size-consistent and polynomial-scaling model chemistries [43–46]. However, these CC methods are not economical enough to be applied to diverse solids and condensed phase problems. Therefore, there is a clear need for quantum chemists to develop a method that is competitive with CC in accuracy and much less costly.

We note that one of the most pressing present-time theoretical challenges is the removal of finite-size effects. This becomes more evident when it comes to distinguishing multiple competing ordered phases of matter. Spontaneous symmetry breaking that forms charge density waves or spin density waves only occurs at the thermodynamic limit. The relative energetics between different phases depend on the size of the system. Therefore, one cannot assess the relative stability of phases using finite-sized cluster models. It is necessary to have a tool to reliably reach the

thermodynamic limit without finite-size effects [46–50]. Such tools often need large supercells (much larger than the minimal unit cell) to thoroughly investigate convergence to the thermodynamic limit, posing a great challenge to method development for simulating correlated solids.

Black-Box Implementation Is Not Required

For both developers and users, having a black-box implementation of a model chemistry is helpful for applying it to a wide variety of systems with little human effort. This has been at the heart of philosophy of modern quantum chemistry owing to Pople. In the author's viewpoint, among other criteria, the black-box implementation may be least important. Customized approaches to specific problems have gained some popularity. They are often necessary for achieving high accuracy with economical computational cost for specific problems.

Classic examples are the multi-reference self-consistent field (MCSCF) [51–58] and multi-reference configuration interaction (MRCI) [59, 60] methods for strongly correlated systems where users have to choose configurations to orbital-optimize or a reference set of configurations on which to add excitations A slightly more black-box approach in this category is CASSCF [51–53] where users only have to specify an active space in which to solve a FCI problem. While MCSCF and MRCI have seen relatively little application, CASSCF has stood out as a useful electron correlation model, though it requires much caution when applying to problems where there is no obvious choice for the active space.

As a more modern example, there are local correlation techniques which take existing correlation methods that satisfy all criteria by Pople (e.g., CCSD(T)) and apply approximations based on the locality of weak correlation. Most approaches involve a tunable parameter (and sometimes multiple parameters) that controls the trade-off between cost and accuracy. This makes the algorithm essentially non-black-box. Users have to check the convergence of the energy with respect to the tunable parameter to ensure the correctness of results that they obtain. Despite this "undesirable" property, local correlation methods remain popular in quantum chemistry and have been applied to numerous problems [61–67] that were simply intractable without them.

Other examples include those methods that yield energies which are not invariant under unitary rotations between occupied-occupied and virtual-virtual orbitals. Widely used single-reference approaches are more or less black-box because their energies are invariant under these rotations. Such invariance allows for a black-box implementation. Namely, once a desired HF or DFT solution is obtained, there is not much caution needed for running such subsequent correlation approaches. Methods

that lack this property can be difficult to use but they often come with other desirable properties such as polynomial scaling and exactness for certain limits. Making these approaches more black-box is an interesting research direction although it is sometimes challenging to make such progress.

We may tolerate non-black-box nature of some methods as long as they can provide reliable solutions to problems in our hand. We emphasize that this does not mean that we should not try to have a black-box approach. Any black-box implementations are highly desirable whenever possible. Our viewpoint is that some methods cannot be made black-box and we should not abandon these approaches simply because of it.

1.3 Challenges Addressed in This Dissertation

As mentioned before, approaches we desire can be somewhat application-specific. We have enough tools to apply to a wide variety of problems, though they may become too costly for large systems. Once we have a method that is targeted to solve a specific class of problems of interest, it is often necessary to have additional tools which could determine whether a given problem can be tackled by the method. Development of such tools that help one choose the right approach is therefore highly desirable.

Distinguishing Weak and Strong Correlation

In Section 1.1, we introduced weak and strong correlation between electrons. Strong correlation is typically difficult to deal with and the applicability of available tools are highly limited in system size. On the other hand, we have many available tools for weak correlation such as PT, which can potentially be applied to systems of thousands of atoms with additional tricks such as locality of weak correlation.

Most approaches to strong correlation problems consist of two steps. First, one builds an "active space" problem, which is to form an effective Hamiltonian for all strongly correlated electrons, and solves this Hamiltonian exactly (or often approximately with high accuracy). Second, one adds weak correlation outside this active space via a CI expansion [68–72], a CC expansion [73–111], or PT [112–119]. The first step of solving an active space problem is normally limited in size as most available tools scale exponentially with the number of electrons. The second step of adding missing weak correlation formally scales polynomially but is usually very complicated in terms of implementation. As such, the resulting model chemistry lacks derivation and implementation of properties beyond energies. If a given system

is only weakly correlated, the situation is much simpler. One can apply a low-order perturbation approach based on a mean-field starting point, Hartree-Fock (HF), and obtain quantitative answers for energies and other properties. Various properties are readily available for simple PT such as second-order Møller-Plesset (MP2) theory. This is due to the fact that our starting point for PT here is a single determinant. In the case of the second step for strong correlation we started from a more complicated active space wavefunction, which poses challenges in implementation and extension of such PT methods. Given this situation, it is preferred to distinguish weak and strong correlation and apply the two-step-strategy of strong correlation to only strongly correlated systems. For weakly correlated systems, such an approach is mostly wasteful and we should attempt to apply a simple approach like MP2.

In the modern era of quantum chemistry, distinguishing these two were normally done by symmetry breaking at the HF level. The meaning of this is most apparent in the HF *variational* energy expression for N-electron systems:

$$\begin{aligned} E_{\mathrm{HF}} &= \inf_{|\Phi\rangle} \frac{\langle\Phi|\hat{H}_{\mathrm{el}}|\Phi\rangle}{\langle\Phi|\Phi\rangle} \\ &= \inf_{\{|\phi_i\rangle\},\mathbf{\Lambda}} \left[\sum_{i=1}^{N_{\mathrm{el}}} \langle\phi_i|\hat{h}|\phi_i\rangle + \frac{1}{2}\sum_{ij}\langle ij||ij\rangle + E_{\mathrm{nuc}} + \sum_{ij}\Lambda_{ij}\langle\phi_i|\phi_j\rangle \right] \end{aligned} \tag{1.6}$$

where $|\Phi\rangle$ is a single Slater determinant made of a set of occupied orbitals $\{|\phi_i\rangle\}$, the one-electron operator $\hat{h}$ is

$$\hat{h} = -\frac{1}{2}\nabla^2 - \sum_A \frac{Z_A}{|\mathbf{r}-\mathbf{R}_A|}, \tag{1.7}$$

the antisymmetrized two-electron integral, $\langle ij||ij\rangle$, reads

$$\langle ij||ij\rangle \equiv \langle ij|ij\rangle - \langle ij|ji\rangle \tag{1.8}$$

with the Coulomb term,

$$\langle ij|ij\rangle = \int_{\mathbf{r}_1,\mathbf{r}_2} \frac{|\phi_i(\mathbf{r}_1)|^2|\phi_j(\mathbf{r}_2)|^2}{|\mathbf{r}_1-\mathbf{r}_2|}, \tag{1.9}$$

and the exchange term,

$$\langle ij|ji\rangle = \int_{\mathbf{r}_1,\mathbf{r}_2} \frac{\phi_i^*(\mathbf{r}_1)\phi_j(\mathbf{r}_1)\phi_j^*(\mathbf{r}_2)\phi_i(\mathbf{r}_2)}{|\mathbf{r}_1-\mathbf{r}_2|}, \tag{1.10}$$

and $\mathbf{\Lambda}$ represents the Lagrange multipliers to enforce orthonormality between orbitals. Eq. (1.6) demonstrates the variational nature of HF. Namely, the HF method produces a variationally optimized Slater determinant that gives an infimum of the energy expression in Eq. (1.6). In practice, one might impose "symmetry constraints" on the form of $|\Phi\rangle$ to obtain a determinant with the same symmetry as the exact ground state of $\hat{H}_{\text{el}}$. The exact ground state has multiple symmetry properties because $\hat{H}_{\text{el}}$ commutes with other operators. The symmetry of exact ground state includes $\hat{S}_z$-symmetry, spin- ($\hat{S}^2$-) symmetry, complex symmetry, and time-reversal symmetry. The symmetry constraints can be understood in terms of working quantities, $\mathbf{C}$ (i.e., molecular orbital coefficients). $\mathbf{C}$ is used to define each molecular orbital (MO) as a linear combination of atomic orbitals (LCAO), that is,

$$\phi_i(\mathbf{r}) = \sum_{\mu} \eta_\mu(\mathbf{r}) C_{\mu i} \tag{1.11}$$

where $\eta_\mu(\mathbf{r})$ denotes an atomic orbital (AO) evaluated at a grid point $\mathbf{r}$. The matrix $\mathbf{C}$ is a transformation matrix that connects MOs with AOs. A most general form of the i-th column (i.e., the i-th MO) in $\mathbf{C}$ is

$$\begin{bmatrix} \mathbf{c}_i^\alpha \\ \mathbf{c}_i^\beta \end{bmatrix} \tag{1.12}$$

where α and β denote the spin-component such that

$$\phi_i(\mathbf{r}) = \sum_{\mu} ((\mathbf{c}_i^\alpha)_\mu \eta_\mu(\mathbf{r}) + (\mathbf{c}_i^\beta)_\mu \eta_\mu(\mathbf{r})). \tag{1.13}$$

A one-body reduced density matrix (1RDM) $\mathbf{P}$ is then composed of a total of four spin-blocks,

$$\mathbf{P} = \mathbf{C}_{\text{occ}} \mathbf{C}_{\text{occ}}^\dagger = \begin{bmatrix} \mathbf{P}^{\alpha\alpha} & \mathbf{P}^{\alpha\beta} \\ \mathbf{P}^{\beta\alpha} & \mathbf{P}^{\beta\beta} \end{bmatrix} \tag{1.14}$$

where $\mathbf{C}_{\text{occ}}$ is the MO coefficient matrix for the occupied orbitals. Possible symmetry constraints on $|\Phi\rangle$ can be understood as restrictions on $\mathbf{P}$. The necessary constraints for representing non-interacting N-electron systems are (1) $\text{tr}(P) = N_{\text{el}}$ and (2) $\mathbf{P}^2 = \mathbf{P}$ (assuming AO basis sets are orthogonal). Depending on the type of HF, one may impose additional constraints on $\mathbf{P}$. In Table 1.1, we present possible HF types along with their restrictions on $\mathbf{P}$. Only RHF possesses all symmetries that the exact ground state has for a given Hamiltonian $\hat{H}_{\text{el}}$. The common wisdom in modern quantum chemistry is that strong correlation exists when RHF is unstable to other HF types. This common wisdom has been challenged by multiple examples [120–

Type	Constraints
RHF	$\mathbf{P}^{\alpha\alpha} = \mathbf{P}^{\beta\beta}$, $\mathbf{P}^{\alpha\beta} = \mathbf{P}^{\beta\alpha} = \mathbf{0}$, $P^{\alpha\alpha}_{\mu\nu} \in \mathbb{R}$
cRHF	$\mathbf{P}^{\alpha\alpha} = \mathbf{P}^{\beta\beta}$, $\mathbf{P}^{\alpha\beta} = \mathbf{P}^{\beta\alpha} = \mathbf{0}$
UHF	$\mathbf{P}^{\alpha\beta} = \mathbf{P}^{\beta\alpha} = \mathbf{0}$, $P^{\alpha\alpha}_{\mu\nu} \in \mathbb{R}$, $P^{\beta\beta}_{\mu\nu} \in \mathbb{R}$
cUHF	$\mathbf{P}^{\alpha\beta} = \mathbf{P}^{\beta\alpha} = \mathbf{0}$
GHF	$P_{\mu\nu} \in \mathbb{R}$
cGHF	None

Table 1.1: Types of HF approaches and their constraints on 1RDM. Note that we assume that orbitals are maximally collinear along the z-axis. For more general classifications without assuming the z-axis being a special axis, see Ch. 3.

127] that often call this "artificial" symmetry breaking. Artificial symmetry breaking occurs due to the lack of weak correlation, not due to the lack of strong correlation. On the contrary, essential symmetry breaking is due to the lack of strong correlation at the HF level and this implies that we need an approach that goes beyond simple PT methods. This artificial symmetry breaking cannot be distinguished from "essential" symmetry breaking solely based on the HF theory. We address this issue based on a correlated orbital theory where orbitals are optimized in the presence of weak correlation (in this case MP2). The resulting method may be useful for treating molecular problems without artifacts from artificial symmetry breaking using HF orbitals, as well as signaling the onset of genuinely strong correlations through the presence of essential symmetry-breaking in its reference orbitals

Exact, Polynomial Description to Strong Spin Correlation

We developed an approach that can describe strong spin correlation (SSC) exactly without invoking an exponential cost wall. SSC is an important class of strong correlation. When there are many spatially separated open-shell electrons, there is only a small energy cost for spin-flips while charge-transfers exhibit a large energy cost. This is the defining property of SSC [128]. There are multiple familiar examples that show emergent SSC between electrons. The most widely known example is multiple bond dissociations in molecules. For instance, dissociating the C-C double bond in an ethene molecule ($H_2C{=}CH_2$) leads to a total of four open-shell electrons that participate in SSC of this molecule. More sophisticated examples include metalloenzymes [129–131] such as the P-center of nitrogenase which involves the so-called FeMoCo moiety [132–135]. Unlike bond dissociations, metalloenzymes exhibit many open-shell electrons even at their equilibrium geometries. This is largely due to the fact that d- or f-electrons tend to be localized in space. Some metalloenzymes may

involve hundreds of open-shell electrons that participate in SSC and thus there is a clear need for an economical method which can handle SSC efficiently.

The common wisdom in modern quantum chemistry is that SSC can be described exactly if one includes all possible spin-couplings for a given number of electrons, N, and a spin-quantum number S. This is the essence of the spin-coupled valence bond (SCVB) or generalized valence bond (GVB) approach. It is undoubtedly the right approach for SSC but the cost for including all possible spin-couplings in SCVB scales exponentially with the number of electrons. The number of independent spin-coupling vectors is given by

$$f(N,S) = \frac{(2S+1)N!}{(\frac{1}{2}N+S+1)!(\frac{1}{2}N-S)!}, \tag{1.15}$$

assuming the $\hat{S}_z$ quantum number $M = S$ [136]. Based on Sterling's approximation, this combinatorial scaling of the spin-coupling dimension can be shown to approach an asymptotic exponential scaling for large N. Similar to other exponential scaling approaches, due to the steep computational scaling, the applicability of SCVB has been limited to systems with a small number of electrons [137–139].

Our approach to this seemingly exponentially difficult problem is the coupled-cluster valence bond (CCVB) approach [140]. We cast the SCVB wavefunction, which contains an exponentially many spin-couplings, into a compact coupled-cluster expansion with only a quadratic number of parameters, $\{t_{KL}\}$. The resulting wavefunction from CCVB is size-consistent, spin-pure (i.e., it is a spin-eigenfunction) and exact for SSC (i.e., exact for multiple bond breaking). Furthermore, the overall cost of the CCVB energy evaluation along with the wavefunction optimization scales only cubically with system size. It turns out that CCVB can describe SSC exactly as long as the UHF energy (see Table 1.1) is exact within the valence active space (where chemical bonds form and break). The UHF energy is exact in this limit because states with different S are all degenerate and all the interacting electrons are high-spin (i.e., no correlation). In such cases, CCVB is exact and maintains the spin-purity.

Some drawbacks and challenges in CCVB were addressed in this dissertation. Those challenges are as follows:

1. The CCVB energy is not invariant under unitary transformations within the occupied-occupied and the virtual-virtual blocks. This makes CCVB highly non-trivial to use even for an expert. If there is a way to improve, it is highly desirable.

2. The CCVB active space is inherently limited to a pairing active space (Ne, No) where we have the same number of electrons and the same number of orbitals

for CCVB to solve. This limits the applicability of CCVB to problems like bond dissociations where such a pairing active space is naturally well-suited.

3. CCVB does not include any ionic excitations between electron pairs. These ionic excitations do not participate in SSC, but they play a crucial role in describing overall electronic structure for systems with mixed SSC and weak correlation.

4. Some problems with SSC are not treatable with CCVB. These examples are those that UHF fails and only cGHF (see Table 1.1) is well-suited among HF approaches.

The drawbacks 1–3 have been addressed by extending CCVB to CCVB with singles and doubles (CCVB-SD) [141, 142] and the drawback 4 have been addressed by extending CCVB further to incorporate missing spin-couplings[143, 144].

1.4 Works Not Mentioned in This Dissertation

There are multiple works that were completed or are in progress as a part of the author's Ph.D. They are omitted in this dissertation for the sake of brevity and flow. We shall briefly mention them for the completeness of this dissertation:

1. An investigation of strong correlation in the context of DFT was carried out using cRHF (see Table 1.1) orbitals [145]. This work offers new insights into the so-called symmetry dilemma in DFT and suggests a new dataset that may be useful for the future XC functional development.

2. The tensor hypercontraction (THC) approach to HF, MP2, and MP3 is revisited with a new viewpoint from low-rank approximations [146–162]. The resulting THC approach requires a single tunable parameter that controls its cost and accuracy and is able to approach the exact answer. The scaling of MP2 and MP3 which are quintic and sextic without THC, respectively, but are only quartic with THC. This is a representative technique of useful non-black-box approaches.

3. A targeted excited state method for CC approaches was developed which can describe doubly excited states that are usually beyond the scope of widely used equation-of-motion CC with singles and doubles (EOM-CCSD). This approach is highly non-black-box and not universally applicable to any excited states. We showed that this tailored approach for double excited states can be indeed useful for some problems.

4. A rather unusual technique in quantum chemistry, the auxiliary-field quantum Monte Carlo (AFQMC) approach, was used to study the uniform electron gas model [163]. This QMC approach propagates a wavefunction in imaginary time and approximates the ground state using the same approach as power methods to obtain the lowest eigenmode of a given matrix. Without the phaseless constraint, AFQMC scales exponentially and therefore the use of the phaseless constraint defined with a trial wavefunction is necessary for the cost-effectiveness at the expense of introducing biases to energies. We attempted to understand the scope of AFQMC with RHF trial wavefunctions in the context of simulating the UEG model.

5. Finite-temperature quantum chemistry is investigated with finite-temperature AFQMC (FT-AFQMC). In particular, the UEG model along with small chemical systems are being assessed with FT-AFQMC with the phaseless constraint. This is an attempt to understand the role of electron correlation at finite temperatures which has been somewhat unexplored in modern quantum chemistry literature.

6. A wavefunction ansatz designed to be used on quantum computers was proposed in the context of the variational quantum eigensolver (VQE) [164]. The ansatz that we proposed is called k-UpCCGSD which can be cheaply implemented on quantum computers (hopefully near-term) [165].

7. Nuclear gradients of the CCVB energy, PT on top of CCVB, and CCVB with valence-optimized doubles (CCVB-VOD) are all under development. These are necessary steps towards solving problems that are not yet possible to solve with existing CCVB tools.

1.5 Outline

Chapter 2

Publication: Joonho Lee and Martin Head-Gordon. "Regularized Orbital-Optimized Second-Order Møller-Plesset Perturbation Theory: A Reliable Fifth-Order Scaling Electron Correlation Model with Orbital Energy Dependent Regularizers". J. Chem. Theory Comput. 2018, 14, 5203–5219.

In order to address the challenge of distinguishing strong and weak correlation, we have developed an approach that optimizes orbitals in the presence of the MP2 correlation energy. The MP2 correlation energy is susceptible to divergence due to the

energy denominator so it is necessary to regularize this singularity to reliably obtain orbitals. This chapter defines such a regularized orbital-optimized MP2 (κ-OOMP2) approach and demonstrates its utility on thermochemistry and non-covalent interaction benchmarks.

Chapter 3

Publication: Joonho Lee and Martin Head-Gordon. "Distinguishing artificial and essential symmetry breaking in a single determinant: approach and application to the C_{60}, C_{36}, and C_{20} fullerenes". Phys. Chem. Chem. Phys. 2019, 21, 4763–4778.

κ-OOMP2 is able to distinguish artificial and essential symmetry breaking and thereby it distinguishes strong and weak correlation more reliably than HF can. We utilize this aspect of κ-OOMP2 to end the controversy about whether C_{60} (Buckminsterfullerene) is strongly correlated. We also analyze a known biradicaloid C_{36} for comparison and as well as C_{20} (the smallest fullerene). The reliability of κ-OOMP2 for distinguishing weak and strong correlation was examined by comparing with other known probes for strong correlation such as natural orbital occupation numbers (in comparison with coupled-cluster methods) and singlet-triplet gaps.

Chapter 4

Publication: Joonho Lee and Martin Head-Gordon. "Two Single-Reference Approaches to Biradicaloid Problems: Complex, Restricted Orbitals and Approximate Spin-Projection Combined With Regularized Orbital-Optimized Møller-Plesset Perturbation Theory". Accepted in J. Chem. Phys.

Utilizing essential symmetry breaking with κ-OOMP2, one can describe singlet biradicaloids. In particular, we examined the use of complex, restricted orbitals and unrestricted orbitals combined with Yamaguchi's approximate spin-projection for describing singlet biradicaloids with a triplet ground state.

Chapter 5

Publication: Joonho Lee, David W. Small, Evgeny Epifanovsky, and Martin Head-Gordon. "Coupled-Cluster Valence-Bond Singles and Doubles for Strongly Correlated Systems: Block-Tensor Based Implementation and Application to Oligoacenes". J. Chem. Theory Comput. 2017, 13, 602–615.

An efficient implementation of CCVB-SD was achieved and we applied CCVB-SD to oligoacenes correlating electrons up to 318 electrons in 318 orbitals. We demon-

strate the utility of CCVB-SD in describing emergent strong correlation present in oligoacenes.

Chapter 6

Publication: Joonho Lee, David W. Small, and Martin Head-Gordon. "Open-Shell Coupled-Cluster Valence-Bond Theory Augmented with an Independent Amplitude Approximation for Three-Pair Correlations: Application to a Model Oxygen-Evolving Complex and Single Molecular Magnet". J. Chem. Phys. 2018, 149, 244121.

We present the development and assessment of open-shell CCVB augmented with three-pair configurations within the independent amplitude approximation (OS CCVB+i3). We numerically demonstrate that OS CCVB+i3 can describe SSC exactly even when CCVB fails. We present numerical experiments on numerous chemical systems such as a model oxygen-evolving complex and a single molecular magnet. We emphasize the remarkable compactness of OS CCVB+i3 wavefunctions for describing SSC.

Chapter 7

We summarize the contents of this dissertation and conclude with some future directions that set new challenges for the future methodology development.

Chapter 2

Regularized Orbital-Optimized Second-Order Møller-Plesset Perturbation Theory

2.1 Introduction

The single-reference second-order Møller-Plesset perturbtation theory (MP2) is one of the simplest correlated wavefunction methods (and therefore one of the most popular ones). There have been some significant developments in improving different aspects of MP2 in the past decade or so and we shall mention those that are particularly relevant to this work.

The development of the resolution-of-identity (RI) technique (or the density-fitting technique) for MP2 was revolutionary.[166, 167] Although RI-MP2 has fundamentally the same computational scaling as MP2 (i.e. $\mathcal{O}(N^5)$), it substantially reduces the prefactor of the algorithm and has allowed for large-scale applications of MP2. RI-MP2 is now considered the *de facto* algorithm for any MP2 calculations except for systems with off-atom electrons such as dipole-bound electrons[168] or electronic resonances.[169] Given its popularity, we shall focus on building a new theory on top of RI-MP2 and we will refer RI-MP2 to as just MP2 for simplicity for the following discussion.

Aside from faster MP2 algorithms, there are two common ways to improve the energetics of MP2: one is the spin component scaled (SCS)-MP2 approach [170–175] and another is the orbital-optimized MP2 (OOMP2) method.[176–178] SCS-MP2 improved the energetics of MP2 for thermochemistry and non-covalent interactions although the optimal scaling parameters are different for these two classes of relative

energies. From an efficiency standpoint, the scaled opposite-spin MP2 (SOS-MP2) method in this category is noteworthy as it is an overall $\mathcal{O}(N^4)$ algorithm while improving the energetics.[171, 173, 175] The idea of SCS-MP2 is also often used in double-hybrid density functional approximations. [179–182] Additionally, overbinding molecular interactions due to inherent errors in MP2 and basis set superposition error were reduced by an attenuated MP2 approach.[183–186]

OOMP2 often produces a qualitatively better set of orbitals for systems where unrestricted Hartree-Fock (UHF) orbitals exhibit artificial spin symmetry breaking. Artificial symmetry breaking is a quite common problem in open-shell systems and polyaromatic hydrocarbons that are weakly correlated systems.[121, 127] In such cases, using UHF orbitals for correlated wave function calculations leads to catastrophically wrong energies and properties.[187–190] The use of Brückner orbitals often improves the results significantly, though obtaining those orbitals is quite expensive. [191, 192] Therefore, OOMP2 was proposed as an economical way to approximate Brückner orbitals. [176] Orbital optimizing at the MP2 level often restores the spin symmetry and results in far better energetics. [176, 177, 193] Furthermore, OOMP2, in principle, removes the discontinuity in the first-order properties that can be catastrophic at the onset of symmetry breaking in MP2.[194] These two observations motivated several research groups to apply [195, 196] and to develop OOMP2 and its variants.[197–204] It was also extended to higher order perturbation theory methods, such as OOMP3 and OOMP2.5.[205–207] The analytic nuclear gradient of OOMP2 was also efficiently implemented [196, 208, 209] and the Cholesky decomposition was also used for an efficient implementation. [210]

However, OOMP2 has shown multiple problems that limit its applicability. First, the inclusion of the MP2 form of the correlation energy in orbital optimization tends to produce very small energy denominators. In some cases, this leads to a divergence of the total energy and it is commonly observed when stretching bonds. Moreover, this is the cause for the significant underestimation of harmonic frequencies at equilibrium geometries.[199] Given that it is very unlikely to observe vanishing energy denominators in finite systems at the HF level, [211] the applicability of MP2 on top of HF orbitals is greater than that of OOMP2.

Second, OOMP2 often does not continuously break spin-symmetry even when there exists a broken-symmetry solution that is lower in energy. [212] To have a continuous transition from a restricted (R) solution to a unrestricted (U) solution, there should be a point at which the lowest eigenvalue of the R to U stability Hessian becomes zero. In the case where two solutions are separated by a barrier, we often observe a discontinuous transition from R to U (or even no transition at all) and there are only positive non-zero eigenvalues in the R to U stability Hessian. We have observed multiple systems where ROOMP2 does not undergo a continuous

transition to UOOMP2 while the corresponding HF calculation does. In this case, this is an artifact of OOMP2 and it is necessary to resolve this issue to reach a proper dissociation limit.

Our group has attempted to solve these two separate issues using a simple regularization scheme that shifts the energy denominator by a constant δ.[199] Despite its simple form, it was effective enough to solve those two issues described above. It is immediately obvious that the energy can no longer diverge. Moreover, as the MP2 energy is damped away, the qualitative behavior of OOMP2 approaches that of HF where we observe continuous transitions from R to U. Razban et al[203] tried to find a regularization parameter δ that solves those two issues within OO-SOS-MP2. Since the desired regularization strength to restore Coulson-Fischer points [213] was too strong (i.e. the true correlation energy attenuated), one faces difficulties in dealing with rather easier problems for MP2, such as typical thermochemistry problems. This led us to considering alternative forms of regularizers which may depend on the orbital energy gap. Ideally, we need a regularizer that leaves the energy contribution from a large denominator unchanged and damps away the contribution from an offending small denominator.

We note that the idea of regularizing perturbation theory has been explored by several others. Other ideas include the level-shifted complete active space second-order perturbation theory (CASPT2),[214] restrained denominator MP2 (RD-MP2),[215] and the recently introduced driven similarity renormalization group (DSRG) methods.[216] In particular the DSRG methods are particularly interesting as they regularize each term differently depending on the associated energy denominator. In fact the regularizers we study here were motivated by DSRG. We also mention that there are other approaches that are computationally as simple as (or cheaper than) MP2 and do not diverge even for metallic systems. These include direct random phase approximation[217] and degeneracy-corrected perturbation theory. [218] We also mention our group's previous work on penalty functions which regularize PT amplitudes.[219] It is worthwhile to mention that there may be formal connections between regularized OOMP2 and correlation theories with screened interactions such as random phase approximation [220] and coupled-pair theories [221] as these all exhibit no singular behavior for metallic systems.

This paper is organized as follows: (1) we review OOMP2 , (2) we describe the regularizers that we used in this work and derive the pertinent orbital gradient of them, (3) we investigate the effect of regularizers on the stability Hessian, (4) we demonstrate preliminary training and test of the new regularizers on the W4-11 set[222], the RSE43 set,[223, 224] and the TA13 set,[225] and (5) we apply these new methods to two chemically interesting biradical molecules.[226, 227]

2.2 Theory

We will use $i, j, k, l, \cdots$ to index occupied orbitals, $a, b, c, d, \cdots$ to index virtual orbitals, and $p, q, r, s, \cdots$ to index either of those two.

2.2.1 OOMP2 Lagrangian in Spin-Orbital Basis

We review the OOMP2 Lagrangian formulation and its orbital gradient within the spin-orbital notation. For generality, we do not assume orbitals to be real.

Hylleraas Functional

The Hylleraas functional J_H is given as

$$\begin{aligned} J_H[\Psi_1] &= \langle\Psi_1|\,\hat{F} - E_0\,|\Psi_1\rangle + \langle\Psi_0|\,\hat{V}\,|\Psi_1\rangle + \langle\Psi_1|\,\hat{V}\,|\Psi_0\rangle \\ &= \langle\Psi_1|\,\hat{F}_N\,|\Psi_1\rangle + \langle\Psi_0|\,\hat{V}_N\,|\Psi_1\rangle + \langle\Psi_1|\,\hat{V}_N\,|\Psi_0\rangle\,, \end{aligned} \tag{2.1}$$

where the subscript N denotes "normal-ordered" operators [228] and the OOMP2 ansatz for $|\Psi_1\rangle$ by definition includes only doubly excited determinants:

$$|\Psi_1\rangle = \hat{T}_2\,|\Psi_0\rangle = \frac{1}{4}\sum_{ijab} t_{ij}^{ab}\,\left|\Psi_{ij}^{ab}\right\rangle. \tag{2.2}$$

In a simpler notation, this functional is

$$J_H[\mathbf{t}] = \mathbf{t}^\dagger\Delta\mathbf{t} + \mathbf{t}^\dagger\mathbf{V} + \mathbf{V}^\dagger\mathbf{t} \tag{2.3}$$

where Δ is a rank-8 tensor defined as

$$\Delta_{ijab}^{klcd} = \langle\Psi_{ij}^{ab}|\hat{F}_N|\Psi_{kl}^{cd}\rangle \tag{2.4}$$

and $\mathbf{V}$ is

$$V_{ab}^{ij} = \langle ab||ij\rangle \tag{2.5}$$

In passing we note that when we include orbital optimization effects $|\Psi_1\rangle$ is no longer composed of canonical orbitals. Instead it is convenient to use pseudocanonical orbitals[229, 230] that diagonalize the occupied-occupied (OO) and the virtual-virtual (VV) blocks of the Fock operator, $\hat{F}$. Strictly speaking, singles contributions do not vanish. However, we argue that this is a part of our ansätz, consistent with the idea of variational Brückner orbitals. Orbital optimization incorporates the most important singles effects. Indeed, the effect of singles was examined in the context of OOMP2 and found negligible as in ref. 177.

MP2 Lagrangian

We construct a Lagrangian that consists of Hylleraas functional J_H and the Hartree-Fock energy E_1 as in

$$\begin{aligned}\mathcal{L}[\mathbf{t},\mathbf{\Theta}] &= E_1[\mathbf{\Theta}] + J_H[\mathbf{t},\mathbf{\Theta}] \\ &= \sum_i \langle i|h|i\rangle + \frac{1}{2}\sum_{ij}\langle ij||ij\rangle + \frac{1}{4}\sum_{ijab}\langle ij||ab\rangle\, t_{ij}^{ab} + \frac{1}{4}\sum_{ijab}(t_{ij}^{ab})^*\,\langle ab||ij\rangle \\ &\quad + \sum_{ij} P_{ij}^{(2)} F_{ji} + \sum_{ab} P_{ab}^{(2)} F_{ba}, \end{aligned} \tag{2.6}$$

where the OO and VV MP2 one-particle density matrices (OPDMs) are

$$P_{ij}^{(2)} = -\frac{1}{2}\sum_{abk}(t_{ik}^{ab})^* t_{jk}^{ab} \tag{2.7}$$

$$P_{ab}^{(2)} = \frac{1}{2}\sum_{ijc}(t_{ij}^{ac})^* t_{ij}^{bc}. \tag{2.8}$$

Assuming pseudocanonical orbitals, the variation in $\mathbf{t}$ yields

$$t_{ij}^{ab} = -\frac{\langle ab||ij\rangle}{\Delta_{ij}^{ab}}, \tag{2.9}$$

where the denominator is defined as a non-negative quantity,

$$\Delta_{ij}^{ab} = \epsilon_a + \epsilon_b - \epsilon_i - \epsilon_j. \tag{2.10}$$

With the optimal amplitudes, J_H yields the familiar MP2 energy expression,

$$E_{\mathrm{MP2}} = -\frac{1}{4}\sum_{ijab}\frac{|\langle ij||ab\rangle|^2}{\Delta_{ij}^{ab}} \tag{2.11}$$

We apply the RI approximation[166, 167] to the two-electron integrals,

$$\langle ij|ab\rangle = \sum_{PQ}(ia|P)(P|Q)^{-1}(Q|jb). \tag{2.12}$$

We further define RI fit coefficients, C_{pq}^P, for the $|pq\rangle$ charge distribution as:

$$C_{pq}^P = \sum_{pqQ}(P|Q)^{-1}(Q|pq), \tag{2.13}$$

and the 3-center, 2-particle density matrix (TPDM) as

$$\Gamma_{ai}^{P} = \sum_{jb} t_{ij}^{ab} C_{jb}^{P}. \tag{2.14}$$

The TPDM piece of the Hylleraas functional then becomes

$$\frac{1}{2} \sum_{iaP} V_{ia}^{P} \, \Gamma_{ai}^{P} + \text{h.c.}, \tag{2.15}$$

where we used

$$V_{ia}^{P} = (ia|P). \tag{2.16}$$

Orbital Optimization

The self-consistent field procedure can be described as rotating N_{mo} orthonormal vectors until an objective function reaches its stationary point. Thus it is possible to relate two different molecular orbital coefficients with a unitary transformation as in

$$\mathbf{C}' = \mathbf{C}\mathbf{U}, \tag{2.17}$$

where $\mathbf{U}$ is a unitary (or orthogonal for real variables) matrix. As both the Hartree-Fock energy and the Hylleraas functional in (2.6) are invariant under OO and VV rotations, we consider only the non-redundant OV orbital rotations. We then write the transformation matrix,

$$\mathbf{U} = \exp[\boldsymbol{\Delta}_{\text{o}} \boldsymbol{\Theta} \boldsymbol{\Delta}_{\text{v}}^{\dagger} - \boldsymbol{\Delta}_{\text{v}} \boldsymbol{\Theta}^{\dagger} \boldsymbol{\Delta}_{\text{o}}^{\dagger}], \tag{2.18}$$

where $\boldsymbol{\Delta}_{\text{o}}$ and $\boldsymbol{\Delta}_{\text{v}}$ are skinny matrices of the dimension $N_{\text{mo}} \times n_{\text{occ}}$ and $N_{\text{mo}} \times n_{\text{vir}}$, respectively, and they have 1's on the diagonal, and $\boldsymbol{\Theta}$ is a matrix of the dimension $n_{\text{occ}} \times n_{\text{vir}}$. It will be useful to expand $\mathbf{U}$,

$$\mathbf{U} = \mathbf{I} + \left(\boldsymbol{\Delta}_{\text{o}} \boldsymbol{\Theta} \boldsymbol{\Delta}_{\text{v}}^{\dagger} - \boldsymbol{\Delta}_{\text{v}} \boldsymbol{\Theta}^{\dagger} \boldsymbol{\Delta}_{\text{o}}^{\dagger} \right) + \mathcal{O}(|\boldsymbol{\Theta}|^2) \tag{2.19}$$

Up to first order in $\boldsymbol{\Theta}$, occupied and virtual orbitals transform in the following way:

$$C'_{\mu i} = C_{\mu i} - \sum_{a} C_{\mu a} \Theta_{ia}^{*} \tag{2.20}$$

$$C'_{\mu a} = C_{\mu a} + \sum_{i} C_{\mu i} \Theta_{ia} \tag{2.21}$$

We now consider the variation of the energy, $\delta\mathcal{L}$, up to first-order in $\mathbf{\Theta}$,

$$\begin{aligned}
\delta\mathcal{L} = & \sum_{ia} \left(-h_{ai}\Theta_{ia} - h_{ia}\Theta^*_{ia}\right) \\
& - \frac{1}{2}\sum_{ija} \Big(\langle ij \,\|\, aj\rangle\, \Theta^*_{ia} + \langle ij \,\|\, ia\rangle\, \Theta^*_{ja} + \langle aj \,\|\, ij\rangle\, \Theta_{ia} + \langle ia \,\|\, ij\rangle\, \Theta_{ja} \Big) \\
& - \sum_{ijc} P^{(2)}_{ij} \left(F_{ci}\Theta_{jc} + F_{jc}\Theta^*_{ic}\right) - \sum_{ijck} P^{(2)}_{ij} \left(\langle jc \,\|\, ik\rangle\, \Theta_{kc} + \langle jk \,\|\, ic\rangle\, \Theta^*_{kc}\right) \\
& + \sum_{kab} P^{(2)}_{ab} \left(F_{ka}\Theta^*_{kb} + F_{bk}\Theta_{ka}\right) - \sum_{abck} P^{(2)}_{ab} \left(\langle bc \,\|\, ak\rangle\, \Theta_{kc} + \langle bk \,\|\, ac\rangle\, \Theta^*_{kc}\right) \\
& + \Bigg[\frac{1}{4}\sum_{ijab} t^{ab}_{ij} \Bigg(- \sum_{c} \Big(\langle cj \,\|\, ab\rangle\, \Theta_{ic} + \langle ic \,\|\, ab\rangle\, \Theta_{jc} \Big) \\
& + \sum_{k} \Big(\langle ij \,\|\, kb\rangle\, \Theta_{ka} + \langle ij \,\|\, ak\rangle\, \Theta_{kb} \Big) \Bigg) + \text{h.c.} \Bigg].
\end{aligned} \tag{2.22}$$

The first line corresponds to the HF orbital gradient and the rest belongs to the MP2 contribution. We apply the RI technique we described before to the last line of Eq. (2.22):

$$\frac{1}{2}\left(-V^P_{ca}\Gamma^P_{ai}\Theta_{ic} - V^P_{cb}\Gamma^P_{bj}\Theta_{jc} + V^P_{ik}\Theta_{ka}\Gamma^P_{ai} + V^P_{jk}\Theta_{kb}\Gamma^P_{bj}\right) + \text{h.c.} \tag{2.23}$$

The orbital optimization treats the real and imaginary parts of Θ_{ia} as separate variables as is done in Wirtinger calculus.[231]

$$\frac{\delta\mathcal{L}}{\delta\text{Re}(\Theta_{kc})} = \frac{\delta\mathcal{L}}{\delta\Theta_{kc}} + \frac{\delta\mathcal{L}}{\delta\Theta^*_{kc}} \tag{2.24}$$

$$\frac{\delta\mathcal{L}}{\delta\text{Im}(\Theta_{kc})} = -i\left(\frac{\delta\mathcal{L}}{\delta\Theta_{kc}} - \frac{\delta\mathcal{L}}{\delta\Theta^*_{kc}}\right) \tag{2.25}$$

where

$$\begin{aligned}
\frac{\delta\mathcal{L}}{\delta\Theta_{kc}} = & - F_{ck} - \sum_{i} F_{ci}P^{(2)}_{ik} + \sum_{a} P^{(2)}_{ca}F_{ak} - \sum_{ij} P^{(2)}_{ij}\,\langle jc \,\|\, ik\rangle - \sum_{ab} P^{(2)}_{ab}\,\langle bc \,\|\, ak\rangle \\
& - \sum_{aP} V^P_{ca}\Gamma^P_{ak} + \sum_{iP} V^P_{ik}\Gamma^P_{ci}
\end{aligned} \tag{2.26}$$

$$\frac{\delta\mathcal{L}}{\delta\Theta^*_{kc}} = \left(\frac{\delta\mathcal{L}}{\delta\Theta_{kc}}\right)^* \tag{2.27}$$

In passing we note that the last two terms in Eq. (2.26) are evaluated by the usual mixed Lagrangian technique as used in the nuclear gradient implementation of RI-MP2. [232]

2.2.2 Regularized OOMP2

Stück and Head-Gordon found a rather disturbing feature of OOMP2 when breaking bonds. [199] The energy denominator Δ_{ij}^{ab} approaches zero near dissociation limits in the case of restricted orbitals if optimized at the MP2 level. This leads to a divergent ROOMP2 solution even when using UOOMP2, as it is variationally preferred. In the perturbation theory literature, this existence of a divergent solution is sometimes referred to as an intruder state problem.

To ameliorate this problem, Stück and Head-Gordon employed a simple level-shift scheme to remove the divergent ROOMP2 solution associated with single bond-breaking and found it somewhat effective. This regularizer will be referred to as a δ-regularizer: $\Delta_{ij}^{ab} \leftarrow \Delta_{ij}^{ab} + \delta$. Some preliminary results on thermochemistry were encouraging with $\delta = 400$ mE_h. However, later it was found that the level-shift parameter to restore Coulson-Fischer points for double and triple bond dissociations is too large to give reasonable thermochemistry results. [203] This sets the main objective of this work. Namely, we are interested in designing a regularizer that can solve the first-order derivative discontinuity and the energy singularity problems while keeping the thermochemistry performance undamaged.

Design principles of regularizers

Ideally, one needs a regularizer that damps away a strongly divergent term while keeping physical correlation terms unchanged. As an attempt to achieve this goal, we propose multiple classes of orbital energy gap dependent regularizers that remove the singularity problem while (hopefully) damaging thermochemistry results to only a small extent.

One may understand the MP2 singularity problem based on the following integral transform:

$$E_{\mathrm{MP2}} = -\frac{1}{4}\sum_{ijab}\int_0^\infty \mathrm{d}\tau\, e^{-\tau\Delta_{ij}^{ab}}|\langle ij||ab\rangle|^2 = \frac{1}{4}\sum_{ijab}\epsilon_{ij}^{ab} \tag{2.28}$$

where

$$\epsilon_{ij}^{ab} = -\int_0^\infty \mathrm{d}\tau\, e^{-\tau\Delta_{ij}^{ab}}|\langle ij||ab\rangle|^2 \tag{2.29}$$

This energy expression is derived from a Laplace transformation of the energy expression in Eq. (2.11) and is a foundation of various linear-scaling MP2 methods.[233–235] When $\Delta_{ij}^{ab} = 0$, the corresponding energy contribution ϵ_{ij}^{ab} is divergent as the integrand does not decay to zero when $\tau \to \infty$.

One may try to regularize ϵ_{ij}^{ab} by changing Δ_{ij}^{ab} to $\Delta_{ij}^{ab} + \delta$ with a positive constant δ so that when $\Delta_{ij}^{ab} = 0$ the integrand decays to zero as $\tau \to \infty$. This corresponds to

the δ-regularizer. Alternatively, one may replace Δ_{ij}^{ab} in the integrand with a function of Δ_{ij}^{ab} that does not go to zero as $\Delta_{ij}^{ab} \to 0$. One such example is

$$\Delta_{ij}^{ab} + \frac{1}{(\alpha + \Delta_{ij}^{ab})^p} \tag{2.30}$$

where $\alpha > 0$ and p is a positive integer which can be chosen empirically. This function has a non-zero asymptote for infinitesimal Δ_{ij}^{ab} and becomes Δ_{ij}^{ab} for large positive values of Δ_{ij}^{ab}. This yields an energy expression,

$$E_{\mathrm{MP2}}(\alpha, p) = -\frac{1}{4} \sum_{ijab} \frac{|\langle ij||ab\rangle|^2}{\Delta_{ij}^{ab} + \frac{1}{(\alpha+\Delta_{ij}^{ab})^p}}, \tag{2.31}$$

and we call this class of regularizers α^p regularizers.

Another way to approach this problem is to change the domain of integration for small Δ_{ij}^{ab} values. The upper limit of the integral should approach ∞ for large Δ_{ij}^{ab} and become a finite value for small Δ_{ij}^{ab} to remove the singularity. A simple way to achieve this is to have a two-parameter integral upper limit $\sigma(\Delta_{ij}^{ab})^p$ where $\sigma > 0$ and p is a positive integer. We call this regularizer, a σ^p-regularizer. The regularized energy expression then reads

$$E_{\mathrm{MP2}}(\sigma, p) = -\frac{1}{4} \sum_{ijab} \frac{|\langle ij||ab\rangle|^2}{\Delta_{ij}^{ab}} \left(1 - e^{-\sigma(\Delta_{ij}^{ab})^p}\right) \tag{2.32}$$

Interestingly, $p = 2$ leads to an energy expression that was derived from the driven similarity renormalization group theory by Evangelista and co-workers.[216]

Lastly, one may modify the two-electron integrals such that the resulting integrand decays to zero when $\Delta_{ij}^{ab} \to 0$. Motivated by the above exponential damping function, we propose to modify V_{ab}^{ij} to

$$W_{ab}^{ij}(\kappa, p) = V_{ab}^{ij} \left(1 - e^{-\kappa(\Delta_{ij}^{ab})^p}\right). \tag{2.33}$$

The regularized energy then reads

$$E_{\mathrm{MP2}}(\kappa, p) = -\frac{1}{4} \sum_{ijab} \frac{|\langle ij||ab\rangle|^2}{\Delta_{ij}^{ab}} \left(1 - e^{-\kappa(\Delta_{ij}^{ab})^p}\right)^2 \tag{2.34}$$

We call this class of regularizers κ^p regularizers.

In this work, we shall investigate the σ^1- and κ^1-regularizers. These were chosen because one can easily write down a Lagrangian that yields the regularized energy expressions and the orbital gradient is not so complicated.

κ^1-Regularizer

We define the following rank-8 tensor $\mathbf{\Sigma}$ that depends on a single parameter β,

$$\Sigma_{ijkl}^{abcd}(\beta) = (e^{\beta \mathbf{F}^{\mathrm{oo}}})_{ik}(e^{\beta \mathbf{F}^{\mathrm{oo}}})_{jl}(e^{-\beta \mathbf{F}^{\mathrm{vv}}})_{ac}(e^{-\beta \mathbf{F}^{\mathrm{vv}}})_{bd} \tag{2.35}$$

where $\mathbf{F}^{\mathrm{oo}}$ and $\mathbf{F}^{\mathrm{vv}}$ are occupied-occupied and virtual-virtual blocks of Fock matrix, respectively. If orbitals are pseudocanonical, $\mathbf{\Sigma}$ becomes much sparser:

$$\Sigma_{ijkl}^{abcd}(\beta) = e^{-\beta \Delta_{ij}^{ab}} \delta_{ik}\delta_{jl}\delta_{ac}\delta_{bd} \tag{2.36}$$

We write the regularized OOMP2 Lagrangian modifying the two-electron integrals in Eq. (2.3),

$$\mathbf{t}^\dagger \mathbf{V} \to \mathbf{t}^\dagger(\mathbf{1} - \mathbf{\Sigma}(\kappa))\mathbf{V} \equiv \mathbf{t}^\dagger \mathbf{W}(\kappa) \tag{2.37}$$

where the damped integral $\mathbf{W}$ is defined as

$$\mathbf{W}(\kappa) = (\mathbf{1} - \mathbf{\Sigma}(\kappa))\mathbf{V} \tag{2.38}$$

Using this, the modified Lagrangian reads

$$\mathcal{L}[\mathbf{t}, \mathbf{\Theta}] = \mathcal{L}_0[\mathbf{t}, \mathbf{\Theta}] - \mathbf{V}^\dagger \mathbf{\Sigma}(\kappa)\mathbf{t} - \mathbf{t}^\dagger \mathbf{\Sigma}(\kappa)\mathbf{V}. \tag{2.39}$$

This leads to modified amplitudes,

$$t_{ij}^{ab} = -\frac{\langle ab||ij\rangle}{\Delta_{ij}^{ab}} \left(1 - e^{-\kappa \Delta_{ij}^{ab}}\right) \tag{2.40}$$

In the limit of $\Delta_{ij}^{ab} \to 0$, $t_{ij}^{ab} \to -\kappa\langle ab||ij\rangle$ as opposed to ∞. The regularized MP2 energy from the modified Lagrangian follows

$$E_{\mathrm{MP2}}(\kappa) = -\frac{1}{4}\sum_{ijab} \frac{|\langle ij||ab\rangle|^2}{\Delta_{ij}^{ab}} \left(1 - e^{-\kappa \Delta_{ij}^{ab}}\right)^2, \tag{2.41}$$

which is the κ^1-OOMP2 energy. We note that $\Delta_{ij}^{ab} \to 0$ does not contribute to the energy. Obviously, the large κ limit recovers the unregularized energy expression.

The orbital gradient is simply the sum of Eq. (2.26) (where $\mathbf{P}^{(2)}$ and $\mathbf{\Gamma}$ are computed with modified amplitudes) and the contribution from the two additional terms in Eq. (2.39). In the pseudocanonical basis,

$$\mathbf{V}^\dagger \mathbf{\Sigma}(\kappa)\mathbf{t} = \frac{1}{4}\sum_{ijab} e^{-\kappa \Delta_{ij}^{ab}} \langle ij||ab\rangle t_{ij}^{ab} \tag{2.42}$$

Differentiating $\langle ij||ab\rangle$ was already explained before, so we focus on the derivative of $e^{\kappa\Delta_{ij}^{ab}}$. We have

$$\frac{\partial e^{\kappa\mathbf{F}^{\mathrm{oo}}}}{\partial\Theta_{kc}} = \kappa\int_0^1 \mathrm{d}\tau\ e^{(1-\tau)\kappa\mathbf{F}^{\mathrm{oo}}}\frac{\partial\mathbf{F}^{\mathrm{oo}}}{\partial\Theta_{kc}}e^{\tau\kappa\mathbf{F}^{\mathrm{oo}}} \tag{2.43}$$

and

$$\frac{\partial F_{ij}}{\partial\Theta_{kc}} = -F_{cj}\delta_{ik} - \langle ic||jk\rangle \tag{2.44}$$

Similarly,

$$\frac{\partial e^{-\kappa\mathbf{F}^{\mathrm{vv}}}}{\partial\Theta_{kc}} = -\kappa\int_0^1 \mathrm{d}\tau\ e^{-(1-\tau)\kappa\mathbf{F}^{\mathrm{vv}}}\frac{\partial\mathbf{F}^{\mathrm{vv}}}{\partial\Theta_{kc}}e^{-\tau\kappa\mathbf{F}^{\mathrm{vv}}} \tag{2.45}$$

and

$$\frac{\partial F_{ab}}{\partial\Theta_{kc}} = F_{ak}\delta_{bc} - \langle ac||bk\rangle \tag{2.46}$$

Generally, one needs to perform an one-dimensional quadrature to compute this contribution to the orbital gradient. In the pseudocanonical basis, the extra contribution to the orbital gradient is given as

$$\begin{aligned}\frac{\partial(\mathbf{V}^\dagger\boldsymbol{\Sigma}(\kappa)\mathbf{t}+\mathrm{h.c.})}{\partial\Theta_{kc}} &= -\sum_{aP}e^{-\kappa\Delta_k^a}V_{ca}^P\tilde{\Gamma}_{ak}^P + \sum_{iP}e^{-\kappa\Delta_i^c}\tilde{\Gamma}_{ci}^P V_{ik}^P \\ &- \kappa\int_0^1\mathrm{d}\tau\ \left(\tilde{F}_{ck}(\tau)e^{(1-\tau)\kappa\epsilon_k} + \tilde{\tilde{F}}_{ck}(\tau)e^{-\tau\kappa\epsilon_c}\right) \\ &- \kappa\int_0^1\mathrm{d}\tau\ \left(\sum_{\mu\nu}\left[\left(X_{\nu\mu}(\tau)-Y_{\nu\mu}(\tau)\right)\langle\mu c||\nu k\rangle\right]\right)\end{aligned} \tag{2.47}$$

where we define

$$\Delta_p^q = \epsilon_q - \epsilon_p, \tag{2.48}$$

$$\tilde{\Gamma}_{ai}^P = \sum_{jb}e^{-\kappa\Delta_j^b}t_{ij}^{ab}C_{jb}^P, \tag{2.49}$$

$$\tilde{F}_{ck}(\tau) = \sum_l F_{cl}e^{\tau\kappa\epsilon_l}(\omega_{lk}^* + \omega_{kl}), \tag{2.50}$$

$$\tilde{\tilde{F}}_{ck}(\tau) = \sum_a(\omega_{ca}+\omega_{ac}^*)e^{-(1-\tau)\kappa\epsilon_a}F_{ak}, \tag{2.51}$$

$$X_{\nu\mu}(\tau) = \sum_{ij}e^{\tau\kappa\epsilon_j}C_{\nu j}(\omega_{ji}^*+\omega_{ij})C_{\mu i}^* e^{(1-\tau)\kappa\epsilon_i} \tag{2.52}$$

$$Y_{\nu\mu}(\tau) = \sum_{ab}e^{-\tau\kappa\epsilon_b}C_{\nu b}(\omega_{ba}+\omega_{ab}^*)C_{\mu a}^* e^{-(1-\tau)\kappa\epsilon_a}, \tag{2.53}$$

$$\omega_{lk} = \sum_{aP} e^{-\kappa\epsilon_a} V_{la}^P \tilde{\Gamma}_{ak}^P, \tag{2.54}$$

and

$$\omega_{ac} = \sum_{iP} e^{\kappa\epsilon_i} \tilde{\Gamma}_{ai}^P V_{ic}^P. \tag{2.55}$$

Those extra terms can be readily implemented to any existing OOMP2 programs and there is only a mild increase in the computational cost. The only additional $\mathcal{O}(N^5)$ step is the formation of $\tilde{\mathbf{\Gamma}}$ in Eq. (2.49) and this can be done at the same time as forming $\mathbf{\Gamma}$.

σ^1-Regularizer

The σ^1-regularizer can be derived from a Hylleraas functional with a set of auxiliary amplitudes $\mathbf{s}$. We write the new Hylleraas functional in the following way:

$$J_H[\mathbf{t}, \mathbf{s}, \mathbf{\Theta}] = \frac{1}{2}\mathbf{s}^\dagger \Delta \mathbf{t} + \frac{1}{2}\mathbf{s}^\dagger \mathbf{W}(\sigma) + \frac{1}{2}\mathbf{t}^\dagger \mathbf{V} + \text{h.c.} \tag{2.56}$$

where $\mathbf{W}(\sigma)$ is the damped integral defined in Eq. (2.38). The modified Hylleraas functional is now a functional of $\mathbf{t}$, $\mathbf{s}$, and $\mathbf{\Theta}$. Stationary conditions on $\mathbf{s}^\dagger$ and $\mathbf{t}^\dagger$ yields

$$\mathbf{s} = -\mathbf{\Delta}^{-1}\mathbf{V}, \tag{2.57}$$

$$\mathbf{t} = -\mathbf{\Delta}^{-1}\mathbf{W}. \tag{2.58}$$

Plugging Eq. (2.57) and Eq. (2.58) to Eq. leads to the following energy expression:

$$E_{\text{MP2}}(\sigma) = -\frac{1}{4}\sum_{ijab} \frac{|\langle ij||ab\rangle|^2}{\Delta_{ij}^{ab}} \left(1 - e^{-\sigma\Delta_{ij}^{ab}}\right), \tag{2.59}$$

which is the σ^1-OOMP2 energy expression. Unlike Eq. (2.41), Eq. (2.59) has non-zero contributions from small Δ_{ij}^{ab} as the limit yields $-\sigma|\langle ij||ab\rangle|^2$. The orbital gradient is more or less the same as that of κ^1-OOMP2. σ^1-OOMP2 can also be implemented with a moderate increase in the computational cost.

2.3 Computational Details

All the calculations presented below are carried out by the development version of Q-Chem. [236] The self-consistent field calculations are based on Q-Chem's new

object-oriented SCF library, `libgscf` and the relevant MP2 components are implemented through Q-Chem's new MP2 library, `libgmbpt`. All those implementations are already at the production level and OpenMP parallelized. All the correlated wave function calculations presented here were performed with all electrons correlated and all virtual orbitals included unless specified otherwise.

The quadrature evaluation in Eq. (2.47) was performed using the standard Gauss-Legendre quadrature. The accuracy of the quadrature for a given quadrature order depends on the orbital energies and thus it is system-dependent. For systems presented below, 20 quadrature points were found to be sufficient. The precise assessment of the accuracy of the quadrature will be an interesting subject for the future study.

2.4 Results and Discussion

For the sake of simplicity, we will refer κ^1 and σ^1-regularizers to as κ- and σ-regularizers, respectively.

2.4.1 ROOMP2 to UOOMP2 Stability Analysis

As noted before, we would like UOOMP2 to spontaneously spin-polarize to reach the proper dissociation limits. Without regularization, it is quite common to observe that UOOMP2 stays on an R solution and never spontaneously polarizes even though there is a more stable U solution that dissociates correctly. This may not be a serious problem if stability analysis can detect those more stable polarized solutions. However, in most cases, there exists a barrier between R and U solutions so that both solutions are stable up to the quadratic stability analysis.

We revisit and assess the new regularizers on the bond-breaking of H_2 (single-bond), C_2H_6 (single-bond), C_2H_4 (double-bond), and C_2H_2 (triple-bond). We present the results for unregularized, κ-, and σ- OOMP2. Interested readers are referred to ref. 203 for the δ-OOMP2 result. The main objective of this section is to find out whether there is a reasonably weak single parameter κ or σ that recovers the Coulson-Fischer points[213] (i.e. the geometries at which spontaneous, continuous symmetry breaking start to occur) for all four cases. All the results are obtained with the cc-pVDZ basis set [237] along with its auxiliary basis set. [238] The diagonalization of the R to U stability Hessian was performed iteratively with the Davidson solver [239] based on the finite difference matrix-vector product technique developed in ref. 212. This technique utilizes the analytic orbital gradient and does not require the implementation of the analytic orbital Hessian.

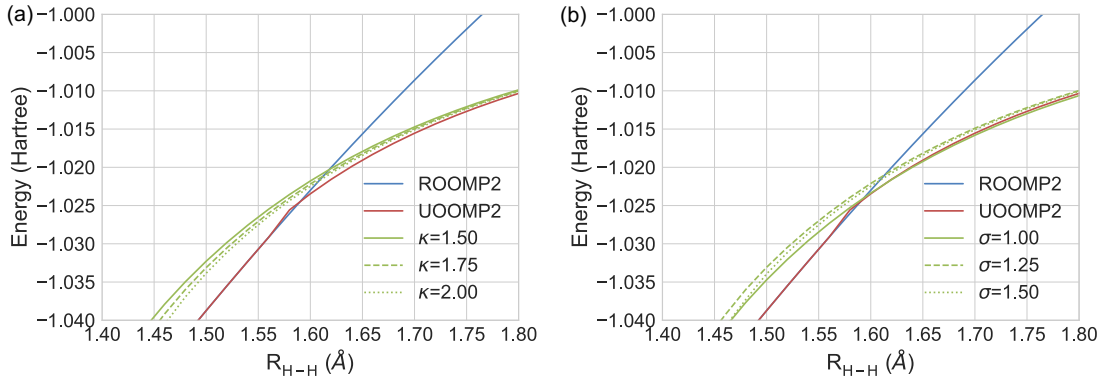

Figure 2.1: The potential energy curve of H_2 within the cc-pVDZ basis set. All the regularized OOMP2 are performed with spin-unrestriction. (a) κ-OOMP2 and (b) σ-OOMP2.

In Figure 2.1, we present the potential energy curve (PEC) of the H_2 dissociation. It is clear that there is a lower U solution starting from 1.6 Å and this is the solution that dissociates properly. However, there is a slight first-order discontinuity between 1.58 Å and 1.60 Å. This was previously noted by one of us in ref. 203. On the other hand, both κ- and σ-UOOMP2 exhibit smooth curves and dissociate properly. We picked the range of κ and σ based on the absolute energies that yield 1-2 mE_h higher than the unregularized one at the equilibrium geometry. The precise determination of those values will be discussed in the next section.

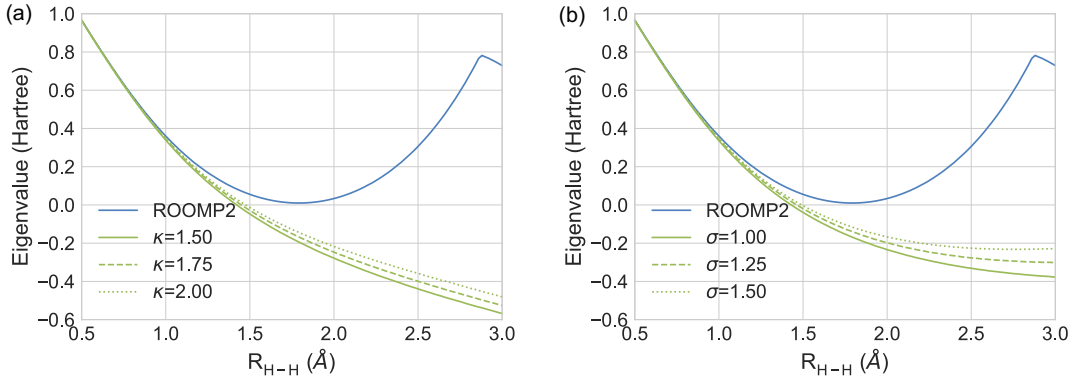

Figure 2.2: The R to U Hessian lowest eigenvalues of H_2 within the cc-pVDZ basis set. (a) κ-OOMP2 and (b) σ-OOMP2.

The continuous transition from R to U in regularized OOMP2 can be understood

based on the R to U Hessian lowest eigenvalues as illustrated in Figure 2.2. The unregularized ROOMP2 exhibits no R to U instability at every given bond distance. In other words, there is no solution that smoothly and barrierlessly connects this R solution to the lower U solution in UOOMP2. This is the source of the first-order discontinuity of ROOMP2 in Fig. 2.1. In contrast to the unregularized ROOMP2 result, both κ- and σ-ROOMP2 exhibit negative eigenvalues after the critical bond length around 1.5 Å. This results into a continuous and smooth transition from the R solution to the U solution as we stretch the bond.

We repeat this analysis for ethane, ethene, and ethyne. The corresponding R to U Hessian lowest eigenvalues are plotted in Figure. 2.3. ROOMP2 shows numerical instabilities in the case of ethene and ethyne whereas both of the regularized ones converge properly. In all cases, the κ and σ regularizers show clear differences. Namely, the σ regularizer shows clearly slower appearance of the negative roots compared to the κ case. Furthermore, the eigenvalue of the σ regularizer tends to turn around after some distance; this is not desirable as there can be a discontinuous transition between R and U solutions depending on where we start. Furthermore, the bond length, at which the Coulson-Fischer point is located, is longer in ethene than in ethyne in the case of σ-OOMP2. Given these results, we would prefer the κ regularizer over the σ regularizer. However, a more detailed assessment is necessary to make a general recommendation.

2.4.2 Training the Regularization Parameter and Its Validation

The W4-11 set

Though the investigation of the stability Hessian eigenvalues was informative, it is not sufficient to suggest a value for the regularization parameter to be used for general chemical applications. Training the regularization parameter on a minimal training set and validating on other test sets will provide a sensible preliminary value.

We chose the W4-11 set developed by Martin and co-workers for the training set. [222] The W4-11 set has played a crucial role in density functional development. The W4-11 set consists of the following subsets: 140 total atomization energies (TAE140), 99 bond dissociation energies (BDE99), 707 heavy-atom transfer (HAT707), 20 isomerization (ISOMER20), and 13 nucleophilic substitution reaction (SN13). MP2 and OOMP2 do not perform very well on this set (i.e. root-mean-square-deviation (RMSD) of 15.10 kcal/mol and 11.08 kcal/mol within the aug-cc-pVTZ basis,[237] respectively). Therefore, it is sensible to choose it as a training set as an attempt to improve upon both MP2 and OOMP2.

The training was done within the aug-cc-pVTZ (aVTZ) basis set [237] along with the corresponding auxiliary basis set.[238] All the calculations are performed with the geometric direct minimization (GDM) algorithm [240] and a stable UHF solution. OO methods used a stable UHF solution as a guess. We also performed additional training at the complete basis set (CBS) limit using the aVTZ and aug-cc-pVQZ (aVQZ) [237] extrapolation (i.e. the TQ extrapolation). [241]

Initially, we optimized only one non-linear parameter (κ or σ) by scanning over [0.05, 4.0]. The optimal values were $\kappa = 1.45$ with the RMSD of 7.09 kcal/mol and $\sigma = 1.00$ with the RMSD of 6.72 kcal/mol as shown in Fig. 2.4 (a). The optimal values change slightly for the TQ extrapolated results as in Fig. 2.4 (b). We have $\kappa = 1.40$ and $\sigma = 0.95$ with the RMSD of 7.80 kcal/mol and 7.28 kcal/mol, respectively. These values are also enough to restore the Coulson-Fischer points in the systems studied before. We recommend those values for general applications.

We also developed a scaled correlation energy variant by adding a linear parameter that scales the overall correlation energy to improve the thermochemistry performance. This is achieved by optimizing a linear parameter c in

$$E_{tot} = E_{HF} + cE_{MP2} \tag{2.60}$$

in addition to the non-linear parameter (κ or σ) for the regularizer. c can be optimized by a means of least-squares-fit. Since changing c alters orbitals, one needs to accomplish self-consistency when optimizing c. We found three self-consistency cycles enough to converge c and present only the final result. For preliminary results, we simply trained this over the TAE-140 set where unregularized OOMP2 performs much worse (an RMSD of 17.48 kcal/mol) than it does in the other subsets of the W4-11 set.

In Figure 2.5, we present the RMSD values of the TAE140 set and the entire W4-11 set as a function of the regularization strength. All the RMSD values are obtained with the scaling factor optimized for the TAE-140 set. In Figure 2.5 (a), we have optimal values of $\kappa = 2.80$ and $\sigma = 2.05$. These values are not enough to restore the Coulson-Fischer points. Validating those values over the entire W4-11 set as in Figure 2.5 (b) shows that those values are not optimal on the entire W4-11 set. The optimal values are $\kappa = 2.25$ and $\sigma = 1.70$ and those are not enough to restore the Coulson-Fischer points.

For general applications, we recommend the values of $\kappa = 1.50$ along with $c = 0.955$ and $\sigma = 1.00$ along with $c = 0.973$. Both yield the RMSD of 6.48 kcal/mol over the entire W4-11 set. We refer each model to as κ-S-OOMP2 and σ-S-OOMP2, respectively. Although the scaling factor is not optimal anymore, those values are still an improvement over their unscaled variants on the W4-11 set. The values are slightly smaller than 1.00 because orbital optimization can often overcorrelate.

	MP2	SCS-MP2	SOS-MP2	OOMP2	SCS-OOMP2	SOS-OOMP2
RMSD	15.10	14.76	15.07	11.08	7.58	5.28
MAD	10.54	10.01	10.30	7.88	5.20	3.81
MAX-MIN	117.44	113.63	117.39	97.05	67.63	51.50

	κ-OOMP2	σ-OOMP2	S-OOMP2	κ-S-OOMP2	σ-S-OOMP2
RMSD	7.09	6.72	6.36	6.48	6.48
MAD	5.03	4.83	4.65	4.75	4.77
MAX-MIN	56.47	53.51	46.91	52.97	52.34

Table 2.1: The W4-11 set RMSD (kcal/mol) of MP2, OOMP2, and their variants. MAD stands for Mean Absolute Deviation and MAX-MIN stands for the difference between maximum and minimum. The colors represent the relative performance of each method; red means the worst and green means the best among the methods presented. For SOS-MP2 and SOS-OOMP2, the Laplace transformation trick is used. All the calculations were performed with the aVTZ basis set.

The TQ extrapolated results are qualitatively similar and we only mention the final results here. We have $\kappa = 1.50$ along with $c = 0.931$ with the RMSD of 6.61 kcal/mol and $\sigma = 1.00$ along with $c = 0.949$ with the RMSD of 6.63 kcal/mol. These are more or less identical results to those of aVTZ with a smaller scaling factor c. Therefore, for the rest of this paper, we will use parameters optimized for the aVTZ basis set.

We summarize the resulting regularized OOMP2 methods in Table 2.1 along with MP2, OOMP2 and other variants of them. All of them were performed with the aVTZ basis set. In particular, we compare the regularized OOMP2 methods with SCS-[170] and SOS-MP2 [171] and their OOMP2 variants.[176, 177] For SCS-MP2 and SCS-OOMP2, $c_{ss} = 1/3$ and $c_{os} = 6/5$ are used.[170, 177] $c_{os} = 1.3$ is used for SOS-MP2[171]and $c_{os} = 1.2$ is used for SOS-OOMP2.[176] For comparison, we developed a single scaling parameter OOMP2 (S-OOMP2) where the parameter was fitted to the TAE140 set. The optimal scaling parameter is $c = 0.90$.

In Table 2.1, MP2 performs the worst among the methods examined in this work and SCS-MP2 and SOS-MP2 provide only a small improvement over MP2. OOMP2 improves about 4 kcal/mol in the RMSD compared to MP2. SCS-OOMP2 shows roughly a factor of 2 improvement over SCS-MP2. SOS-OOMP2 performs the best among the methods presented and shows a 2.5 times smaller RMSD than that of SOS-MP2. RMSD, MAD, and MAX-MIN show the same trend.

The unscaled regularized OOMP2 methods, κ-OOMP2 and σ-OOMP2, both provide improved energetics compared to the unregularized one. They are comparable to SCS-OOMP2 and SOS-OOMP2. However, it should be noted that the regularization parameters are optimized for the W4-11 set. It is not so surprising that κ-OOMP2

and σ-OOMP2 perform relatively well.

S-OOMP2 performs better than those unscaled regularized OOMP2. Given that S-OOMP2 was trained over only the TAE140 set, this is an interesting outcome. Adding regularizers to S-OOMP2 provides no improvement and it makes the performance little worse. However, the regularization is necessary to restore the Coulson-Fischer points for molecules studied in the previous section. We also note that κ-S-OOMP2 and σ-S-OOMP2 exhibit a more or less identical performance in terms of RMSD, MAD, and MAX-MIN.

The RSE43 set

We also validate the regularized OOMP2 methods on the RSE43 set [224] where unregularized OOMP2 performs nearly perfectly.[177] The RSE43 has total 43 radical stabilization energies and all of them are energies of a reaction where a methyl radical abstracts a hydrogen from a hydrocarbon. The original RSE43 set reference values were not considered of very high quality[224] and thus we use the updated reference data based on the work by Grimme and co-workers.[223]

We compare MP2, OOMP2, their variants, and three combinatorially designed density functionals (ωB97X-V, ωB97M-V, and B97M-V) developed in our group. ωB97X-V is a range-separated generalized gradient approximation (GGA) hybrid functional with the VV10 dispersion tail and ωB97M-V is a range-separated meta GGA with the VV10 dispersion tail. B97M-V is a meta GGA pure functional with the VV10 dispersion tail. All DFT calculations are performed with the aVQZ basis set [237] and all the MP2 and OOMP2 calculations are done with the aVTZ basis set.[237] MP2 calculations are performed with a stable UHF solution and OOMP2 calculations started from a stable UHF solution.

The RSE43 set RMSD values are presented in Table 2.2. DFT functionals outperform MP2, SCS-MP2, and SOS-MP2. The poor quality of those MP2 methods is likely because of the artificial spin symmetry breaking at the HF level. DFT functionals are in general less prone to the artificial spin symmetry breaking problem. ωB97X-V and ωB97M-V exhibit nearly identical results and B97M-V is roughly twice worse than those two in terms of RMSD, MAD, and MAX-MIN.

Orbital optimization generally improves the energetics here. SOS-OOMP2 does not outperform OOMP2 and SCS-OOMP2 in this case. S-OOMP2 is comparable to OOMP2 and SCS-OOMP2. κ-OOMP2 and σ-OOMP2 along with their scaled variants are comparable to the unregularized ones. Adding linear parameters on top of those to scale the MP2 correlation energy does not alter the results significantly. Since the regularization damps out the absolute MP2 energy quite significantly, this is a non-trivial and exciting result.

	ωB97X-V	ωB97M-V	B97M-V	MP2	SCS-MP2	SOS-MP2
RMSD	1.10	0.93	2.44	4.51	5.05	5.34
MAD	0.44	0.44	0.95	2.41	2.56	2.64
MAX-MIN	2.53	2.75	5.81	17.32	19.14	20.08

	OOMP2	SCS-OOMP2	SOS-OOMP2	κ-OOMP2	σ-OOMP2	S-OOMP2	κ-S-OOMP2	σ-S-OOMP2
RMSD	0.58	0.80	1.50	0.88	0.87	0.62	0.97	0.94
MAD	0.45	0.30	0.52	0.43	0.41	0.35	0.42	0.40
MAX-MIN	2.56	1.38	3.07	1.87	1.69	1.69	1.96	1.81

Table 2.2: The RSE43 set RMSD (kcal/mol) of ωB97X-V, ωB97M-V, and B97M-V, MP2, OOMP2, and their variants. MAD stands for Mean Absolute Deviation and MAX-MIN stands for the difference between maximum and minimum. The colors represent the relative performance of each method; red means the worst and green means the best among the methods presented.

The TA13 set

We further test our new methods on the TA13 set.[225] This dataset involves 13 radical-closed-shell non-bonded interaction energies. We used the aVTZ basis set [237] and counterpoise corrections to mitigate basis set superposition error (BSSE). Examining spin-contamination, one data point, CO^+, was found to be an outlier. The UHF $\langle S^2 \rangle$ for CO^+ is 0.98, which deviates significantly from its ideal value of 0.75. With OOMP2, the zeroth order $\langle S^2 \rangle$ is 0.76, which is quite close to the ideal value. The same is observed in the case of regularized OOMP2.

In Table 2.3, we present the interaction energy errors for each data point of MP2, OOMP2, and their variants. Going from MP2 to OOMP2, there are several noticeable changes. The problematic HF$-CO^+$ interaction is handled much better with OO. Another problematic case in MP2 is the H_2O-F interaction and this is also improved with OO. Overall, without OO, SCS-MP2 and SOS-MP2 are not any better than MP2. Comparing SCS- and SOS-OOMP2 with OOMP2, scaling does not help improve the energetics of OOMP2 and in fact tends to make it worse. κ- and σ-OOMP2 perform more or less the same, as do their scaled variants. Regularization keeps the performance of OOMP2 unchanged. The regularized ones perform better than simple scaled OOMP2 methods (i.e. SCS-OOMP2, SOS-OOMP2, and S-OOMP2). It is interesting that the one-parameter model, S-OOMP2, performs better than the more widely used two-parameter models, SCS-OOMP2 and SOS-OOMP2.

In Table 2.4, we present the statistical errors of MP2, OOMP2, and their variants on the TA13 set. OOMP2 performs the best among the methods presented here. We note that ωB97M-V has an RMSD of 2.75 kcal/mol, [242] a little worse than OOMP2.

Complexes	MP2	SCS-MP2	SOS-MP2	OO-MP2	SCS-OO-MP2	SOS-OO-MP2	κ-OO-MP2	σ-OO-MP2	S-OO-MP2	κ-S-OO-MP2	σ-S-OO-MP2
H_2O-Al	1.42	2.77	3.45	0.76	2.18	3.00	1.00	1.06	1.13	1.13	1.15
H_2O-Be^+	2.38	2.84	3.08	2.67	3.09	3.09	1.84	1.71	2.45	1.85	1.68
H_2O-Br	1.11	2.01	2.45	0.23	1.39	2.22	0.95	1.03	0.79	1.11	1.15
HOH-CH_3	0.14	0.49	0.66	-0.01	0.39	0.67	0.08	0.12	0.16	0.14	0.16
H_2O-Cl	1.32	2.20	2.64	0.13	1.37	2.26	0.94	1.03	0.77	1.11	1.16
H_2O-F	4.25	5.33	5.87	-1.10	1.75	3.84	0.50	0.79	0.86	1.10	1.21
H_2O-Li	1.58	2.10	2.36	1.20	1.92	2.27	1.32	1.28	1.35	1.38	1.32
H_2O-HNH_2^+	-0.80	0.12	0.58	-0.73	0.21	0.71	-1.18	-1.18	-0.55	-1.05	-1.12
H_2O-NH_3^+	1.43	2.22	2.62	0.06	1.18	2.04	0.43	0.54	0.71	0.66	0.69
FH-BH_2	0.14	0.51	0.70	-0.04	0.39	0.69	0.00	0.04	0.15	0.08	0.09
HF-CO^+	-5.07	-5.22	-5.30	0.96	2.08	2.83	0.35	0.48	1.44	0.64	0.64
FH-NH_2	-0.13	0.62	1.00	-0.25	0.56	0.98	-0.54	-0.53	-0.09	-0.44	-0.48
FH-OH	0.27	0.76	1.00	0.16	0.69	0.98	0.01	0.02	0.28	0.08	0.05

Table 2.3: The counterpoise corrected interaction energy errors (kcal/mol) of MP2, OOMP2, and their variants in the 13 data points in TA13.

	MP2	SCS-MP2	SOS-MP2	OOMP2	SCS-OOMP2	SOS-OOMP2
RMSD	2.14	2.65	2.94	0.96	1.56	2.22
MAD	1.41	1.61	1.71	0.67	0.70	0.89
MSE	0.62	1.29	1.62	0.31	1.32	1.97
MAX-MIN	9.32	10.55	11.17	3.77	2.88	3.18

	κ-OOMP2	σ-OOMP2	S-OOMP2	κ-S-OOMP2	σ-S-OOMP2
RMSD	0.88	0.91	1.04	0.98	0.98
MAD	0.60	0.62	0.57	0.64	0.66
MSE	0.44	0.49	0.73	0.60	0.59
MAX-MIN	3.02	2.89	3.00	2.90	2.80

Table 2.4: The TA13 set RMSD (kcal/mol) of MP2, OOMP2, and their variants. MAD stands for Mean Absolute Deviation, MSE stands for Mean Signed Error, MAX-MIN stands for the difference between maximum and minimum. The colors represent the relative performance of each method; red means the worst and green means the best among the methods presented.

OOMP2, SCS-OOMP2, and SOS-OOMP2 all improved the numerical performance compared to their parent methods. Regularized OOMP2 methods perform very well and unscaled ones perform better than the scaled ones. We also presented mean signed errors (MSEs) which are often used to infer a potential bias in statistical data. The MSEs are all positive in Table 2.4 and would be smaller if we performed a TQ extrapolation along with counterpoise corrections.[243] In summary, we found that regularization does not damage the performance of OOMP2 in describing non-bonded interactions in the TA13 set. Overall, κ-OOMP2 performs the best in the TA13 set among those tested.

2.4.3 Application to Organic Singlet Biradicaloids

Organic biradicaloids are not very common to observe experimentally because they are quite unstable. Indeed, a molecule with a singlet biradical ground state is typically a contradiction. A singlet biradicaloid is the ground state due to the presence of some closed shell character.[244] They may appear in numerous interesting chemical reactions as a transition state.[245] In this section, we will study two experimentally observed organic singlet biradicaloids.[226, 227]

One may attempt to use Yamaguchi's approximate spin-projected UMP2 (AP-UMP2) approach [246, 247] to spin-project the broken-symmetry (BS) $M_S = 0$ UMP2 state to obtain the spin-pure energy of the $S = 0$ state. Assuming we have only singlet and triplet states that contribute to the $M_S = 0$ state, one can easily

work out the spin-pure singlet energy based on $\langle S^2 \rangle$:

$$E_{S=0} = \frac{E_{\mathrm{BS}} - (1-\alpha)E_{S=1}}{\alpha} \tag{2.61}$$

where

$$\alpha = \frac{\langle S^2 \rangle_{S=1} - \langle S^2 \rangle_{\mathrm{BS}}}{\langle S^2 \rangle_{S=1} - \langle S^2 \rangle_{S=0}} \tag{2.62}$$

The projection is exact only if there is only one spin-contaminant (i.e. the triplet state since we are interested in the singlet state). There are numerous ways to evaluate $E_{S=1}$ and $\langle S^2 \rangle_{S=1}$. We will choose the simplest way which is to assume $E_{S=1} \approx E_{M_S=1}$ and replace $\langle S^2 \rangle_{S=1}$ with $\langle S^2 \rangle_{M_S=1}$. This requires $M_S = 1$ calculations in addition to $M_S = 0$ calculations. For this reason UMP2 cannot be reliably applied to the singlet state ($S = 0$) as the $M_S = 0$ UHF state is often massively spin-contaminated. The core orbitals are assumed to be more or less the same between $M_S = 0$ and $M_S = 1$.

In passing, we note that more satisfying AP-UMP2 results may be obtained via the approach by Malrieu and co-workers which makes these assumptions exact in the case of biradicaloids.[248–250] This is achieved by allowing unrestriction only within the two electrons in two orbitals (2e,2o) active space with a possibility of using restricted open-shell formalism. Furthermore, a common set of core orbitals is used for the BS state and the $S = 1$ state. Our group explored a similar approach called unrestricted in active pairs[251] which can be combined with the AP formula to produce a spin-pure energy.

It is common to observe $\langle S^2 \rangle_{\mathrm{BS}} >> 1$ with a stable $M_S = 0$ UHF solution of biradicaloids and thus it can be dangerous to apply the spin-projection. Moreover, the $M_S = 1$ state tends to be also spin-contaminated in biradicaloids. As a solution to this problem, one may try to use UOOMP2 to obtain minimally spin-contaminated $M_S = 0, 1$ states. This is not always possible due to the inherent numerical instability of UOOMP2 that commonly arises when applied to strongly correlated systems like biradicaloids. Indeed, for the biradicaloids studied here, we were not able to obtain the UOOMP2 energies due to this instability.

It is then natural to use regularized UOOMP2 to obtain the $M_S = 0, 1$ states of those systems. With the regularizers developed in this work, we do no longer run into the numerical instability. Therefore, the combination of regularized UOOMP2 and Yamaguchi's spin projection is quite attractive for simulating the electronic structure of biradicaloids. We note that AP-UOOMP2 is formally extensive as long as biradicaloism is not exceeded (i.e. spin-contamination is limited to a two-electron manifold).

In passing, we note that the first order correction to $\langle S^2 \rangle$ for regularized OOMP2 can be obtained in the same way as the usual MP2 method.[176] The only difference

M_S	κ-OOMP2	σ-OOMP2	κ-S-OOMP2	σ-S-OOMP2
0	0.00 (1.211)	0.00 (1.145)	0.00 (1.238)	0.00 (1.173)
1	1.95 (2.117)	1.62 (2.091)	2.07 (2.129)	1.74 (2.104)
2	46.07 (6.115)	45.23 (6.091)	45.99 (6.126)	45.26 (6.104)

Table 2.5: Spin-gaps (kcal/mol) of HZD from regularized UOOMP2 methods developed in this work. The numbers in parentheses are the corresponding $\langle S^2 \rangle$ value.

for κ-OOMP2 is that we use regularized amplitudes instead of the unmodified ones. In the case of σ-OOMP2, we get a half contribution from the regularized ones and another half from the unregularized ones. This is obvious from the form of the modified TPDMs in each regularized OOMP2.

Heptazethrene Dimer (HZD)

Oligozetherens have been experimentally synthesized and characterized as stable singlet biradicaloids. [160] Similar to oligoacenes, they exhibit a polyradicaloid character in the background along with a strong biradicaloid character. There have been experimental interests in synthesizing tetraradicaloids using heptazethrenes. In particular, the experimental and theoretical work by Wu and co-workers has drawn our attention where they successfully synthesized heptazetherene dimer (HZD) as an attempt to synthesize a stable singlet tetraradicaloid. [226] Using unrestricted CAM-B3LYP [252] density functional calculations, they characterized a strong biradicaloid character along with a very small tetraradicaloid character. They conclude that this compound should be better described as a biradicaloid and our work here also confirms this conclusion as we shall see.

The geometry was taken from ref. 226 and shown in Fig. 2.6. We used the cc-pVDZ basis set [237] and the corresponding auxiliary basis set.[238] Furthermore, the frozen core approximation was employed to reduce the computational cost.

In Table 2.5, we present the spin gaps and $\langle S^2 \rangle$ of HZD using regularized UOOMP2 methods developed in this work. The gap between the $M_S = 0$ and $M_S = 1$ states is very small. Furthermore, the $M_S = 0$ state is heavily spin contaminated. This is a signature of biradicaloids. The $\langle S^2 \rangle$ values of the $M_S = 1, 2$ states are relatively close to the corresponding spin-pure states. There is also roughly a gap of 45 kcal/mol between the triplet and the quintet state and this supports that HZD is not a tetraradicaloid and better described as a biradicaloid. Given those observations, this system is well suited for Yamaguchi's AP. Applying AP will yield a lower singlet state than the $M_S = 0$ state and thus provide a larger singlet-triplet gap.

	κ-OOMP2	σ-OOMP2	κ-S-OOMP2	σ-S-OOMP2
α	0.428	0.452	0.418	0.442
ΔE_{S-T}	4.55	3.59	4.96	3.95

Table 2.6: The spin-projected single-triplet gap ΔE_{S-T} (kcal/mol) of HZD from regularized AP-UOOMP2 methods. α is the spin-projection coefficient used to obtain the projected energy in Eq. (2.61).

In Table 2.6, the spin-projection coefficient α and the resulting spin-projected singlet-triplet gap are presented. Different methods exhibit a different magnitude of α and ΔE_{S-T} and the range of ΔE_{S-T} is from 3.59 kcal/mol to 4.96 kcal/mol which is roughly a 1.4 kcal/mol variation. We also note that there is a roughly 1 kcal/mol difference between κ and σ regularizers in both unscaled and scaled variants. The scaled variants have a 0.5 kcal/mol larger ΔE_{S-T} compared to their corresponding unscaled variants. Regardless of which regularized OOMP2 we use, ΔE_{S-T} is small enough that this molecule is undoubtedly a biradicaloid. The extent of biradicaloid character can be inferred from the value of α in Table 2.6. $\alpha = 0.5$ is the perfect biradical limit and HZD shows $\alpha = 0.40 - 0.45$. This suggests that the stability of HZD may be attributed to some closed-shell configuration contribution.

Pentaarylbiimidazole (PABI) complex

Recently, Miyasaka, Abe, and co-workers studied a photochromic radical dimer, pentaarylbiimidazole (PABI) by a means of ultrafast spectroscopy. [227] Without any external perturbations, PABI stays as its closed conformer shown in Fig. 2.7 (a). This stable conformation is closed-shell and does not exhibit any biradicaloid characters. Once a laser field is applied, the closed conformation undergoes a transition to its excited state and a subsequent relaxation back to the ground state surface. During this dynamics, the C-N bond in the middle in Fig. 2.7 (a) gets dissociated, which results in two possible conformers, open 1 and open 2, depicted in Fig. 2.7 (b) and (c), respectively. These two conformers were computationally shown [227] to exhibit quite strong biradicaloid characters, which drew our attention.

As understanding the dynamics in the system requires a reliable method for treating excited states and strongly correlated ground state, Miyasaka, Abe, and co-workers applied extended multi-state complete active space second-order perturbation theory (XMS-CASPT2). [253] Here we will compare AP-UOOMP2 ground state results against XMS-CASPT2 (4e, 6o).

All the geometries are obtained from ref. 227 and we used def2-SVP [254] and the corresponding density-fitting basis [255] for the study of this molecule. The frozen

$\langle S^2 \rangle$	κ-OOMP2	σ-OOMP2	κ-S-OOMP2	σ-S-OOMP2
open 1 ($M_S = 0$)	0.918	0.897	0.929	0.911
open 1 ($M_S = 1$)	2.026	2.023	2.030	2.026
open 2 ($M_S = 0$)	0.906	0.880	0.918	0.896
open 2 ($M_S = 1$)	2.027	2.023	2.031	2.027

Table 2.7: The $\langle S^2 \rangle$ values of regularized UOOMP2 methods.

core approximation was employed.

The closed conformation exhibits $\langle S^2 \rangle_0 = 3.31$ at the $M_S = 0$ UHF level which is attributed to artificial symmetry breaking. To support this, we ran κ-S-OOMP2 and σ-S-OOMP2 with κ and σ ranging from 0.05 to 4.0. The scaling factors for each κ and σ are the optimal values which yielded Fig. 2.5. The κ values greater than 0.2 and all values of σ were enough to restore the restricted spin symmetry. This strongly suggests that the closed conformation is a closed-shell molecule with no strong correlation.

The open 1 and open 2 conformations are heavily spin-contaminated at the $M_S = 0$ UHF level as they have $\langle S^2 \rangle_0 = 4.41$ and $\langle S^2 \rangle_0 = 4.47$, respectively. These two cases are particularly interesting because if the regularization strength is too weak then it fully restores the spin-symmetry and yields a closed-shell solution. κ-S-OOMP2 requires κ less than 3.8 for open 1 and κ less than 3.5 to observe spin-symmetry breaking. At $\kappa = 1.5$ (recommended value), each conformer has $\langle S^2 \rangle = 0.929$ and $\langle S^2 \rangle = 0.918$, respectively. This supports the conclusion that both open 1 and open 2 are biradicaloids as pointed in ref.227. A similar result was found for σ-S-OOMP2 as well.

In Table 2.7, we present the $\langle S^2 \rangle$ values of the $M_S = 0, 1$ states of open 1 and open 2. Different flavors of regularized OOMP2 do not deviate significantly from each other. The $M_S = 1$ states are all almost spin-pure whereas the $M_S = 0$ states are spin-contaminated. As the $\langle S^2 \rangle$ values of the $M_S = 0$ states are close to 1.0, those states exhibit significant biradicaloid character. Therefore, these two systems are perfect candidates for the Yamaguchi's AP scheme.

Applying the AP scheme to spin-purify the spin-contaminated $M_S = 0$ energies of open 1 and open 2 leads to the various OOMP2 relative energies shown in Table 2.8. The results in Table 2.8 show almost no quantitative differences between different regularized OOMP2 methods. It is interesting that the system is quite insensitive to what flavor of OOMP2 we use. Compared to XMS-CASPT2, the relative energies of regularized OOMP2 for open 1 and open 2 are roughly 5 kcal/mol higher. The relative energies between open 1 and open 2 are reproduced by every regularized

	XMS-CASPT2[1]	κ-OOMP2	σ-OOMP2	κ-S-OOMP2	σ-S-OOMP2
closed	0	0	0	0	0
open 1	32.03	37.13	36.52	36.21	35.97
open 2	33.57	38.79	38.11	37.78	37.50

Table 2.8: The relative energies (kcal/mol) of the three conformers of PABI from XMS-CASPT2 and regularized AP-UOOMP2 methods. [1] The XMS-CASPT2 numbers were taken from ref. 227 and the active space used was (4e, 6o).

OOMP2 presented: open 2 is about 1.5 kcal/mol higher than open 1. While the regularized OOMP2 methods agree with XMS-CASPT2 on a very small relative energy scale between open 1 and open 2, they differ significantly from XMS-CASPT2 for the relative energy between closed and open conformations. It is unclear whether this small active space XMS-CASPT2 is a reliable method for this problem just as it is unclear that regularized OOMP2 is quantitatively accurate. This is an interesting system to further study using a recently developed couple-cluster method in our group that can handle a much larger active space. [142]

In summary, we applied the regularized OOMP2 methods developed in this work to obtain relative energies of three conformations of PABI. Two of the three conformations were found to be strong biradicaloids which agree well with what was found with the XMS-CASPT2 study before. We also found that the different regularized OOMP2 methods do not differ significantly from each other.

2.5 Conclusions

Orbital-optimized second order Møller-Plesset perturbation theory (OOMP2) is an inexpensive approach to obtaining approximate Brückner orbitals, and thereby cutting the umbilical cord between MP2 and mean-field Hartree-Fock (HF) orbitals. This has demonstrated benefits for radicals and systems where HF exhibits artificial symmetry-breaking. [176] However the limited MP2 correlation treatment can introduce artifacts of its own, because the MP2 correlation energy diverges as the HOMO-LUMO gap approaches zero. One striking example is that restricted and unrestricted orbital solutions are each local minima for molecules with stretched bond-lengths – in other words there is no Coulson-Fischer point [212, 213] where the restricted orbital solution becomes unstable to spin polarization! It has been previously recognized that some type of regularization is necessary to avoid such divergences. Simple level shifts have been explored,[199] but are inadequate in general

because the size of the level shift needed to ensure a Coulson-Fischer point in general is so large that the MP2 correlation effects are grossly attenuated.[203]

In this work we have therefore developed and assessed two new regularization approaches, called κ-OOMP2 and σ-OOMP2, which both have the feature that the strength of regularization is largest as the HOMO-LUMO gap approaches zero, and becomes zero as the gap becomes large. This way the total correlation energy is not greatly attenuated even with quite strong regularization. The regularization strength in each case is controlled by a single parameter (i.e. κ and σ) which has units of inverse energy so that small values correspond to strong regularization. Despite the greater complexity of these regularizers relative to a simple level shift, they can be quite efficiently implemented in conjunction with orbital optimization, at a cost that is not significantly increased relative to unmodified OOMP2. These models can be used with just the single parameter, or, alternatively, an additional parameter corresponding to scaling the total correlation energy (i.e. S-OOMP2) can be included as well.

The main conclusions from the numerical tests and assessment of the regularizers are as follows:

1. *Regularization.* We assessed the performance of the new regularizers on single, double and triple bond-breaking problems, to determine the weakest regularizers that can properly restore the Coulson-Fischer (CF) points across these systems. The conclusion is very encouraging: a regularization parameter of $\kappa \leq 1.5\ E_{\mathrm{h}}^{-1}$ is capable of correctly restoring the CF points on all of these systems. For $\kappa = 1.5\ E_{\mathrm{h}}^{-1}$ regularization applied the ethane, ethene, ethyne series, the CF distance, r_{CF} is much shorter for the two latter systems as is appropriate for the physics of the method. The σ regularization is clearly less satisfactory in this regard, as $r_{\mathrm{CF}}(\mathrm{C_2H_2}) > r_{\mathrm{CF}}(\mathrm{C_2H_4})$ for the smallest $\sigma = 1.0\ E_{\mathrm{h}}^{-1}$ value considered, and the lowest eigenvalue of the stability matrix does not always show monotonic behavior as a function of bond-stretching displacements.

2. *Scaling.* We examined the performance of OOMP2 with and without regularizers, as well as with and without scaling (S) of the total correlation energy on two datasets representing thermochemical energy differences (W4-11) and radical stabilization energies (RSE43) and one dataset representing radical-closed-shell non-bonded interaction energies (TA13). The TAE140 subset of the W4-11 set was used to train scaling factors. The results show that unregularized OOMP2 over-emphasizes correlation effects, as the optimal scaling factor is only 0.9. By contrast, choosing a physically appropriate κ value of $1.45\ E_{\mathrm{h}}^{-1}$ is appropriate for use without scaling, by reducing the tendency of

orbital optimization to over-correlate through smaller energy gaps. A slight improvement in numerical results can be obtained with a scaled κ-S-OOMP2 method, using $\kappa = 1.5\ E_{\mathrm{h}}^{-1}$ and $c = 0.955$. Broadly similar conclusions hold for σ regularization. The regularized OOMP2 methods perform slightly better than OOMP2 for the TA13 set, and slightly worse for the RSE43 set.

3. *Chemical application to singlet biradicaloids.* We applied these regularized OOMP2 methods to two experimentally relevant organic biradicaloids, the heptazethrene dimer (HZD) and the pentaarylbiimidazole complex (PABI). We emphasize that unmodifed OOMP2 diverges for these systems and the regularization is necessary to obtain energies in a numerically stable way. We combined the regularized OOMP2 methods with Yamaguchi's approximate projection scheme to spin-purify $M_S = 0$ energies of the biradicaloids. We found that all four regularized OOMP2 methods developed in this work perform equally well.

4. *Recommendation.* Given the documented failures of OOMP2 for bond-breaking without regularization, and its related tendency to over-correlate, it cannot be recommended for general chemical applications despite its formal advantages. Fortunately, the $\kappa = 1.45\ E_{\mathrm{h}}^{-1}$ regularization introduced here appears to resolve all of these issues in a way that is as satisfactory as could be hoped for, given that MP2 itself is inherently incapable of solving strong correlation problems (i.e. spin-polarization should occur in such cases). We recommend κ-OOMP2 as a more robust replacement for OOMP2. We believe that it may also be valuable as a way of realizing well-behaved orbital optimized double hybrid density functionals[200, 204] in the future.

Beyond stabilizing the OOMP2 method, the new regularizers introduced in this work may also have other interesting and potentially useful applications in electronic structure theory. For example, they can be applied to Møller-Plesset theory without orbital optimization. At the MP2 level this will alter the relative energies of RMP2 and UMP2 in a way that raises the RMP2 energy when energy gaps are small, possibly avoiding artifacts that occur in that regime. It may also be interesting to explore the effect on higher order correlation energies, such as MP3 or MP4, or the triples correction to methods such as coupled cluster theory with singles and doubles, CCSD(T). Orbital optimization can also be performed with coupled cluster doubles (i.e. OO-CCD),[256] and for cases where electron correlation effects are strong, regularization may be also be useful to ensure the correct presence of Coulson-Fischer points. Likewise regularizers may be helpful to avoid non-variational failures of coupled cluster theory without orbital regularization. Of course, it is an open

question whether the forms we have presented here are appropriate for these non-MP2 applications or not.

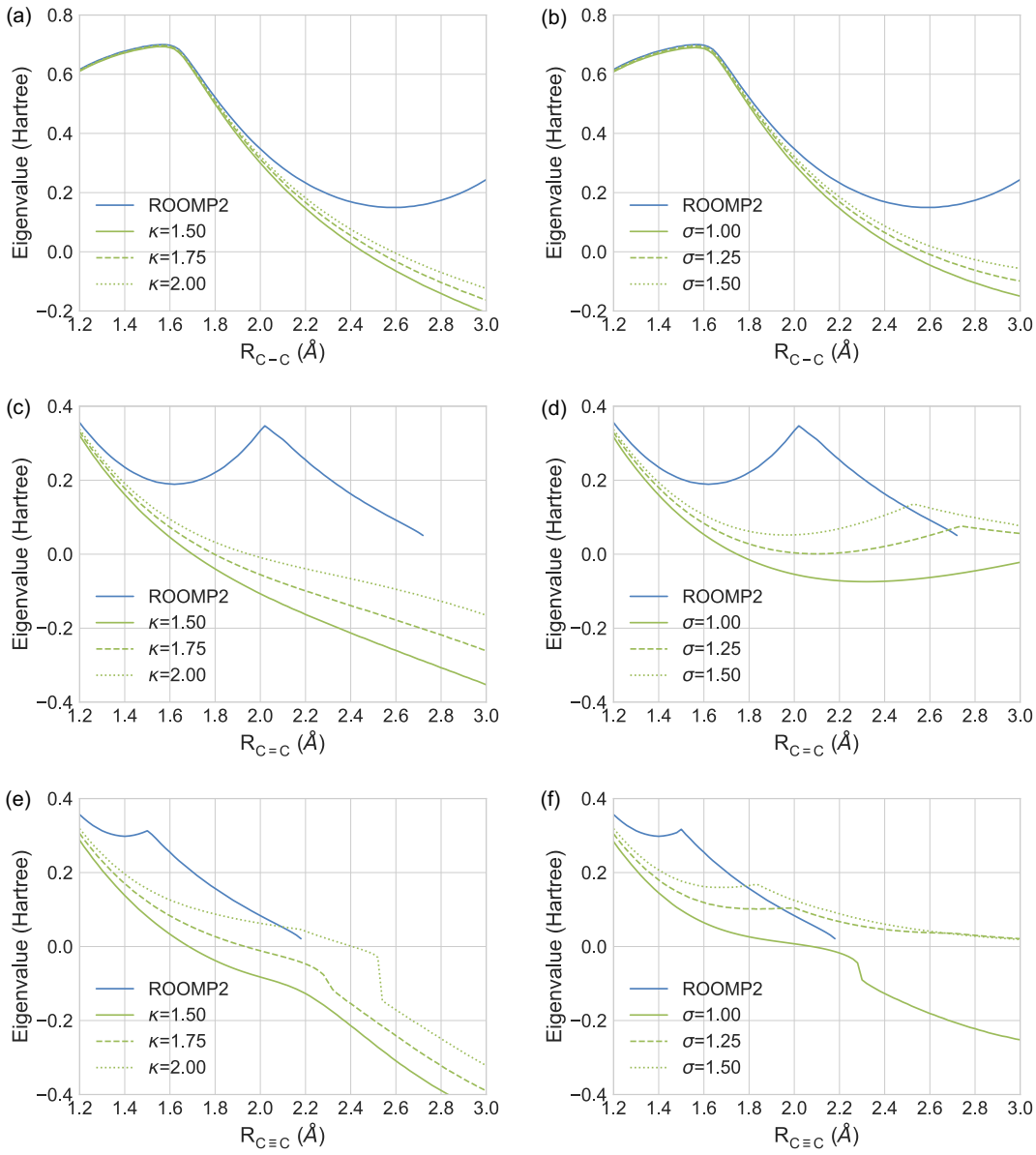

Figure 2.3: The R to U Hessian lowest eigenvalues of ethane, ethene and ethyne within the cc-pVDZ basis set. (a) Ethane with κ-ROOMP2. (b) Ethane with σ-ROOMP2. (c) Ethene with κ-ROOMP2. (d) Ethene with σ-ROOMP2. (e) Ethyne with κ-ROOMP2. (f) Ethyne with σ-ROOMP2. Note that discontinuities in the plots indicate discontinuous transitions in the corresponding ROOMP2 curves. ROOMP2 does not converge after 2.72 Å for ethene and 2.18 Å for ethyne.

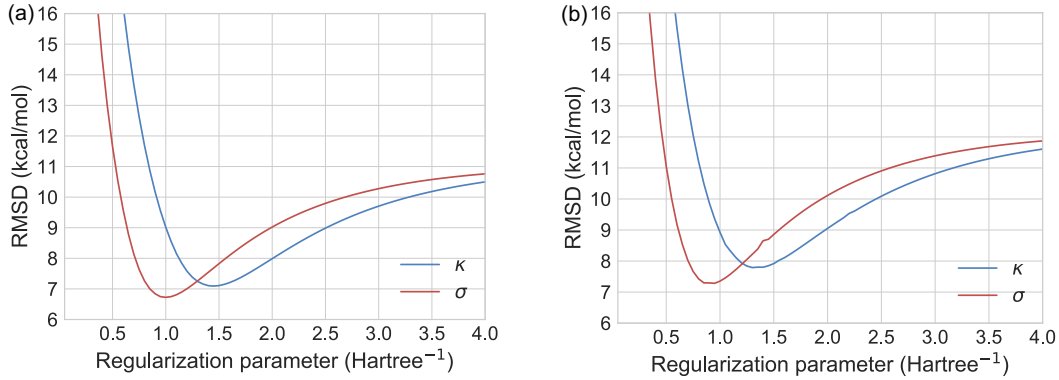

Figure 2.4: The W4-11 set RMSD (kcal/mol) as a function of regularization parameter κ and σ. (a) aVTZ and (b) TQ extrapolated results. The optimal values are κ =1.45 E_h^{-1} and $\sigma = 1.0\ E_h^{-1}$ for aVTZ and $\kappa = 1.40\ E_h^{-1}$ and $\sigma = 0.95\ E_h^{-1}$ for the TQ extrapolated case.

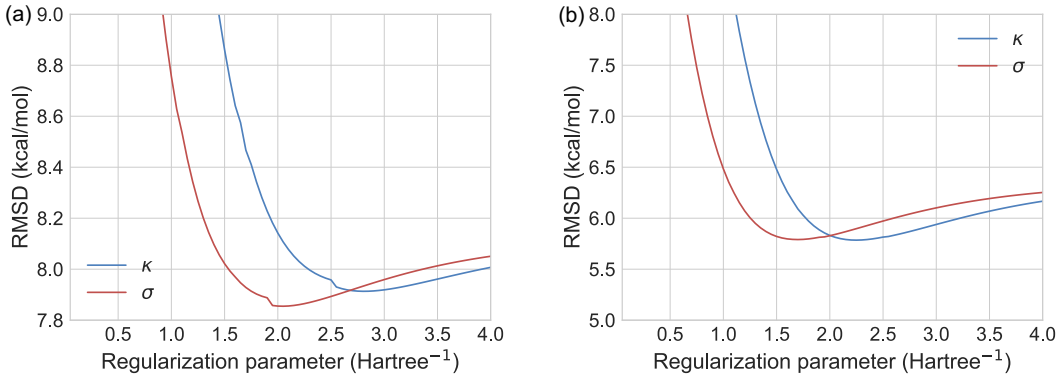

Figure 2.5: (a) The TAE140 set RMSD and (b) the W4-11 set RMSD as a function of regularization parameter κ and σ where the scaling parameter c for each data point is optimal within the TAE-140 set. Discontinuities are caused by the appearance of different orbital solutions in the MR16 subset of the TAE140 set. The basis set used was aVTZ.

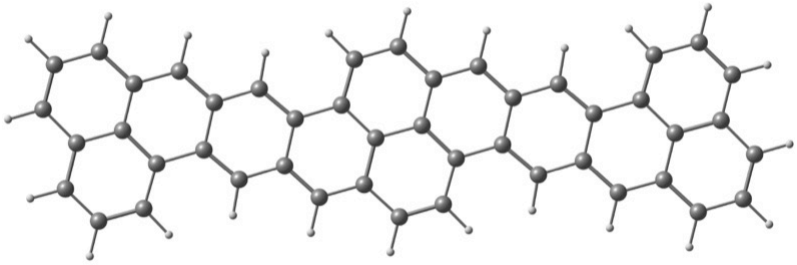

Figure 2.6: The molecular structure of heptazetherene dimer (HZD). White: H and Grey: C

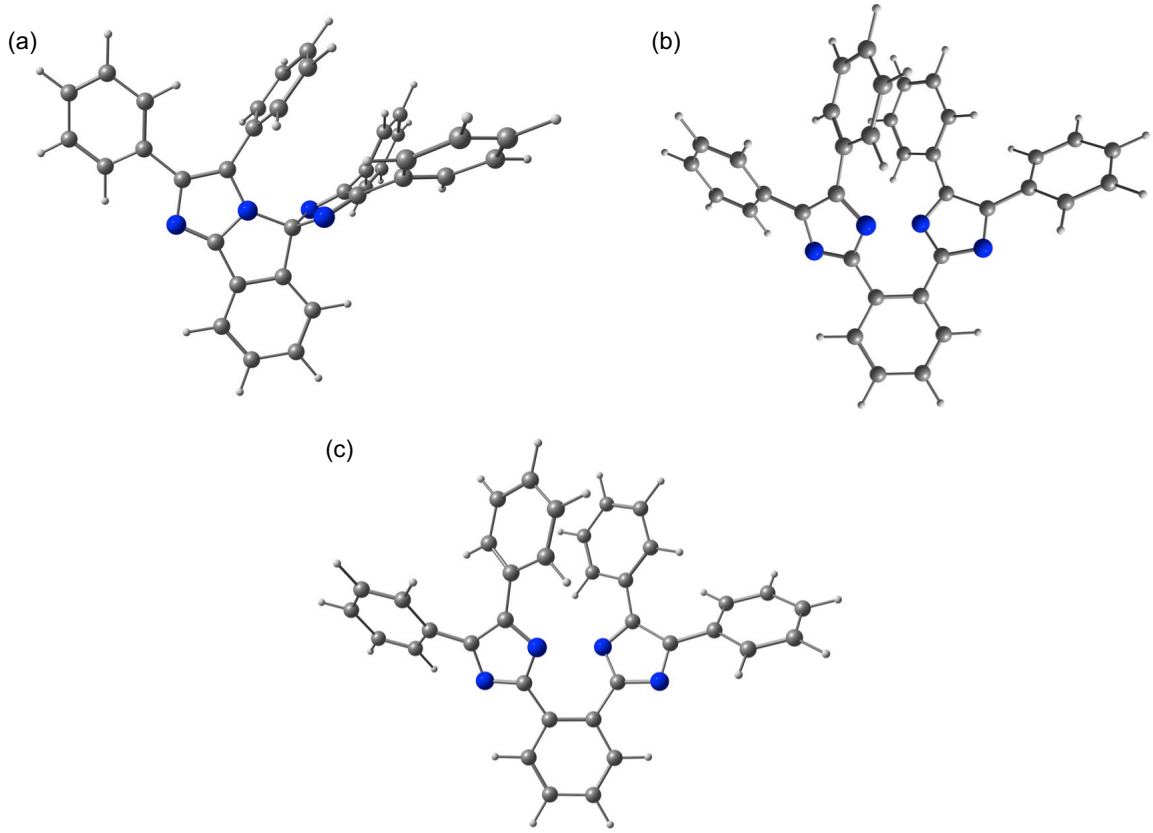

Figure 2.7: The molecular structures of PABI: (a) closed, (b) open 1 and (c) open 2. White: H, Grey: C, and Blue: N.

Chapter 3

Distinguishing Artificial and Essential Symmetry Breaking in a Single Determinant

3.1 Introduction

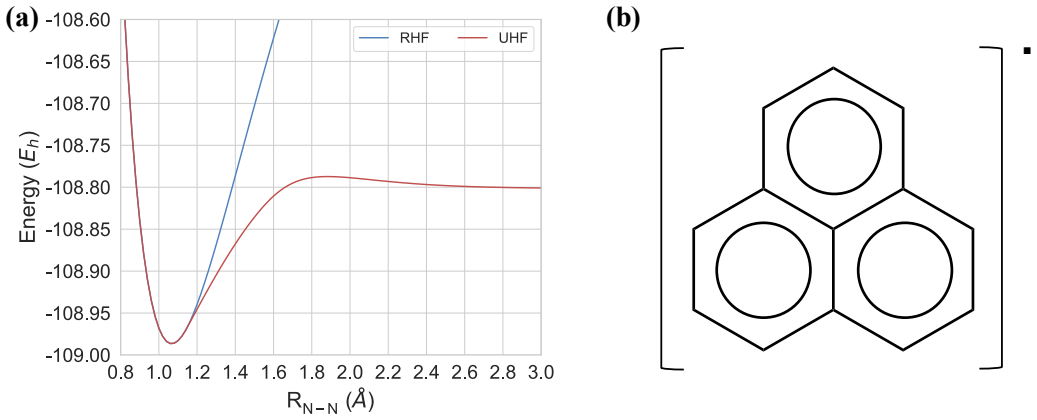

Figure 3.1: (a) Bond dissociation of N_2 in the cc-pVTZ basis set and (b) a phenalenyl radical. In (a), RHF stands for spin-restricted Hartree-Fock and UHF stands for spin-unrestricted Hartree-Fock. The Coulson-Fischer point is located at 1.16 Å.

The conventional wisdom in quantum chemistry is that spin symmetry-breaking is often necessary for describing strongly correlated systems that are beyond the scope of single-reference wavefunctions with spin-restricted orbitals.[257, 258] A familiar ex-

ample, illustrated in Figure 3.1 (a) is the spin-polarization that occurs in homolytic bond-breaking at the Coulson-Fischer point,[213] leading to spin-unrestricted fragments at separation. We can say that this is *essential symmetry-breaking*, because without it, the character of a one-determinant wavefunction is fundamentally wrong (it has ionic character at dissociation). This is analogous to the fact that the exact wavefunction in this recoupling regime has *essential* multiconfigurational character, and is not qualitatively similar to a single determinant of spin-restricted orbitals. In other words, essential symmetry-breaking yields qualitatively better energies because it captures some aspects of electron correlation relative to a spin-restricted determinant.

However, *artificial symmetry breaking* has appeared in numerous systems including open-shell systems and polyaromatic hydrocarbons. [120–127] It is "artificial" in the sense that these systems are not strongly correlated and a single Slater determinant wavefuction with restricted orbitals should be a faithful representation. However, employing unrestricted Hartree-Fock (UHF) wavefunctions often yields significantly spin-contaminated results, which then generally give poor energetics. An example is the doublet phenalenyl radical, shown in Figure 3.1 (b), which is quite stable, with known solution chemistry.[259, 260] Yet UHF/6-31G* calculations lead to $\langle \hat{S}^2 \rangle = 2.08$ rather than 0.75,[176] even though there is no obvious "essential" electron correlation effect that is captured by this extensive spin symmetry-breaking. Rather we might say that this "artificial" symmetry-breaking is lowering the energy by recovering a bit of the dynamical correlation.

It is another difficult *symmetry dilemma* as to how to distinguish a genuine symmetry breaking from an artificial one. [261] At the mean-field level, spontaneous symmetry breaking occurs to lower the mean-field electronic energy. Broken symmetry solutions are variationally preferred due to the very limited form of a single deteminant wavefunction. However, subsequent correlated wavefunction calculations (particularly those that include perturbative corrections) on top of broken symmetry orbitals often yield qualitatively incorrect energetics and properties.[122, 123, 126, 187–190, 262]

To mitigate this problem, it is often preferred to employ approximate Brückner orbitals.[191, 192, 263, 264] The exact Brückner orbitals may be obtained from an exact wavefunction by enforcing the zero singles constraint (i.e. the defining property of Brückner orbitals).[265, 266] Having an exact wavefunction is not a realistic assumption so, in practice, one may utilize coupled-cluster doubles (CCD) to obtain so-called Brückner doubles (BD).[192] Our group proposed a variational formulation of BD, called orbital-optimized doubles (OD), which optimizes orbitals in the presence of the CCD correlation energy.[256, 267]

One major drawback of OD (or BD) is that its computational complexity scales

sextically with system size. A more economical way to obtain approximate Brückner orbitals with fifth-order complexity is to use orbital-optimized second-order Møller-Plesset theory (OOMP2).[176] OOMP2 has been successfully applied to shed light on artificial spin-symmetry breaking problems.[195, 196] It also improves energetics of radical-involving systems drastically compared to regular MP2.[177, 268]

Although OOMP2 has shown its utility in the aforementioned examples, it also has two disturbing features.[199, 203] First, its potential energy surface often exhibits a first-order derivative discontinuity even though the electronic energy is minimized with respect to orbitals which should give only a second-order derivative discontinuity. This is a consequence of the disappearance of Coulson-Fischer points.[213] Second, it often finds a divergent energy solution (i.e. $E = -\infty$) by preferring an unphysical zero-gap restricted solution. We argue that these two drawbacks were satisfactorily solved and thoroughly analyzed in our previous work where we employed an orbital energy dependent regularizer.[269]

Fullerenes have attracted great attention in physical chemistry and interested readers are referred to ref. 270, an excellent textbook which summarizes the history of fullerenes in physical chemistry, and references therein. Starting from the smallest fullerene, C_{20},[271] fullerenes are made solely of carbon and exhibit uncommon cage geometries. These extraordinary features of fullerenes are interesting on their own. What is surprising from an electronic structure standpoint is that many of these fullerenes exhibit complex generalized Hartree-Fock (cGHF) solutions as discovered by Jiménez-Hoyos et al.[272] These symmetry-broken cGHF solutions were interpreted as an indicator of polyradicaloid character of fullerenes. This is unexpected because experimentally synthesized fullerenes are quite stable and thus these stable ones are likely closed-shell in character.

The most striking conclusion of Jiménez-Hoyos and co-workers' work is that buckminsterfullerene, C_{60}, is polyradicaloid because of the existence of a cGHF solution. This contradicts our group's previous attempt at characterizing the electron correlation of C_{60}. Our group discovered a restricted (R) to unrestricted (U) instability in C_{60} at the HF level.[195] We carefully assessed the nature of spin-symmetry breaking in comparison with C_{36} which is known to be strongly correlated. For C_{60} RMP2 yielded a more reasonable single-triplet gap than UMP2 and scaled opposite spin OOMP2 restored the spin-symmetry. For these reasons, our conclusion was that C_{60} is not strongly correlated and should be described as a closed-shell molecule.

In this work, we address this controversy on symmetry breaking of C_{60} and characterize the electron correlation of related molecules (i.e., C_{20} and C_{36}) using the recently developed regularized OOMP2 (κ-OOMP2)[269] and coupled-cluster valence bond with singles and doubles (CCVB-SD) methods.[141, 142]

3.2 Theory

We will use $i, j, k, l, \cdots$ to index occupied orbitals, $a, b, c, d, \cdots$ to index virtual orbitals, and $p, q, r, s, \cdots$ to index either of those two. n_α denotes the number of α electrons, n_β denotes the number of β electrons, n_{mo}^σ is the number of molecular orbitals of spin σ, and n_{so} is the number of spin orbitals.

3.2.1 Classification of HF Solutions

Fukutome pioneered the group-theoretic classification of non-relativistic HF solutions.[273] There are a total of eight distinct classes based on the symmetry of the electronic Hamiltonian (complex conjugation ($\hat{K}$), time-reversal ($\hat{\Theta}$), and spin-operators $\hat{S}_{\mathbf{n}}$ where $\mathbf{n}$ is a collinear axis and $\hat{S}^2$). We will follow the classification by Stuber and Paldus,[274] which is identical to Fukutome's classification with a different name for each class. The eight different classes are: restricted HF (RHF), complex RHF (cRHF), unrestricted HF (UHF), complex UHF (cUHF), generalized HF (GHF), and complex GHF (cGHF) along with paired UHF (pUHF) and paired GHF (pGHF). For the purpose of this work, we discuss symmetry breaking of $\hat{K}$, $\hat{S}_{\mathbf{n}}$, and $\hat{S}^2$ and do not discuss $\hat{\Theta}$. Therefore, there is no distinction between complex solutions and paired solutions since they differ only by time-reversal symmetry. We will thus discuss a total of six classes of HF solutions of each fullerene presented below, which are summarized in Table 3.1.

$\hat{K}$	$\hat{S}^2$	$\hat{S}_{\mathbf{n}}$	Stuber-Paldus
Conserved	Conserved	Conserved	RHF
Broken	Conserved	Conserved	cRHF
Conserved	Broken	Conserved	UHF
Broken	Broken	Conserved	cUHF
Conserved	Broken	Broken	GHF
Broken	Broken	Broken	cGHF

Table 3.1: Classification of HF solutions relevant in this work. $\hat{K}$ is a complex conjugation operator and $\hat{S}^2$ and $\hat{S}_{\mathbf{n}}$ are spin operators. Note that we do not distinguish between complex conjugation symmetry breaking and time-reversal symmetry breaking for the purpose of this work.

3.2.2 Generalized MP2

GHF eliminates the distinction between α and β spin orbitals characteristic of UHF.[273–278] Instead each electron occupies a spin-orbital that can be an arbitrary linear combination of α and β basis functions. We refer to such an orbital as a generalized spin-orbital (GSO). The usual spin-orbital MP2 energy expression reads,

$$E_{\mathrm{MP2}} = E_0 - \frac{1}{4}\sum_{ijab}\frac{|\langle ij||ab\rangle|^2}{\Delta_{ij}^{ab}}, \tag{3.1}$$

where E_0 is the energy of the reference HF determinant and the remainder is the MP2 correlation energy. Δ_{ij}^{ab} is a non-negative orbital energy gap defined as

$$\Delta_{ij}^{ab} = \epsilon_a + \epsilon_b - \epsilon_i - \epsilon_j, \tag{3.2}$$

and a two-electron integral $(ia|jb)$ is

$$(ia|jb) = \int_{\mathbf{r_1},\mathbf{r_2}} \frac{\phi_i(\mathbf{r_1})^*\phi_a(\mathbf{r_1})\phi_j(\mathbf{r_2})^*\phi_b(\mathbf{r_1})}{||\mathbf{r_1}-\mathbf{r_2}||_2}. \tag{3.3}$$

and an antisymmetrized integral is

$$\langle ij||ab\rangle = (ia|jb) - (ib|ja) \tag{3.4}$$

The evaluation of a two-electron integral with GSOs can be achieved in the following way:

$$(ia|jb) = (i^\alpha a^\alpha|j^\alpha b^\alpha) + (i^\alpha a^\alpha|j^\beta b^\beta) + (i^\beta a^\beta|j^\alpha b^\alpha) + (i^\beta a^\beta|j^\beta b^\beta) \tag{3.5}$$

where we used the fact that each GSO, $|\phi_p\rangle$, has an α and a β component

$$|\phi_p\rangle = \begin{pmatrix} \phi_p^\alpha \\ \phi_p^\beta \end{pmatrix}. \tag{3.6}$$

We did not include the contributions with mixed spin components on electron 1 or 2 (e.g., $(i^\alpha a^\beta|j^\alpha b^\alpha)$) because they are zero upon the spin integration. Having expanded out the two-electron integral this way, the implementation of GMP2 is (at least conceptually) trivial on top of an existing MP2 program.

The resolution of the identity approximation can be also applied to Eq. (3.5) using [166, 167]

$$(i^{\sigma_1}a^{\sigma_1}|j^{\sigma_2}b^{\sigma_2}) = \sum_{PQ}(i^{\sigma_1}a^{\sigma_1}|P)(P|Q)^{-1}(Q|j^{\sigma_2}b^{\sigma_2}) \tag{3.7}$$

where $(i^{\sigma_1}a^{\sigma_1}|P)$ represents a 2-electron 3-center Coulomb integral and $(P|Q)$ is the metric matrix of the above decomposition which is a 2-electron 2-center Coulomb integral among auxiliary basis functions.

The scaling of RI-cGMP2 is the same as RI-RMP2 or RI-UMP2 (i.e., $\mathcal{O}(N^5)$). However, it carries a large prefactor compared to RI-RMP2 or RI-UMP2. The bottleneck of RI-MP2 is forming two-electron integrals in Eq. (3.7). In the case of RI-RMP2 this step scales $\mathcal{O}(n_\alpha^2(n_{\text{mo}}^\alpha - n_\alpha)^2 n_{\text{aux}})$ whereas RI-UMP2 scales $\mathcal{O}((n_\alpha^2(n_{\text{mo}}^\alpha - n_\alpha)^2 + n_\beta^2(n_{\text{mo}}^\beta - n_\beta)^2 + n_\alpha n_\beta(n_{\text{mo}}^\alpha - n_\alpha)(n_{\text{mo}}^\beta - n_\beta))n_{\text{aux}})$. Assuming $n_\alpha = n_\beta$, RI-UMP2 is three times more expensive than RI-RMP2. In the case of RI-GMP2, we have a scaling of $\mathcal{O}(n_{\text{elec}}^2(n_{\text{so}} - n_{\text{elec}})^2 n_{\text{aux}})$. Assuming $n_{\text{elec}} = 2n_\alpha$ and $n_{\text{so}} = 2n_{\text{mo}}^\alpha$, we conclude that RI-GMP2 is 16 times more expensive than RI-RMP2. RI-cGMP2 carries an extra factor of four due to complex arithmetic operations. Overall, RI-cGMP2 is 64 times more expensive than RI-RMP2. Since we will be studying reasonably large systems, this non-negligible prefactor will limit the applicability of RI-cGMP2 in this study.

We will use the RI approximation throughout this work so we shall drop "RI" and refer to "RI-MP2" as "MP2".

3.2.3 Regularized Orbital-Optimized MP2

When orbital-optimizing Eq. (3.1), it is sometimes observed that the energy tends to $-\infty$. This divergence is attributed to the development of a small denominator, $\Delta_{ij}^{ab} \to 0$ for some i, j, a, b. While simple level shifts were first explored[199, 203] they proved inadequate. In essence, such large level shifts were needed[203] (10–30 eV) that results, while stable, could be inferior to the unregularized theory. To better mitigate this problem, we proposed a regularized MP2 method whose energy reads

$$E_{\text{MP2}}(\kappa) = E_0 - \frac{1}{4}\sum_{ijab} \frac{|\langle ij||ab\rangle|^2}{\Delta_{ij}^{ab}} \left(1 - e^{-\kappa\Delta_{ij}^{ab}}\right)^2 \tag{3.8}$$

where $\kappa > 0$ is a single empirical parameter that controls the strength of regularization. The exponential damping function ensures that small denominators cannot contribute to the final energy. Orbital-optimizing Eq. (3.8) yields κ-OOMP2 which we thoroughly analyzed and benchmarked in our previous work.[269] $\kappa = 1.45\ E_h^{-1}$ was recommended as it appeared to combine favorable recovery of Coulson-Fischer points with good numerical performance.

3.2.4 Classification of OOMP2 Solutions

The classification of OOMP2 solutions can be done in the same way as that of HF solutions. The classification needs to incorporate the MP2 correction to the one-particle density matrix (1PDM) and the first-order correction to the spin expectation values.

The norm of the imaginary part of the 1PDM, ξ, diagnoses the fundamental complexity of a wavefunction at the one-body level.[279] This was sufficient for testing the fundamental complexity of OOMP2 solutions studied in this work. However, in principle, one may consider a more sophisticated diagnostic tool that involves higher order density matrices. The expression for the correlated 1PDM of OOMP2 methods is given in the Appendix.

The first-order correction to the spin expectation values are needed to compute the first-order correction to a spin covariance matrix $\mathbf{A}$ defined as

$$A_{ij} = \langle \hat{S}_i \hat{S}_j \rangle - \langle \hat{S}_i \rangle \langle \hat{S}_j \rangle \tag{3.9}$$

The nullity of this matrix determines the collinearity of a given wavefunction as noted by Small et al.[277] If there is a zero eigenvalue associated with an eigenvector $\mathbf{n}$, the wavefunction is collinear along this axis $\mathbf{n}$. The real part of $\mathbf{A}$ is a positive semidefinite matrix and the smallest eigenvalue, μ_0, can be used to quantify the non-collinearity of a given wavefunction. This applies to not only non-interacting wavefunctions such as HF states but also correlated states such as MP1 wavefunctions. We present the formula for computing the first-order correction to $\mathbf{A}$ in the Appendix.

As a side note, during the course of finishing this work, we found that the expression for the first-order correction to $\langle \hat{S}^2 \rangle$ presented in ref. 176 is off by a factor of two and the one in ref. 268 is off by a factor of four from the correct expression. This is clear from looking at a more general expression given in the Appendix.

3.2.5 Coupled-Cluster Methods

Restricted CC with singles and doubles (RCCSD) generally fails to describe strongly correlated systems and often exhibits non-variationality in such systems. Recently, we proposed coupled-cluster valence bond with singles and doubles (CCVB-SD) as a simple alternative that modifies the parametrization of quadruple excitations in RCCSD. [141] CCVB-SD is better than RCCSD at handling strong correlation as it can describe bond dissociations exactly within a valence active space as long as UHF (or UCCSD) can. This property is inherited from a much simpler correlation model, CCVB.[128, 140, 143, 144, 280, 281] Furthermore, CCVB-SD was

successfully applied to oligoacenes which exhibit emergent strong correlations while RCCSD showed non-variationality.[142] It is clear from our experience that strong correlation is present when we observe qualitative differences between CCVB-SD and RCCSD. This can be shown in terms of working equations. CCVB-SD modifies the quadruples in RCCSD which plays a crucial role in describing strong correlation. This modification becomes negligible if no substantial connected quadruples are needed and therefore in such cases there is no strong correlation. Comparing those CC methods will shed light on the electron correlation effects in the fullerenes.

3.3 Probes for Artificial Symmetry Breaking

3.3.1 Probe 1: Symmetry Breaking Landscape from κ-OOMP2

One way to address the problem of distinguishing between essential symmetry breaking (driven by missing static correlation effects) and artificial symmetry breaking (driven by missing dynamical correlation effects) in HF calculations is to apply a method that optimizes the orbitals including only dynamical correlation but not the static or essential correlation. With such an approach, artificial symmetry breaking will be virtually eliminated because dynamic correlation effects are explicitly included and are therefore removed as a driving force for symmetry breaking. Essential symmetry breaking remains because no static correlation is included to handle strong correlation problems.

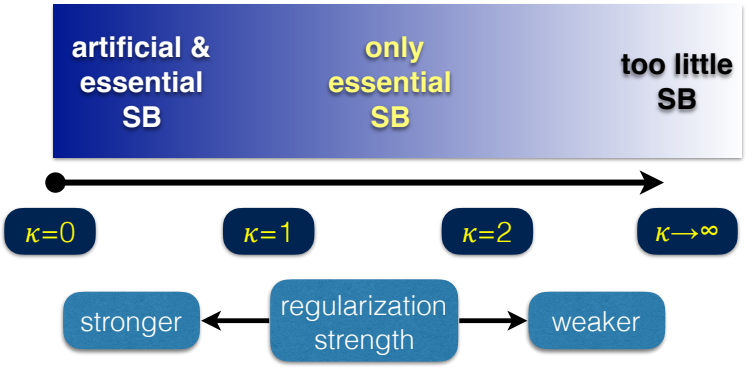

Figure 3.2: Illustration of artificial and essential symmetry breaking (SB) in κ-OOMP2 as a function of κ. $\kappa \in [1.0, 2.0]$ exhibits only essential SB.

The κ-OOMP2 method is such a theory for reasons that are summarized in Figure 3.2. Varying the regularization parameter over the range [0.5, 4.0] for which this method has been parameterized yields a survey of how symmetry breaking depends on regularization strength. Regularization that is weak ($\kappa > 2$) defines methods that strongly favor symmetry-restoration, and will often be below the true energy. For example, in bond-breaking, Coulson-Fischer points are pushed to very long bond-lengths, and eventually are even lost. This arises because weak regularization includes part of the exaggerated MP2 description of the (potentially strong) paired correlations associated with small promotion energies. Thus the limit of very weak regularization ($\kappa \to \infty$) may not even admit essential symmetry breaking for strongly correlated systems.

By contrast regularization that is strong ($\kappa < 1$) will potentially admit both essential and artificial symmetry breaking, because part of the dynamical correlation is also attenuated. This is most clearly seen by considering κ-OOMP2, where the limit as $\kappa \to 0$ recovers HF theory, with all its symmetry breaking characteristics and the limit of $\kappa \to \infty$ recovers unregularized OOMP2 with its (a) overestimation of static correlation with restricted orbitals and (b) loss of Coulson-Fischer points. Finally, the intermediate regime, which we view here as roughly $\kappa \in [1.0, 2.0]$, presents a transition between strong and weak regularization. The value of $\kappa = 1.45$ which was selected to yield useful accuracy and restore Coulson-Fischer points, as discussed previously,[269] lies in this region.

We can use the κ-dependence of symmetry breaking in κ-OOMP2 to characterize its nature. For an even electron system that exhibits symmetry breaking at the HF level, using κ-OOMP2 at a fixed geometry as a function of κ will yield a critical value, κ_c above which symmetry restoration is complete. If κ_c is large enough (weak regularization, for instance $\kappa_c > 2$), so that Coulson-Fischer points are not properly restored in bond-breaking, then we conclude that the HF symmetry breaking was essential in character, since so too is that of κ-OOMP2. On the other hand, if κ_c is small enough (strong regularization, for instance $\kappa_c < 1$) then we are well into the regime where Coulson-Fischer points exist, and we must therefore conclude that the HF symmetry breaking was artificial in character, because symmetry breaking is readily quenched in κ-OOMP2, even with strong regularization.

3.3.2 Probe 2: Singlet-Triplet Gap

A singlet-triplet gap measures the energy cost for breaking a pair of electrons that are singlet coupled. This would be much smaller than a usual single bond energy if two electrons are spatially well separated and singly occupying each orbital. This is the case for biradicaloids where singlet-triplet gaps less than 10 kcal/mol are

commonly observed.[245] On the other hand, if the gap is large then the molecule is best described as a closed-shell molecule. A precise experimental value for this gap is available for C_{60} and therefore this is a good probe especially for C_{60}. In this work, we define this as $\Delta E_{S-T} = E_T - E_S$ where E_S and E_T are singlet and triplet energies, respectively.

3.3.3 Probe 3: Correlated 1PDM

We will investigate two quantities that can be obtained from the correlated unrelaxed 1PDM of CC wavefunctions (RCCSD and CCVB-SD). The first one is natural orbital occupation numbers (NOONs) which are eigenvalues of the 1PDM. For a perfect closed-shell molecule, the NOONs would be either 0.0 (empty) or 2.0 (doubly occupied). For a perfect biradical system, there should be two eigenvalues of 1.0 as well. In general, the NOONs will be distributed between 0.0 and 2.0. A polyradicaloid must have multiple eigenvalues that significantly deviate from 0.0 and 2.0.

The second quantity that we will report is Head-Gordon's number of unpaired electrons (NUE),[282]

$$\mathrm{NUE} = \sum_i \min(2 - n_i, n_i) \tag{3.10}$$

where i is summed over all natural orbitals and n_i is the occupation number of the i-th natural orbital. This takes the entire spectrum of NOONs and reduces it to a single scalar value that quantifies strong correlation. In the case of a perfect closed-shell molecule, NUE is zero. Molecules with open-shell character will exhibit larger NUE values. When these quantities show a qualitative difference between RCCSD and CCVB-SD for a given system, we conclude that the system is strongly correlated and vice versa.

3.4 Results

We investigated the C_{60}, C_{36}, and C_{20} fullerenes. We studied a total of five different geometries of C_{20} whereas only one conformation for other fullerenes was studied. All HF calculations were performed with wavefunction stability analysis to ensure the local stability of solutions. The pertinent cGHF electronic Hessian is provided in the Appendix. All calculations were carried out with a development version of `Q-Chem`.[236] All plots were generated with `Matplotlib` [283] and all molecular figures were generated with `Chemcraft`.[284]

Obtaining quantitatively accurate answers with CC methods is very computationally intensive for fullerenes so we look for qualitative answers by comparing them to

various OOMP2 methods. We will employ the STO-3G basis set in order to exaggerate the effect of strong correlation and discuss the implication within this basis set as well as the frozen core approximations. We only present the CC data for C_{60} and C_{36} here; the CC data for C_{20} showed the same conclusions as the other analyses based on OOMP2 we present below.

3.4.1 The Nature of Electron Correlation in C_{60}

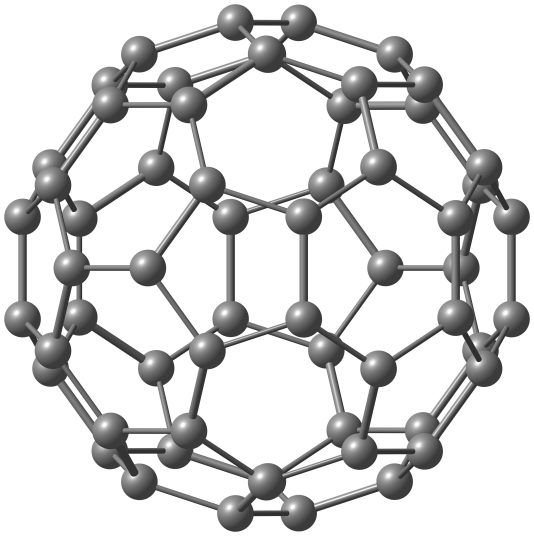

Figure 3.3: The I_h molecular structure of C_{60}.

C_{60} is a well-known electron paramagnetic resonance silent molecule[285] and its geometry is shown in Figure 3.3. Therefore, it is undoubtedly a molecule with a singlet ground state. Furthermore, its stability has suggested that it is a closed shell molecule.[286] This is why it was surprising to observe the existence of R to U symmetry breaking of C_{60} at the HF level.[195] This R to U symmetry breaking was in the end characterized as artificial based on analyses using OOMP2 and the single-triplet gap. Later, Jiménez-Hoyos et al. found a cGHF solution for C_{60} and concluded that C_{60} is strongly correlated (or polyradicaloid) based on this broken-symmetry HF solution.[272] This was surprising to us because C_{60} has been hardly suggested to be polyradicaloid and is also very stable in experiments. Therefore, we revisit this problem with κ-OOMP2 and CC methods and try to determine whether C_{60} is strongly correlated.

Symmetry Breaking Landscape

Due to limited computational time, we could obtain the symmetry breaking landscape of this molecule only within a minimal basis set, STO-3G.[287] We took the cGHF optimized geometry of C_{60} from Jiménez-Hoyos and co-workers' work. As it is well known, the STO-3G basis set exaggerates strong correlation and facilitates symmetry breaking. The critical κ values obtained from minimal basis set calculations would therefore be a good estimate on the upper bound of κ_c.

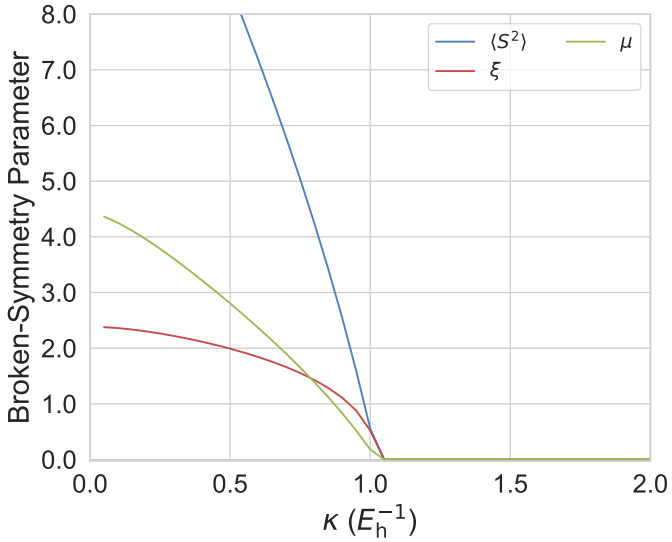

Figure 3.4: Measures of symmetry breaking ($\langle S^2 \rangle$, ξ, and μ) as a function of the regularization strength κ for C_{60} (I_h). The plots characterize symmetry-breaking/restoration in κ-OOMP2.

In Figure 3.4, we present the symmetry breaking landscape of C_{60}. For $\kappa < 1.05$, $\langle S^2 \rangle$, ξ, and μ exhibit a steep increase as κ decreases. Eventually, the curve reaches the cGHF solution at the limit of $\kappa \to 0$. $\kappa = 1.05$ is enough to restore all symmetries that were broken at the HF level. This critical value is not large enough to be safely in the range of essential symmetry breaking illustrated in Section 3.3.1. Therefore we conclude that the symmetry breaking at the HF level is *artificial*. We also confirmed the symmetry restoration at $\kappa = 1.45$ with κ-OOMP2 within the VDZ (i.e., cc-pVDZ[237] without polarization) basis set. Therefore, we believe that the basis set incompleteness error will not affect this qualitative conclusion.

Method	$\Delta E_{\text{S-T}}$	$\langle \hat{S}^2 \rangle_{M_S=0}$	$\langle \hat{S}^2 \rangle_{M_S=1}$
RHF	65.63	0.000	2.000
RMP2	57.42	0.000	2.000
SCS-RMP2	59.44	0.000	2.000
SOS-RMP2	60.45	0.000	2.000
UHF	45.23	6.708	8.560
UMP2	77.39	5.566	7.401
UOOMP2	19.48	0.000	2.043
SCS-UOOMP2	28.53	0.000	2.002
SOS-UOOMP2	35.72	0.000	1.995
κ-UOOMP2	49.23	0.000	2.002
Experiment[288]	36.95 $\pm$ 0.02		

Table 3.2: The singlet-triplet gap $\Delta E_{\text{S-T}}$ (kcal/mol) of C_{60} from various methods. The expectation values of $\langle \hat{S}^2 \rangle$ for $M_S = 0$ and $M_S = 1$ states are presented as well. Note that these values include correlation corrections to $\langle \hat{S}^2 \rangle$.

Singlet-Triplet Gap

In Table 3.2, we present the singlet-triplet gap of C_{60} computed with various MP2 methods. Here, we used the cc-pVDZ basis set[237] along with the corresponding auxiliary basis set.[238] For OO methods, we performed orbital optimization starting from stable UHF solutions. The results presented in Table 3.2 generally agree with what Stück and Head-Gordon reported.[195]

The singlet-triplet gap predicted by HF is better with UHF (45.23 kcal/mol) than with RHF (65.63 kcal/mol) in comparison to the experimental value (36.95 $\pm$ 0.02 kcal/mol). UHF exhibits striking spin-contamination and this is improved to a small extent with UMP2. The singlet-triplet gap of UMP2 is much worse than that of UHF, going from 45.23 kcal/mol to 77.39 kcal/mol whereas RMP2 improves the gap by 8 kcal/mol compared to RHF. It is clear that a better reference for subsequent correlation calculations is RHF not UHF. We also compare RMP2 with spin-component scaled MP2 [170](SCS-MP2) and scaled opposite-spin MP2[171] (SOS-MP2). The singlet-triplet gap is quite insensitive to the choice of scaling factors.

OOMP2 methods successfully remove heavy spin-contamination observed at the HF level. While in terms of $\langle \hat{S}^2 \rangle$ unregularized OOMP2 and its scaled variants are desirable, a striking underestimation of the gap is alarming. In particular, compared to their non-OO variants these gaps are severely underestimated. We suspect that this is due to overcorrelating the $M_S = 1$ state via OO. Unlike the non-OO variants,

unregularized (i.e., $\kappa \to \infty$) OO methods are sensitive to the scaling parameters. We observe that the gap from SOS-UOOMP2 is only off by 1 kcal/mol from the experimental value. This is likely a fortuitous outcome.

It is interesting that this unphysical overcorrelation of the triplet state seems to be resolved with κ-UOOMP2. κ-UOOMP2 exhibits an error of 12 kcal/mol which is likely due to the limited treatment of electron correlation. It will be interesting to resolve this remaining error using higher order perturbation theory or, perhaps, coupled-cluster methods.

Correlated 1PDM

We then obtain NOONs from OOMP2 methods and analyze them. We will discuss three unregularized OOMP2 methods, OOMP2, SCS-OOMP2,[177] and SOS-OOMP2[176] along with κ-OOMP2. In Figure 3.5, different OOMP2 methods exhibit more or less identical NOONs. We could not find unrestricted solutions for any of these methods. This reflects the simplicity of the electronic structure of C_{60}. A noticeable reduction in open-shell character is observed in κ-OOMP2 compared to other OOMP2 methods. These NOONs are far from the usual values for orbitals with open-shell character in strongly correlated wavefunctions (i.e., values between 1.30 and 0.70).

Likewise, the NOONs from CC methods presented in Figure 3.6 strongly suggest that this molecule is *not strongly correlated*. RCCSD and CCVB-SD exhibit visually identical distributions. Indeed, the NOONs of the highest occupied NO (HONO) and the lowest unoccupied NO (LUNO) are (1.87, 0.14) for both methods. These values are comparable to naphthalene's NOONs computed with CCVB-SD. Evidently, naphthalene is not a strongly correlated system, which implies that neither is C_{60}.

Method	STO-3G	cc-pVDZ
OOMP2	8.04 (0.13)	14.03 (0.23)
SCS-OOMP2	7.67 (0.13)	12.63 (0.21)
SOS-OOMP2	6.92 (0.12)	11.02 (0.18)
κ-OOMP2	3.86 (0.06)	8.08 (0.13)
RCCSD	9.48 (0.16)	
CCVB-SD	9.19 (0.15)	

Table 3.3: Number of unpaired electrons (NUE) of C_{60} computed from various methods. The numbers in parentheses are NUE per carbon atom.

In Table 3.3, we present NUEs (Eq. (3.10)) of C_{60} computed by various methods. With a larger basis set (cc-pVDZ), NUEs are larger than those of STO-3G.This

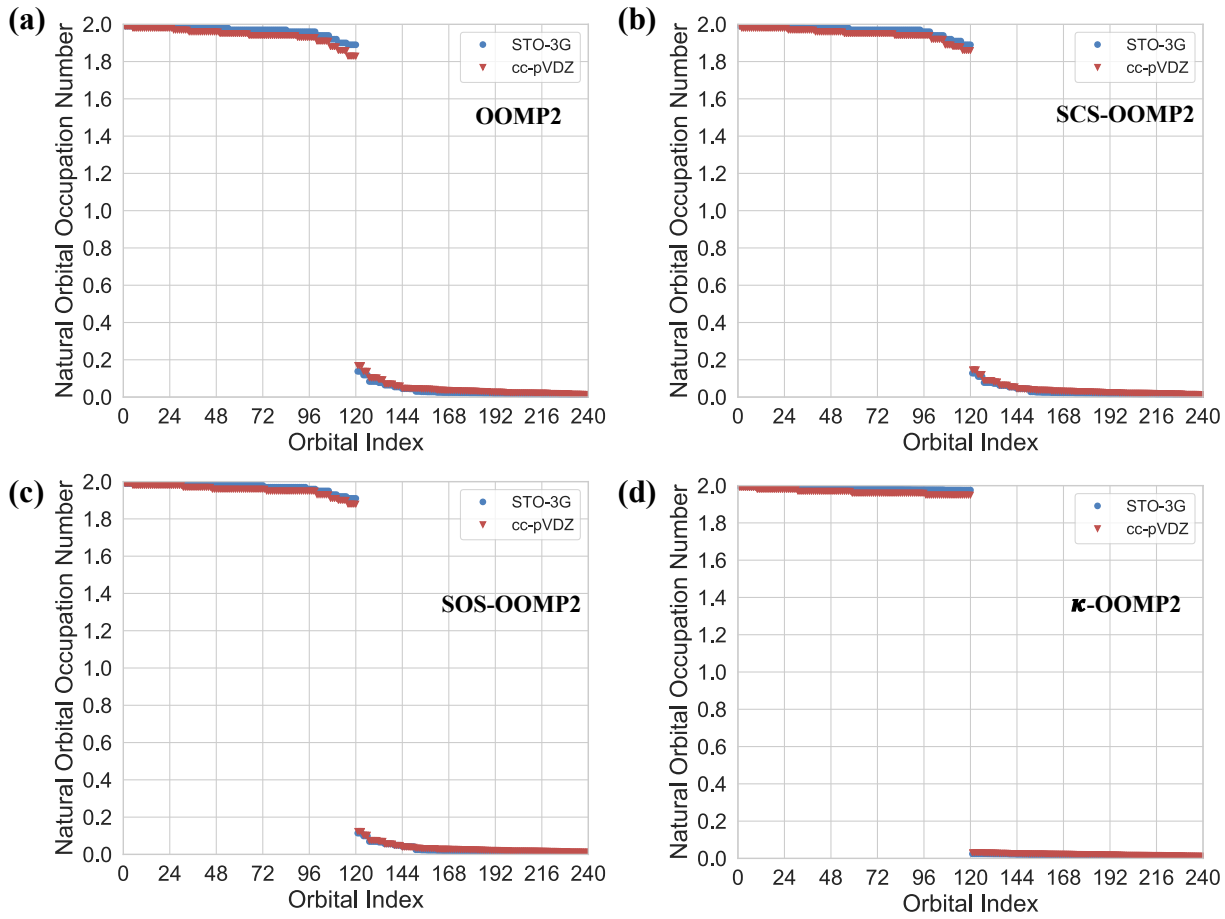

Figure 3.5: Natural orbital occupation numbers of C_{60} within a valence active space from (a) OOMP2, (b) SCS-OOMP2, (c) SOS-OOMP2, and (d) κ-OOMP2. Note that there were no unrestricted solutions found for any of these methods.

reflects the increase in open-shell character due to dynamic correlation. We once again observe almost no differences between RCCSD and CCVB-SD. Overall, there are about 0.06 to 0.16 unpaired electrons per C atom in C_{60} within the STO-3G basis set. As each C atom has four valence electrons, this amounts only 1.6–4.0% of the total number of electrons. Therefore, the polyradicaloid character in C_{60} is only marginal from the global electronic structure viewpoint.

Based on these analyses, we conclude that C_{60} should be considered a closed-shell molecule and *not strongly correlated*. Thus the very interesting cGHF solution reported previously[272] should be considered as an artificial rather than an essential

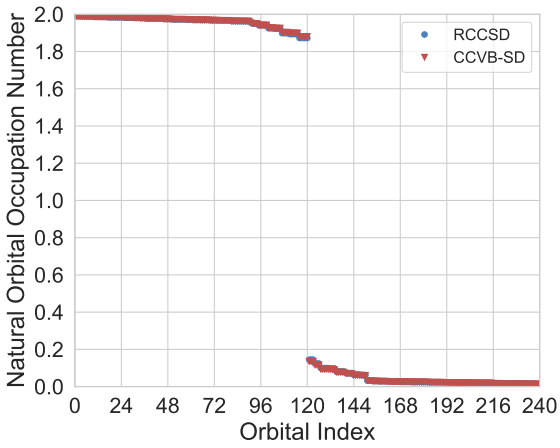

Figure 3.6: Natural orbital occupation numbers of C_{60} within the minimal basis set, STO-3G, from RCCSD and CCVB-SD. Two sets of data points are very close to each other so the blue circles lie right below the red triangles.

symmetry breaking. This conclusion will be also supported by comparing with our next molecule, C_{36} which is a well-known biradicaloid.

3.4.2 The Nature of Electron Correlation in C_{36}

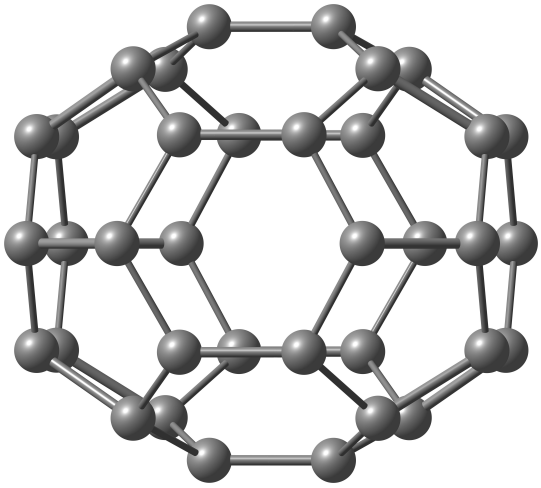

Figure 3.7: The D_{6h} molecular structure of C_{36}.

The D_{6h} structure of C_{36} shown in Figure 3.7 has been known to exhibit strong

biradicaloid character.[289] This has been of great interest both experimentally[290] and theoretically.[289, 291–297] The D_{6h} structure is supported by the ^{13}C NMR spectrum exhibiting a single peak.[290] Different computational methods suggested different structures and even different multiplicities. There is no doubt that C_{36} exhibits complex electronic structure and is a strongly correlated system.

Stück and Head-Gordon studied this prototypical strongly correlated system using unregularized SOS-OOMP2 before. Fortunately, unregularized OOMP2 did not diverge even with this substantial biradicaloid character. What was not explicitly mentioned in this previous work is that OOMP2 in fact yields a restricted solution when starting from an unrestricted solution. Since unregularized OOMP2 unphysically prefers restricted solutions (closely connected to its singularity problem), this is not unexpected. This also suggests that whether unregularized OOMP2 restores broken symmetry is not a definitive probe to characterize strong electron correlation in a given system (it is the $\kappa \to \infty$ limit shown in Fig. 3.2). We will see how κ-OOMP2 resolves this artifact and can be used to probe strong correlation in this system.

We obtained the D_{6h} molecular structure of C_{36} via geometry optimization with restricted density functional calculations using the BLYP exchange-correlation functional[298, 299] and the 6-31G(d) basis set.[300] The geometry optimization was performed with a D_{6h} geometric constraint so the optimization was not allowed to break this spatial symmetry. We do not think that this geometry is quantitatively accurate but for the purpose of this work, it should be sufficient.

Symmetry Breaking Landscape

We computed a landscape of symmetry breaking as a function of κ within the 6-31G basis set[301] along with the cc-pVDZ auxiliary basis set.[238] This may not be quantitatively accurate, but it should be enough to draw qualitative conclusions. Figure 3.8 shows that C_{36} exhibits multiple classes of one-particle wavefunctions as a function of κ. As noted by Jiménez-Hoyos et al,[272] at the HF level there exists a cGHF solution. This is clearly evident in Figure 3.8 for $\kappa < 1.00$, since we have nonzero $\langle S^2 \rangle$, ξ, and μ. ξ and μ vanish at their critical value $\kappa_c = 1.00$ and only unrestricted solutions were obtained for $\kappa \in [1.00, 2.45]$. For $\kappa > 2.45$, only restricted solutions were found. These solutions are consistent with Stück and Head-Gordon's work which used unregularized SOS-OOMP2.[195] This landscape has more structure than that of C_{60} (see Fig. 3.4) which reflects the increased complexity of the electronic structure of C_{36}.

The κ value within the essential symmetry breaking region exhibits only unrestricted solutions. Therefore, complex generalized solutions reflect artificial symme-

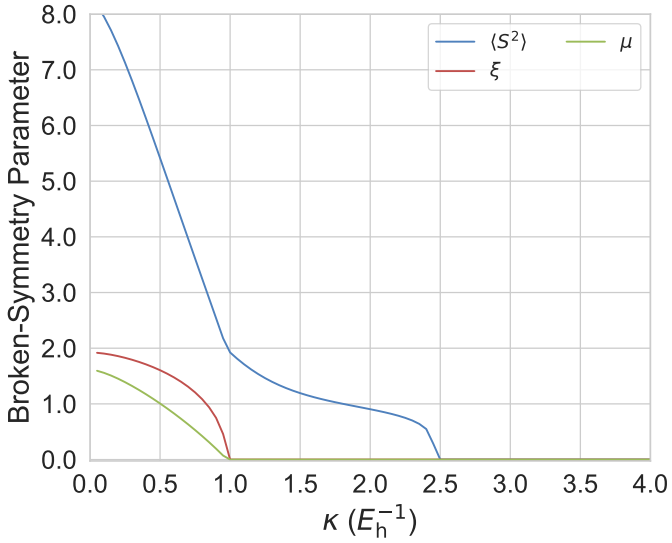

Figure 3.8: Measures of symmetry breaking ($\langle S^2 \rangle$, ξ, and μ) as a function of the regularization strength κ for C_{36} (D_{6h}). The plots characterize symmetry-breaking/restoration in κ-OOMP2.

try breaking while restricted solutions exhibit artificial symmetry restoration. Since C_{36} is a well-known singlet biradicaloid, one would expect an unrestricted solution with an $\langle S^2 \rangle$ value between 0.0 and 2.0 (i.e., there is only triplet contaminant). Interestingly, this is what was obtained from κ-OOMP2 with $\kappa = 1.45$ (as described in Figure 3.8). Based on the existence of this essential symmetry breaking, we conclude that C_{36} is strongly correlated.

Singlet-Triplet Gap

We will focus on determining whether unscaled κ-OOMP2 with $\kappa = 1.45$ (i.e., the recommended default κ-OOMP2 method[269]) works quantitatively well compared to other MP2 approaches. We observed the same cG to U partial symmetry restoration with $\kappa = 1.45$ within the cc-pVDZ basis set. Therefore, due to limited computational resources, for the cc-pVTZ basis set[237, 238] we only ran unrestricted calculations. In Table 3.4, we present the singlet-triplet gap ($\Delta E_{\text{S-T}}$) computed with various MP2 approaches. Since there is no reliable experimental gap available, we shall compare our results against multi-reference MP2 (MRMP2) results.[289] The MRMP2 results were obtained with the 6-31G(d) basis set and a small active space, (2e, 4o), complete active space self-consistent field (CASSCF) reference state. These might not be a

Method	$\Delta E_{\text{S-T}}$	$\langle \hat{S}^2 \rangle_{M_S=0}$	$\langle \hat{S}^2 \rangle_{M_S=1}$
RHF	-19.69	0.000	2.000
RMP2	21.81	0.000	2.000
SCS-RMP2	17.10	0.000	2.000
SOS-RMP2	14.75	0.000	2.000
UHF	32.29	7.448	8.793
UMP2	42.73	6.428	7.795
UOOMP2	15.85	0.000	2.070
SCS-UOOMP2	30.76	0.000	1.978
SOS-UOOMP2	22.91	0.000	2.002
κ-UOOMP2	4.42	0.959	2.008
AP+κ-UOOMP2	8.46		
MRMP2[289]	8.17		

Table 3.4: The singlet-triplet gap $\Delta E_{\text{S-T}}$ (kcal/mol) of C_{36} from various methods. The expectation values of $\langle \hat{S}^2 \rangle$ for $M_S = 0$ and $M_S = 1$ states are presented as well. Note that these values include correlation corrections to $\langle \hat{S}^2 \rangle$. All but MRMP2 results were obtained with the cc-pVTZ basis set.[237] MRMP2 results in ref. 289 were obtained with a D_{6h} geometry within the 6-31G(d) basis set. MRMP2 was performed on a CASSCF solution with a (2e, 4o) active space.

highly accurate reference result, but it can serve as a qualitative answer.

RHF predicts a triplet ground state, a qualitatively wrong result. RMP2, SCS-RMP2,[170] and SOS-RMP2[171] correct the sign of the gap. They are quite far away from the multi-reference MP2 (MRMP2) result and this is because the singlet biradicaloid character of the true ground state cannot be captured by doubly occupying restricted orbitals. UHF and UMP2 are heavily spin-contaminated and predict significantly large gaps. We note that the MP2 treatment cannot clean up heavy spin-contamination present at the UHF level. As a result, these gaps are qualitatively incorrect as they are too large to support the singlet biradicaloid character.

Spin symmetry breaking iscompletely removed with unregularized OOMP2 methods. The UOOMP2 gap is smaller than RMP2. However, SCS- and SOS-MP2 methods predict much larger gaps with OO than those without OO. This is likely due to overcorrelating the singlet state. This is the case where OOMP2 (or κ-OOMP2 for $\kappa \to \infty$) yields too little symmetry breaking as explained in Section 3.3.1.

κ-UOOMP2 yields a broken-symmetry solution for $M_S = 0$ and $\langle \hat{S}^2 \rangle$ is 0.959. This is of strong singlet biradicaloid character and serves as a good candidate for Yamaguchi's approximate spin-projection (AP)[246] to obtain better energetics. The

use of AP in conjunction with κ-UOOMP2 was first discussed in ref. 269. Without AP, the gap was predicted to be 4.42 kcal/mol. This is small enough to conclude that C_{36} is a singlet biradicaloid, but the gap is underestimated due to spin-contamination. Applying AP lowers the singlet energy by 4 kcal/mol which yields a gap of 8.46 kcal/mol. This is quite close to the reference MRMP2 energy. However, a more precise benchmark is highly desirable in the future to draw a more definitive conclusion. Nevertheless, the result suggests that C_{36} is strongly correlated which agrees with the conclusion drawn based on the symmetry breaking landscape.

Correlated 1PDM

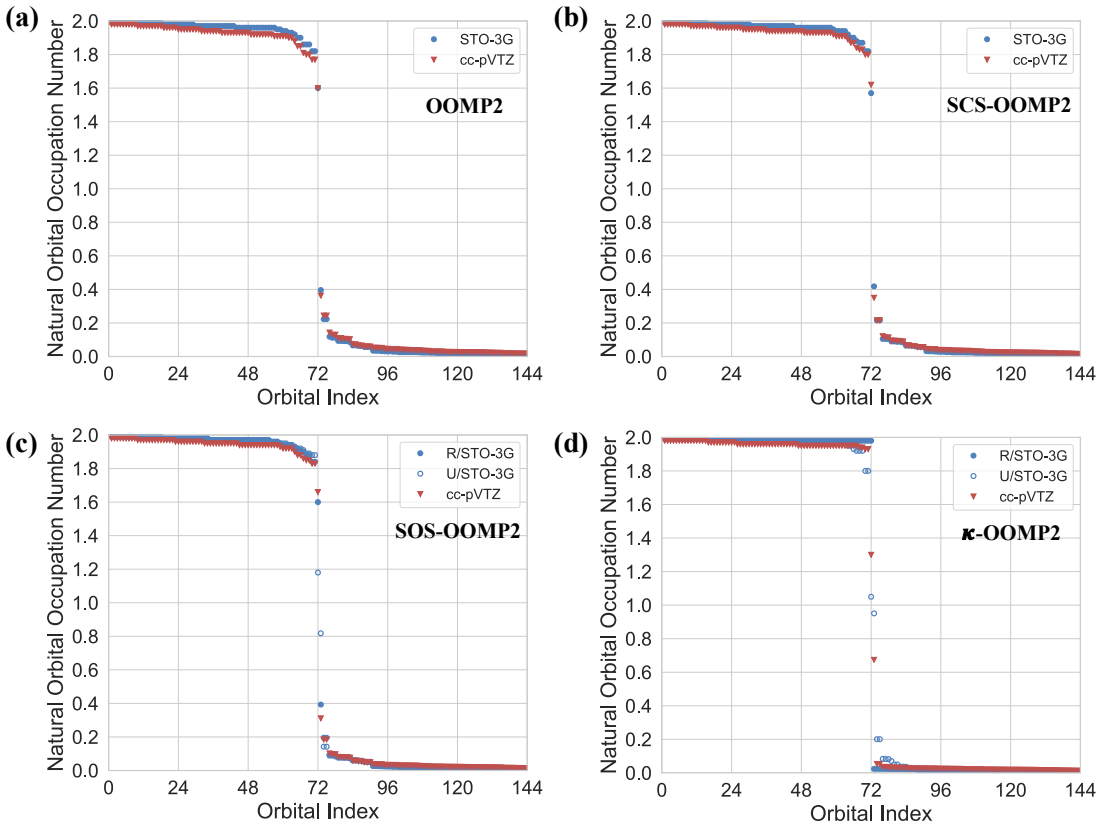

Figure 3.9: Natural orbital occupation numbers of C_{36} within the valence space from (a) OOMP2, (b) SCS-OOMP2, (c) SOS-OOMP2, and (d) κ-OOMP2. Note that there were no unrestricted solutions found for OOMP2 and SCS-OOMP2. Furthermore, the solution from κ-OOMP2 with cc-pVTZ is unrestricted.

In Figure 3.9, we discuss NOONs of C_{36} from the various OOMP2 methods that were used in the previous sections. For STO-3G, OOMP2, SOS-OOMP2, and κ-OOMP2 exhibit clear emergent singlet biradicaloid character. It is clear that NOONs exhibit more open-shell character than those of C_{60} Interestingly, we could isolate an unrestricted STO-3G solution with SOS-OOMP2 by reading in an unrestricted κ-OOMP2 solution. We could not isolate such a solution with the cc-pVTZ basis set. The R to U symmetry breaking of SOS-OOMP2 is interesting in that the unrestricted solution is 21 mE_h higher in energy than the restricted one. Within the cc-pVTZ basis set, OOMP2, SCS-OOMP2, and SOS-OOMP2 all predict very similar NOONs and they exhibit only slight singlet biradicaloid character. On the other hand, κ-OOMP2 exhibits very strong biradicaloid character characterized by an unrestricted solution. HONO and LUNO for this unrestricted solution in the cc-pVTZ basis set have NOONs of 1.30 and 0.67, respectively. The true ground state would have less polarized NOONs than κ-OOMP2.

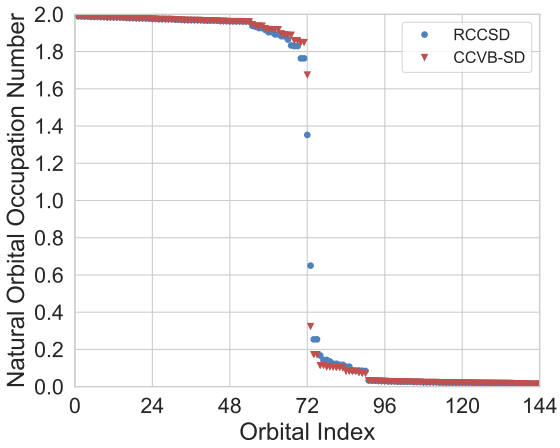

Figure 3.10: Natural orbital occupation numbers of C_{36} within the minimal basis set, STO-3G, from RCCSD and CCVB-SD.

In Figure 3.10, we show NOONs from two CC methods, RCCSD and CCVB-SD. As was noted before, RCCSD and CCVB-SD show qualitative differences when the system is strongly correlated.[141, 142] In particular, RCCSD clearly overcorrelates and likely exhibits non-variationality.[142] These trends are well reflected in Figure 3.10. The NOONs of the HONO and the LUNO are (1.35, 0.65) and (1.68, 0.32) for RCCSD and CCVB-SD, respectively. These two sets of NOONs show clear differences in that RCCSD exhibits far more open-shell character than does CCVB-SD. We also note that the CCVB-SD value (1.68, 0.32) is comparable to NOONs of an acene of

length 12 we studied in ref. 142. This is quite substantial strong correlation.

Method	STO-3G/R	STO-3G/U	cc-pVTZ
OOMP2	6.45 (0.18)	N/A	10.76 (0.30)
SCS-OOMP2	6.24 (0.17)	N/A	9.75 (0.27)
SOS-OOMP2	5.66 (0.16)	6.17 (0.17)[1]	8.52 (0.24)
κ-OOMP2	2.31 (0.06)	5.58 (0.15)[1]	6.94 (0.19)[1]
RCCSD	8.23 (0.23)	N/A	
CCVB-SD	6.65 (0.18)	N/A	

Table 3.5: Number of unpaired electrons (NUE) of C_{36} computed from various methods. For SOS-OOMP2 and κ-OOMP2 with STO-3G, we present NUE for both restricted and unrestricted solutions. The first value corresponds to the restricted one and the second corresponds to the unrestricted one. The numbers in parentheses are NUE per carbon atom. STO-3G/R indicates restricted calculations with STO-3G while STO-3G/U indicates unrestricted calculations with STO-3G. The cc-pVTZ calculations are done with spin-unrestricted calculations and broken symmetry solutions are indicated by a superscript 1. [1] Spin-unrestricted solutions.

We present the NUEs computed from the various methods examined here in Table 3.5. Compared to Table 3.3, all the NUEs are smaller with C_{36} than with C_{60}. However, this is simply due to the fact that there are more electrons in C_{60}. With a proper normalization (i.e., NUE per C atom), it is clear that C_{60} exhibits less open-shell character than C_{36}.

For OOMP2 methods, the open-shell character increases going from STO-3G to cc-pVTZ. Although HONO and LUNO exhibit less polarization, the other orbitals exhibit more open-shell character with a larger basis set. This can be understood as having more dynamic correlation effects and smaller correlation within a valence space in the cc-pVTZ basis set.

Comparing NUEs of RCCSD and CCVB-SD clearly suggests that RCCSD overcorrelates the system. Therefore, this also suggests that C_{36} is strongly correlated.

3.4.3 The Nature of Electron Correlation in C_{20}

Lastly, we obtain the landscape of symmetry breaking of a smaller fullerene, C_{20}. We have established that all three probes we used yield a consistent conclusion for C_{60} and C_{36}. Therefore, we believe that it is sufficient to use this single probe to obtain an answer to a qualitative question: is C_{20} strongly correlated?

Jahn-Teller distorted structures

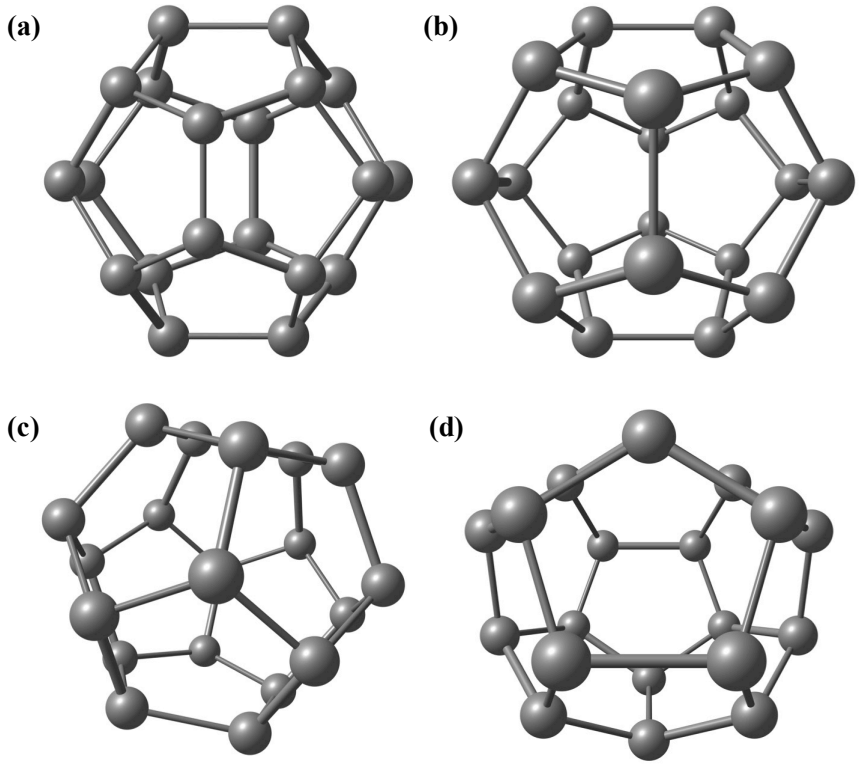

Figure 3.11: Four Jahn-Teller distorted isomers of C_{20}: (a) C_{2h}, (b) D_{2h}, (c) C_i, and (d) D_{3h}.

C_{20} has attracted a lot of attention since it is the smallest possible fullerene suggested by graph-theoretic analyses.[302] The existence of its cage geometry was controversial for some time,[303–310] but eventually it was experimentally observed in 2000.[271] Since then, there have been a lot of quantum chemistry studies of C_{20} which focus on relative energetics of different conformers such as bowl, cage, and ring.[297, 311–316] Here we focus on multiple Jahn-Teller distorted conformations of the cage geometry (C_{2h}, D_{2h}, C_i, and D_{3h}).

Manna and Martin carried out a careful study of relative energies among the Jahn-Teller distorted conformers of C_{20}. [316] They used state-of-the-art wavefunction methods in conjunction with high-quality density functional theory calculations. We took molecular geometries of C_{20} from ref. 316 which were optimized with PBE0 and the cc-pVTZ basis set. These geometries are shown in Figure 3.11. Our focus in this section is on the artificial symmetry breaking in these molecules. We studied these

within the cc-pVDZ basis set[237] along with the appropriate auxiliary basis set.[238] In Table 3.6, we present the classification of HF solutions of these molecules. Since they are commonly thought of as closed-shell molecules, it is striking that RHF is always unstable under spin-symmetry breaking for these molecules.

Geometry	$\hat{K}$	$\hat{S}^2$	$\hat{S}_{\mathbf{n}}$	Stuber-Paldus	$\langle S^2 \rangle_0$	ξ_0	μ_0
C_{2h}	Broken	Broken	Broken	cGHF	5.395	1.117	0.816
D_{2h}	Broken	Broken	Broken	cGHF	5.397	1.626	0.818
C_i	Broken	Broken	Conserved	cUHF	5.101	1.074	0.000
D_{3h}	Broken	Broken	Conserved	cUHF	5.100	1.247	0.000

Table 3.6: Classification of HF solutions of C_{20} isomers along with the corresponding $\langle S^2 \rangle_0$, ξ_0, and μ_0. The subscript 0 denotes that these properties are computed at the HF level.

We will first discuss the cGHF solutions found in C_{2h} and D_{2h}. Although the two geometries differ by 29 mE_h in terms of the nuclear repulsion energy, the cGHF energies differ only by 10 μE_h. This means that the nuclear configurations are very different but the total energy, which includes nuclear repulsion energy and electronic energy, is nearly degenerate. While this accidental near-degeneracy is surprising, the appearance of non-collinear solutions is also striking since this molecule should be considered closed-shell.[297, 303, 308, 317] We will now see how regularized OOMP2 restores this artificial symmetry breaking starting from these broken symmetry solutions as a function of the regularization strength.

In Figure 3.12, $\langle S^2 \rangle$, ξ, and μ are plotted as a function of κ for C_{2h} and D_{2h} geometries. Although two cGHF solutions exhibit quantitative similarity in $\langle S^2 \rangle$, ξ, and μ as shown in Table 3.6, κ_c values for each quantity shows a qualitative difference.

In the case of the C_{2h} geometry (Figure 3.12 (a)), κ_c values are 1.00, 0.80 and 0.80 for $\langle S^2 \rangle$, ξ, and μ, respectively. This suggests that for $\kappa \in [0.80, 1.00]$ there are unrestricted solutions for this system. Moreover, the symmetry restoration of complex and non-collinearity occurs at the same time. The $\langle S^2 \rangle$ restoration requires stronger MP2 correlation energies than ξ and μ. The D_{2h} geometry exhibits a different behavior. The κ_c values for $\langle S^2 \rangle$, ξ, and μ are 1.00, 1.00, and 0.80, respectively. In this case, for $\kappa \in [0.80, 1.00]$ there are complex, unrestricted solutions. The U to G symmetry breaking is easier to restore than complex and unrestriction based on the relative magnitude of κ_c values. These κ_c values are in the artificial symmetry breaking range discussed in Section 3.3.1. Therefore, we conclude that this symmetry breaking is *artificial*.

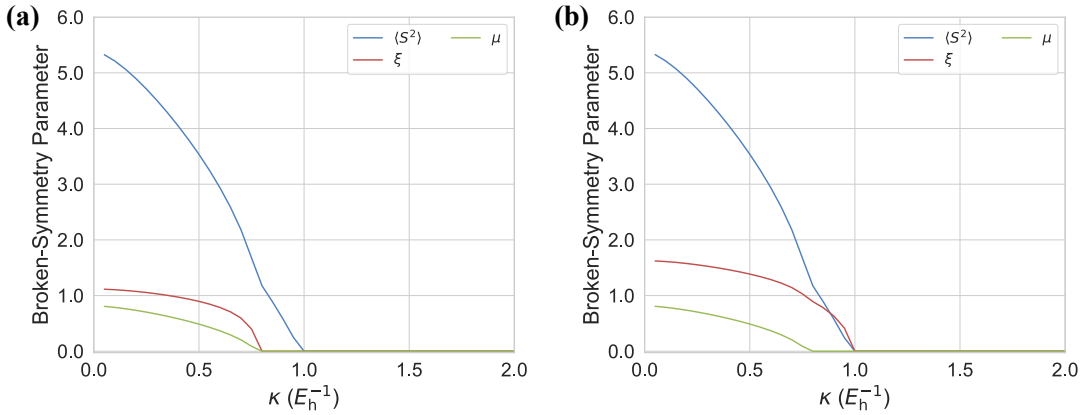

Figure 3.12: Measures of symmetry breaking ($\langle S^2 \rangle$, ξ, and μ) as a function of the regularization strength κ for (a) C_{20} (C_{2h}) and (b) C_{20} (D_{2h}). The plots characterize symmetry-breaking/restoration in κ-OOMP2.

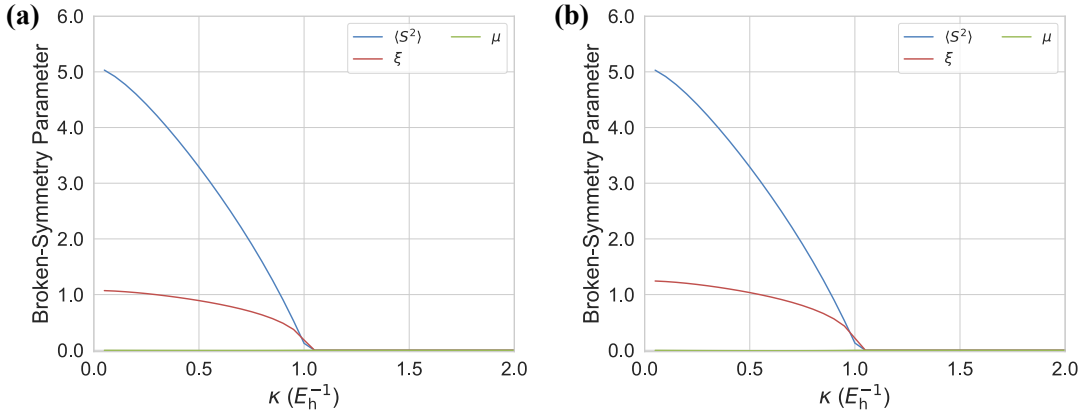

Figure 3.13: Measures of symmetry breaking ($\langle S^2 \rangle$, ξ, and μ) as a function of the regularization strength κ for (a) C_{20} (C_i) and (b) C_{20} (D_{3h}). The plots characterize symmetry-breaking/restoration in κ-OOMP2.

There are a total of two cUHF solutions in the C_i and D_{3h} geometries. The nuclear repulsion energies of these molecules differ by 29 mE_h and the cUHF solutions differ only by 10 μE_h. This appearance of electronic degeneracy is similar to the two cGHF solutions of the same molecule. In Figure 3.13, the three measures of symmetry breaking is shown as a function of κ for these two geometries. Clearly, μ is zero at every regularization strength so there is no generalized solution for these geometries. Although there were qualitative differences in κ_c between C_{2h} and D_{2h},

C_i and D_{3h} show identical κ_c values for $\langle S^2 \rangle$ and ξ. The κ_c values are 1.05 for both of the symmetries, which is in the artificial symmetry breaking range. Therefore, this symmetry breaking should also be considered *artificial*.

We emphasize these findings about four different geometries of C_{20} agree with previous studies by others[297, 303, 308, 317]: C_{20} is a singlet closed-shell molecule and there is no strong correlation in this molecule as long as the geometry is Jahn-Teller distorted.

Dodecahedral (I_h) Structure

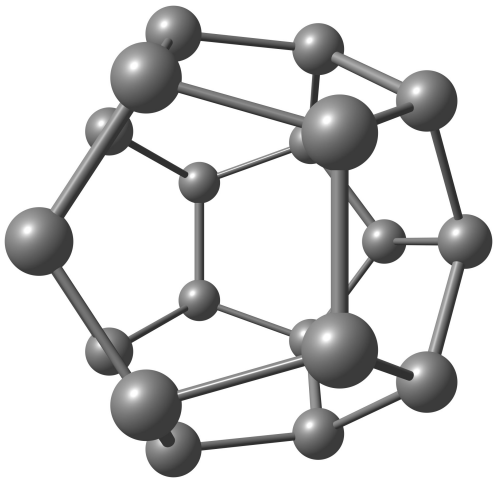

Figure 3.14: The dodecahedral molecular structure of C_{20}.

It is possible to force strong correlation by enforcing a higher symmetry. It is very likely that small fluctuations would be sufficient to break any degeneracies present in a higher symmetry and results into a more stable and lower symmetry geometry. This is the origin of commonly observed Jahn-Teller distortions. It is very surprising that a dodecahedral geometry (I_h) was found to be the global minimum with cGHF in the work by Jiménez-Hoyos et al.[272] We took the geometry from their work (shown in Figure 3.14) and ran the same analysis to see how symmetry breaking plays a role in describing the electron correlation of this molecule.

In Figure 3.15, we present a symmetry breaking landscape of the dodecahedral geometry. It has more structure than other previous cases. There is a discontinuous jump in μ going from $\kappa = 1.05$ to $\kappa = 1.10$. This is due to the existence of two distinct low-lying solutions: complex, generalized and complex, unrestricted solutions. The gap between these two competing solutions is controlled by κ and around $\kappa = 1.10$

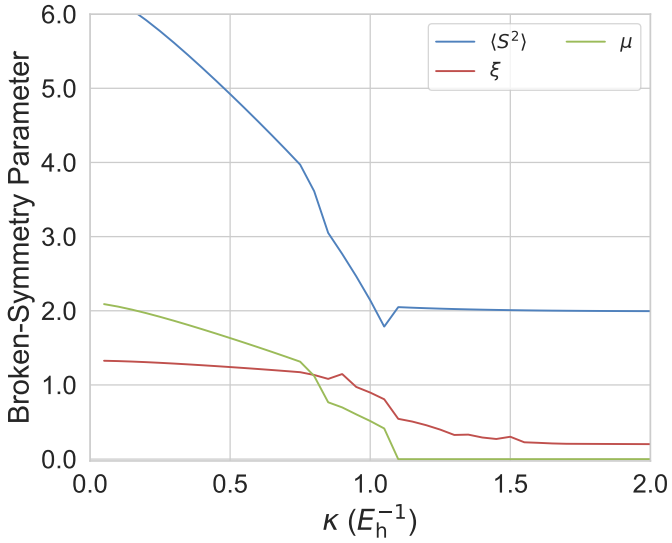

Figure 3.15: Measures of symmetry breaking ($\langle S^2 \rangle$, ξ, and μ) as a function of the regularization strength κ for C_{20} with a dodecahedral geometry. The plots characterize symmetry-breaking/restoration in κ-OOMP2.

the relative energetics becomes reversed. For $\kappa > 1.10$, cU solutions are found to be the lowest energy solution.

$\langle \hat{S} \rangle$ suggests that a triplet state (with complexity) is the ground state of this system for reasonable κ values. At $\kappa = 1.45$, we examined the energy lowering from complexity by comparing the energy between U and cU solutions. We found that these solutions are degenerate as well.

This intricate landscape of symmetry breaking indicates that the system is likely strongly correlated under this geometry. Furthermore, a definitive answer to this question was obtained from equation-of-motion spin-flip coupled-cluster with singles and doubles (EOM-SF-CCSD) within the cc-pVDZ basis set starting from an $M_S = 1$ κ-OOMP2 orbitals. The $M_S = 1$ unrestricted CCSD calculation has $\langle \hat{S}^2 \rangle = 2.02$ which should serve as a good reference state for a subsequent spin-flip calculation. The EOM-SF-CCSD[318] calculation yielded a near-exact degeneracy between singlet and triplet states (i.e., near-zero singlet-triplet gap) and this strongly suggests that the system is strongly correlated. This is also consistent with the prediction by molecular orbital theory.[319]

Therefore, we confirm that the claim by Jiménez-Hoyos et al. is correct that C_{20} at the I_h geometry is strongly correlated. The next question is then whether this geometry is the actual ground state conformation of C_{20}. Given the near-zero singlet-

triplet gap of the I_h geometry, C_{20} would be quite reactive and unstable. However, experimental findings suggest that C_{20} is not as reactive as a pure biradical.[320] It is likely that the global minimum structure would be one of the Jahn-Teller distorted structures or other structures such as bowl suggested in literature. We present the κ-OOMP2 energies of the five geometries of C_{20} examined here in Table 3.7. It is clear that the Jahn-Teller distorted geometries are nearly degenerate and the icosahedral geometry is higher in energy. However, these geometries were optimized with different levels of theory, so more conclusive results should be obtained with optimized geometries at κ-OOMP2. This would be an interesting research direction to pursue in the future.

Geometry	κ-OOMP2	Relative Energy
C_{2h} [1]	-759.15036	0.01
D_{2h} [1]	-759.15037	0.00
C_i [1]	-759.15032	0.03
D_{3h} [1]	-759.15030	0.04
I_h [2]	-759.12120	18.31

Table 3.7: κ-OOMP2 ($\kappa = 1.45$) energies (E_h) of C_{20} in the geometries examined in this work with the cc-pVDZ basis set and their relative energies (kcal/mol). [1] The geometry was taken from ref. 316 which was optimized with PBE0 and the cc-pVTZ basis set. [2] The geometry was taken from ref. 272 which was optimized with cGHF and the 6-31G(d) basis set.

3.5 Summary

We have presented an unbiased analysis to determine whether fullerenes, C_{20}, C_{36}, and C_{60}, are strongly correlated. At the Hartree-Fock level, this was already done based on the existence of complex, generalized Hartree-Fock (cGHF) solutions in the work by Jiménez-Hoyos et al. As it is common to observe artificial symmetry at the HF level in innocent (i.e., not strongly correlated) systems, we analyzed these solutions beyond the HF level. This was achieved with three different probes.

First, we used the recently developed regularized orbital-optimized second-order Møller-Plesset perturbation theory (κ-OOMP2) to obtain landscapes of symmetry breaking parameters for spin operators $\hat{S}^2$ and $\hat{S}_{\mathbf{n}}$ and complex operator $\hat{K}$ as a function of the regularization strength κ. The critical strength κ_c was then used to determine whether a given fullerene is strongly correlated. If κ_c is around 1.0, which

is far stronger than the optimal κ we determined in our previous work, we concluded that the symmetry breaking at the HF level is artificial.

Second, we obtained the singlet-triplet gaps of these fullerenes and quantified strong correlation in them. A singlet-triplet gap measures an energy cost of unpairing an electron pair and this energy cost should be small if the system has strong biradicaloid character.

Lastly, we studied strong correlation within a minimal basis using two coupled-cluster (CC) methods along with various unregularized OOMP2 methods and κ-OOMP2. The two methods used in this work are restricted CC with singles and doubles (RCCSD) and CC valence-bond with singles and doubles (CCVB-SD). Based on our previous work,[142] it is well understood that there is a qualitative difference between RCCSD and CCVB-SD when strong correlation is present. This qualitative difference was probed with natural orbital occupation numbers (NOONs). NOONs from CCVB-SD were in general qualitatively consistent with NOONs from κ-OOMP2 for the systems we considered in this work. Based on these three independent probes, we reached the following conclusions.

C_{60} is *not strongly correlated* and the symmetry breaking present in its cGHF solution is *artificial* based on all three probes. The critical κ values for each symmetry breaking is in the range of artificial symmetry breaking. Its singlet-triplet gap is large in both experiments and computations. Furthermore, RCCSD and CCVB-SD show nearly identical behavior. Therefore, the molecule should be described as a closed shell molecule. This is not surprising due to the fact that it is electron paramagnetic resonance silent and found stable in experiments. This then contradicts the conclusion drawn by Jiménez-Hoyos and co-workers.

On the other hand, C_{36} within the D_{6h} point group is strongly correlated. In particular, it is a singlet biradicaloid where unrestricted treatment in conjunction with Yamaguchi's approximate projection can be used to obtain a qualitatively (and even quantitatively) correct answer. The cGHF solution found by Jiménez-Hoyos et al is likely an artifact due to the limited treatment of electron correlation: the complex and $\langle \hat{S}_{\mathbf{n}} \rangle$ symmetry breakings are *artificial*. However, since breaking $\langle \hat{S}^2 \rangle$ symmetry was found to be *essential*, we conclude that this system is strongly correlated. The singlet-triplet gap of this molecule was found to be small and a qualitative difference between the NOONs of RCCSD and CCVB-SD was observed. All three probes indicate that the symmetry breaking in C_{36} is *essential* and C_{36} is strongly correlated.

Lastly, we applied the first probe to the smallest fullerene C_{20}. A total of five geometries of C_{20} considered in this work all exhibit symmetry breaking. All of the Jahn-Teller distorted geometries (C_{2h}, D_{2h}, C_i, and D_{3h}) were found not to be strongly correlated and the underlying Hartree-Fock symmetry breaking is therefore *artificial*. On the other hand, the fully symmetric dodecahedral geometry (I_h) was

found to be strongly correlated. In particular, it exhibits a near-zero singlet-triplet gap.

It is the central message of this paper that not every symmetry breaking in a HF solution indicates strong correlation. Many symmetry breakings in Hartree-Fock are simply due to its lack of dynamic correlation, which can be properly recovered by perturbation theory such as MP2. κ-OOMP2 emerges as a method that captures dynamic correlation, and attenuates all strong correlation. This is visually evident in plots of NOONs for C_{60} for example (Figure 3.5(d)). As a result, κ-OOMP2 removes artificial symmetry breaking in its reference determinant. However, essential symmetry breaking due to lack of static (or strong) correlation remains. This is visually evident in plots of NOONs for C_{36} for example (Figure 3.9(d)). The analyses we presented here can be used to probe strong correlation in numerous chemical systems especially when one is unsure about using single-reference methods.

3.6 Appendix

The Appendix includes the equations for the correlated one-particle density matrix of MP2, the derivation for the non-collinearity test of MP1 wavefunctions and the orbital Hessian of cGHF wavefunctions.

3.6.1 One-Particle Density Matrix of MP2

For OOMP2 methods, we compute the correlated 1PDM using

$$P_{ij}^{(2)} = -\frac{1}{2}\sum_{abk}(t_{ik}^{ab})^* t_{jk}^{ab} \tag{3.11}$$

$$P_{ab}^{(2)} = \frac{1}{2}\sum_{ijc}(t_{ij}^{ac})^* t_{ij}^{bc}. \tag{3.12}$$

where the first is the MP2 correction to the occupied-occupied (OO) block of the 1PDM and the second is the correction to the virtual-virtual (VV) block. For κ-OOMP2, the amplitudes used in Eq. (3.11) and Eq. (3.12) are regularized. Moreover, κ-OOMP2 has an extra term to the OO and VV blocks,

$$X_{ij} = -\kappa\int_0^1 \mathrm{d}\tau e^{\tau\kappa\epsilon_i}(\omega_{ij}^* + \omega_{ji})e^{(1-\tau)\kappa\epsilon_j} \tag{3.13}$$

$$Y_{ab} = \kappa\int_0^1 \mathrm{d}\tau e^{-\tau\kappa\epsilon_a}(\omega_{ab} + \omega_{ba}^*)e^{-(1-\tau)\kappa\epsilon_b} \tag{3.14}$$

where ω_{ij} and ω_{ab} are defined as follows:

$$\omega_{ij} = \sum_{aP} e^{-\tau\kappa\epsilon_a} V_{ia}^P \tilde{\Gamma}_{aj}^P \tag{3.15}$$

and

$$\omega_{ab} = \sum_{iP} e^{\tau\kappa\epsilon_i} \tilde{\Gamma}_{ai}^P V_{ib}^P \tag{3.16}$$

where V_{ia}^P is the 3-center 2-electron integrals and $\tilde{\Gamma}_{ai}^P$ reads

$$\tilde{\Gamma}_{ai}^P = \sum_{jb} t_{ij}^{ab} V_{jb}^P \tag{3.17}$$

The resulting κ-OOMP2 1PDM is then obtained by summing the usual MP2 contribution and the regularization correction terms (Eq. (3.13) and Eq. (3.14)). In other words, we have

$$\tilde{P}_{ij}^{(2)} = P_{ij}^{(2)} + X_{ij} \tag{3.18}$$

$$\tilde{P}_{ab}^{(2)} = P_{ab}^{(2)} + Y_{ab} \tag{3.19}$$

These $\tilde{P}_{ij}^{(2)}$ and $\tilde{P}_{ab}^{(2)}$ are the *relaxed* 1PDMs of κ-OOMP2. More details are available in ref. 269.

3.6.2 Non-Collinearity Test of MP1 Wavefunctions

In order to perform the non-collinearity test on an MP1 wavefunction, one needs first-order corrections to $\langle \hat{S}_i \rangle$ and $\langle \hat{S}_i \hat{S}_j \rangle$ where $i, j \in \{x, y, z\}$. The first-order correction to $\langle \hat{O} \rangle$ for an operator $\hat{O}$ is defined as follows:

$$\langle \hat{O} \rangle_1 = \langle \Psi_1 | \hat{O} | \Psi_0 \rangle + \langle \Psi_0 | \hat{O} | \Psi_1 \rangle. \tag{3.20}$$

This can be derived from the derivative with respect to λ of the first-order MP energy expression $E^{(1)}$ with a modified Hamiltonian, $\hat{H} + \lambda \hat{O}$. We enumerate the expectation value of each spin operator using this formula. For $\langle \hat{S}^2 \rangle$, one may use the following identity:

$$\hat{S}^2 = \hat{S}_z + \hat{S}_z^2 + \hat{S}_- \hat{S}_+, \tag{3.21}$$

where

$$\hat{S}_z = \frac{1}{2} \sum_p \left(\hat{a}_{p_\alpha}^\dagger \hat{a}_{p_\alpha} - \hat{a}_{p_\beta}^\dagger \hat{a}_{p_\beta} \right) \tag{3.22}$$

$$\hat{S}_+ = \hat{S}_x + i\hat{S}_y = \sum_p \hat{a}^\dagger_{p_\alpha}\hat{a}_{p_\beta} \tag{3.23}$$

$$\hat{S}_- = \hat{S}_x - i\hat{S}_y = \sum_p \hat{a}^\dagger_{p_\beta}\hat{a}_{p_\alpha} \tag{3.24}$$

One can evaluate $\langle \hat{S}_i \hat{S}_j \rangle$ for $i, j \in \{x, y\}$ using $\langle \hat{S}_i \hat{S}_j \rangle$ for $i, j \in \{+, -\}$. We choose to work with these ladder operators for simplicity.

With a cGHF reference, the zeroth order expectation values are as follows:[277, 278]

$$\langle \hat{S}_z \rangle_0 = \frac{1}{2}\sum_i \left(\langle i_\alpha | i_\alpha \rangle - \langle i_\beta | i_\beta \rangle\right) \tag{3.25}$$

$$\langle \hat{S_+} \rangle_0 = \langle \hat{S_-} \rangle_0^* = \sum_i \langle i_\alpha | i_\beta \rangle \tag{3.26}$$

$$\begin{aligned}\langle \hat{S}_z^2 \rangle_0 =& \frac{1}{4}\sum_i \left(\langle i_\alpha | i_\alpha \rangle + \langle i_\beta | i_\beta \rangle\right) \\ &+ \frac{1}{4}\sum_{ij}\sum_{\sigma\in\{\alpha,\beta\}} \left(\langle i_\sigma | i_\sigma \rangle \langle j_\sigma | j_\sigma \rangle - \langle i_\sigma | j_\sigma \rangle \langle j_\sigma | i_\sigma \rangle\right) \\ &+ \frac{1}{4}\sum_{ij} \left(\langle i_\beta | j_\beta \rangle \langle j_\alpha | i_\alpha \rangle - \langle i_\alpha | i_\alpha \rangle \langle j_\beta | j_\beta \rangle + \text{h.c.}\right)\end{aligned} \tag{3.27}$$

$$\langle \hat{S}_- \hat{S}_+ \rangle_0 = \sum_i \langle i_\beta | i_\beta \rangle + \sum_{ij} \left(\langle i_\alpha | i_\beta \rangle \langle j_\beta | j_\alpha \rangle - \langle i_\beta | j_\alpha \rangle \langle j_\alpha | i_\beta \rangle\right) \tag{3.28}$$

$$\langle \hat{S}_+ \hat{S}_- \rangle_0 = \sum_i \langle i_\alpha | i_\alpha \rangle + \sum_{ij} \left(\langle i_\alpha | i_\beta \rangle \langle j_\beta | j_\alpha \rangle - \langle i_\beta | j_\alpha \rangle \langle j_\alpha | i_\beta \rangle\right) \tag{3.29}$$

$$\langle \hat{S}_- \hat{S}_- \rangle_0 = \langle \hat{S}_+ \hat{S}_+ \rangle_0^* = \sum_{ij} \left(\langle i_\beta | i_\alpha \rangle \langle j_\beta | j_\alpha \rangle - \langle j_\beta | i_\alpha \rangle \langle i_\beta | j_\alpha \rangle\right) \tag{3.30}$$

$$\begin{aligned}\langle \hat{S}_+ \hat{S}_z \rangle_0 = \langle \hat{S}_z \hat{S}_- \rangle_0^* =& -\frac{1}{2}\sum_i \langle i_\alpha | i_\beta \rangle + \frac{1}{2}\sum_{ij} \left(\langle i_\alpha | i_\beta \rangle \langle j_\alpha | j_\alpha \rangle - \langle j_\alpha | i_\beta \rangle \langle i_\alpha | j_\alpha \rangle\right) \\ &- \frac{1}{2}\sum_{ij} \left(\langle i_\alpha | i_\beta \rangle \langle j_\beta | j_\beta \rangle - \langle i_\beta | j_\beta \rangle \langle j_\alpha | i_\beta \rangle\right)\end{aligned} \tag{3.31}$$

$$\begin{aligned}\langle \hat{S}_- \hat{S}_z \rangle_0 = \langle \hat{S}_z \hat{S}_+ \rangle_0^* =& \frac{1}{2}\sum_i \langle i_\beta | i_\alpha \rangle + \frac{1}{2}\sum_{ij} \left(\langle i_\beta | i_\alpha \rangle \langle j_\alpha | j_\alpha \rangle - \langle i_\alpha | j_\alpha \rangle \langle j_\beta | i_\alpha \rangle\right) \\ &- \frac{1}{2}\sum_{ij} \left(\langle i_\beta | i_\alpha \rangle \langle j_\beta | j_\beta \rangle - \langle i_\beta | j_\beta \rangle \langle j_\beta | i_\alpha \rangle\right)\end{aligned} \tag{3.32}$$

where we used the fact that each orbital is of the spinor form in Eq. (3.6) and we define

$$\langle p_{\sigma_1}|q_{\sigma_2}\rangle = \int_{\mathbf{r}} (\phi_p^{\sigma_1}(\mathbf{r}))^* \phi_q^{\sigma_2}(\mathbf{r}). \tag{3.33}$$

We note that there is no spin integration in Eq. (3.33). These are used to compute the covariance matrix $A_{ij} = \langle \hat{S}_i \hat{S}_j \rangle - \langle \hat{S}_i \rangle \langle \hat{S}_j \rangle$. As noted before, the eigenspectrum of $\mathbf{A}$ determines whether the GHF wavefunction is genuinely non-collinear. The wavefunction is collinear if and only if there is a zero eigenmode.

Similarly, the first-order corrections to these expectation values can be obtained from

$$\langle \hat{O} \rangle_1 = \frac{1}{4} \sum_{ijab} \left(t_{ij}^{ab}\right)^* \langle \Psi_{ij}^{ab} | \hat{O} | \Psi_0 \rangle + \frac{1}{4} \sum_{ijab} \langle \Psi_0 | \hat{O} | \Psi_{ij}^{ab} \rangle t_{ij}^{ab} \tag{3.34}$$

This can be easily computed as follows:

$$\langle \hat{S}_z \rangle_1 = \langle \hat{S}_+ \rangle_1 = \langle \hat{S}_- \rangle_1 = 0 \tag{3.35}$$

$$\begin{aligned} \langle \hat{S}_z^2 \rangle_1 = \frac{1}{4} \sum_{\substack{i<j \\ a<b}} \left(t_{ij}^{ab}\right)^* \sum_{\sigma \in \{\alpha,\beta\}} (2\langle a_\sigma | i_\sigma \rangle \langle b_\sigma | j_\sigma \rangle - 2\langle a_\sigma | j_\sigma \rangle \langle b_\sigma | i_\sigma \rangle) \\ + \frac{1}{4} \sum_{\substack{i<j \\ a<b}} \left(t_{ij}^{ab}\right)^* (-2\langle a_\alpha | i_\alpha \rangle \langle b_\beta | j_\beta \rangle + 2\langle a_\beta | j_\beta \rangle \langle b_\alpha | i_\alpha \rangle \\ - 2\langle a_\beta | i_\beta \rangle \langle b_\alpha | j_\alpha \rangle + 2\langle a_\alpha | j_\alpha \rangle \langle b_\beta | i_\beta \rangle) + \text{h.c.} \end{aligned} \tag{3.36}$$

$$\begin{aligned} \langle \hat{S}_- \hat{S}_+ \rangle_1 = \langle \hat{S}_+ \hat{S}_- \rangle_1 = \sum_{\substack{i<j \\ a<b}} (t_{ij}^{ab})^* (\langle a_\beta | i_\alpha \rangle \langle b_\alpha | j_\beta \rangle - \langle a_\alpha | j_\beta \rangle \langle b_\beta | i_\alpha \rangle \\ + \langle a_\alpha | i_\beta \rangle \langle b_\beta | j_\alpha \rangle - \langle a_\beta | j_\alpha \rangle \langle b_\alpha | i_\beta \rangle) + \text{h.c.} \end{aligned} \tag{3.37}$$

$$\begin{aligned} \langle \hat{S}_- \hat{S}_- \rangle_1 = \langle \hat{S}_+ \hat{S}_+ \rangle_1^* = \sum_{\substack{i<j \\ a<b}} (t_{ij}^{ab})^* \left(2\langle a_\beta | i_\alpha \rangle \langle b_\beta | j_\alpha \rangle - 2\langle a_\beta | j_\alpha \rangle \langle b_\beta | i_\alpha \rangle\right) \\ + \sum_{\substack{i<j \\ a<b}} (t_{ij}^{ab}) \left(2\langle i_\beta | a_\alpha \rangle \langle j_\beta | b_\alpha \rangle - 2\langle j_\beta | a_\alpha \rangle \langle i_\beta | b_\alpha \rangle\right) \end{aligned} \tag{3.38}$$

$$\begin{aligned}\langle \hat{S}_+ \hat{S}_z \rangle_1 = \langle \hat{S}_z \hat{S}_- \rangle_1^* = \frac{1}{2} \sum_{\substack{i<j \\ a<b}} (t_{ij}^{ab})^* (&\langle a_\alpha | i_\beta \rangle \langle b_\alpha | j_\alpha \rangle - \langle a_\alpha | j_\alpha \rangle \langle b_\alpha | i_\beta \rangle \\ &+ \langle a_\alpha | i_\alpha \rangle \langle b_\alpha | j_\beta \rangle - \langle a_\alpha | j_\beta \rangle \langle b_\alpha | i_\alpha \rangle - \langle a_\alpha | i_\beta \rangle \langle b_\beta | j_\beta \rangle \\ &+ \langle a_\beta | j_\beta \rangle \langle b_\alpha | i_\beta \rangle - \langle a_\beta | i_\beta \rangle \langle b_\alpha | j_\beta \rangle + \langle a_\alpha | j_\beta \rangle \langle b_\beta | i_\beta \rangle) \\ + \frac{1}{2} \sum_{\substack{i<j \\ a<b}} t_{ij}^{ab} (&\langle i_\alpha | a_\alpha \rangle \langle j_\alpha | b_\beta \rangle - \langle j_\alpha | a_\beta \rangle \langle i_\alpha | b_\alpha \rangle \\ &+ \langle i_\alpha | a_\beta \rangle \langle j_\alpha | b_\alpha \rangle - \langle j_\alpha | a_\alpha \rangle \langle i_\alpha | b_\beta \rangle - \langle i_\beta | a_\beta \rangle \langle j_\alpha | b_\beta \rangle \\ &+ \langle j_\alpha | a_\beta \rangle \langle i_\beta | b_\beta \rangle - \langle i_\alpha | a_\beta \rangle \langle j_\beta | b_\beta \rangle + \langle j_\beta | a_\alpha \rangle \langle i_\alpha | b_\beta \rangle)\end{aligned} \tag{3.39}$$

$$\begin{aligned}\langle \hat{S}_- \hat{S}_z \rangle_1 = \langle \hat{S}_z \hat{S}_+ \rangle_1^* = \frac{1}{2} \sum_{\substack{i<j \\ a<b}} (t_{ij}^{ab})^* (&\langle a_\beta | i_\alpha \rangle \langle b_\alpha | j_\alpha \rangle - \langle a_\alpha | j_\alpha \rangle \langle b_\beta | i_\alpha \rangle \\ &+ \langle a_\alpha | i_\alpha \rangle \langle b_\beta | j_\alpha \rangle - \langle a_\beta | j_\alpha \rangle \langle b_\alpha | i_\alpha \rangle - \langle a_\beta | i_\alpha \rangle \langle b_\beta | j_\beta \rangle \\ &+ \langle a_\beta | j_\beta \rangle \langle b_\beta | i_\alpha \rangle - \langle a_\beta | i_\beta \rangle \langle b_\beta | j_\alpha \rangle + \langle a_\beta | j_\alpha \rangle \langle b_\beta | i_\beta \rangle) \\ + \frac{1}{2} \sum_{\substack{i<j \\ a<b}} t_{ij}^{ab} (&\langle i_\alpha | a_\alpha \rangle \langle j_\beta | b_\beta \rangle - \langle j_\beta | a_\alpha \rangle \langle i_\alpha | b_\alpha \rangle \\ &+ \langle i_\beta | a_\alpha \rangle \langle j_\alpha | b_\alpha \rangle - \langle j_\alpha | a_\alpha \rangle \langle i_\beta | b_\alpha \rangle - \langle i_\beta | a_\beta \rangle \langle j_\beta | b_\alpha \rangle \\ &+ \langle j_\beta | a_\alpha \rangle \langle i_\beta | b_\beta \rangle - \langle i_\beta | a_\alpha \rangle \langle j_\beta | b_\beta \rangle + \langle j_\beta | a_\beta \rangle \langle i_\beta | b_\alpha \rangle)\end{aligned} \tag{3.40}$$

3.6.3 Complex Generalized HF

The variation in the energy expression reads

$$\begin{aligned}\delta E = \sum_{ia} (-h_{ai} \delta\Theta_{ia} - h_{ia} \delta\Theta_{ia}^*) - \frac{1}{2} \sum_{ija} \Big(&\langle ij \parallel aj \rangle \, \delta\Theta_{ia}^* + \langle ij \parallel ia \rangle \, \delta\Theta_{ja}^* \\ &+ \langle aj \parallel ij \rangle \, \delta\Theta_{ia} + \langle ia \parallel ij \rangle \, \delta\Theta_{ja} \Big)\end{aligned} \tag{3.41}$$

where $\delta\Theta_{ia}$ is an infinitesimal orbital rotation. This energy variation can be used to compute orbital gradient and similarly orbital hessian.

Orbital Gradient

We compute the gradient of E with respect to the real and imaginary part of $\mathbf{\Theta}$,

$$\frac{\partial E}{\partial \mathrm{Re}(\Theta_{ia})} = -\left[h_{ai} + J_{ai} - K_{ai}\right] + \mathrm{h.c.} = -h_{ai} - \sum_k \langle ak||ik\rangle - h_{ia} - \sum_k \langle ik||ak\rangle \quad (3.42)$$

$$\frac{\partial E}{\partial i\mathrm{Im}(\Theta_{ia})} = -\left[h_{ai} + J_{ai} - K_{ai}\right] - \mathrm{h.c.} = -h_{ai} - \sum_k \langle ak||ik\rangle + h_{ia} + \sum_k \langle ik||ak\rangle \quad (3.43)$$

Orbital Hessian

Similarly, the variation of orbital gradient reads

$$\begin{aligned}\delta\frac{\partial E}{\partial \mathrm{Re}(\Theta_{ia})} =& \sum_j \left(-h_{ji}\delta\Theta^*_{ja} + h_{ab}\delta\Theta^*_{bi}\right) + \sum_k \left(-\sum_j \delta\Theta^*_{aj}\langle jk||ik\rangle + \sum_b \delta\Theta^*_{bi}\langle ak||bk\rangle\right) \\ &+ \sum_{kb} \delta\Theta^*_{bk}\langle ak||ib\rangle + \sum_{kb}\delta\Theta_{bk}\langle ab||ik\rangle + \mathrm{h.c.} \end{aligned} \quad (3.44)$$

and

$$\begin{aligned}\delta\frac{\partial E}{\partial i\mathrm{Im}(\Theta_{ia})} =& \sum_j \left(-h_{ji}\delta\Theta^*_{ja} + h_{ab}\delta\Theta^*_{bi}\right) + \sum_k \left(-\sum_j \delta\Theta^*_{aj}\langle jk||ik\rangle + \sum_b \delta\Theta^*_{bi}\langle ak||bk\rangle\right) \\ &+ \sum_{kb} \delta\Theta^*_{bk}\langle ak||ib\rangle + \sum_{kb}\delta\Theta_{bk}\langle ab||ik\rangle - \mathrm{h.c.} \end{aligned} \quad (3.45)$$

These are then used to obtain orbital hessian:

$$\begin{aligned}\frac{\partial^2 E}{\partial \mathrm{Re}(\Theta_{ia})\partial \mathrm{Re}(\Theta_{jb})} =& \Bigg[-\delta_{ab}\left(h_{ji} + \sum_k \langle jk||ik\rangle\right) + \delta_{ij}\left(h_{ab} + \sum_k \langle ak||bk\rangle\right) \\ &+ \langle aj||ib\rangle + \langle ab||ij\rangle\Bigg] + h.c \end{aligned} \quad (3.46)$$

$$\begin{aligned}\frac{\partial^2 E}{\partial i\mathrm{Im}(\Theta_{ia})\partial i\mathrm{Im}(\Theta_{jb})} =& \Bigg[\delta_{ab}\left(h_{ji} + \sum_k \langle jk||ik\rangle\right) - \delta_{ij}\left(h_{ab} + \sum_k \langle ak||bk\rangle\right) \\ &- \langle aj||ib\rangle + \langle ab||ij\rangle\Bigg] + h.c \\ =& -\frac{\partial^2 E}{\partial \mathrm{Im}(\Theta_{ia})\partial \mathrm{Im}(\Theta_{jb})} \end{aligned} \quad (3.47)$$

$$\frac{\partial^2 E}{\partial \mathrm{Im}(\Theta_{ia})\partial \mathrm{Re}(\Theta_{jb})} = i\left[-\langle aj||ib\rangle + \langle ab||ij\rangle - h.c.\right] \tag{3.48}$$

$$\frac{\partial^2 E}{\partial \mathrm{Re}(\Theta_{ia})\partial \mathrm{Im}(\Theta_{jb})} = -i\left[-\langle aj||ib\rangle + \langle ab||ij\rangle - h.c.\right] \tag{3.49}$$

Chapter 4

Two Single-Reference Approaches to Singlet Biradicaloid Problems

4.1 Introduction

Strong correlation is usually associated with multiple open-shell electrons that are antiferromagnetically coupled into a low-spin state.[321–323] For instance, molecular magnets with multiple metal centers,[144, 324–327] non-innocent ligands,[328, 329] metalloenzymes,[129–131] and oligoacenes[142, 330–332] exhibit strong correlation. Of such cases, singlet biradicaloids exhibit the simplest form of strong correlation.[244, 245, 333–337] As this is usually outside the scope of single-reference electronic structure methods, it is common to employ multiconfigurational methods.[58, 338, 339] A brute-force approach to treat this strong correlation is complete active space self-consistent field (CASSCF) with an active space of two electrons in two orbitals (2e, 2o). However, CASSCF does not incorporate electron correlation outside the active space so subsequent dynamic correlation treatments[112, 118, 340] are necessary for quantitatively correct answers. A related single reference approach is to start from the triplet single determinant (i.e., $M_S = 1$) and flip a spin to access the $M_S = 0$ manifold, either using configuration interaction (CI)[325, 341–344] or coupled-cluster (CC) via the equation of motion approach.[318, 334, 345]

Alternatively, one could try to treat such systems using single-reference methods with the help of *essential* symmetry breaking. It is essential in the sense that the qualitative character of a single-determinant wavefunction is fundamentally wrong without essential breaking. A majority of *essential* symmetry breaking is spin-restricted (R) to spin-unrestricted (U) symmetry breaking, namely spin-polarization. In the case of singet biradicaloids, such essential symmetry breaking can be combined with

Yamaguchi's approximate spin-projection (AP) to produce spin-pure energies.[246, 346–352] The applicability of AP is dependent on whether the underlying wavefunction contains only one contaminant. It is an exact projection only if there is one single contaminant. This sets a limit to $\langle \hat{S}^2 \rangle$ of broken-symmetry $M_S = 0$ solutions to be effective for AP: $0.0 \leq \langle \hat{S}^2 \rangle \leq 2.0$.

UHF is heavily spin-contaminated for most biradicaloids. For instance, this was observed by us in the heptazethrene dimer (HZD) where broken-symmetry UHF yields $\langle \hat{S}^2 \rangle = 6.3$ in the cc-pVDZ basis set.[269] The subsequent correlation treatment based on these UHF solutions via second-order Møller-Plesset perturbation theory (MP2) is not effective in removing such heavy spin contamination. It is possible to employ orbital optimized MP2 (OOMP2) as an attempt to produce a reference determinant with only essential symmetry breaking (i.e., $\langle \hat{S}^2 \rangle \approx 1.0$). However, it is likely that OOMP2 produces a divergent solution or a restricted solution that is unphysically low in energy if not divergent.[199, 203] As a solution to this problem, we employed regularized OOMP2 (κ-OOMP2) to treat HZD. [269] In contrast to our previous δ-OOMP2 (regularized with a constant level-shift), κ-OOMP2 determines the strength of regularization of individual correlation energy contributions depending on the orbital energy gap associated with them. κ-OOMP2, in turn, achieves both the recovery of Coulson-Fischer points[213] and favorable thermochemistry performance, which was found to be challenging for δ-OOMP2 to achieve.[203] Returning to the HZD example, κ-OOMP2 with unrestricted orbitals (κ-UOOMP2) produces $\langle \hat{S}^2 \rangle = 1.2$ which is well-suited for subsequent AP treatment. Generally speaking, κ-UOOMP2 with AP (AP+κ-UOOMP2) is a simple and robust way to treat biradicaloids which captures both static and dynamic correlation. We will further highlight this particular combination of AP and κ-UOOMP2 later in this work.

A rather rarer class of *essential* symmetry breaking, which is another focus of this work, is real, R to complex, R (cR) symmetry breaking. This is referred to as "complex-polarization" in this work. Complex polarization was known for many years in the context of some strongly correlated molecules such as O_2 ($^1\Delta_g$).[353–361] Our group established its connection to generalized valence bond perfect pairing (GVB-PP)[362] using the complex pairing theorem.[279] When such solutions exist, complex restricted Hartree-Fock (cRHF) can indeed capture some aspects of GVB-PP and behaves qualitatively better than RHF. It was shown that the subsequent correlation treatment, cRMP2, yields quantitatively more accurate results than RMP2 for systems examined in ref. 279. Moreover, cRMP2 outperformed UMP2 especially when there is a strong mixing between singlet and triplet states.

Our recent work illustrated a way to obtain such essential symmetry breaking with κ-OOMP2.[363] Therein we discussed how to remove *artificial* spin-polarization using κ-OOMP2 with complex, generalized (cG) orbitals. It is artificial because

orbital optimization in the presence of dynamic correlation such as MP2 (or other approaches for approximate Brückner orbitals) may remove such symmetry breaking. Artificial symmetry breaking occurs at the HF level not due to the lack of ability to describe strong correlation but because of the lack of dynamic correlation treatment. In ref. 363, we show that it is possible to distinguish artificial and essential symmetry breaking based on κ-OOMP2. Interested readers are referred to ref. 363 and we will further review some aspects of this relevant to this work in Section 4.2.2. In addition to *essential* spin-symmetry breaking, it is also possible to explore *essential* complex-polarization within the κ-OOMP2 method, which will combine the strengths of cRMP2 and κ-OOMP2. Namely, κ-cROOMP2 is able to describe multireference systems whenever complex-polarization is relevant.

For general biradicaloid systems, it is natural to consider AP and cR methods as simple single-reference alternatives to multi-reference and spin-flip methods. In particular, these are far simpler to implement than typical multi-reference second-order perturbation theory.[112, 118] Compared to AP, cR methods offer more straightforward formalisms for response theory. For example, cRMP2 has the identical response theory formalism to that of usual MP2 and there is no need to derive additional terms. The analytic nuclear derivatives of AP methods have been derived and implemented at the mean-field level,[346, 347, 350, 351] but there has been no study on response theory of correlated wavefunction methods with AP. While the formal and practical simplicity of cR methods is very desirable, its limited applicability due to the rareness of cR solutions makes it less appealing.

In this work we will explore several biradicaloid systems that exhibit cRHF solutions and discuss the applicability of κ-cROOMP2 and AP+κ-UOOMP2. In particular, we will compare κ-cROOMP2 and AP+κ-UOOMP2 in these systems and discuss the similarities and differences between them. For simplicity, we will limit our discussion to HF, MP2 and κ-OOMP2 although other variants of MP2 and OOMP2, such as spin-component scaled methods,[170, 171] can also be combined with cR orbitals or AP.

4.2 Theory

We will use $i, j, k, l, \cdots$ to index occupied orbitals, $a, b, c, d, \cdots$ to index virtual orbitals, and $p, q, r, s, \cdots$ to index either of those two.

4.2.1 Review of cRHF and Complex Polarization

The complex restricted Hartree-Fock (cRHF) energy is given by

$$E_{\mathrm{HF}} = 2\,\mathrm{tr}\,(\mathbf{PH}_0) + 2\,\mathrm{tr}\,(\mathbf{PJ}) - \mathrm{tr}\,(\mathbf{PK}) + E_{\mathrm{nuc}} \tag{4.1}$$

where $\mathbf{P}$ is the one-particle reduced density matrix (1PDM), $\mathbf{H}_0$ is the one-electron Hamiltonian, $\mathbf{J}$ and $\mathbf{K}$ are the Coulomb and exchange matrices, and E_{nuc} is the nuclear repulsion energy. In cRHF, we allow the molecular orbital (MO) coefficient matrix $\mathbf{C}$ to be complex and as a result $\mathbf{P}$ may become complex. As mentioned in ref. 279, a cRHF solution is "fundamentally complex" if and only if the norm of the imaginary part of $\mathbf{P}$ is non-zero.

The use of complex restricted (cR) orbitals for multi-reference problems has been known for many years in electronic structure theory[353–361] but they have been rarely employed in practice. The major reason for this underappreciation is due to the rareness of genuine cR solutions. Small et al. established the connection between cRHF and GVB-PP and as a result, we have a better understanding of why cR solutions are rare and when to expect them.[279]

Within a single pair of electrons, the R to cR instability is driven by the energy lowering due to a PP-like (or CAS(2,2)-like) configuration. However, a cRHF wavefunction also necessarily contains an open-shell singlet (OSS)-like configuration which is usually energetically high. The competition between the PP-like contribution (energy-lowering versus R) and the OSS-like contribution (energy-raising versus R) determines the R to cR instability. When the PP stabilization is greater than the OSS energetic cost, we observe the R to cR instability. This is, however, not very common to observe and this explains the rareness of cRHF solutions. As we will see, some singlet biradicaloids exhibit complex-polarization and therefore cRHF can serve as a faithful starting point for subsequent correlation treatments. The relative energetics between PP-like terms and OSS-like terms change in the presence of correlation treatment. Therefore, it is reasonable to expect that some cRHF solutions are *artificial* and they would lead to cRMP2 energies that are much higher than RMP2. We will encounter an example that demonstrates this later in the paper.

It is useful to run internal stability analysis to ensure the local stability of cRHF solutions. We provide the electronic Hessian of the energy expression in Eq. (4.1) in Appendix.

4.2.2 Regularized OOMP2 with cR orbitals: κ-cROOMP2

The MP2 energy expression with cRHF orbitals reads

$$E_{\text{cRMP2}} = E_{\text{HF}} + \sum_{ijab} \tau_{ij}^{ab} \, (ia|jb) \tag{4.2}$$

where i and j are occupied spatial orbitals, a and b are unoccupied spatial orbitals, $(ia|jb)$ represents the two-electron four-center integrals and the spin-adapted amplitudes τ are

$$\tau_{ij}^{ab} = -\frac{2\,(ia|jb)^* - (ib|ja)^*}{\Delta_{ij}^{ab}}. \tag{4.3}$$

Δ_{ij}^{ab} is a positive energy denominator defined as

$$\Delta_{ij}^{ab} = \epsilon_a + \epsilon_b - \epsilon_i - \epsilon_j, \tag{4.4}$$

where ϵ_p denotes canonical orbital energies. Orbital optimization of Eq. (4.2) yields orbital-optimized MP2 (OOMP2). As mentioned in Section 4.1, OOMP2 has two major issues that limits its applicability. First, as we optimize orbitals in the presence of correlation energy, Δ_{ij}^{ab} can become very small and the resulting energy can become non-variational and even approach divergence.[199] Second, as a result OOMP2 may *unphysically* prefer restricted solutions and remove the Coulson-Fischer point.[203] Our group has developed a regularization scheme which fixes these two major issues in OOMP2.[269]

The orbital-energy-dependent regularization introduced in ref. 269 modifies the two-electron integrals in the correlation energy contribution in Eq. (4.2). The resulting κ-cRMP2 energy expression reads

$$E_{\kappa\text{-cRMP2}} = E_{HF} + \sum_{ijab} \tilde{\tau}_{ij}^{ab*} \, (ia|jb) \, (1 - e^{-\kappa\Delta_{ij}^{ab}}) \tag{4.5}$$

where the regularized amplitudes are

$$\tilde{\tau}_{ij}^{ab} = \tau_{ij}^{ab}(1 - e^{-\kappa\Delta_{ij}^{ab}}) \tag{4.6}$$

Orbital optimizing Eq. (4.5) defines the κ-OOMP2 method (in this case κ-cROOMP2). It is immediately obvious that the correlation energy can no longer diverge even when $\Delta_{ij}^{ab} = 0$. Based on carbon-carbon single, double, and triple bond breaking, we showed that the Coulson-Fischer point is recovered. Combining recovery of Coulson-Fischer points with reasonable performance for a thermochemistry benchmark, $\kappa = 1.45$ was recommended for chemical applications.[269] We also showed

that $\kappa \in [1.0, 2.0]$ (which comfortably includes $\kappa = 1.45$ in the middle) yields only *essential* symmetry breaking and can remove *artificial* HF symmetry breaking in fullerenes.[363] This is because κ-OOMP2 describes dynamic correlation, but regularization has removed the inaccurate description of static correlation present in conventional MP2.

Distinguishing artificial and essential symmetry breaking based on κ-OOMP2 may seem arbitrary. However, in ref. 363 we compared this diagnosis of strong correlation with other approaches such as natural orbital occupation numbers and more sophisticated coupled-cluster methods. All these three independent probes suggested that C_{60} is not strongly correlated and C_{36} is strongly correlated. As such, κ-OOMP2 can reliably probe the underlying symmetry breaking and answer whether it is artificial (not strongly correlated) or essential (strongly correlated). κ-OOMP2 will be used to probe essential symmetry breaking and strong correlation in another fullerene C_{30} below.

The implementation of κ-cROOMP2 was accomplished closely following the spin-orbital implementation described in ref. 269. We apply the resolution-of-the-identity approximation to $(ia|jb)$,

$$(ia|jb) = \sum_{PQ} (ia|P) (P|Q)^{-1} (Q|jb) = \sum_{P} (ia|P) C_{jb}^{P} \tag{4.7}$$

where P and Q are auxiliary basis indices and we define the expansion coefficients of an occupied-virtual product $|jb)$ as:

$$C_{jb}^{P} = \sum_{Q} (P|Q)^{-1} (Q|jb) \tag{4.8}$$

The spin-adapted two-particle density matrix (2PDM) consists of two parts: one is the usual MP2 2PDM contribution,

$$\Gamma_{ai}^{P} = 2 \sum_{jb} C_{jb}^{P} \tilde{\tau}_{ij}^{ab}, \tag{4.9}$$

and another is the modification due to the regularizer,

$$\tilde{\Gamma}_{ai}^{P} = 2 \sum_{jb} C_{jb}^{P} \tilde{\tau}_{ij}^{ab} e^{-\kappa(\epsilon_b - \epsilon_j)} \tag{4.10}$$

Similarly, the spin-adapted 1PDM also consists of two parts: the first is the usual MP2 1PDM contributions,

$$P_{ij}^{(2)} = -2 \sum_{abk} (\tilde{\tau}_{ik}^{ab})^* \frac{(ka|jb)^*}{\Delta_{ij}^{ab}} \tag{4.11}$$

$$P_{ca}^{(2)} = 2\sum_{ijb}(\tilde{\tau}_{ij}^{ab})^* \frac{(ic|jb)^*}{\Delta_{ij}^{cb}} \tag{4.12}$$

and the second is the modification from the regularizer,

$$\tilde{P}_{ij}^{(2)} = -\kappa \int_0^1 \mathrm{d}\tau e^{\tau\kappa\epsilon_i}(\omega_{ij}^* + \omega_{ji})e^{(1-\tau)\kappa\epsilon_j} = -(\omega_{ij}^* + \omega_{ji})\left(\frac{e^{\kappa\epsilon_i} - e^{\kappa\epsilon_j}}{\epsilon_i - \epsilon_j}\right) \tag{4.13}$$

$$\tilde{P}_{ab}^{(2)} = \kappa \int_0^1 \mathrm{d}\tau e^{-\tau\kappa\epsilon_a}(\omega_{ab} + \omega_{ba}^*)e^{-(1-\tau)\kappa\epsilon_b} = (\omega_{ab} + \omega_{ba}^*)\left(\frac{e^{-\kappa\epsilon_a} - e^{-\kappa\epsilon_b}}{\epsilon_b - \epsilon_a}\right) \tag{4.14}$$

where the definition of ω_{ij} and ω_{ab} follows:

$$\omega_{ij} = \sum_{aP} e^{-\kappa\epsilon_a}(ia|P)\tilde{\Gamma}_{aj}^{P} \tag{4.15}$$

and

$$\omega_{ab} = \sum_{iP} e^{\kappa\epsilon_i}\tilde{\Gamma}_{ai}^{P}(ib|P) \tag{4.16}$$

These spin-adapted quantities can be used to produce appropriate orbital gradients for orbital optimization. Interested readers are referred to ref. 269 for more technical details. In passing we mention that Eq. (4.13) and Eq. (4.14) were computed via a one-dimensional Legendre quadrature previously,[269] but in the pseudocanonical basis, it can be done analytically as shown above.

We apply the frozen-core approximation to the systems considered in this paper. This adds orbital rotation parameters between frozen core and occupied orbitals to the orbital optimization problem. We present the pertinent orbital gradient equations and explain some numerical difficulties we encountered with this optimization problem in the Appendix.

4.2.3 Yamaguchi's Approximate Spin-Projection

The approximate spin-projection method proposed by Yamaguchi [246] has been widely used in a wide variety of strong correlation problems.[246, 346–352] Its working equation is very simple and it usually takes at most two separate single point calculations for two different M_S values to perform the projection. When projecting a triplet state out of an $M_S = 0$ broken symmetry solution, one can use the following equation which is derived using $\langle S^2 \rangle$:

$$E_{S=0} = \frac{E_{\mathrm{BS}} - (1-\alpha)E_{S=1}}{\alpha} \tag{4.17}$$

where the spin-coupling coefficient α is

$$\alpha = \frac{\langle S^2 \rangle_{S=1} - \langle S^2 \rangle_{\mathrm{BS}}}{\langle S^2 \rangle_{S=1} - \langle S^2 \rangle_{S=0}} \tag{4.18}$$

There are multiple ways to obtain $E_{S=1}$ and $\langle S^2 \rangle_{S=1}$. The simplest way is to use a high spin $M_S = 1$ calculation to obtain $E_{S=1}$ at the same level of theory as E_{BS}. Therefore, we need a total of two unrestricted calculations, $M_S = 0$ and $M_S = 1$. Evidently, if the singlet is heavily spin-contaminated the above spin-coupling equation is no longer valid. Furthermore, we need a nearly spin-pure value of $\langle S^2 \rangle$ for the $M_S = 1$ state. As we shall see later, κ-UOOMP2 can accomplish these objectives.

4.3 Applications

We will study multiple biradicaloid systems that have one pair of electrons that exhibit *essential* complex-polarization or spin-polarization. In other words, the singlet ground state of these systems involve a pair of open-shell electrons. Throughout the examples presented below, we will see how κ-cROOMP2 and/or AP+κ-UOOMP2 can be used for these singlet biradicaloids and also compare their strengths and weaknesses.

All calculations were performed with a development version of Q-Chem.[236] For κ-OOMP2 methods, we took a stable HF solution as an initial set of orbitals unless mentioned otherwise. All plots were generated with `Matplotlib` [283] and all molecular figures were generated with `Chemcraft`.[284]

4.3.1 TS12 Set: Triplet-Singlet Gaps

We will consider triplet-singlet gaps ($\Delta E_{\text{T-S}} = E_{\mathrm{S}} - E_{\mathrm{T}}$) of atoms and diatomics whose ground state is triplet. Systems with a triplet ground state are likely to have a (near) degeneracy between highest occupied molecular orbital (HOMO) and lowest unoccupied molecular orbital (LUMO) so these are also likely to have near-degenerate OSS-like and PP-like configurations. Therefore, for these molecules, there is a good chance for *essential* complex polarization to occur.

We will compare HF, MP2, and κ-OOMP2 methods with different types of orbitals for treating the singlet ground state of the following molecules: C, NF, NH, NO^-, O_2, O, PF, PH, S_2, S, Si, and SO. The reference triplet-singlet gaps as well as the equilibrium bond length of diatomics for each electronic state were taken from

the NIST Chemistry WebBook.[364] Individual references for these experimental values and geometries are given in the Appendix. We validated the experimental gaps against near-exact full configuration interaction calculations using the heat-bath algorithm developed by Holmes and co-workers.[365] The theoretical estimation lies within 1.0 kcal/mol of the experimental values and we provide these data in the Appendix. This data set will be referred to as the "TS12" set for the rest of this manuscript.

In benchmarking HF, MP2, and κ-OOMP2 methods, we employed the aug-cc-pVQZ basis set[237, 366] along with its auxiliary basis set.[238] The frozen core approximation was used for all correlated wavefunction calculations. Unrestricted orbitals are used for the triplet state ($M_S = 1$).

	$M_S = 0$	$M_S = 1$	Triplet	Singlet
C	1.018	2.010	^{3}P	^{1}D
NF	1.015	2.023	$X^3\Sigma^-$	$a^1\Delta$
NH	1.012	2.017	$X^3\Sigma^-$	$a^1\Delta$
NO^-	1.031	2.052	$X^3\Sigma^-$	$a^1\Delta$
O_2	1.023	2.049	$X^3\Sigma_g^-$	$a^1\Delta_g$
O	1.009	2.009	^{3}P	^{1}D
PF	1.047	2.035	$X^3\Sigma^-$	$a^1\Delta$
PH	1.039	2.029	$X^3\Sigma^-$	$a^1\Delta$
S_2	1.062	2.060	$X^3\Sigma_g^-$	$a^1\Delta_g$
S	1.033	2.013	^{3}P	^{1}D
Si	1.047	2.015	^{3}P	^{1}D
SO	1.051	2.058	$X^3\Sigma^-$	$a^1\Delta$

Table 4.1: The UHF $\langle S^2 \rangle$ values of the molecules in the test set considered in this work and the term symbol for each electronic state considered in the TS12 set.

For the molecules in the TS12 set, using real, restricted orbitals for the singlet ground state is fundamentally incorrect as it cannot capture the biradicaloid character of the singlet ground state. UHF orbitals are heavily spin-contaminated as the singlet ground state is a strong biradicaloid. This is well illustrated in Table 4.1. The $M_S = 0$ states exhibit $\langle S^2 \rangle = 1.0$ which indicates nearly perfect singlet biradicals. The $M_S = 1$ states are more or less spin-pure which validates the use of UHF orbitals for $M_S = 1$ states. Therefore, UHF and UMP2 are expected to perform very poorly on this test set. However, all these $\langle S^2 \rangle$ values are very well-suited for the AP approach. Therefore, one may expect that AP+UMP2 and AP+κ-UOOMP2

perform similarly well. We will see whether these predictions are indeed true in the TS12 set.

	Expt.	RHF	UHF	RMP2	UMP2
C	29.14	26.59	-15.37	13.85	-13.58
NF	34.32	31.54	-14.80	10.99	-17.23
NH	35.93	30.59	-16.72	15.90	-17.29
NO^-	17.30	29.60	-2.11	5.53	-7.74
O_2	22.64	32.54	-5.45	6.15	2.72
O	45.37	34.72	-22.79	19.71	-22.10
PF	20.27	25.37	-11.89	10.80	-9.06
PH	21.90	24.35	-11.93	11.66	-10.17
S_2	13.44	21.03	-5.70	4.48	-5.01
S	26.41	26.52	-15.75	14.21	-12.19
Si	18.01	20.13	-11.77	10.12	-7.76
SO	18.16	24.77	-6.94	3.94	-9.84
RMSD	N/A	27.66	13.04	11.60	12.42
MSD	N/A	27.31	-11.77	10.61	-10.77

Table 4.2: The experimental triplet-singlet gap $\Delta E_{\text{T-S}}(= E_S - E_T)$ (kcal/mol) of various atoms and diatomics and the deviation (kcal/mol) in $\Delta E_{\text{T-S}}$ obtained with HF and MP2 using restricted and unrestricted orbitals. RMSD stands for root-mean-square-deviation and MSD stands for mean-signed-deviation.

First, we discuss HF and MP2 with real, restricted (R) and real, unrestricted orbitals (U). The results of these methods are presented in Table 4.2. Based on the mean-signed-deviation (MSD) of each method, it is evident that restricted orbitals overestimate the gap whereas unrestricted orbitals underestimate the gap. This suggests that the singlet ground state of these molecules is too high in energy when described by R orbitals and too low in energy when described by U orbitals. This is expected for RHF because closed-shell electronic structure produced by R orbitals should be less stable than an open-shell one. It is also expected for UHF, as the triplet ground state is lower in energy than the singlet ground state, triplet-singlet spin contamination lowers the energy of $M_S = 0$ unrestricted state. With the MP2 level of correlation, these failures of R and U orbitals do not disappear. RMP2 has an RMSD of 11.60 kcal/mol and UMP2 has an RMSD of 12.42 kcal/mol.

How does κ-OOMP2 change this conclusion? As long as R or U orbitals are employed, very similar behavior is observed. As it is typical for RMP2 to overestimate correlation energies for singlet biradicaloids, we expect κ-ROOMP2 to produce larger

	κ-ROOMP2	κ-UOOMP2
C	15.71	-13.97
NF	12.07	-17.31
NH	17.46	-17.04
NO^-	10.59	-6.71
O_2	11.18	-10.18
O	20.67	-22.02
PF	14.06	-9.85
PH	14.68	-10.53
S_2	10.34	-5.25
S	16.19	-12.86
Si	12.91	-9.43
SO	10.09	-8.54
RMSD	14.18	12.85
MSD	13.83	-11.97

Table 4.3: The deviation (kcal/mol) in $\Delta E_{\text{T-S}}(= E_S - E_T)$ obtained with different MP2 and OOMP2 methods with complex, restricted (cR) orbitals. RMSD stands for root-mean-square-deviation and MSD stands for mean-signed-deviation.

triplet-singlet gaps than those of RMP2. This is mainly due to the regularization which is more effective on the singlet states here. Since none of the systems exhibit *artificial* spin-symmetry breaking (as presented in Table 4.1), it is expected that κ-UOOMP2 methods do not significantly change the energetics of these systems.

In Table 4.3, we see that the κ-ROOMP2 gaps are all greater than the RMP2 gaps in Table 4.2, which confirms our prediction. For κ-UOOMP2, the gaps are all within 2 kcal/mol from those of UMP2 except O_2. In O_2, the difference between these two methods is 12.90 kcal/mol. This is due to the underlying *artificial* reflection spatial symmetry breaking in addition to the *essential* spin symmetry breaking in the UHF $M_S = 0$ solution. The *artificial* symmetry breaking is removed with κ-UOOMP2 while the essential one still persists.

We discuss whether these unrestricted states serve as reasonable bases to apply AP as well as whether cR orbitals can improve these catastrophic failures of HF, MP2, and κ-OOMP2 with R and U orbitals. The results of cR and AP methods are presented in Table 4.4. Neither cRHF nor AP+UHF produces satisfying results due to the lack of dynamic correlation. Moreover, cRHF and AP+UHF show significant differences in all molecules (the smallest difference is 4.21 kcal/mol and the largest one is 15.75 kcal/mol!). With MP2, cRMP2 is quite satisfying in that it has an

	cRHF	AP+UHF	cRMP2	AP+UMP2	κ-cROOMP2	AP+ κ-UOOMP2
C	9.83	-1.24	1.36	3.61	2.04	2.38
NF	12.71	4.86	-1.70	1.41	-1.28	0.93
NH	11.04	2.63	0.59	3.14	1.44	3.38
NO^-	17.42	13.21	-0.72	2.50	2.74	4.41
O_2	17.85	11.69	-2.26	29.34	1.50	3.02
O	10.44	-0.01	0.65	3.51	1.04	3.38
PF	12.62	-3.01	0.94	3.49	3.42	1.38
PH	11.41	-1.45	0.91	2.98	3.26	1.73
S_2	12.59	2.53	-1.70	4.22	3.22	3.33
S	11.22	-4.53	1.43	3.79	2.73	1.81
Si	9.10	-5.03	1.45	3.86	3.27	-0.18
SO	13.89	4.76	-3.49	-0.79	1.50	1.63
RMSD	12.78	5.98	1.64	9.00	2.45	2.58
MSD	12.51	2.03	-0.21	5.09	2.07	2.27

Table 4.4: The deviation (kcal/mol) in $\Delta E_{\text{T-S}}(= E_S - E_T)$ obtained with HF, MP2, and κ-OOMP2 with approximate spin-projection (AP) and complex, restricted (cR) orbitals. Note that the AP procedure was carried out using the first-order corrected spin expectation values in the case of UMP2 and κ-UOOMP2. RMSD stands for root-mean-square-deviation and MSD stands for mean-signed-deviation.

RMSD of 1.64 kcal/mol with an MSD of -0.21 kcal/mol. The TS12 set can indeed be described properly with cR orbitals. On the other hand, the performance of AP+UMP2 is somewhat disappointing as it is poorer than cRMP2. In particular, an error of 29.34 kcal/mol in the case of O_2 is a striking outlier. This is due to spatial symmetry breaking in UHF $M_S = 0$ which cannot be fixed by UMP2 but can be fixed by κ-UOOMP2. Other than O_2, we observe a non-negligible difference (5.92 kcal/mol) in S_2 which is also caused by spatial symmetry breaking in the UHF solution. All the other molecules exhibit 2-3 kcal/mol differences between these two methods.

Orbital optimization in the presence of MP2 yields significantly better AP results but κ-cROOMP2 produces slightly worse results than cRMP2. The slight degradation in performance of cRMP2 in κ-cROOMP2 shows an interesting trend. All data points show larger triplet-singlet gaps with κ-cROOMP2 than with cRMP2. This indicates that there may be some overcorrelation problems with cRMP2 which is being regularized by κ-cROOMP2. Given the substantially better performance of

κ-cROOMP2 compared to its R and U versions, this result is still very encouraging. Moreover, we emphasize that it is only κ-OOMP2 orbitals that yield quantitatively similar results between cR and AP approaches by harnessing only *essential* symmetry breaking.

For the rest of this work, we will further numerically show the quantitative similarity between AP+κ-UOOMP2 and κ-cROOMP2 beyond model systems.

4.3.2 Reactivity of Deprotonated Cysteine Ion with O_2 ($^1\Delta_g$)

There are not so many chemical systems for which cR methods can be a useful alternative to standard multi-reference methods. Any systems involving singlet oxygen (O_2 ($^1\Delta_g$)) are good candidates. In particular, singlet oxygen appears frequently in reactions in biological systems. [367] An example that we will study here is the reaction between an amino acid, cysteine (Cys) and singlet oxygen. Cys is one of the five amino acids that are susceptible to singlet oxygen attack.[368] Because of the multi-reference nature of singlet oxygen, studying reactivity of Cys is challenging for single-reference methods. As shown in Section 4.3.1, O_2 ($^1\Delta_g$) exhibits *essential* complex polarization. Therefore, this is an interesting example for comparing AP and cR approaches.

Lu et al. studied the reactivity of Cys ions with O_2 ($^1\Delta_g$) using Yamaguchi's AP.[159] As mentioned earlier, In the case of singlet oxygen, the only spin contaminant is the triplet ground state. Therefore, AP is well-suited for this case. What Lu and co-workers found is that the reactivity of Cys ions with singlet oxygen is much smaller than that of neutral Cys. This was shown by a high activation barrier along a reactive pathway.

We will study a reaction between deprotonated Cys ([Cys-H]$^-$) and singlet oxygen. Although there are multiple local minima geometries available, we investigated the lowest energy geometries from among those which Lu and co-workers reported. The molecular geometries of the precursor and transition state are shown in Figure 4.1. Lu and co-workers optimized the geometries at the level of B3LYP with the 6-31+G(d) basis set *with restricted orbitals*.

The precursor in Figure 4.1 has substantial open-shell character due to the presence of singlet oxygen, but the transition state (TS) is a closed-shell molecule because of the formation of a persulfoxide. It is possible that the geometry optimization of the precursor (Figure 4.1 (a)) may produce a qualitatively wrong geometry when performed with restricted orbitals. We independently investigated this using unrestricted orbitals and could not find a local minimum similar to Figure 4.1 (a). A

precise determination of the precursor geometry would be interesting to study in the future using cR orbitals or AP methods.

Nonetheless, for present purposes we studied this system using the RB3LYP geometries from those of Lu and co-workers for single point cR and AP calculations. We employed the cc-pVTZ basis set[237] and the associated auxiliary basis set.[238] For the computational efficiency, the frozen core approximation was used for correlated wavefunction calculations. The goal of our study is to demonstrate the power of cR orbitals in comparison to AP methods (and conventional R and U orbitals) for the open-shell singlet precursor geometry.

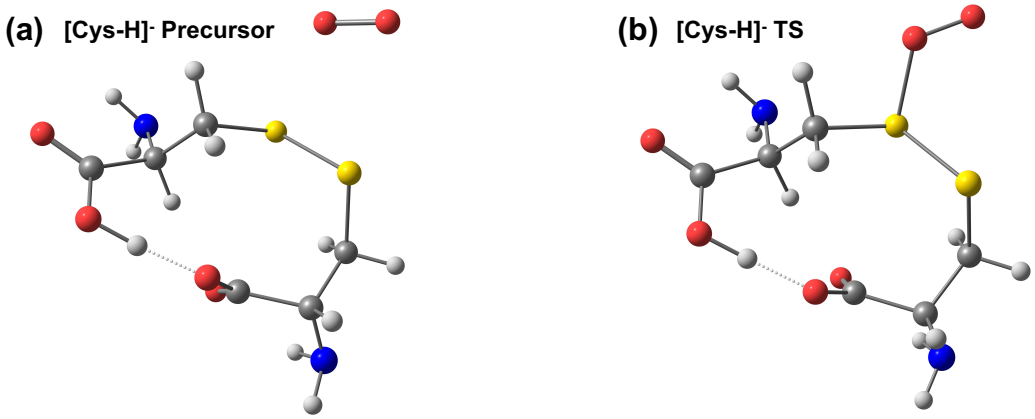

Figure 4.1: Molecular geometries for (a) the precursor and (b) the transition state (TS) for $[\text{Cys-H}]^- + O_2$. The Cartesian coordinates for each geometry were taken from ref. 159.

Method	ΔE	$\langle \hat{S}^2 \rangle_{M_S=0}$
RHF	9.79	0.000
cRHF	16.93	0.000
UHF	45.17	1.023
AP+UHF	33.71	

Table 4.5: The activation energy ΔE (kcal/mol) of $[\text{Cys-H}]^- + O_2$ from various types of HF. The expectation values of $\langle \hat{S}^2 \rangle$ for the $M_S = 0$ state of the precursor are presented as well.

We first discuss how different types of HF methods perform in predicting the reaction energy barrier (i.e., E(TS) - E(precursor)). We compare the use of R, U, and cR orbitals for the precursor. The precursor RHF energy should be much

higher than cRHF whereas the UHF energy should be too low since the triplet contaminant is much more stable. Therefore, a back-of-the-envelope estimation for the relative energy barrier ordering is RHF < cRHF < UHF. This is indeed supported by numerical results presented in Table 4.5.

The relative activation energy ordering will change based on the subsequent correlation treatment. For instance, UHF orbitals are heavily spin-contaminated so the subsequent UMP2 correlation energy will be underestimated, which then leads to a substantially smaller energy barrier than for UHF. Similarly, RHF orbitals should also lead to somewhat high energy when combined with MP2, which then yields a smaller energy barrier than that of cRMP2. Therefore, it is expected that the relative energy barrier ordering of MP2 methods is cR > R > U.

Method	ΔE	$\langle \hat{S}^2 \rangle_{M_S=0}$
RMP2	19.89	0.000
cRMP2	19.47	0.000
UMP2	4.04	1.024
AP+UMP2	-18.32	

Table 4.6: The activation energy ΔE (kcal/mol) of $[\text{Cys-H}]^-+\text{O}_2$ from various types of HF. The expectation values of $\langle \hat{S}^2 \rangle$ for the $M_S = 0$ state of the precursor are presented as well.

In Table 4.6, we observe the following trend instead: cR ≈ R > U. It is perhaps surprising that cR and R produce more or less the same energy barriers. There is quite strong complex polarization within a pair of electrons which led to a substantial energy lowering at the HF level. Evidently, despite the poor RHF reference, RMP2 recovers more correlation energy than cRMP2, perhaps because of overcorrelating small gap contributions.

Lastly, we note that there is a significant energy difference between AP+UMP2 and cRMP2 similar to the O_2 triplet-singlet gap result observed in Section 4.3.1. However, this is mainly due to the qualitative difference between cR and U solutions. Spin-contamination often drives artifacts in the spin-density distribution which cannot be easily fixed by a posteriori spin projection methods. However, this can potentially be fixed by orbital optimizing in the presence of correlation as we shall see.

In Table 4.7, we present the activation barrier obtained using various types of κ-OOMP2 methods and two popular, combinatorially optimized density functional theory (DFT) methods (ωB97X-V[369] and ωB97M-V[370]). First, we note that κ-cROOMP2 and AP+κ-UOOMP2 predict a barrier within 1 kcal/mol from each other.

Method	ΔE	$\langle \hat{S}^2 \rangle_{M_S=0}$
κ-ROOMP2	8.21	0.000
κ-cROOMP2	10.17	0.000
κ-UOOMP2	19.70	0.968
AP+κ-UOOMP2	9.30	0.000
UωB97X-V	24.72	0.970
AP+UωB97X-V	15.80	
UωB97M-V	20.42	0.943
AP+UωB97M-V	11.03	

Table 4.7: The activation energy ΔE (kcal/mol) of [Cys-H]$^-$+O_2 from various OOMP2 and DFT methods. The expectation values of $\langle \hat{S}^2 \rangle$ for the $M_S = 0$ state of the precursor are presented as well. Note that these values include correlation corrections to $\langle \hat{S}^2 \rangle$ wherever appropriate.

This is because the κ-UOOMP2 $M_S = 0$ state no longer has any artificial symmetry breaking and produces a solution with only essential spin-symmetry breaking. κ-ROOMP2 is similar to κ-OOMP2 with cR or AP despite the lack of open-shell character in the wavefunction. The R to cR instability at the κ-OOMP2 level causes an energy lowering of only about 2 kcal/mol. κ-UOOMP2 overestimates the gap by a factor of 2 compared to the corresponding AP results.

To see how well κ-cROOMP2 and AP+κ-UOOMP2 perform, we also compare this with two DFT methods. Without AP, both DFT methods with U orbitals predict the barrier too high. With AP, ωB97X-V predicts a barrier of 15.80 kcal/mol while ωB97M-V predicts a barrier of 11.03 kcal/mol. There is a quite significant functional dependence on the barrier height with the AP prescription (this may be related to the fact that $\langle \hat{S}^2 \rangle$ cannot be rigorously evaluated: the expectation value of the KS determinant is used). A barrier height of about 10 kcal/mol was obtained with κ-cROOMP2, AP+κ-cROOMP2, and AP+ωB97M-V and an even higher height with AP+ωB97X-V. All of these suggest that the reactivity of [Cys-H]$^-$ with O_2 ($^1\Delta_g$) is moderate at room temperature. In passing, we note that a higher level benchmark data would be desirable, using more sophisticated and computationally demanding methods such as equation of motion spin-flip coupled-cluster with singles and doubles (EOM-SF-CCSD).[318] This will be interesting to study in the future.

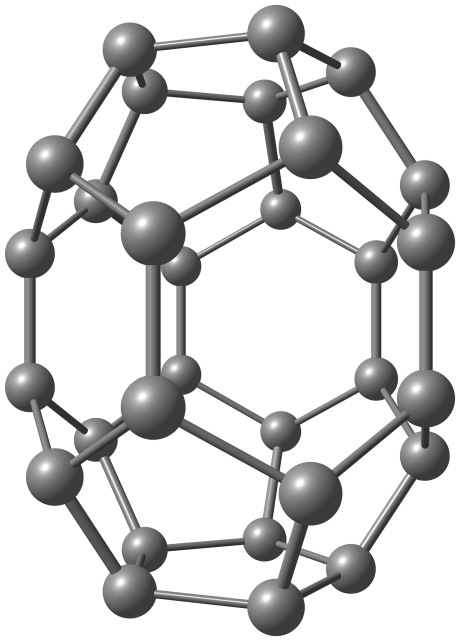

Figure 4.2: Molecular geometries of C_{30} (D_{5h}). The Cartesian coordinates for this geometry used in this work are provided in the Appendix.

4.3.3 Triplet-Singlet Gap of C_{30}

Fullerenes are an interesting class of molecular clusters that are made solely of carbon atoms. They all form intriguing cage structures and often are stable enough to be experimentally synthesized. C_{30} is one of the smaller fullerenes and it has been quite challenging to isolate C_{30} experimentally due to its instability. It was pointed out in several experimental[310] and theoretical[319, 371] studies that the highest symmetry structure, D_{5h}, is highly reactive. This particular molecular geometry is presented in Figure 4.2.

The molecular geometries used in this work are optimized with unrestricted B97M-V[372] for each M_S state, with D_{5h} geometry within the cc-pVDZ basis set.[237] As this system is biradicaloid, the geometry of the $M_S = 0$ state may require special care, but for simplicity we employed unrestricted calculations. The $\langle S^2 \rangle$ values of each state with this particular functional is 1.020 and 2.013, respectively. We provide the geometries of C_{30} used in this work in the Appendix. Details about the geometries will not alter the qualitative conclusion we are drawing in this section as long as the underlying point group symmetry is D_{5h}.

Jiménez-Hoyos and co-workers reported the existence of complex generalized HF

(cGHF) solutions for C_{30} (D_{5h}) and concluded that C_{30} is a polyradicaloid based on the cGHF solution.[272] Due to its pronounced strong correlation, it is not surprising to observe symmetry breaking at the HF level. However, one may wonder if breaking every symmetry from RHF to cGHF is *essential* since UHF is sufficient for most singlet biradicaloid systems.

We have developed a computational strategy which can identify *artificial* symmetry breaking at the HF level using κ-OOMP2 with cG orbitals.[363] We scan over a range of κ values (i.e., the regularization strength) and compute the critical regularization strength, κ_c, to break/restore a given symmetry. Symmetry breaking with $\kappa_c \in [0.0, 1.0]$ is categorized as *artificial* symmetry breaking, $\kappa_c \in [1.0, 2.0]$ is *essential* symmetry breaking, and symmetry restoration for $\kappa_c > 2.0$ may be considered to be *artificial* restoration (i.e., too little symmetry breaking). The symmetry landscape of C_{30} will help to identify the character of *essential* symmetry breaking in this system.

We obtained the symmetry breaking landscape of C_{30} within the 6-31G basis set[301] along with the cc-pVDZ auxiliary basis set.[238] The frozen core approximation was used for computational efficiency. We focused on three symmetry breaking parameters: the spin expectation value $\langle \hat{S}^2 \rangle$, the non-collinearity order parameter μ,[277] and the fundamental complexification measure ξ.[279, 363]

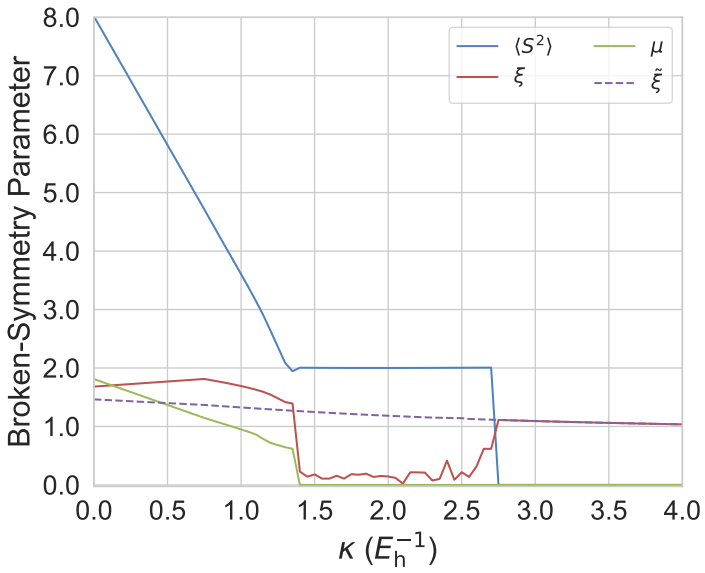

Figure 4.3: Measures of symmetry breaking ($\langle S^2 \rangle$, ξ, and μ) as a function of the regularization strength κ for C_{30} (D_{5h}). $\tilde{\xi}$ is the complex broken-symmetry parameter of κ-cROOMP2. These quantities characterize symmetry-breaking/restoration in κ-OOMP2.

In Figure 4.3, we see that $\kappa_c = 1.40$ for μ, $\kappa_c = 2.70$ for $\langle S^2 \rangle$, and there is no obvious symmetry restoration for ξ. Compared to our previous work on characterizing other fullerenes such as C_{60} and C_{36}, this landscape is more complex than the well-known biradicaloid C_{36}. Between $\kappa = 1.40$ and $\kappa = 2.70$, cU solutions are found. It is interesting that for $\kappa > 2.70$ cR solutions are most stable and there are no U or cU solutions. R solutions are commonly observed in the weak regularization regime, $\kappa > 2.0$, but cR solutions are quite unusual to observe. It turns out that this complex symmetry breaking in κ-cROOMP2 exists for all κ values as shown with the purple dashed line in Figure 4.3. With κ-cGOOMP2 with $\kappa < 2.70$, κ-cROOMP2 solutions are higher in energy than other spin symmetry broken solutions. This is why these solutions are only observed with very weak regularization in the landscape. Based on these results, we conclude that the symmetry breaking of $\langle S^2 \rangle$, ξ, and μ is *essential* and this molecule is strongly correlated.

Method	$\Delta E_{\text{T-S}}$	$M_S = 0$	$M_S = 1$
RHF	10.94	0.00	2.00
UHF	-13.07	7.18	8.15
cRHF	10.86	0.00	2.00
RMP2	-25.62	0.00	2.00
UMP2	-8.39	6.34	7.33
cRMP2	-27.50	0.00	2.00
κ-ROOMP2	5.36	0.00	2.00
κ-UOOMP2	1.84	1.02	2.00
κ-cROOMP2	3.93	0.00	2.00
AP+κ-UOOMP2	3.75		2.00

Table 4.8: The triplet-singlet gap $\Delta E_{\text{T-S}} (= E_S - E_T)$ (kcal/mol) of C_{30} from various methods. The expectation values of $\langle \hat{S}^2 \rangle$ for $M_S = 0$ and $M_S = 1$ states are presented as well. Note that these values include correlation corrections to $\langle \hat{S}^2 \rangle$.

We also computed the triplet-singlet gap of C_{30} using HF, MP2, and κ-OOMP2 methods with multiple types of orbitals. At $\kappa = 1.45$ with the cc-pVDZ basis set, we found a κ-cUOOMP2 solution (with $\langle S^2 \rangle = 2.0$) when started from a cGHF solution. This triplet κ-cUOOMP2 solution was found to be almost exactly degenerate with a triplet κ-UOOMP2 solution. Therefore, for the remaining discussion we employed κ-UOOMP2 for the triplet state.

The computed triplet-singlet gaps are presented in Table 4.8, which are obtained with the cc-pVTZ basis set. Without correlation, RHF and cRHF predict very large gaps with a triplet ground state whereas UHF predicts a large gap with a singlet

ground state. The MP2 correction on top of these reference states all prefers the singlet state with a significant spin gap. This is a qualitative failure of the MP2-level correlation treatment.

κ-OOMP2 provides a significant improvement over the MP2 results. κ-ROOMP2 predicts the sign of the gap correctly with a gap of 5.36 kcal/mol. κ-cROOMP2 yields a slightly smaller gap than κ-ROOMP2 and the energy lowering from complex polarization is only about 1.43 kcal/mol. κ-UOOMP2 yields almost a perfect open-shell solution (i.e., $\langle S^2 \rangle \approx 1.0$), so AP+$\kappa$-UOOMP2 is effective for this system. AP+κ-UOOMP2 predicts more or less the same gap as κ-cROOMP2 and the difference between two is only 0.18 kcal/mol. In terms of the triplet-singlet gap, all of the κ-OOMP2 approaches predict the biradicaloid character of C_{30}.

Although the triplet-singlet gap from the R methods is similar to the cR methods, the use of R orbitals breaks the spatial symmetry (D_{5h}) of C_{30}. This is evident when looking at the Mulliken population of individual carbon atoms. To illustrate this, we present the Mulliken population of the five carbon atoms in the top pentagon of C_{30} in Figure 4.2. Obviously, they are all equivalent due to the D_{5h} symmetry, but using restricted or unrestricted orbitals breaks this symmetry as shown in Table 4.9. Thus geometry optimization with other methods than cR methods will likely break this spatial symmetry. This is not because of the Jahn-Teller distortion but because of the *artificial* spatial symmetry breaking present at the electronic level. In passing we mention than orbital-optimizing the spin-projected energy in Eq. (4.17) could potentially yield qualitatively better density than κ-UOOMP2.[349]

RHF	UHF	cRHF	κ-ROOMP2	κ-UOOMP2	κ-cROOMP2
0.0083	0.0001	0.0179	-0.0027	0.0111	0.0099
0.0105	0.0001	0.0179	0.0067	0.0109	0.0099
0.0290	-0.0034	0.0179	0.0187	0.0093	0.0099
0.0290	0.0056	0.0179	0.0187	0.0120	0.0099
0.0105	-0.0034	0.0179	0.0067	0.0092	0.0099

Table 4.9: Mulliken population of the five carbon atoms in the top pentagon in C_{30} shown in Figure 4.2.

In summary, in this example we showed that κ-cROOMP2 is better suited than AP+κ-UOOMP2 in the presence of high point group symmetry such as D_{5h}. Although they both yield similar energies, the underlying wavefunction breaks spatial symmetry if not treated with cR orbitals. This highlights the unique utility of electronic structure methods with cR orbitals whenever complex polarization is *essential*.

4.3.4 Stable Organic Triplet Biradical

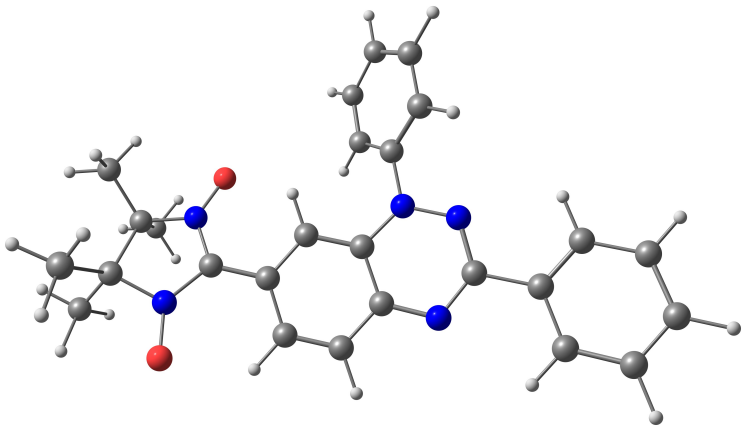

Figure 4.4: Molecular geometries of the organic biradical studied here. The Cartesian coordinates for this geometry used in this work are taken from ref. 373.

Although organic triplet biradicals are very rare to isolate due to their normally high reactivity, there have been some reports of synthesizing stable ones.[245, 374] Indeed, many stable singlet biradicaloids are stable because of some closed shell character.[244] Since triplet biradicals lack in any closed shell character, it is difficult to observe stable ones. Gallagher and co-workers synthesized an organic biradical with a triplet ground state.[373] This biradical has quite robust stability compared to usual biradicals and survives at 140 °C without significant decomposition. Experimentally the triplet-singlet gap of this molecule was measured to be about 0.5 kcal/mol. However, such a small gap allows for a thermal mixture of singlet and triplet states as temperature is raised to ambient conditions and above.

Gallagher and co-workers suggested a modification to this synthesized complex and hypothesized a triplet ground state, aiming for a larger triplet-singlet gap than 0.5 kcal/mol.[373] The structure of this proposed molecule is presented in Figure 4.4. They supported their claim using UB3LYP/6-31G(d,p) calculations which yielded a gap of 3.5 kcal/mol for this newly suggested complex. Our goal is to confirm whether this hypothesis is correct using κ-cROOMP2 and/or AP+κ-UOOMP2. We studied this system within the cc-pVDZ basis set[237] and its auxiliary basis set[238] with the frozen-core approximation and the geometries were taken from ref. 373 which

were optimized at the UB3LYP/6-31G(d,p) level. This proposed system was recently synthesized and characterized with $\Delta E_{TS} \geq 1.7$ kcal/mol.[375]

Unlike other examples presented above, there are no obvious symmetry constraints that give rise to a R to cR instability in this system. This is why it is interesting that there is a R to cR instability at the HF level (see Table 4.10). However, this complex polarization turns out to be *artificial* and κ-OOMP2 with $\kappa = 1.45$ yields only a restricted solution. Therefore, in this case κ-cROOMP2 is not applicable whereas AP+κ-UOOMP2 is well-suited.

Method	$\Delta E_{\text{T-S}}$	$M_S = 0$	$M_S = 1$
RHF	63.56	0.00	2.00
UHF	12.44	6.25	7.69
cRHF	63.49	0.00	2.00
RMP2	29.88	0.00	2.00
UMP2	-8.64	2.56	3.86
cRMP2	48.97	0.00	2.00
κ-UOOMP2	1.48	1.02	2.03
AP+κ-UOOMP2	2.97		2.00
κ-cR/ROOMP2	36.23	0.00	2.00

Table 4.10: The triplet-singlet gap $\Delta E_{\text{T-S}}(= E_S - E_T)$ (kcal/mol) of the biradical system in Figure 4.4 from various methods. The expectation values of $\langle \hat{S}^2 \rangle$ for $M_S = 0$ and $M_S = 1$ states are presented as well. Note that these values include correlation corrections to $\langle \hat{S}^2 \rangle$.

In Table 4.10, the triplet-singlet gap of this system is presented. At the HF level, none of the orbital types predict small enough gaps to be considered to be a biradical. RHF and cRHF states are nearly degenerate and thus the complex polarization is not as strong as other examples presented before. UHF exhibits striking spin-symmetry breaking and predicts a much smaller spin gap than RHF and cRHF.

The MP2 treatment on top of these reference HF determinants does not improve these poor energetics. There is about a 20 kcal/mol energy difference between RMP2 and cRMP2 and RMP2 is lower in energy than cRMP2. This may indicate *artificial* complex polarization which indeed turns out to be the case in this system (vide infra). UMP2 removes a large portion of the spin contamination present at the HF level, but it still is heavily spin-contaminated. As a result, it predicts the sign of the gap incorrectly.

κ-UOOMP2 predicts a reasonably small gap with satisfying spin contamination for the singlet state ($\langle S^2 \rangle \approx 1.0$) and almost no spin contamination for the triplet

state. With the AP scheme, the gap is predicted to be 2.97 kcal/mol. This supports the original hypothesis[373] made by experimentalists that this system has a gap larger than 0.5 kcal/mol, with a triplet ground state. This is also in agreement with the recent experiment which studied this system.[375] Lastly, we note that κ-cROOMP2 collapses to a real, restricted solution and yields a substantially larger gap (36.23 kcal/mol), because this method does not adequately describe the strongly correlated singlet.

In summary, in this example, AP+κ-UOOMP2 successfully describes the biradicaloid character of the singlet state in the molecule whereas κ-cROOMP2 cannot describe such character because there is no cR solution at the κ-OOMP2 level.

4.4 Conclusions

In this work, we examined two single-reference approaches based on regularized orbital-optimized Møller-Plesset perturbation theory (κ-OOMP2) that exploit *essential* symmetry breaking to describe singlet biradicaloids. Combined with Yamaguchi's approximate projection (AP), unrestricted κ-OOMP2 (κ-UOOMP2) offers a way to access almost spin-pure singlet energies. Alternatively, complex, restricted κ-OOMP2 (κ-cROOMP2) can describe biradicaloid character if there is complex polarization. We compared these two methods over a variety of systems: a total of 12 triplet-singlet gaps in the TS12 set, the barrier height of a reaction between a cysteine ion and a singlet oxygen molecule, the C_{30} (D_{5h}) fullerene, and lastly an organic biradical with a triplet ground state. We summarize the major conclusions from these numerical experiments as follows:

1. Without orbital optimization at the MP2 level, Hartree-Fock (HF) orbitals tend to exhibit *artificial* symmetry breaking in singlet biradicaloids. In the case of cRHF, this is sometimes reflected in spurious charge distribution of molecules whereas it often manifests as heavy spin contamination (and commonly also spurious charge distribution) in UHF. In such cases, we recommend κ-OOMP2 which is an electronic structure tool that removes most *artificial* symmetry breaking and yields orbitals with only *essential* symmetry breaking.

2. κ-cROOMP2 is recommended whenever there is *essential* complex polarization. This is due to the fact that κ-UOOMP2 manifests not only spin-symmetry breaking but also spatial symmetry breaking which cannot be purified with the AP scheme.

3. When there is no *essential* complex polarization but only *essential* spin polarization, AP+κ-UOOMP2 is recommended. cR solutions are rare in nature and it is difficult to observe them with systems without point group symmetry. Therefore, the applicability of AP+κ-UOOMP2 is broader than that of κ-cROOMP2.

Strong correlation is a difficult problem to solve and there is no universal approach to it other than brute-force approaches such as complete active space methods.[58] However, at least for two-electron strong correlation problems studied here, either κ-cROOMP2 or AP+κ-UOOMP2 can be a single-reference electronic structure method that correctly describes strong correlation character. It will be interesting to apply these tools to a broader range of chemical systems along with more developments on their response theory such as excited states and analytic nuclear gradients in the future. The presented approaches, which use cR orbitals or AP, can be extended to higher order single-reference correlation methods such as coupled-cluster with singles and doubles (CCSD) and third-order Møller-Plesset perturbation theory (MP3).

4.5 Appendix

The Appendix discusses the frozen core and frozen virtual approximation in κ-OOMP2 and includes the theoretical reference data of TS12 set and the Cartesian coordinate of C_{30}.

4.5.1 Frozen Core and Frozen Virtual Approximation

Here, we use IJK... to denote frozen core orbitals and ABC... to denote frozen virtual orbitals. As in the main manuscript, we use ijk.. for active occupied orbitals and abc... for active virtual orbitals.

The frozen core approximation limits the correlation energy calculation to all electrons but core electrons. Similarly, the frozen virtual approximation limits the virtual space of correlation energy to be all virtuals but frozen virtuals. The orbital optimization with these frozen degrees of freedom (DOFs) becomes somewhat complicated because it adds more subspaces to consider compared to the one without frozen DOFs. Namely, the orbital rotation matrix has the following block structure:

$$\mathbf{\Theta} = \begin{bmatrix} 0 & \Theta_{Ik} & \Theta_{Ia} & \Theta_{IA} \\ -\Theta_{Ik}^* & 0 & \Theta_{ia} & \Theta_{iA} \\ -\Theta_{Ia}^* & -\Theta_{ia}^* & 0 & \Theta_{aB} \\ -\Theta_{IA}^* & -\Theta_{iA}^* & -\Theta_{aB}^* & 0 \end{bmatrix} \tag{4.19}$$

where we assumed that the orbital space is ordered as frozen core (C), active occupied (O), active virtual (V), and frozen virtual (fV). This define non-redundant parameters in the exponential parametrization of orbital rotation in our problem. In other words, we have

$$\mathbf{C}' = \mathbf{C} \exp(\mathbf{\Theta}) \tag{4.20}$$

where $\mathbf{C}$ denotes the orbital coefficient at a given point and $\mathbf{C}'$ defines the rotation of these orbitals by $\mathbf{\Theta}$. We did not include C-C, O-O, V-V, and fV-fV rotations since both Hartree-Fock (HF) and Møller-Plesset energies are invariant under these rotations. This is exactly why one could canonicalize orbitals within these blocks without changing the underlying energy and that is the basis we used in this work as well.

Here, we list expressions for non-trivial orbital gradient of each block that involves frozen orbitals. We first define the orbital gradient L_{pq} as

$$L_{pq} = \frac{\partial \mathcal{L}}{\partial \Theta_{qp}} \tag{4.21}$$

where $\mathcal{L}$ is the MP2 Lagrangian defined in ref. 269. The C-fV block is the same as the HF orbital gradient so we will not write this down. The other blocks involve correlation energy contribution in general and therefore we present here the explicit forms: the C-O block reads

$$L_{Ki} = \sum_{j} \left(P_{ij} + \tilde{P}_{ij}\right) F_{jK} + \sum_{aQ} (aK|Q) \left(\Gamma^{Q}_{ia} - \tilde{\Gamma}^{Q}_{ia}\right) \tag{4.22}$$

where P_{ij}, $\tilde{P}_{ij}$, $\mathbf{\Gamma}$, and $\tilde{\mathbf{\Gamma}}$ are defined in the main text (i.e., Eqns (4.9), (4.10), (4.11), and (4.13)), the C-V block reads

$$L_{Ka} = -\sum_{iQ} (iK|Q) \left(\Gamma^{Q}_{ai} - \tilde{\Gamma}^{Q}_{ai}\right) - \sum_{ij} \left(P_{ij} + \tilde{P}_{ij}\right) \langle ja \,\|\, iK\rangle - \sum_{bc} \left(P_{cb} + \tilde{P}_{cb}\right) \langle ba \,\|\, cK\rangle \,, \tag{4.23}$$

the O-fV block reads

$$L_{iA} = \sum_{aQ} (Aa|Q) \left(\Gamma^{Q}_{ai} - \tilde{\Gamma}^{Q}_{ai}\right) - \sum_{jk} \left(P_{jk} + \tilde{P}_{jk}\right) \langle kA \,\|\, ji\rangle - \sum_{bc} \left(P_{cb} + \tilde{P}_{cb}\right) \langle bA \,\|\, ci\rangle \,, \tag{4.24}$$

and lastly the V-fV block reads

$$L_{aB} = \sum_{c} \left(P_{ca} + \tilde{P}_{ca}\right) F_{Bc} - \sum_{iQ} (Bi|Q) \left(\Gamma^{Q}_{ia} - \tilde{\Gamma}^{Q}_{ia}\right) \tag{4.25}$$

For an approximate second-order optimization method such as geometric direct minimization (GDM), Broyden-Fletcher-Goldfarb-Shanno (BFGS), and etc., it is important to have a reasonable approximation to the inverse of the exact Hessian $\mathbf{H}$. This is usually achieved by approximating the diagonal elements of $\mathbf{H}^{-1}$ by a simple orbital energy gap expression,

$$\mathbf{P}_{ia,ia} = (\epsilon_a - \epsilon_i)^{-1} \tag{4.26}$$

where $\mathbf{P}$ is the preconditioner (up to some constant) that can be used in GDM or BFGS. This is usually a good approximation due to the following reasons: (1) HF orbital hessian is diagonally dominant and the orbital gap term contributes most to the diagonal elements and (2) the correlation contribution to the orbital Hessian is generally smaller than that of HF. In the presence of frozen DOFs, this form of preconditioner should be applied with great caution. This is because HF energy is invariant under C-O and V-fV rotations. In other words, for C-O and V-fV DOFs one needs to derive a different form of preconditioner that involves only correlation contributions. Surprisingly, we found the corresponding Hessian to be generally near-singluar, which makes the optimization of those variables quite challenging. Indeed, this approach can take about 50-60 iterations to converge even when started from a nearly converged solution (the norm of orbital gradient is about $1e^{-4}$). This approach will be referred to as `Algorithm 1`.

Due to this optimization challenge, we tried an alternative optimization strategy where we consider only C-V, O-V, and O-fV rotations. The Hessian of these rotations is well-conditioned so this optimization should be relatively more stable. Here, we choose a rather unusual representation for evaluating orbital gradient. Namely, we pseudocanonicalize C∪O and V∪fV though C-O and V-fV rotations change the energy. Frozen core orbitals and frozen virtual orbitals are then determined based on the orbital energies in the pseudocanonical basis. L_{Ka} and L_{iA} are identical to Eq. (4.23) and Eq. (4.24), respectively, except that now we incorporate the effect of C-O and V-fV rotations into the density matrix:

$$P_{Ki} = \frac{1}{\epsilon_i - \epsilon_K} \sum_{aQ} (aK|Q) \left(\Gamma^Q_{ia} - \tilde{\Gamma}^Q_{ia} \right) \tag{4.27}$$

and

$$P_{aB} = \frac{1}{\epsilon_a - \epsilon_B} \sum_{iQ} (iB|Q) \left(\Gamma^Q_{ai} - \tilde{\Gamma}^Q_{ai} \right) \tag{4.28}$$

These density matrix expressions are also used in the derivation of frozen orbital MP2 analytic nuclear gradient.[232] This approach will be referred to as `Algorithm`

2. Although `Algorithm 2` performed very well (i.e., it takes about 10-15 iterations when starting from a superposition of atomic density guess), all the numerical results we presented in the main text are based on `Algorithm 1` described above. We also note that response equations of frozen orbital OOMP2 when optimized with `Algorithm 2` can be more involved than in the case of `Algorithm 1`.

We close this section with numerical results that support that `Algorithm 2` is in fact a close approximation to `Algorithm 1`. As an example, we present the κ-ROOMP2 results for the TS12 set. All calculations were run with a converged RHF guess and we report the number of iterations to converge to a threshold of $1e^{-8}$ for root-mean-squared orbital gradient. According to Table 4.11, it is evident that `Algorithm 2` takes far less iterations than `Algorithm 1` with an energy difference of 1–0.1 mE_h. Since `Algorithm 2` is a variational upper bound of `Algorithm 1`, it is expected that relative energies such as triplet-singlet gaps would have even smaller differences. Indeed, for TS12 set, the differences in the triplet-singlet gaps between two algorithms are found to be less than 0.1 kcal/mol as illustrated in Table 4.12.

System	`Algorithm 1`		`Algorithm 2`		E_{diff}
	E	n_{iter}	E	n_{iter}	
C	-37.690362513	16	-37.690067032	8	0.295
NF	-154.201650852	72	-154.201482123	13	0.169
NH	-55.047151603	24	-55.047033847	10	0.118
NO^-	-129.686138434	75	-129.686059952	15	0.078
O_2	-150.106253507	42	-150.106160845	13	0.093
O	-74.870856816	18	-74.870757388	9	0.099
PF	-440.563185799	86	-440.562525083	13	0.661
PH	-341.348436231	53	-341.347730464	10	0.706
S_2	-795.383381169	68	-795.382002596	11	1.379
S	-397.565198508	37	-397.564061508	9	1.137
Si	-288.858231640	30	-288.857705318	9	0.526
SO	-472.772158481	84	-472.771421737	13	0.737

Table 4.11: The comparison of two orbital optimization algorithms for frozen core ROOMP2 calculations on the TS12 set. Energy, E, is in E_h and the energy difference between two algorithms, E_{diff}, is in mE_h.

In the future, we will explore these two algorithms to determine what is the best practice of running frozen orbital OOMP2 calculations.

System	`Algorithm 1`	`Algorithm 2`	E_{diff}
C	44.883	44.849	-0.034
NF	46.375	46.393	0.018
NH	53.362	53.388	0.026
NO^-	27.867	27.89	0.023
O_2	33.782	33.82	0.038
O	65.985	66.036	0.051
PF	34.378	34.335	-0.043
PH	36.626	36.577	-0.049
S_2	23.804	23.778	-0.026
S	42.656	42.601	-0.055
Si	30.954	30.918	-0.036
SO	28.262	28.244	-0.018

Table 4.12: The comparison of two orbital optimization algorithms for frozen core ROOMP2 calculations on the TS12 set: the triplet-singlet energies (kcal/mol), $\Delta E_{\text{S-T}}$, and the differences (kcal/mol) between two algorithms are presented.

4.5.2 TS12 Set

In the TS12 set, there are a total of 8 diatomics and we provide the bond lengths of each molecule in Table 4.13 along with pertinent publications. The references are for atoms as follows: C,[376] Si,[377] O,[378] and S.[379]

	$S = 1$	$S = 0$	Refs.
NF	1.31698	1.3079	380
NH	1.034	1.0362	381
NO^-	1.258	1.262	382383
O_2	1.20752	1.2156	384
PF	1.5897	1.5849	385
PH	1.422_3	1.430_2	386387
S_2	1.889_2	1.898_3	388
SO	1.48108_7	1.4919_7	389390

Table 4.13: The interatomic distance (Å) of diatomic molecules in the TS12 set.

4.5.3 Heat-Bath Configuration Interaction Benchmarks

We also crosschecked the experimental ΔE_{ST} values of these molecules against heat-bath configuration interaction (HCI) calculations.[391] Our goal was not to produce high-quality theoretical benchmark results with HCI. Instead, we wanted to check the experimental values within 1 kcal/mol. Obviously, a more thorough theoretical benchmark study is desirable but we believe that it will not affect the conclusion of this work. HCI energies are not invariant under unitary transformations between orbitals. Often, choosing orbitals is crucial in obtaining high-quality energies. We therefore ran small active space (20–30 orbitals) HCI with self-consistent field (HCISCF) to obtain orbitals and performed HCI without the active space (i.e., only with the frozen core approximation).

A summary of the HCI calculations (with the aug-cc-pVQZ basis set) performed in this work is given in Table 4.14. The two parameters ϵ_1 and ϵ_2 control the number of determinants included in the variational and second-order perturbational (PT2) energies, respectively. We tuned the ϵ_1 parameter such that with a tight $\epsilon_2 < 10^{-6}$ the PT2 contribution (ΔE_{PT2}) does not exceed 10 kcal/mol. Ideally, it would be the best to match ΔE_{PT2} contributions for $M_S = 0$ and $M_S = 1$ for good error cancelation when computing the energy differences. This was found to be somewhat difficult to achieve in general. Nevertheless, we observe a good agreement between HCI and experimental values in general.

4.5.4 Cartesian Coordinates of C_{30}

We optimized the geometry of $M_S = 0$ and $M_S = 1$ with the B97M-V functional[372] and cc-pVDZ basis set[237] using unrestricted orbitals. We present the Cartesian coordinates for each geometry below.

System	M_S	Dets	ϵ_1	ϵ_2	ΔE_{PT2}	$\Delta E_{\text{S-T}}$	E_{diff}
C	0	42049	7.50×10^{-05}	1.00×10^{-06}	-0.03(0)	29.40(0)	0.26(0)
	1	5686	5.00×10^{-04}	1.00×10^{-06}	-0.20(0)		
NF	0	9342972	5.00×10^{-05}	1.00×10^{-08}	-6.09(6)	33.24(6)	0.54(6)
	1	8182669	5.00×10^{-05}	1.00×10^{-08}	-4.86(2)		
NH	0	845036	5.00×10^{-05}	1.00×10^{-06}	-0.41(0)	36.57(1)	0.64(1)
	1	388415	7.50×10^{-05}	1.00×10^{-06}	-0.42(0)		
NO^-	0	10255619	5.00×10^{-05}	1.00×10^{-08}	-7.39(14)	18.30(14)	1.00(14)
	1	23755485	2.50×10^{-05}	1.00×10^{-08}	-3.54(5)		
O_2	0	9051071	5.00×10^{-05}	1.00×10^{-08}	-4.69(2)	22.33(7)	-0.31(7)
	1	8879015	5.00×10^{-05}	1.00×10^{-08}	-4.38(6)		
O	0	448149	5.00×10^{-05}	1.00×10^{-06}	-0.12(0)	45.71(0)	0.34(0)
	1	201697	7.50×10^{-05}	1.00×10^{-06}	-0.13(0)		
PF	0	13511473	3.75×10^{-05}	1.00×10^{-08}	-3.77(6)	21.06(7)	0.78(7)
	1	10943112	3.75×10^{-05}	1.00×10^{-08}	-3.13(4)		
PH	0	742478	5.00×10^{-05}	1.00×10^{-06}	-0.91(0)	22.11(0)	0.20(0)
	1	534296	5.00×10^{-05}	1.00×10^{-06}	-0.61(0)		
S_2	0	18265003	2.50×10^{-05}	1.00×10^{-08}	-7.41(10)	12.95(14)	-0.49(14)
	1	15790755	2.50×10^{-05}	1.00×10^{-08}	-5.99(10)		
S	0	438077	5.00×10^{-05}	1.00×10^{-06}	-0.38(0)	26.22(0)	-0.20(0)
	1	314915	5.00×10^{-05}	1.00×10^{-06}	-0.26(0)		
Si	0	44589	7.50×10^{-05}	1.00×10^{-06}	-0.06(0)	17.96(0)	-0.05(0)
	1	4329	5.00×10^{-04}	1.00×10^{-06}	-0.41(0)		
SO	0	14066327	3.75×10^{-05}	1.00×10^{-08}	-9.05(5)	17.52(7)	-0.63(7)
	1	24049522	2.50×10^{-05}	1.00×10^{-08}	-5.81(5)		

Table 4.14: A summary of HCI calculations: (1) the number of determinants (Dets) and two threshold parameters (ϵ_1 and ϵ_2) are also presented for each M_S state, (2) the magnitude of the PT2 correction (kcal/mol), ΔE_{PT2}, is given, and (3) the triplet-singlet energies (kcal/mol), $\Delta E_{\text{S-T}}$, computed with HCI and the differences (kcal/mol) between HCI and experimental gaps (E_{diff}) are presented.

Atom	X	Y	Z
C	1.2291469539	0.0000000000	2.5955841295
C	2.0010162987	0.0000000000	1.4148129741
C	1.7164173296	-1.2470501857	-0.6979480205
C	1.7164173296	-1.2470501857	0.6979480205
C	0.3798272973	-1.1689882200	2.5955841295
C	0.6183480423	-1.9030795901	1.4148129741
C	-0.9944007743	-0.7224744524	2.5955841295
C	-0.6556130810	-2.0177695862	-0.6979480205
C	-0.6556130810	-2.0177695862	0.6979480205
C	-1.6188561916	-1.1761678700	1.4148129741
C	0.6183480423	-1.9030795901	-1.4148129741
C	-0.9944007743	0.7224744524	2.5955841295
C	-2.1216084971	0.0000000000	-0.6979480205
C	-2.1216084971	0.0000000000	0.6979480205
C	-1.6188561916	1.1761678700	1.4148129741
C	-1.6188561916	-1.1761678700	-1.4148129741
C	0.3798272973	1.1689882200	2.5955841295
C	-0.6556130810	2.0177695862	-0.6979480205
C	-0.6556130810	2.0177695862	0.6979480205
C	0.6183480423	1.9030795901	1.4148129741
C	-1.6188561916	1.1761678700	-1.4148129741
C	1.7164173296	1.2470501857	-0.6979480205
C	1.7164173296	1.2470501857	0.6979480205
C	2.0010162987	0.0000000000	-1.4148129741
C	0.6183480423	1.9030795901	-1.4148129741
C	1.2291469539	0.0000000000	-2.5955841295
C	0.3798272973	1.1689882200	-2.5955841295
C	-0.9944007743	0.7224744524	-2.5955841295
C	-0.9944007743	-0.7224744524	-2.5955841295
C	0.3798272973	-1.1689882200	-2.5955841295

Table 4.15: The Cartesian coordinates (Å) of the geometry of C_{30} ($M_S = 0$) used in this work. The corresponding total energy of B97M-V/cc-pVDZ at this geometry is -1142.80050744412 E_h.

Atom	X	Y	Z
C	1.2289392980	0.0000000000	2.5951347450
C	2.0011617189	0.0000000000	1.4145443520
C	1.7168626316	-1.2473737166	-0.6976786167
C	1.7168626316	-1.2473737166	0.6976786167
C	0.3797631281	-1.1687907275	2.5951347450
C	0.6183929796	-1.9032178929	1.4145443520
C	-0.9942327771	-0.7223523953	2.5951347450
C	-0.6557831713	-2.0182930702	-0.6976786167
C	-0.6557831713	-2.0182930702	0.6976786167
C	-1.6189738390	-1.1762533458	1.4145443520
C	0.6183929796	-1.9032178929	-1.4145443520
C	-0.9942327771	0.7223523953	2.5951347450
C	-2.1221589207	0.0000000000	-0.6976786167
C	-2.1221589207	0.0000000000	0.6976786167
C	-1.6189738390	1.1762533458	1.4145443520
C	-1.6189738390	-1.1762533458	-1.4145443520
C	0.3797631281	1.1687907275	2.5951347450
C	-0.6557831713	2.0182930702	-0.6976786167
C	-0.6557831713	2.0182930702	0.6976786167
C	0.6183929796	1.9032178929	1.4145443520
C	-1.6189738390	1.1762533458	-1.4145443520
C	1.7168626316	1.2473737166	-0.6976786167
C	1.7168626316	1.2473737166	0.6976786167
C	2.0011617189	0.0000000000	-1.4145443520
C	0.6183929796	1.9032178929	-1.4145443520
C	1.2289392980	0.0000000000	-2.5951347450
C	0.3797631281	1.1687907275	-2.5951347450
C	-0.9942327771	0.7223523953	-2.5951347450
C	-0.9942327771	-0.7223523953	-2.5951347450
C	0.3797631281	-1.1687907275	-2.5951347450

Table 4.16: The Cartesian coordinates (Å) of the geometry of C_{30} ($M_S = 1$) used in this work. The corresponding total energy of B97M-V/cc-pVDZ at this geometry is -1142.803154404 E_h.

Chapter 5

Coupled-Cluster Valence-Bond Singles and Doubles for Strongly Correlated Systems

5.1 Introduction

Strong correlations are an important subject of active research in the field of electronic structure theory. Systems with d or f orbitals such as metalloenzymes[392] like photosystem II [393, 394] are well known strongly correlated systems. Polyradicaloid systems such as molecules near bond-breaking[395] and polyaromatic hydrocarbons,[226, 396–399] also belong to this category. Phenomena driven by correlations between electrons that lie outside perturbative regimes such as high-T_C superconductivity[400] and Kondo problems[401] are also inherently strong correlation problems. Describing these systems and phenomena requires proper treatment of strong correlations to obtain at least a qualitatively correct description.

One of the most popular approaches in quantum chemistry to address these problems is the use of brute-force algorithms such as complete active space self-consistent field (CASSCF).[58] The applicability of CASSCF is limited by the need to solve the full configuration interaction (FCI) problem within an active space, which has a computational cost that scales exponentially with the number of electrons in the active space. To extend the applicability of CASSCF, enormous efforts have been made on developing more efficient approximate FCI solvers such as Alavi and co-worker's FCI quantum monte carlo (FCIQMC) [402, 403] and White's density matrix renormalisation group (DMRG).[34–36, 404, 405] FCIQMC uses importance sampling techniques of QMC to solve the FCI problem and shows a weaker exponential scaling compared

to the traditional determinant based exact FCI solver. [406, 407] DMRG was originally designed for solving one-dimensional (1D) lattice systems and encodes the most important degrees of freedom between neighbouring sites using singular value decompositions of density matrices. DMRG is a polynomial-scaling method for 1D systems with short-range interactions, but is still an exponential-scaling method for general systems of higher dimensions or with long-range interactions. These two independent approaches have been applied to non-trivial chemical systems small enough to afford these brute force approaches.[38–42, 408–410] It is, however, highly desirable to develop polynomial-scaling methods that can qualitatively capture strong correlations in systems where FCIQMC and DMRG become intractable.

Another common approach to strong correlations is multi-reference coupled-cluster (MRCC) theory. [411–413] The basic idea is to include physically relevant higher cluster excitations by employing multiple determinants in the reference state that are difficult to access in the usual single reference approaches. MRCC approaches can be categorised into (1) state-universal [73–78] and (2) valence-universal [79–87] that are often referred to as genuine MRCC approaches and (3) state-specific approaches.[88–111] The first two suffer from the appearance of intruder states [414–417] and require solving for several eigenstates simultaneously, many of which can be irrelevant to the problem. The third approach can avoid these problems but usually at the expense of the explicit inclusion of higher excitations. These are still active areas of research in the pursuit of strong correlations, and interested readers are referred to ref. 412 and references therein.

Another interesting, formally simpler, and often computationally more tractable approach than those mentioned above, is single-reference coupled-cluster (SRCC) theory. SRCC singles and doubles with non-iterative triples (CCSD(T)) is a *de facto* standard approach for non-strongly correlated systems.[418] Its non-variational failure for strongly correlated systems when used with restricted Hartree-Fock (RHF) references has inspired development of new methods.

The simplest possible (and thus the most widely used) fix to this problem is to use an unrestricted HF (UHF) reference at the expense of spin symmetry. However, many studies have indicated that UCCSD or UCCSD(T) misses a fair amount of correlations in the so-called spin-recoupling regime, an intermediate regime between equilibrium and bond-dissociation. [419] More crucially, these methods fail to provide a quantitatively accurate singlet-triplet gaps due to severe spin contaminations. Using UHF references is thus not satisfying for general applications.

An alternative approach without increasing the substitution level (i.e. with only singles and doubles substitutions), is to correct for higher excitations in a non-iterative fashion. This is done in the methods of moments coupled cluster approximations including renormalised and completely renormalised variants.[420–428] Instead

of evaluating the energy using projection equations, more stable approaches include evaluating it variationally [429–431] or through approximations to the variational evaluation, such as unitary CC (UCC),[432–435] extended CC (ECC),[436–441] and quadratic CC (QCC).[442–444] Instead of evaluating the energy using projection equations, more stable approaches include evaluating it variationally with either an expectation value ansatz[429–431] or a unitary ansatz[432–435] and approximations to the variational evaluation such as extended CC (ECC)[436–441] and quadratic CC (QCC).[442–444] These have shown improved energetics in strongly correlated systems, but none of them are an ultimate solution to the problem. Increasing the substitution levels systematically, such as up to triples (RCCSDT) [445] and up to quadruples (RCCSDTQ), [446] is another approach at the expense of steep scaling costs ($n_{\text{occ}}^3 n_{\text{vir}}^5$ and $n_{\text{occ}}^4 n_{\text{vir}}^6$, respectively).

Recently, our group has developed a local correlation model for strong correlations, the hierarchical perfect n-tuples model (e.g. perfect quadruples (PQ), perfect hextuples (PH), etc.). [447–450] It explicitly incorporates higher cluster operators up to n-tuples in a very restricted form to better preserve computational feasibility. The use of localised orbitals is essential in this approach as thethe limited number of higher excitations will be most effective among orbitals that are spatially close. The price we pay for this is the lack of orbital-invariance within occupied-occupied and virtual-virtual rotations.The price we pay for this is that the energy is no longer invariant with respect to occupied-occupied and virtual-virtual rotations. Moreover, simultaneous multiple bond-breaking will require a higher n-tuples model, which becomes intractable quickly.

Another simple and yet very effective approach are the spin-flip methods pioneered by Krylov and co-workers. [318, 334, 345, 451] Equation-of-motion spin-flip coupled cluster (EOM-SF-CC) theory is based on the observation that restricted open-shell HF (ROHF) can qualitatively describe strongly correlated systems in a high-spin state such as triplet stretched H_2. At the level of singles and doubles, EOM-SF-CCSD describes the singlet ground state as an excitation or a deexcitation from a high-spin CCSD wavefunction. It has been widely used for diradical systems. [334] The major drawback of this approach is that systems with many strongly correlated electrons would require the use of extremely high-spin reference whose orbitals are far from being suitable to describe singlet ground states.

There have been proposals that remove certain quadratic terms in doubles (D) amplitudes equations in RCCSD to mimic the effects of triples and quadruples (TQ) and greatly improve the accuracy for strongly correlated systems. Many of them were originally motivated by the cost reduction when ignoring some non-linear terms, but later it was realised that discarding such terms can vastly improve the accuracy in molecules near quasi-degeneracy. The main goal in this research direction is to

account approximately for higher excitations (T, Q, ...) whilst retaining formal properties of RCCSD such as size-extensivity, orbital invariance within occupied-occupied and virtual-virtualenergy-invariance with respect to occupied-occupied and virtual-virtual rotations, and exactness for non-interacting two electron systems.

This approach was pioneered by Paldus and co-workers who developed approximate coupled-pairs with quadruples (ACPQ) [452, 453] which has inspired many subsequent developments. ACPQ was motivated by the structure of Q extracted from a cluster analysis of a broken-symmetry wavefunction such as UHF and projected HF (PHF), which cancels certain quadratic terms when studying strongly correlated limits of the Pariser-Parr-Pople model.[453] This provided justification for related approaches such as ACP-D45 [454, 455] and approximate CCD (ACCD) [456, 457] . Linearised CC, [458] 2CC, [459] and coupled electron pair approximation (CEPA) and its variants [460, 461] also belong to this category.

A more recent approach in this category is the distinguishable cluster approximation (DCA) [462] where a diagram corresponding to direct exchange of two doubles amplitudes is discarded. It was suggested as an *ad hoc* modification to RCCD (called DCD) and later derived from a screened Coulomb formalism. [463] DCD and its variants (Brueckner DCD, orbital-optimised DCD and DCSD) [462–465] all do not "turn over" when breaking N_2 in a double-zeta basis. Despite its promising earlier results its non-interative triples version (DCSD(T)) shows a similar non-variational failure to that of CCSD(T) for bond-breaking [463] when applied to N_2 in a triple-zeta basis. This suggests that an alternative way to include T perhaps in a non-iterativean iterative fashion should be explored.

Another recent approach in this category is singlet-paired CCSD (CCSD0) proposed by Bulik *et al.* [466] The singlet doubles operator in RCCSD can be divided into symmetric singlet doubles (or singlet-pairing doubles) and antisymmetric singlet doubles (or triplet-pairing doubles). This splitting of the doubles operator was extensively exploited in orthogonally spin adapted formula,[467–470] and it will be reviewed later in this paper as well. In CCSD0, the antisymmetric singlet doubles operator is completely removed by ansatz. Removing those terms improves the performance of the theory for bond dissociations, although when applied to N_2 in a minimal basis it does not reach the correct asymptote.[466][471] Moreover, the contribution from the removed antisymmetric singlet doubles is not negligible in general. For instance, N_2 at equilibrium in a double-zeta basis has non-negligible dynamic correlations coming from the antisymmetric doubles. Neglecting these correlations results in the CCSD0 energy being too high not only at the dissociation limit but also at the equilibrium geometry.[466] Furthermore, Their recent efforts of incorporating antisymmetric singlet doubles with the frozen symmetric singlet doubles amplitudes suggest that an alternative route should be investigated.[472]

We would also like to mention externally corrected CCSD [473] which employs TQ obtained from external wavefunctions such as CASSCF, [474, 475] valence-bond (VB), [476–478] broken-symmetry HF. [452, 479, 480] In particular CCSDQ', pioneered by Paldus, Piecuch and co-workers, [452, 480] has similarities to the method to be discussed in this paper. In CCSDQ', one augments CCSD amplitudes equations with Q obtained from a cluster analysis of projection-after-variation PHF wavefunctions. [481] The resulting wavefunction is rigorously spin-pure, and it showed promising results on simple MR systems such as H_4 and H_8. In passing, we note that CCSDQ' (or CCDQ') is closely related to aforementioned ACPQ, the major difference being that CCSDQ' is not a self-contained method.

Two of us (D.W.S and M.H.G.) introduced coupled-cluster valence-bond theory singles and doubles (CCVB-SD) as a simple modification to RCCSD to describe strongly correlated *closed-shell* systems. [141] As opposed to completely removing certain quadratic terms from RCCSD or using external sources for higher excitations, CCVB-SD directly models Q with its D. The way it models Q originated from a simpler model, CCVB, which yields a spin-pure wavefunction and can describe simultaneous multiple bond breaking at a cost dominated by integral transformations.[128, 140, 280] CCVB was formulated based on the recognition of a modified cluster expansion hidden in PHF. In this regard CCVB-SD is similar in spirit to ACPQ and CCSDQ'. The similarity between CCVB-SD and ACPQ was noticed in ref. 141. The key distinction is CCVB-SD is self-contained, unlike CCSDQ', and removes certain quadratic terms in RCCSD by solving modified amplitudes equations as opposed to discarding such terms *a priori*, as in ACPQ.

In CCVB-SD, a singlet doubly-excited configuration is constructed by pairing an occupied orbital with a virtual orbital and coupling two triplets out of such two pairs to form an overall singlet state. This is how CCVB encodes interpair correlations, and the remaining higher-order correlations enter through the aforementioned modified cluster expansion. CCVB-SD successfully combines advantages of RCCSD and CCVB: it preserves all the formal properties of RCCSD mentioned above and describes valence correlations correctly even near multiple bond dissociations. Another viewpoint is obtained by noting that CCVB generalizes PHF, removing the latter's size inconsistency, and CCVB-SD generalizes CCVB. Therefore, CCVB-SD is an effective combination of PHF and coupled cluster. The value of finding such a combination was emphasized in a recent paper.[482] We also note that CCVB-SD naturally contains the antisymmetric doubles that are discarded in CCSD0. When properly implemented, CCVB-SD should scale the same as does RCCSD, which is $n_{\mathrm{occ}}^2 n_{\mathrm{vir}}^4$. Its result for the triple-bond dissociation of N_2 in a minimal basis shows its ability to capture strong correlations in the valence space as it reaches the correct asymptote. [141]

The main objective of this paper is to provide detailed information about a new production-level implementation of CCVB-SD and discuss its applicability to systems of hundreds of strongly correlated electrons with an application to emergent many-electron correlations in oligoacenes,[38, 39, 330, 483–491] which have been the focus of much recent attention. This paper is organised as follows: (1) we review and discuss the CCVB-SD wavefunction ansatz from a different angle than what is discussed in ref.141, (2) we discuss the derivation of CCVB-SD Λ-equation, (3) we illustrate how we implement the CCVB-SD T-amplitudes equation and Λ-equation solvers into a block-tensor based coupled-cluster code, and (4) we apply CCVB-SD to oligoacenes and discuss strong correlations in their ground state.

5.2 The Model

In CCVB-SD, the wavefunction ansatz is given through quadruples level as [141]

$$|\Psi\rangle = \left(\hat{\mathrm{I}} + \hat{\mathcal{T}}_1 + \frac{1}{2}\hat{\mathcal{T}}_1^2 + \hat{\mathcal{S}} + \frac{1}{6}\hat{\mathcal{T}}_1^3 + \frac{1}{2}\hat{\mathcal{S}}\hat{\mathcal{T}}_1^2 + \hat{\mathcal{S}}\hat{\mathcal{T}}_1 + \frac{1}{24}\hat{\mathcal{T}}_1^4 + \frac{1}{2}\hat{\mathcal{S}}^2 - \frac{1}{2}\hat{\mathrm{I}}_S\hat{\mathcal{Q}}^2\right)|\Phi_0\rangle\,, \tag{5.1}$$

where $|\Phi_0\rangle$ denotes a singlet reference, $\hat{\mathcal{T}}_1$ represents the singles operator, the doubles operator $\hat{\mathcal{S}}$ creates singlet doubly-excited configurations, the doubles operator $\hat{\mathcal{Q}}$ creates quintet doubly-excited configurations, and $\hat{\mathrm{I}}_S$ is a general singlet-subspace projection operator which can be written as a sum of outer products of orthonormal singlet states $\{|\Phi_\mu\rangle\}$,

$$\hat{\mathrm{I}}_S = |\Phi_0\rangle\langle\Phi_0| + \sum_{ia}|\Phi_i^a\rangle\langle\Phi_i^a| + \sum_{ijab}\left|\Phi_{ij}^{ab}\right\rangle\left\langle\Phi_{ij}^{ab}\right| + \cdots. \tag{5.2}$$

This ansatz includes full singles and doubles operators, and thus it is exact for non-interactingisolated two-electron systems. The $\hat{\mathcal{Q}}^2\hat{\mathrm{I}}_S\hat{\mathcal{Q}}^2$ term represents an approximate connected quadruples contribution that plays a key role in capturing strong correlations in CCVB-SD.

Based on this wavefunction ansatz, the CCVB-SD energy and amplitudes equations follow

$$E = \langle\Phi_0|\, e^{-\hat{\mathcal{G}}}\hat{\mathcal{H}}e^{\hat{\mathcal{G}}}\,|\Phi_0\rangle = \langle\Phi_0|\left(e^{-\hat{\mathcal{G}}}\hat{\mathcal{H}}e^{\hat{\mathcal{G}}} - \hat{\mathcal{H}}\;\hat{\mathrm{I}}_S\frac{1}{2}\hat{\mathcal{Q}}^2\right)|\Phi_0\rangle\,, \tag{5.3}$$

$$0 = \langle\Delta_\mu|\left(e^{-\hat{\mathcal{G}}}\hat{\mathcal{H}}e^{\hat{\mathcal{G}}} - \hat{\mathcal{H}}\;\hat{\mathrm{I}}_S\frac{1}{2}\hat{\mathcal{Q}}^2\right)|\Phi_0\rangle\,, \tag{5.4}$$

where the primary cluster operator $\hat{\mathcal{G}}$ is defined as

$$\hat{\mathcal{G}} = \hat{\mathcal{T}}_1 + \hat{\mathcal{S}}, \tag{5.5}$$

and $|\Delta_\mu\rangle$ represents an excited determinant in the spin-orbital basis including singly-excited ones $\left|\Delta_{i_{\sigma_1}}^{a_{\sigma_1}}\right\rangle$ and doubly-excited ones $\left|\Delta_{i_{\sigma_1} j_{\sigma_2}}^{a_{\sigma_1} b_{\sigma_2}}\right\rangle$. We note that in the second equality in Eq. (5.3) we used

$$\langle\Phi_0|\left(\hat{\mathcal{H}}\ \hat{\mathrm{I}}_S \frac{1}{2}\hat{\mathcal{Q}}^2\right)|\Phi_0\rangle = 0, \tag{5.6}$$

which is a consequence of the Slater rules. CCVB-SD formally includes other higher disconnected excitations beyond quadruples, but we only need up to quadruples for the purpose of solving the amplitude equations.

It is important to note that the amplitudes of $\hat{\mathcal{S}}$ parametrise the amplitudes of $\hat{\mathcal{Q}}$. This connection is most succinct if we use the following configurations for the singlet doubles subspace, indexed by spatial orbitals and grouped into 2 categories: $|^S\Phi_{ij}^{ab}\rangle$ and $|^A\Phi_{ij}^{ab}\rangle$ where the superscripts S and A denote symmetry and antisymmetry under the permutation of spatial orbital indices (i.e. i↔j, a↔b), respectively. This construction is based on the orthogonal spin-adapted 4-electron singlet configurations discussed extensively elsewhere.[467–470] As illustrated in Fig. 5.1, the symmetric state is constructed by taking two singlets from (ij) (a 2-particle geminal made from occupied levels i and j) and (ab) (a 2-particle geminal made from virtual levels a and b) to form a 4-electron singlet. The antisymmetric state, on the other hand, is built coupling two triplets from (ij) and (ab) to form an overall singlet.

In terms of excitations from a singlet reference $|\Phi_0\rangle$, the construction of $|^S\Phi_{ij}^{ab}\rangle$ and $|^A\Phi_{ij}^{ab}\rangle$ can be carried out using spin-adapted geminal (or pair) operators. The singlet annihilation operator $\hat{\sigma}_{pq}$ and the three triplet annihilation operators ($^{-1}\hat{\tau}_{pq}$, $^{0}\hat{\tau}_{pq}$, $^{1}\hat{\tau}_{pq}$) for each M_S are defined as follows:

$$\hat{\sigma}_{pq} = \frac{1}{\sqrt{2}}\left(\hat{a}_{q_\beta}\hat{a}_{p_\alpha} + \hat{a}_{p_\beta}\hat{a}_{q_\alpha}\right), \tag{5.7}$$

$$^{-1}\hat{\tau}_{pq} = \hat{a}_{q_\beta}\hat{a}_{p_\beta}, \tag{5.8}$$

$$^{0}\hat{\tau}_{pq} = \frac{1}{\sqrt{2}}\left(\hat{a}_{q_\beta}\hat{a}_{p_\alpha} - \hat{a}_{p_\beta}\hat{a}_{q_\alpha}\right), \tag{5.9}$$

and

$$^{1}\hat{\tau}_{pq} = \hat{a}_{q_\alpha}\hat{a}_{p_\alpha}. \tag{5.10}$$

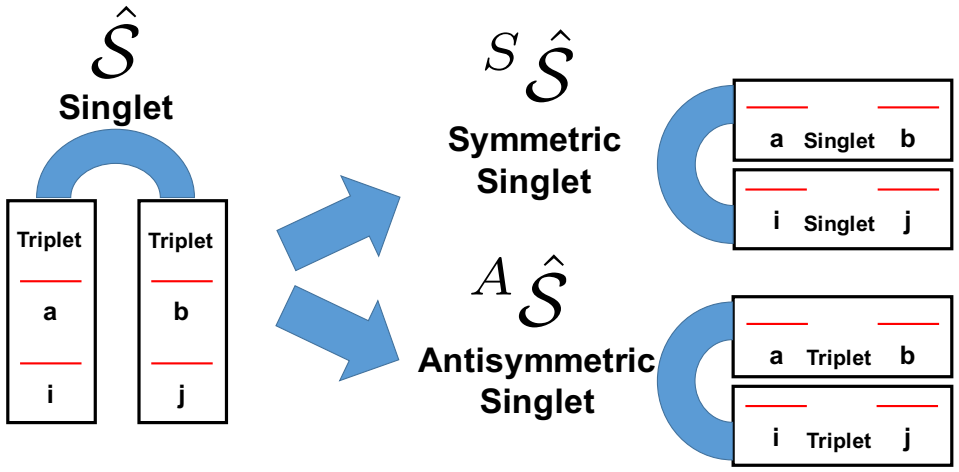

Figure 5.1: An illustration of the decomposition of singlet doubles space into antisymmetric and symmetric singlet parts.

Applying these operators to $|\Phi_0\rangle$, $|{}^{S}\Phi_{ij}^{ab}\rangle$ and $|{}^{A}\Phi_{ij}^{ab}\rangle$ follow

$$\begin{aligned} |{}^{S}\Phi_{ij}^{ab}\rangle &= {}^{ss}\hat{\Sigma}_{ij}^{ab}\,|\Phi_0\rangle \\ &= \frac{1}{2}\left(|\Delta_{i_\beta j_\alpha}^{b_\beta a_\alpha}\rangle + |\Delta_{i_\alpha j_\beta}^{b_\alpha a_\beta}\rangle + |\Delta_{i_\beta j_\alpha}^{a_\beta b_\alpha}\rangle + |\Delta_{i_\alpha j_\beta}^{a_\alpha b_\beta}\rangle\right), \end{aligned} \tag{5.11}$$

and

$$\begin{aligned} |{}^{A}\Phi_{ij}^{ab}\rangle &= {}^{tt}\hat{\Sigma}_{ij}^{ab}\,|\Phi_0\rangle \\ &= \frac{1}{\sqrt{12}}\left(|\Delta_{i_\beta j_\alpha}^{b_\beta a_\alpha}\rangle + |\Delta_{i_\alpha j_\beta}^{b_\alpha a_\beta}\rangle - |\Delta_{i_\beta j_\alpha}^{a_\beta b_\alpha}\rangle - |\Delta_{i_\alpha j_\beta}^{a_\alpha b_\beta}\rangle - 2\,|\Delta_{i_\beta j_\beta}^{a_\beta b_\beta}\rangle - 2\,|\Delta_{i_\alpha j_\alpha}^{a_\alpha b_\alpha}\rangle\right), \end{aligned} \tag{5.12}$$

where

$${}^{ss}\hat{\Sigma}_{ij}^{ab} = \hat{\sigma}_{ab}^{\dagger}\hat{\sigma}_{ij}, \tag{5.13}$$

and

$${}^{tt}\hat{\Sigma}_{ij}^{ab} = \frac{1}{\sqrt{3}}\left(-{}^{0}\hat{\tau}_{ab}^{\dagger}\,{}^{0}\hat{\tau}_{ij} - {}^{-1}\hat{\tau}_{ab}^{\dagger}\,{}^{-1}\hat{\tau}_{ij} - {}^{1}\hat{\tau}_{ab}^{\dagger}\,{}^{1}\hat{\tau}_{ij}\right). \tag{5.14}$$

In the case of $|{}^{S}\Phi_{ij}^{ab}\rangle$, $\hat{\sigma}_{ij}$ removes a singlet from $|\Phi_0\rangle$ and in its place creates another singlet with $\hat{\sigma}_{ab}^{\dagger}$. Unsurprisingly, the result is a doubly-substituted singlet configuration. Constructing $|{}^{A}\Phi_{ij}^{ab}\rangle$ is similar except that we must ensure that the resulting configuration is singlet. For example, ${}^{0}\hat{\tau}_{ij}$ removes a triplet from the reference and

replaces it with another triplet via ${}^0\hat{\tau}^\dagger_{ab}$, but if we had stopped there, the configuration would still have a quintet component. In any case, the underlying concept in this viewpoint of the singlet doubles space is that we are removing two electrons of a given spin from the reference and replacing them with two electrons of the same spin. In passing, we note that this construction verifies the earlier assertion about the permutation symmetry of the two states as

$$|{}^S\Phi^{ab}_{ij}\rangle = |{}^S\Phi^{ba}_{ij}\rangle = |{}^S\Phi^{ab}_{ji}\rangle = |{}^S\Phi^{ba}_{ji}\rangle\,, \tag{5.15}$$

and

$$|{}^A\Phi^{ab}_{ij}\rangle = -\,|{}^A\Phi^{ba}_{ij}\rangle = -\,|{}^A\Phi^{ab}_{ji}\rangle = |{}^A\Phi^{ba}_{ji}\rangle\,. \tag{5.16}$$

We also note that Eq. (5.11) is not normalised for cases with repeated indices, but it is consistent with our definition of ${}^S\hat{\mathcal{S}}$ shown below. With these, the singlet doubles operator $\hat{\mathcal{S}}$ thus separates into two orbital-invariant pieces

$$\hat{\mathcal{S}} = {}^S\hat{\mathcal{S}} + {}^A\hat{\mathcal{S}}, \tag{5.17}$$

where the symmetric part of $\hat{\mathcal{S}}$ is

$${}^S\hat{\mathcal{S}} = \frac{1}{4}\sum_{ijab} {}^S S^{ab}_{ij}\, {}^{ss}\hat{\Sigma}^{ab}_{ij}, \tag{5.18}$$

and the antisymmetric part of $\hat{\mathcal{S}}$ is

$${}^A\hat{\mathcal{S}} = \frac{1}{4}\sum_{ijab} {}^A S^{ab}_{ij}\, {}^{tt}\hat{\Sigma}^{ab}_{ij}. \tag{5.19}$$

${}^S S^{ab}_{ij}$ and ${}^A S^{ab}_{ij}$ have the same index symmetry as the corresponding substitution operators (i.e. they follow the same symmetry as Eq. (5.15) and Eq. (5.16), respectively). These two sets of amplitudes constitute two tensors ${}^S\mathbf{S}$ and ${}^A\mathbf{S}$, each of size $n^2_{\text{occ}} n^2_{\text{vir}}$. Because the amplitude indices are for spatial orbitals, the tensors will be referred to as being "spinless". In contrast to this, tensors indexed with spin orbitals will be referred to as "spinful" tensors. For completeness, we write $\hat{\mathcal{S}}$ in terms of spin blocks of its spinful counterpart $\hat{s}$ as in

$$\hat{\mathcal{S}} = \sum_{ijab} s^{a_\alpha b_\beta}_{i_\alpha j_\beta} \hat{a}^\dagger_{a_\alpha}\hat{a}^\dagger_{b_\beta}\hat{a}_{j_\beta}\hat{a}_{i_\alpha} + \frac{1}{4}\sum_{ijab} s^{a_\alpha b_\alpha}_{i_\alpha j_\alpha}\left(\hat{a}^\dagger_{a_\alpha}\hat{a}^\dagger_{b_\alpha}\hat{a}_{j_\alpha}\hat{a}_{i_\alpha} + \hat{a}^\dagger_{a_\beta}\hat{a}^\dagger_{b_\beta}\hat{a}_{j_\beta}\hat{a}_{i_\beta}\right), \tag{5.20}$$

$$\hat{\mathcal{S}} = \frac{1}{4}\sum_{ijab} s^{a_\alpha b_\alpha}_{i_\alpha j_\alpha}\left(\hat{a}^\dagger_{a_\alpha}\hat{a}^\dagger_{b_\alpha}\hat{a}_{j_\alpha}\hat{a}_{i_\alpha} + \hat{a}^\dagger_{a_\beta}\hat{a}^\dagger_{b_\beta}\hat{a}_{j_\beta}\hat{a}_{i_\beta}\right) + \sum_{ijab} s^{a_\alpha b_\beta}_{i_\alpha j_\beta}\hat{a}^\dagger_{a_\alpha}\hat{a}^\dagger_{b_\beta}\hat{a}_{j_\beta}\hat{a}_{i_\alpha}, \tag{5.21}$$

where the summations run over spatial orbitals, the first term denotes the same spin block of $\hat{s}$ and the second term is the opposite spin block of $\hat{s}$.

When acting on $|\Phi_0\rangle$, $\hat{\mathcal{Q}}$ creates a linear combination of quintet configurations. Because the maximum spin for four electrons is quintet, it is clear that each quintet double should be obtained by removing a triplet from the reference and replacing it with another triplet. We have

$$\hat{\mathcal{Q}} = \frac{1}{4} \sum_{ijab} Q_{ij}^{ab} \, {}^{tt}\hat{\kappa}_{ij}^{ab}, \tag{5.22}$$

where

$${}^{tt}\hat{\kappa}_{ij}^{ab} = \frac{1}{\sqrt{6}} \left(-2 \, {}^{0}\hat{\tau}_{ab}^{\dagger} \, {}^{0}\hat{\tau}_{ij} + {}^{-1}\hat{\tau}_{ab}^{\dagger} \, {}^{-1}\hat{\tau}_{ij} + {}^{1}\hat{\tau}_{ab}^{\dagger} \, {}^{1}\hat{\tau}_{ij} \right), \tag{5.23}$$

and $\mathbf{Q}$ is another spinless antisymmetric tensor of size $n_{\text{occ}}^2 n_{\text{vir}}^2$. The action of ${}^{tt}\hat{\kappa}_{ij}^{ab}$ creates a quintet configuration as in

$$|{}^{Q}\Phi_{ij}^{ab}\rangle = {}^{tt}\hat{\kappa}_{ij}^{ab} \, |\Phi_0\rangle \tag{5.24}$$

$$= \frac{1}{\sqrt{6}} \left(|\Delta_{i_\beta j_\alpha}^{b_\beta a_\alpha}\rangle + |\Delta_{i_\alpha j_\beta}^{b_\alpha a_\beta}\rangle - |\Delta_{i_\beta j_\alpha}^{a_\beta b_\alpha}\rangle - |\Delta_{i_\alpha j_\beta}^{a_\alpha b_\beta}\rangle + |\Delta_{i_\beta j_\beta}^{a_\beta b_\beta}\rangle + |\Delta_{i_\alpha j_\alpha}^{a_\alpha b_\alpha}\rangle \right). \tag{5.25}$$

We can now describe the correspondence between $\mathbf{S}$ and $\mathbf{Q}$, which is given by

$$Q_{ij}^{ab} = -2 \, {}^{A}S_{ij}^{ab}. \tag{5.26}$$

This indicates that $\mathbf{Q}$ is independent of ${}^{S}\mathbf{S}$ and parametrised by ${}^{A}\mathbf{S}$. This is intuitive given that ${}^{A}\mathbf{S}$ and $\mathbf{Q}$ have the same permutational symmetry in the spatial orbitals, or alternatively they are both obtained by substituting triplets within the reference. The detailed proof of Eq. (5.26) is available in Appendix of this article.

The physical meaning of ${}^{S}\hat{\mathcal{S}}$ and ${}^{A}\hat{\mathcal{S}}$ may be better understood in the language of valence bond theory.[492] ${}^{S}\hat{\mathcal{S}}$ contains perfect-pairing (PP) [493] terms which are important pieces of strong correlations that describe intrapair correlations. In addition to PP terms, it also has important interpair correlations such as ionic excitations between two pairs. On the other hand, ${}^{A}\hat{\mathcal{S}}$ corresponds to interpair correlations which are not captured by ${}^{S}\hat{\mathcal{S}}$ but are important to describe polyradical character of systems. ${}^{A}\mathbf{S}$ parametrises quadruples in a different way than they are parametrised in RCCSD. If ${}^{A}\mathbf{S}$ is small, then $\mathbf{Q}$ is small and so is the difference between the CCVB-SD and RCCSD results. In this sense, CCVB-SD theory asserts that ${}^{A}\mathbf{S}$ is the operative element (at least for the doubles) in RCCSD's failure to correctly describe strong correlations. This also stands in contrast to the CCSD0 method [466] which removes ${}^{A}\mathbf{S}$ or ${}^{A}\hat{\mathcal{S}}$ entirely.

5.3 CCVB-SD Lagrangian and Λ–equation

Following Eq. (5.3) and (5.4), we establish the CCVB-SD Lagrangian defined as

$$\mathcal{L}(\hat{\mathcal{T}}_1, \hat{\mathcal{S}}, \hat{\Lambda}) = \langle \Phi_0 | \left(\hat{\mathrm{I}} + \hat{\Lambda} \right) \left(e^{-\hat{\mathcal{G}}} \hat{\mathcal{H}} e^{\hat{\mathcal{G}}} - \hat{\mathcal{H}}\ \hat{\mathrm{I}}_S \frac{1}{2} \hat{\mathcal{Q}}^2 \right) | \Phi_0 \rangle \,, \tag{5.27}$$

where $\hat{\Lambda}$, a deexcitation operator multiplied by Lagrange's multipliers, is defined as

$$\begin{aligned} \hat{\Lambda} &= \hat{\Lambda}_1 + \hat{\Lambda}_2 \\ &= \sum_{ia} \Lambda_i^a \hat{E}_a^i + \frac{1}{2} \sum_{ijab} \Lambda_{ij}^{ab} \hat{E}_a^i \hat{E}_b^j, \end{aligned} \tag{5.28}$$

with the unitary-group generator

$$\hat{E}_i^a = \hat{a}_{a_\alpha}^\dagger \hat{a}_{i_\alpha} + \hat{a}_{a_\beta}^\dagger \hat{a}_{i_\beta}. \tag{5.29}$$

If we did not have the quintet contribution, we would have exactly the same Lagrangian as RCCSD. Finding a stationary point of $\mathcal{L}$ with respect to the variations of t_i^a, ${}^S S_{ij}^{ab}$, and ${}^A S_{ij}^{ab}$ yields the CCVB-SD Λ-equation. For the singles equations, it can be easily shown that the resulting equation is essentially identical to the one for RCCSD with the cluster operator $\hat{\mathcal{G}}$. [494] Below we shall discuss how the doubles equations differ from the usual RCCSD Λ-equation.

From Eq. (5.26),

$$\frac{\partial \hat{\mathcal{Q}}}{\partial\, {}^A S_{ij}^{ab}} = -2\, {}^{tt}\hat{\kappa}_{ij}^{ab}, \tag{5.30}$$

and the quintet contribution for the Λ-equation follows

$$2 \langle \Phi_0 | \left(\hat{\mathrm{I}} + \hat{\Lambda} \right) \left(\hat{\mathcal{H}}\ \hat{\mathrm{I}}_S\, {}^{tt}\hat{\kappa}_{ij}^{ab} \hat{\mathcal{Q}} \right) | \Phi_0 \rangle = 2 \langle \Phi_0 | \hat{\Lambda}_2 \hat{\mathcal{H}}\ \hat{\mathrm{I}}_S\, {}^{tt}\hat{\kappa}_{ij}^{ab} \hat{\mathcal{Q}} | \Phi_0 \rangle \,. \tag{5.31}$$

Using

$$\langle \Phi_0 | \left(\hat{\mathrm{I}} + \hat{\Lambda}_2 \right) e^{-\hat{\mathcal{Q}}} [\hat{\mathcal{H}}, {}^{tt}\hat{\kappa}_{ij}^{ab}] e^{\hat{\mathcal{Q}}} | \Phi_0 \rangle = \langle \Phi_0 | \hat{\Lambda}_2 \hat{\mathcal{H}}\ \hat{\mathrm{I}}_S\, {}^{tt}\hat{\kappa}_{ij}^{ab} \hat{\mathcal{Q}} | \Phi_0 \rangle \,, \tag{5.32}$$

the quintet contribution can be reshaped similarly to the RCCD Λ-equation expression with the doubles operator being $\hat{\mathcal{Q}}$.

Using this, the CCVB-SD Λ-equation in a spatial-orbital form for each variation with respect to ${}^{S}S_{ij}^{ab}$ and ${}^{A}S_{ij}^{ab}$ is written as

$$\frac{\partial \mathcal{L}}{\partial\, {}^{S}S_{ij}^{ab}} = 0 \rightarrow \langle \Phi_0 | \left(\hat{\mathrm{I}} + \hat{\Lambda}\right) e^{-\hat{\mathcal{G}}} \left[\hat{\mathcal{H}}, {}^{ss}\hat{\Sigma}_{ij}^{ab}\right] e^{\hat{\mathcal{G}}} |\Phi_0\rangle = 0, \tag{5.33}$$

$$\begin{aligned}\frac{\partial \mathcal{L}}{\partial\, {}^{A}S_{ij}^{ab}} = 0 \rightarrow &\langle \Phi_0 | \left(\hat{\mathrm{I}} + \hat{\Lambda}\right) e^{-\hat{\mathcal{G}}} \left[\hat{\mathcal{H}}, {}^{tt}\hat{\Sigma}_{ij}^{ab}\right] e^{\hat{\mathcal{G}}} |\Phi_0\rangle \\ &+ 2 \langle \Phi_0 | \left(\hat{\mathrm{I}} + \hat{\Lambda}_2\right) e^{-\hat{\mathcal{Q}}} [\hat{\mathcal{H}}, {}^{tt}\hat{\kappa}_{ij}^{ab}] e^{\hat{\mathcal{Q}}} |\Phi_0\rangle = 0.\end{aligned} \tag{5.34}$$

This can be further simplified to more familiar forms [494],

$$\langle \Phi_0 | \left(\bar{\mathcal{H}}^{\hat{\mathcal{G}}} + \left[\hat{\Lambda}, \bar{\mathcal{H}}^{\hat{\mathcal{G}}}\right] + \sum_{kc} \bar{\mathcal{H}}^{\hat{\mathcal{G}}} |\Phi_k^c\rangle \langle \Phi_k^c| \hat{\Lambda}_1 \right) |{}^{S}\Phi_{ij}^{ab}\rangle = 0, \tag{5.35}$$

$$\begin{aligned}&\langle \Phi_0 | \left(\bar{\mathcal{H}}^{\hat{\mathcal{G}}} + \left[\hat{\Lambda}, \bar{\mathcal{H}}^{\hat{\mathcal{G}}}\right] + \sum_{kc} \bar{\mathcal{H}}^{\hat{\mathcal{G}}} |\Phi_k^c\rangle \langle \Phi_k^c| \hat{\Lambda}_1 \right) |{}^{A}\Phi_{ij}^{ab}\rangle \\ &\quad + 2 \langle \Phi_0 | \left(\bar{\mathcal{H}}^{\hat{\mathcal{Q}}} + \left[\hat{\Lambda}_2, \bar{\mathcal{H}}^{\hat{\mathcal{Q}}}\right] \right) |{}^{Q}\Phi_{ij}^{ab}\rangle = 0,\end{aligned} \tag{5.36}$$

where we define

$$\bar{\mathcal{H}}^{\hat{\mathcal{O}}} = e^{-\hat{\mathcal{O}}} \hat{\mathcal{H}} e^{\hat{\mathcal{O}}}. \tag{5.37}$$

Eq. (5.35) can be used to update the symmetric part of Λ_{ij}^{ab} (i.e. ${}^{S}\Lambda_{ij}^{ab}$) whilst Eq. (5.36) can be used to update the antisymmetric part of Λ_{ij}^{ab} (i.e. ${}^{A}\Lambda_{ij}^{ab}$) .

5.3.1 Unrelaxed PDMs

It can be verified that the expression of the CCVB-SD one-particle density matrix (1PDM) is identical to that of RCCSD.[494] On the other hand, the expression for the two-particle density matrix (2PDM) has an extra term associated with $\hat{\mathcal{Q}}$. To see this, we define a spin-orbital tensor of size $2(n_{\mathrm{occ}} + n_{\mathrm{vir}})^4$ (having both same-spin and opposite-spin blocks) that represents the CCVB-SD unrelaxed 2PDM:

$$\xi_{r_{\sigma_1} s_{\sigma_2}}^{p_{\sigma_1} q_{\sigma_2}} = \langle \Phi_0 | \left(\hat{\mathrm{I}} + \hat{\Lambda}\right) \left(e^{-\hat{\mathcal{G}}} (\hat{a}_{p_{\sigma_1}}^{\dagger} \hat{a}_{q_{\sigma_2}}^{\dagger} \hat{a}_{s_{\sigma_2}} \hat{a}_{r_{\sigma_1}}) e^{\hat{\mathcal{G}}} - \frac{1}{2} (\hat{a}_{p_{\sigma_1}}^{\dagger} \hat{a}_{q_{\sigma_2}}^{\dagger} \hat{a}_{s_{\sigma_2}} \hat{a}_{r_{\sigma_1}}) \hat{\mathrm{I}}_S \hat{\mathcal{Q}}^2 \right) |\Phi_0\rangle \tag{5.38}$$

$$= {}^{\hat{\mathcal{G}}}\xi_{r_{\sigma_1} s_{\sigma_2}}^{p_{\sigma_1} q_{\sigma_2}} + {}^{\hat{\mathcal{Q}}}\xi_{r_{\sigma_1} s_{\sigma_2}}^{p_{\sigma_1} q_{\sigma_2}}, \tag{5.39}$$

where

$${}^{\hat{\mathcal{G}}}\xi_{r_{\sigma_1} s_{\sigma_2}}^{p_{\sigma_1} q_{\sigma_2}} = \langle \Phi_0 | \left(\hat{\mathrm{I}} + \hat{\Lambda}\right) e^{-\hat{\mathcal{G}}} (\hat{a}_{p_{\sigma_1}}^{\dagger} \hat{a}_{q_{\sigma_2}}^{\dagger} \hat{a}_{s_{\sigma_2}} \hat{a}_{r_{\sigma_1}}) e^{\hat{\mathcal{G}}} |\Phi_0\rangle, \tag{5.40}$$

and

$$ {}^{\hat{\mathcal{Q}}}\xi^{p_{\sigma_1}q_{\sigma_2}}_{r_{\sigma_1}s_{\sigma_2}} = -\frac{1}{2}\left\langle\Phi_0\right|(\hat{\mathrm{I}}+\hat{\Lambda})(\hat{a}^\dagger_{p_{\sigma_1}}\hat{a}^\dagger_{q_{\sigma_2}}\hat{a}_{s_{\sigma_2}}\hat{a}_{r_{\sigma_1}})\hat{\mathrm{I}}_S\hat{\mathcal{Q}}^2\left|\Phi_0\right\rangle. \tag{5.41} $$

${}^{\hat{\mathcal{G}}}\xi$ is the RCCSD contribution with the cluster operator $\hat{\mathcal{G}}$, and ${}^{\hat{\mathcal{Q}}}\xi$ is an extra term coming from $\hat{\mathcal{Q}}$. It is clear that the second term contributes to only OOVV blocks (i.e. $\xi^{i_{\sigma_1}j_{\sigma_2}}_{a_{\sigma_1}b_{\sigma_2}}$) because $\hat{\mathcal{Q}}^2$ produces quadruply excited configurations. We then use a similar trick used in Eq. (5.32) to write the extra term in the following form:

$$ {}^{\hat{\mathcal{Q}}}\xi^{p_{\sigma_1}q_{\sigma_2}}_{r_{\sigma_1}s_{\sigma_2}} = -\left\langle\Phi_0\right|(\hat{\mathrm{I}}+\hat{\Lambda}_2)e^{-\hat{\mathcal{Q}}}(\hat{a}^\dagger_{i_{\sigma_1}}\hat{a}^\dagger_{j_{\sigma_2}}\hat{a}_{b_{\sigma_2}}\hat{a}_{a_{\sigma_1}})\hat{\mathrm{I}}_S e^{\hat{\mathcal{Q}}}\left|\Phi_0\right\rangle. \tag{5.42} $$

Having these unrelaxed PDMs allows for computing unrelaxed one-electron and two-electron properties.

As the formation of relaxed PDMs (i.e. response equations) for CCVB-SD remains unchanged from RCCSD, [494] all the relaxed properties of CCVB-SD are computed by usual ways as is done for RCCSD. The analytical gradients can be readily implemented in general coupled-cluster codes.

5.4 Block-Tensor Implementation of CCVB-SD

In this section, we use uppercase letters such as S, ${}^SS$, ${}^AS$, Q, Λ, ${}^S\Lambda$, and ${}^A\Lambda$ to indicate spinless tensors or operators as before, and lowercase letters such as s, q, μ, ν , λ, ρ, ζ, and ξ are used for spinful tensors, i.e. ones with spin-orbital indices.

5.4.1 Tensorial Properties of Doubles Operators

In a spin-orbital based implementation, $\hat{\mathcal{S}}$ is represented by a set of amplitudes $s^{a_{\sigma_1}b_{\sigma_2}}_{i_{\sigma_1}j_{\sigma_2}}$ as shown in Eq. (5.21). With this, we can extract ${}^A\mathbf{S}$:

$$ {}^AS^{ab}_{ij} = \frac{1}{\sqrt{12}}\left(s^{b_\beta a_\alpha}_{i_\beta j_\alpha} + s^{b_\alpha a_\beta}_{i_\alpha j_\beta} - s^{a_\beta b_\alpha}_{i_\beta j_\alpha} - s^{a_\alpha b_\beta}_{i_\alpha j_\beta} - 2s^{a_\beta b_\beta}_{i_\beta j_\beta} - 2s^{a_\alpha b_\alpha}_{i_\alpha j_\alpha}\right). \tag{5.43} $$

This form, however, poses a little challenge when embedded into block-tensor based codes as accessing individual elements of tensors will be highly inefficient. Manipulating such equations in terms of block tensors instead of individual elements is thus valuable.

`Q-Chem`'s[236] coupled-cluster code, `ccman2`, extensively employs the block tensors implemented in a general tensor library called `libtensor`. [495] In `libtensor`, any doubles amplitudes of the form $o^{a_{\sigma_1}b_{\sigma_2}}_{i_{\sigma_1}j_{\sigma_2}}$ are stored only with non-zero, symmetry-unique blocks, called canonical blocks. For instance, when unrestricted orbitals are

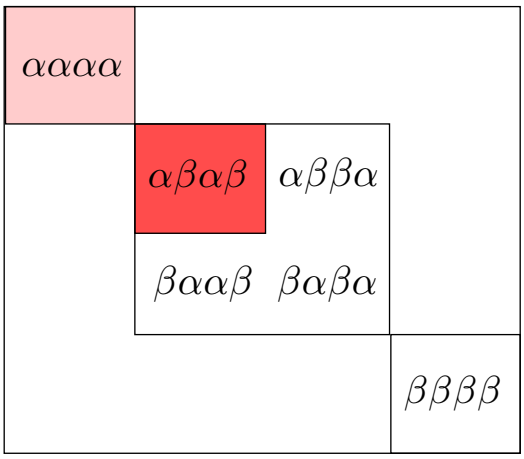

Figure 5.2: The data structure of block tensors of order 4. Colored blocks are only canonical blocks for tensors with restricted orbitals, and $(\alpha\alpha\alpha\alpha)$ block can be obtained from $(\alpha\beta\alpha\beta)$ block in the case of singlet operators.

used there are three canonical blocks (i.e. $(\alpha\alpha\alpha\alpha)$, $(\beta\beta\beta\beta)$, $(\alpha\beta\alpha\beta)$) out of the total six blocks illustrated in Figure 5.2. In the case of restricted orbitals and closed-shell molecules (or more generally singlet operators), one needs only opposite-spin blocks (i.e. $(\alpha\beta\alpha\beta)$) to form the entire tensor. This is because restricted orbitals imply the $\alpha \leftrightarrow \beta$ symmetry and for singlet operators same-spin blocks can be obtained by antisymmetrising opposite-spin blocks.

This can be seen from the form of a singlet configuration $|\Phi\rangle = \hat{\mathcal{S}}\,|\Phi_0\rangle$. The projection of this state onto the same-spin space is simply obtained as

$$s_{i_\alpha j_\alpha}^{a_\alpha b_\alpha} = \langle \Delta_{i_\alpha j_\alpha}^{a_\alpha b_\alpha} | \hat{\mathcal{S}} | \Phi_0 \rangle = -\frac{1}{\sqrt{3}}\, {}^{A}S_{ij}^{ab}. \tag{5.44}$$

Similarly, the opposite-spin projection is

$$s_{i_\alpha j_\beta}^{a_\alpha b_\beta} = \langle \Delta_{i_\alpha j_\beta}^{a_\alpha b_\beta} | \hat{\mathcal{S}} | \Phi_0 \rangle = \frac{1}{2}\, {}^{S}S_{ij}^{ab} - \frac{1}{\sqrt{12}}\, {}^{A}S_{ij}^{ab}, \tag{5.45}$$

$$s_{i_\alpha j_\beta}^{b_\alpha a_\beta} = \langle \Delta_{i_\alpha j_\beta}^{b_\alpha a_\beta} | \hat{\mathcal{S}} | \Phi_0 \rangle = \frac{1}{2}\, {}^{S}S_{ij}^{ab} + \frac{1}{\sqrt{12}}\, {}^{A}S_{ij}^{ab}. \tag{5.46}$$

This shows that for any combination of (i, j) and (a, b) including $i = j$ or $a = b$

$$s_{i_\alpha j_\alpha}^{a_\alpha b_\alpha} = s_{i_\alpha j_\beta}^{a_\alpha b_\beta} - s_{i_\alpha j_\beta}^{b_\alpha a_\beta}. \tag{5.47}$$

Similarly, one can show

$$s_{i_\alpha j_\alpha}^{a_\alpha b_\alpha} = \frac{1}{2}\left(s_{i_\alpha j_\beta}^{a_\alpha b_\beta} - s_{i_\alpha j_\beta}^{b_\alpha a_\beta} + s_{j_\alpha i_\beta}^{b_\alpha a_\beta} - s_{j_\alpha i_\beta}^{a_\alpha b_\beta} \right). \tag{5.48}$$

As long as restricted orbitals are employed, both Eq. (5.47) and Eq. (5.48) are identical. The latter is preferred for the purpose of demonstration because it is easier to see the full antisymmetrisation with respect to permuting either occupied orbitals or virtual orbitals. Symbolically, we write thisEq. (5.48) as

$$\mathtt{SS(s)} = \frac{1}{2}\,\mathtt{asymm_O[asymm_V[OS(s)]]}, \tag{5.49}$$

where $\mathtt{SS}(\cdot)$ denotes the same-spin block of a given tensor as in

$$\mathtt{SS(s)}^{ab}_{ij} = s^{a_\alpha b_\alpha}_{i_\alpha j_\alpha}, \tag{5.50}$$

$\mathtt{OS}(\cdot)$ denotes the opposite-spin block of a given tensor as in

$$\mathtt{OS(s)}^{ab}_{ij} = s^{a_\alpha b_\beta}_{i_\alpha j_\beta}, \tag{5.51}$$

and $\mathtt{asymm_O}[\cdot]$ and $\mathtt{asymm_V}[\cdot]$ perform antisymmetrisation of a given tensor over occupied and virtual spatial indices, respectively. Similarly, we define symmetrisation of a given tensor as $\mathtt{symm_O}[\cdot]$ and $\mathtt{symm_V}[\cdot]$ over occupied and virtual spatial indices, respectively. In passing, we note that Eq. (5.44) implies that the spinless antisymmetric part of a singlet tensor is obtained simply scaling the same-spin component of the corresponding singlet spinful tensor. This is again in the symbolic form:

$$\mathtt{^A S} = -\sqrt{3}\ \mathtt{SS(s)}. \tag{5.52}$$

We then illustrate the tensorial properties of $\mathbf{Q}$ which will be useful to derive block-tensor equations. It can be read from Eq. (5.25) that (similarly to Eq. (5.44))

$$\mathtt{SS(q)} = \frac{1}{\sqrt{6}}\,\mathtt{Q}. \tag{5.53}$$

and $(\alpha\alpha\alpha\alpha)$ and $(\beta\beta\beta\beta)$ blocks of $\mathbf{q}$ are identical. Combining this with Eq. (5.26) and Eq. (5.52), we arrive at

$$\mathtt{SS(q)} = \frac{-2}{\sqrt{6}}\,\mathtt{^A S} = \sqrt{2}\ \mathtt{SS(s)}. \tag{5.54}$$

This shows how the same-spin block of the spinful tensor $\mathbf{q}$ is related to the same-spin block of a singlet tensor $\mathbf{s}$. Also, the opposite spin-block of $\mathbf{q}$ is

$$\mathtt{OS(q)} = -\,\mathtt{SS(q)}, \tag{5.55}$$

and this contrasts with Eq. (5.49), which manifests a different tensorial property of singlet and quintet tensors.

5.4.2 T-Amplitude Solver

The singles equation is identical to RCCSD with the doubles operator $\hat{\mathcal{G}}$, so we will focus on solving the doubles equation. Based on the properties of the doubles operators appearing in CCVB-SD discussed above, CCVB-SD can be efficiently implemented in a block-tensor based coupled cluster codes. The CCVB-SD amplitude equation reads

$$\rho^{a_{\sigma_1}b_{\sigma_2}}_{i_{\sigma_1}j_{\sigma_2}}(\hat{\mathcal{G}}) = \mu^{a_{\sigma_1}b_{\sigma_2}}_{i_{\sigma_1}j_{\sigma_2}}(\hat{\mathcal{G}}) - \left(\nu^{a_{\sigma_1}b_{\sigma_2}}_{i_{\sigma_1}j_{\sigma_2}}(\hat{\mathcal{Q}}) - \langle a_{\sigma_1}b_{\sigma_2} \parallel i_{\sigma_1}j_{\sigma_2}\rangle\right) = 0, \tag{5.56}$$

where we define

$$\mu^{a_{\sigma_1}b_{\sigma_2}}_{i_{\sigma_1}j_{\sigma_2}}(\hat{\mathcal{O}}) = \left\langle \Delta^{a_{\sigma_1}b_{\sigma_2}}_{i_{\sigma_1}j_{\sigma_2}} \middle| \bar{\mathcal{H}}^{\hat{\mathcal{O}}} \middle| \Phi_0 \right\rangle, \tag{5.57}$$

and

$$\nu^{a_{\sigma_1}b_{\sigma_2}}_{i_{\sigma_1}j_{\sigma_2}}(\hat{\mathcal{O}}) = \left\langle \Delta^{a_{\sigma_1}b_{\sigma_2}}_{i_{\sigma_1}j_{\sigma_2}} \middle| \hat{\mathrm{I}}_S \bar{\mathcal{H}}^{\hat{\mathcal{O}}} \middle| \Phi_0 \right\rangle. \tag{5.58}$$

$\mu(\hat{\mathcal{O}})$ can be obtained easily with any existing coupled-cluster codes whereas computing $\nu(\hat{\mathcal{O}})$ is not as straightforward. Below we illustrate how to solve this amplitudes equation with details on computing $\nu(\hat{\mathcal{Q}})$ from $\mu(\hat{\mathcal{Q}})$:

1. Perform the block-tensor operation demonstrated in Eq. (5.54) based on **s** either from the previous iteration or an initial guess. This gives `SS(q)` and then performing the operation in Eq. (5.55) yields the full **q** tensor.

2. Form $\mu(\hat{\mathcal{Q}})$ defined in Eq. (5.57). This can be achieved with any standard coupled-cluster codes.

3. $\nu(\hat{\mathcal{Q}})$ is obtained through a spin-projection of $\mu(\hat{\mathcal{Q}})$ onto a 4-electron singlet subspace. Since $\nu(\hat{\mathcal{Q}})$ is strictly a singlet, we can utilize the tensorial properties of general singlet tensors discussed above. The upshot is that we only need to obtain `OS(`ν`(`$\hat{\mathcal{Q}}$`))` and `SS(`ν`(`$\hat{\mathcal{Q}}$`))` will be obtained using Eq. (5.49). For the sake of simplicity, we write μ and ν to indicate $\mu(\hat{\mathcal{Q}})$ and $\nu(\hat{\mathcal{Q}})$, respectively.

   The element wiseelement-wise definition of ν is well described in the appendix of ref.141, which can be further simplified to

$$\begin{aligned}\nu^{a_\alpha b_\beta}_{i_\alpha j_\beta} &= \frac{1}{6}\left(\mu^{b_\beta a_\alpha}_{i_\beta j_\alpha} + \mu^{b_\alpha a_\beta}_{i_\alpha j_\beta} + 2\mu^{a_\beta b_\alpha}_{i_\beta j_\alpha} + 2\mu^{a_\alpha b_\beta}_{i_\alpha j_\beta} + \mu^{a_\beta b_\beta}_{i_\beta j_\beta} + \mu^{a_\alpha b_\alpha}_{i_\alpha j_\alpha}\right) \\ &= \frac{1}{3}\left(\mu^{b_\alpha a_\beta}_{i_\alpha j_\beta} + 2\mu^{a_\alpha b_\beta}_{i_\alpha j_\beta} + \mu^{a_\alpha b_\alpha}_{i_\alpha j_\alpha}\right),\end{aligned} \tag{5.59}$$

where we used $\mu^{a_\alpha b_\beta}_{i_\alpha j_\beta} = \mu^{a_\beta b_\alpha}_{i_\beta j_\alpha}$. We then write this in a block-tensor form:

$$\mathtt{OS}(\nu) = \frac{1}{3}\left(\mathtt{OS}(\mu) + \mathtt{symm_V}[\mathtt{OS}(\mu)] + \mathtt{SS}(\mu)\right). \tag{5.60}$$

The same-spin blocks are obtained using Eq. (5.49). In passing, we note that Eq. (5.59) gives a correct singlet tensor even when there are repeated indices. One can verify that this single operation yields all the spin-projected opposite-spin blocks of the tensor described in the appendix of ref.141.

After evaluating $\rho(\hat{\mathcal{G}})$, a standard Jacobi iteration along with Pulay's direct inversion of the iterative subspace (DIIS) [496] can be used to solve for the amplitudes. This completes the implementation of the CCVB-SD T-amplitude solver. The computational cost of CCVB-SD has a larger prefactor (roughly twice larger) than RCCSD due to the need for constructing $\nu(\hat{\mathcal{Q}})$. As its asymptotic scaling is the same as RCCSD ($n^2_{\mathrm{occ}} n^4_{\mathrm{vir}}$), this is considered a minor drawback. More detailed information on the performance of this implementation is available in the applications discussed later.

5.4.3 Λ-Equation Solver

We define a general spin-orbital tensor γ that can be readily computed in usual coupled cluster programs as follows,

$$\gamma^{a_{\sigma_1} b_{\sigma_2}}_{i_{\sigma_1} j_{\sigma_2}}(\hat{\mathcal{O}}) = \langle \Phi_0 | \left(\bar{\mathcal{H}}^{\hat{\mathcal{O}}} + \left[\hat{\Lambda}, \bar{\mathcal{H}}^{\hat{\mathcal{O}}}\right] + \sum_{kc} \bar{\mathcal{H}}^{\hat{\mathcal{O}}} \left|\Phi^c_k\right\rangle \left\langle \Phi^c_k \right| \hat{\Lambda}_1 \right) \left| \Delta^{a_{\sigma_1} b_{\sigma_2}}_{i_{\sigma_1} j_{\sigma_2}} \right\rangle. \tag{5.61}$$

Using this tensor and Eq. (5.11), Eq. (5.35) can be achieved by

$$\frac{1}{2}\,\mathtt{symm_V}[\mathtt{symm_0}[\mathtt{OS}(\gamma(\hat{\mathcal{G}}))]], \tag{5.62}$$

whereas with Eq. (5.12) and Eq. (5.25), Eq. (5.36) can be written as

$$\begin{aligned} &\frac{1}{\sqrt{3}}\left(-\frac{1}{2}\,\mathtt{asymm_V}[\mathtt{asymm_0}[\mathtt{OS}(\gamma(\hat{\mathcal{G}}))] - 2\,\mathtt{SS}(\gamma(\hat{\mathcal{G}}))\right) \\ &+ \frac{4}{\sqrt{6}}\left(-\frac{1}{2}\,\mathtt{asymm_V}[\mathtt{asymm_0}[\mathtt{OS}(\gamma(\hat{\mathcal{Q}}))] + \mathtt{SS}(\gamma(\hat{\mathcal{Q}}))\right). \end{aligned} \tag{5.63}$$

Combining these with Eq. (5.45), a full update of $\mathtt{OS}(\lambda)$ is obtained. As λ is a singlet spin-orbital tensor, we can simply obtain the same-spin block using Eq. (5.49).

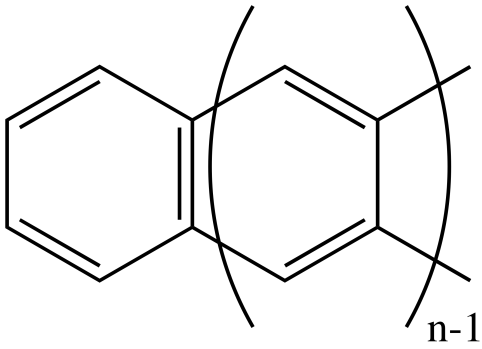

Figure 5.3: The chemical structure of n-acene ($C_2H_4C_{4n}H_{2n}$).

5.4.4 Unrelaxed PDMs

The form presented in Eq. (5.42) is not convenient to use because of the singlet projection operator appearing in the middle of two non-singlet operators. Thus, it is natural to form separate expressions for the symmetric part and the antisymmetric part of the 2PDM tensor similarly to what is proposed in the Λ-equation solver. We define a spin-orbital tensor

$$\zeta^{i_{\sigma_1} j_{\sigma_2}}_{a_{\sigma_1} b_{\sigma_2}} = -\left\langle \Phi_0 \right| \left(\hat{\mathrm{I}} + \hat{\Lambda}_2\right) e^{-\hat{\mathcal{Q}}} (\hat{a}^\dagger_{i_{\sigma_1}} \hat{a}^\dagger_{j_{\sigma_2}} \hat{a}_{b_{\sigma_2}} \hat{a}_{a_{\sigma_1}}) e^{\hat{\mathcal{Q}}} \left| \Phi_0 \right\rangle , \tag{5.64}$$

and this can be easily computed in the same way as RCCD. Using Eq. (5.45), $\mathtt{OS}(\hat{\mathcal{Q}}\xi)$ is obtained as

$$\begin{aligned} \mathtt{OS}(\hat{\mathcal{Q}}\xi) = & \frac{1}{4}\, \mathtt{symm_V}[\mathtt{symm_0}[\mathtt{OS}(\zeta)]] \\ & + \frac{1}{3}\left(\frac{1}{4}\, \mathtt{asymm_V}[\mathtt{asymm_0}[\mathtt{OS}(\zeta)] + \mathtt{SS}(\zeta)\right). \end{aligned} \tag{5.65}$$

As $\hat{\mathcal{Q}}\xi$ is a singlet tensor, we can use Eq. (5.49) to form $\mathtt{SS}(\hat{\mathcal{Q}}\xi)$ based on $\mathtt{OS}(\hat{\mathcal{Q}}\xi)$ obtained above.

5.5 Applications to oligoacenes

The acenes, illustrated in Fig. 5.3, are known to exhibit emergent strong correlations as their length grows and thus they provide a well-defined platform for testing novel approaches for strong correlations. There have been numerous studies on oligoacenes using various methods such as CASSCF,[330, 483] DMRG-CASCI,[38, 39]

variational 2-RDM methods,[484–486] adaptive CI (ACI),[487] multi-reference averaged quadratic coupled cluster (MR-AQCC),[497, 498] and density functional theory (DFT) based methods such as DFT/MRCI,[488] thermally-assisted-occupation DFT (TAO-DFT),[489] fractional-spin DFT (FS-DFT),[490] and particle-particle random-phase approximation (pp-RPA).[491] Although RCCSD has been applied to short acenes (n≤7)[483, 499, 500], there is no study on longer acenes using RCCSD mainly because of their known failures for strongly correlated systems.

We compare absolute energies and natural orbital occupation numbers of different SRCC methods against the exact answers taken from ref.38 up to 12-acene with all π-electrons correlated. The natural orbital occupation numbers for SRCC are computed with symmetrised 1PDMs. Symmetrised 1PDMs yield very similar results to unsymmetrised ones. We further study and discuss higher acenes (n>12) using CCVB-SD with a well-defined model geometry ($R_{C-C} = 1.3964\mathring{A}$, $R_{C-H} = 1.0755\mathring{A}$) not only correlating π-electrons but correlating all the valence electrons. All the calculations presented below employ a minimal basis (STO-3G) and are performed with the development version of `Q-Chem`.[236] All the plots were generated with `matplotlib`.[283]

5.5.1 Comparison against DMRG with all π-electrons correlated

We first examine whether using RHF orbitals is valid for these systems because the quality of RHF orbitals often degrades for strongly correlated systems. Optimised doubles (OD) [178, 267] or orbital-optimised CCD yields nearly identical energies to those of RCCSD, implying that RHF orbitals are qualitatively correct. Due to convergence issues, OD was performed only up to 6-acene, so, to further examine the efficacy of using RHF orbitals, we also carried out test CCVB-SD calculations with RBLYP orbitals. The use of RBLYP orbitals does not yield qualitatively different results. Therefore, the numbers reported in Table 5.1 are all obtained using stable RHF orbitals that are spatially symmetric.

For weakly correlated systems, RCCSD and CCVB-SD yield almost identical results and the deviation between the two becomes more significant for the systems with strong correlations. For the acenes shown in Table 5.1, the RCCSD energies are significantly lower than those of CCVB-SD, which hints at a non-variational failure of RCCSD. More specifically, as illustrated in Table 5.1, RCCSD and OD may be starting to "turn over" at 6-acene because the error in correlation energies is smaller in 6-acene than in 5-acene. Moreover, the RCCSD(T) energies are lower than those of DMRG. Fig. 5.4 demonstrates that the correlation energy error per acene unit

n	DMRG	CCVB-SD	RCCSD	RCCSD(T)	OD	QCCD	QCCD(2)
2	-378.862173	9.472	2.509	-0.499	2.550	5.102	2.915
3	-529.721682	14.671	4.472	-0.784	4.538	8.766	5.071
4	-680.578678	20.481	6.103	-1.888	6.203	13.000	7.653
5	-831.434630	26.941	7.142	-4.185	7.254	17.846	10.706
6	-982.290070	34.822	6.432	-9.609	6.114	23.989	14.750
8	-1284.000964	54.051	DNC	DNC	DNC	DNC	DNC
10	-1585.713311	71.973	DNC	DNC	DNC	DNC	DNC
12	-1887.425575	89.154	DNC	DNC	DNC	DNC	DNC

Table 5.1: Reference absolute energies (in Hartrees) from the π-space DMRG calculations of ref.38 and deviations (in mH) of several methods from the DMRG values. Geometries are also taken from ref.38 which were optimised at the level of UB3LYP/6-31G* with $S = 0$. The number of renormalised states, M, of DMRG calculations is 1000. The DMRG calculation for n=12 was not fully converged with respect to M. Calculations with convergence problems are indicated by DNC. RHF orbitals are used for CCVB-SD, RCCSD, and RCCSD(T) whereas OD, QCCD, and QCCD(2) are computed with optimised orbitals.

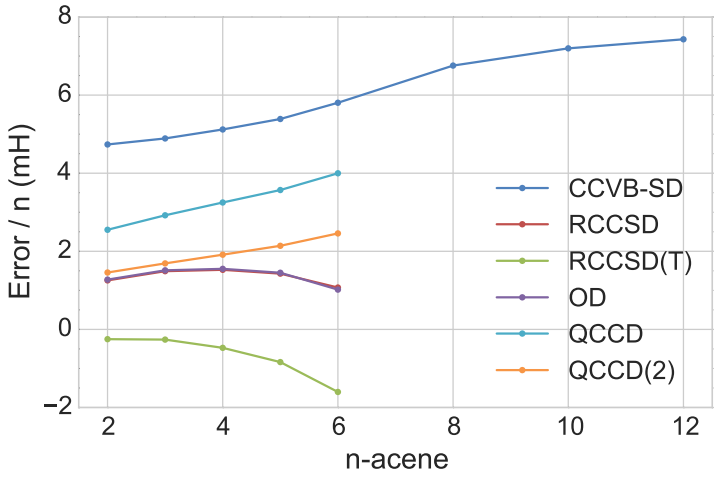

Figure 5.4: The correlation energy error with respect to DMRG per acene unit of different coupled-cluster methods. We note that the OD curve is right on top of the RCCSD one.

in CCVB-SD reaches a plateau value as the system size increases. It confirms that the correlation energy error in CCVB-SD is size-extensive. Furthermore, RCCSD,

RCCSD(T), and OD turn over at 5-acene. In the end, they must plateau since they are all size-extensive.

We confirm whether RCCSD behaves non-variationally by performing orbital-optimised QCCD [442] where the left eigenfunction is improved by including a de-excitation operator up to quadratic terms and the right eigenfunction remains the same as that of RCCD. This more balanced treatment of the left eigenfunction allows for an energy evaluation closer to that of variational CC.

Table 5.1 shows that the QCCD energies are above the RCCSD energies for every acene considered here. As QCCD energies are closer to the true variational CCSD energies,[430, 442] we conclude that RCCSD behavesmay be behaving non-variationally even for short acenes. It is interesting that even a seemingly innocent molecule like naphthalene apparently shows non-variationality of RCCSD given that this behaviour has been mostly observed for molecules near bond dissociations. In passing, we note that CCVB-SD does not show any convergence issues unlike the others presented here and this is likely due to the approximate inclusion of connected quadruples that stablisesstabilises singles and doubles amplitudes.

Neither QCCD nor CCVB-SD is variational, so either could in principle exhibit non-variationality. In other words, both CCVB-SD and QCCD [430] can legitimately be below variational CCSD. QCCD cannot reach the correct limit for bond-breaking while CCVB-SD can.[442] Yet CCVB-SD yields higher energies for the acenes. This suggests that QCCD may be also exhibiting non-variationality. It will be interesting to see other approaches such as unitary CCSD[432–435] and extended CCSD[436–441] to further investigate this. In passing we note that, unlike RCCSD(T), the QCCD(2) energiesthe energies of QCCD(2),[444] which is a perturbative correction of a similar level of theory to RCCSD(T), are above the DMRG energies for acenes up to n = 6. It will be interesting to see whether QCCD(2) will become lower than DMRG for longer acenes. Given that the NOONs of QCCD and CCVB-SD are very similar and their energies are yet very different, it will be interesting to compare a perturbative correction to CCVB-SD and QCCD(2) in the future.

We then discuss the natural orbital occupation numbers (NOONs) of each method. The NOONs of RCCSD show larger polyradical character than that of DMRG, which indicates RCCSD's tendency to overcorrelate these systems. The NOONs of QCCD are less polarised than those of CCSDRCCSD and they are very similar to those of CCVB-SD. The NOONs of CCVB-SD show similar trends to DMRG's, but with smaller radical character. This may, in part, be due to missing connected higher-than-double excitations in CCVB-SD that may be necessary to better describe correlations of acenes. We discuss more in depth the nature of correlations in oligoacenes in a separate study.

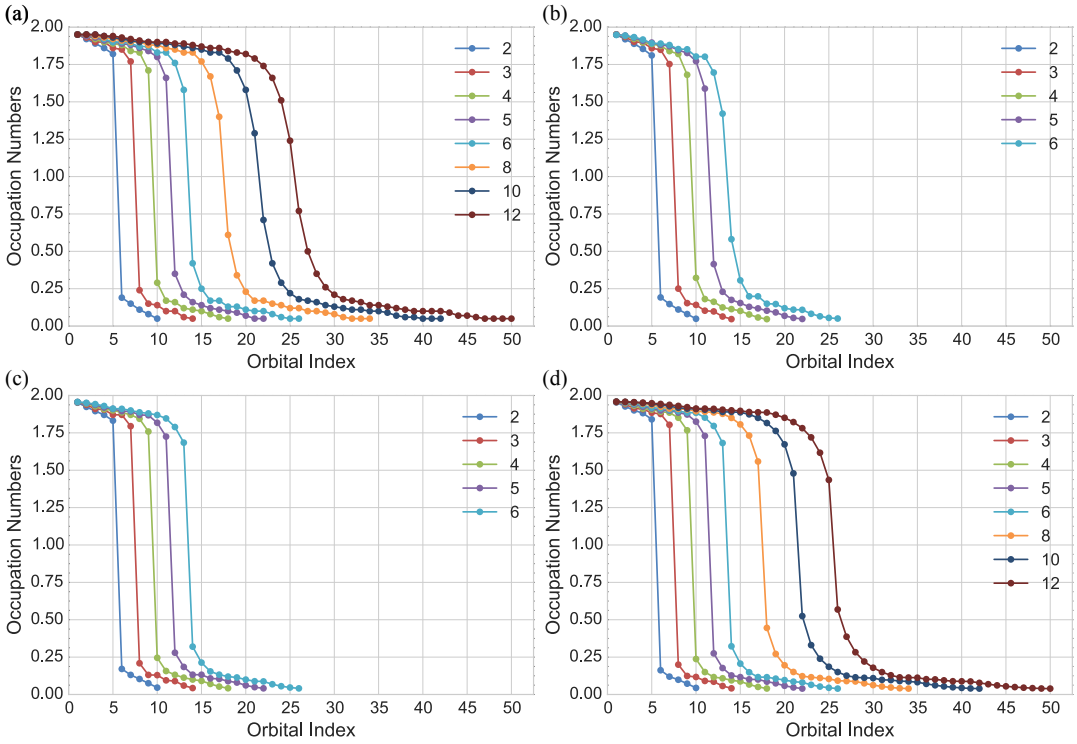

Figure 5.5: Natural orbital occupation numbers from (a) DMRG, (b) RCCSD, (c) QCCD, and (d) CCVB-SD.

5.5.2 Application of CCVB-SD to longer acene oligomers

We apply CCVB-SD to a model geometry up to 23-acene with all π-electrons correlated and up to 17-acene with all valence electrons correlated. As mentioned earlier, the lengths of all C-C and C-H bonds are fixed at 1.3964 Å and 1.0755 Å, respectively. The angle between three neighboring carbons and the angle between H$-$C$-$C are fixed at 120° to ensure D_{2h} symmetry.

The NOONs for these series are shown in Fig. 5.6. Compared to the results from the UB3LYP geometries used above, there is virtually no difference in the NOONs. It has been pointed out that small changes in geometries of oligoacenes do not alter their NOONs.[39] Regardless of whether all π-electrons are correlated or all valence electrons are correlated, both cases exhibit a plateau region as the acene chain length increases.

Mizukami *et al.* applied DMRG with $M = 256$ to a model geometry (R_{C-C}(shorter) = 1.402Å, R_{C-C}(longer) = 1.435Å, R_{C-H} = 1.010Å) up to 25-acene with all π-electrons

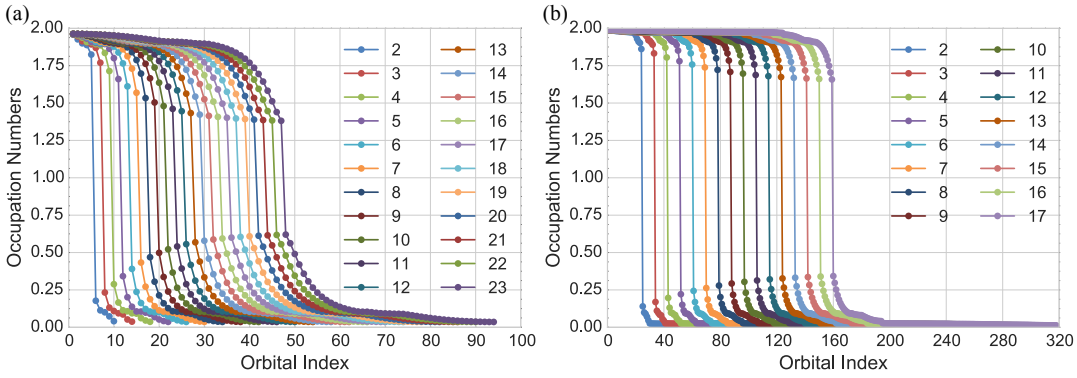

Figure 5.6: Natural orbital occupation numbers of model geometries (R_{C-C} = 1.3964 Å, R_{C-H} = 1.0755 Å) from CCVB-SD with (a) all π-electrons correlated and (b) all valence electrons correlated. The largest calculation in (b) correlates 318 electrons in 318 orbitals.

correlated, which is slightly different than the one used in this study.[39] Fitting the NOONs of HONO (highest occupied natural orbital with occupation greater than 1) and LUNO (lowest unoccupied natural orbital with occupation less than 1) to analytical functions in Fig 5.6 (a), the asymptotes for (HONO, LUNO) were found to be (1.36, 0.64) for CCVB-SD, whilst the ref. 39 authors obtained (1.30, 0.70) for DMRG.[501] Those $M = 256$ DMRG calculations were far from being converged with respect to the number of renormalised states and thus we expect the exact asymptotes to be closer to 1.0 for both HONO and LUNO. The π-space CCVB-SD asymptote is less radicaloid, but it qualitatively captures the emergent strong correlations present in oligoacenes.

The progression of emergent strong correlations as a function of the length of acenes when correlating all valence electrons has not yet been well-characterised mainly because of the absence of suitable quantum chemistry models. The significant progress that has been made in developing FCIQMC[402, 403] and DMRG[34–36, 404, 405] allows treatment of systems with approximately 100 electrons in 100 orbitals at near benchmark accuracy. However, correlating all valence electrons of the oligoacenes requires an active space much larger than this limit (e.g. even 5-acene (pentacene) has 102 electrons in 102 orbitals for the full-valence space). On the other hand, more economical wavefunction based methods such as RCCSD cannot properly describe systems with emergent strong correlations of many electrons as shown in the previous section.

Here, we apply CCVB-SD to oligoacenes up to 17-acene correlating all valence

electrons, which yields a maximum active space of 318 electrons and 318 orbitals. The largest CCVB-SD calculation took little less than two hours per iteration using 32 cores in AMD Opteron Processor 6376. Under the same condition, RCCSD took roughly an hour per iteration, which confirms that the computational cost of CCVB-SD is twice larger than RCCSD.

Comparing NOONs of both casesπ-space and full-valence space calculations as illustrated in Fig. 5.6, it is interesting to note that the radical character in terms of NOONs is considerably less prominent for the full-valence calculations. This may be understood similarly to the way we understand two-configuration SCF (TCSCF) wavefunctions that tend to yield larger amplitudes on the excited determinants compared to the exact answers. Therefore, one would expect more radicaloid (closer to 1) NOONs for truncated active space calculations, which in our case are π-space calculations. The NOONs from the full-valence calculations also reach a plateau region as the system grows and the asymptote is (1.63, 0.37) for (HONO, LUNO).

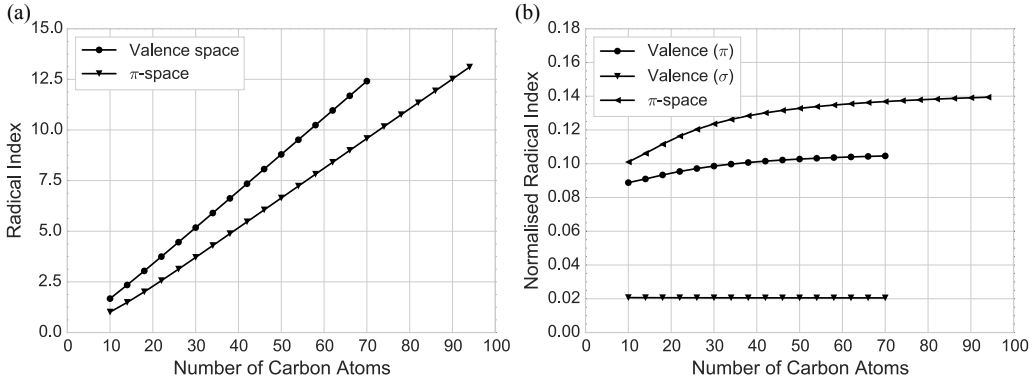

Figure 5.7: (a) Radical index as a function of the number of carbon atoms, and (b) normalised radical index as a function of the number of carbon atoms.

We further compute the radical index (RI) of oligoacenes. The RI, proposed by Head-Gordon [282], is a measure of the number of radical electrons in a system. Although in terms of NOONs of HONO and LUNO the valence calculations seem to exhibit smaller radical characters than the π-space calculations, the net RI is larger in the valence calculations as illustrated in Fig. 5.7 (a). This is because there are 4–5 times more correlated electrons in the valence calculations than in the π-space calculations. Therefore, we separate σ-NOs and π-NOs in the valence calculations and divide the RI by the number of σ or π-electrons, respectively. This normalised RI (NRI) directly indicates the average radical character per electron in a system and the NRI closer to 1.0 indicates more of radical character. For example, an ideal

diradical would yield NRI of 1.0 within (2,2) active space. We classify HONO - $n_\pi/2$ +1 to HONO and LUNO to LUNO + $n_\pi/2$ - 1 as π-NOs and the rest of NOs as σ-NOs. This is justified because the NOs in this range are each of π character.The π-NOs and σ-NOs are classfied by their irreducible representations as the NOs from CCVB-SD are all spatially symmetric in the systems considered in this work.

With this classification, the resulting NRI is depicted in Fig. 5.7 (b). Unsurprisingly, the σ-NOs in the valence calculations do not show any noticeable changes in the NRI and their NRIs are much smaller than those of π-NOs. The NRI of valence-π is smaller than that of π-space calculations, which is consistent with what is observed in the NOONs. The NRIs of π-NOs increase as system grows and they reach bulk values in both valence and π-space calculations. This clearly shows the progressive emergent radical character in the π-space of oligoacenes. In passing, we note that increasing the basis beyond STO-3G is expected to show a further reduction in the largest NOONs for virtuals and this is an interesting subject of future study.

5.6 Conclusions and Outlook

In this paper, we summarized the CCVB-SD electron correlation method in terms of orthogonally spin-adapted doubles operators and derived its Λ-equation and unrelaxed density matrices. We also described a block-tensor based implementation of CCVB-SD and showed a large-scale application to acene oligomers correlating up to 318 electrons in 318 orbitals.

Studying oligoacenes with CCVB-SD and other single reference CC methods, several interesting results were found: (1) Even for naphthalene, a significant difference in energy between RCCSD and QCCD was found, which suggests non-variational behaviour of RCCSD. This non-variational behaviour becomes more pronounced for larger acenes. (2) CCVB-SD qualitatively captures strong correlations of acenes based on the comparison between NOONs from CCVB-SD and DMRG[38, 39] and (3) correlating all valence electrons shows a significantly smaller radical character in the π-space than when correlating only the π-electrons, but it still shows progressive emergent strong correlations as system grows.

Lack of connected excitation beyond double in CCVB-SD is possibly the largest missing contribution, with triples (T) being the leading correction. In the future, modifications of CCVB-SD to include T (and beyond) are desirable. There are many ways to pursue this direction including non-iterative approaches as is done in similarity-transformed perturbation theory, [502] CCSD(T), [418] and optimised-inner-projection method that has been applied to incorporate T into ACPQ.[503–505] Approximating T in a non-iterativea self-contained iterative fashion using singles

and doubles similarly to the way CCVB-SD approximates connected quadruples (Q) would be formally and computationally more satisfying but is still an open question.

There are other future extensions of CCVB-SD to consider such as linear-response CC (LR-CC) [506] or equation-of-motion CC (EOM-CC) [507] for excited states and open-shell CCVB-SD similar to open-shell CCVB. [281] As CCVB-SD handles valence correlations well, for basis sets larger than minimal basis, it would be beneficial to develop valence optimised CCVB-D similarly to valence optimised doubles (VOD).[256] It will be interesting to study mechanisms of reactions involving strongly correlated transition states such as pericyclic reactions using algorithms such as nudged elastic band [508, 509] and growing string methods. [510–513] The production-level implementation of CCVB-SD energy and gradients described in this paper will facilitate these exciting developments and applications.

5.7 Appendix

5.7.1 Proof of Eq. (5.26)

We begin with Eq. (63) and Eq. (64) of ref. 141 in our present notation,

$$\hat{\mathcal{S}} = \frac{1}{2} \sum_{ijab} S_{ij}^{ab}\, \hat{\Sigma}_{ij}^{ab}, \tag{5.66}$$

$$\hat{\mathcal{Q}} = \frac{1}{2} \sum_{ijab} S_{ij}^{ab}\, {}^{tt}\hat{\kappa}_{ij}^{ab} \tag{5.67}$$

$$= \sum_{\substack{i<j \\ a<b}} \left(S_{ij}^{ab} - S_{ji}^{ab} \right) {}^{tt}\hat{\kappa}_{ij}^{ab}, \tag{5.68}$$

where t_{ij}^{ab}, $\mathcal{S}_{ij}^{ab}$, and $\mathcal{Q}_{ij}^{ab}$ in ref. 141 correspond to S_{ij}^{ab}, $\hat{\Sigma}_{ij}^{ab}$, and ${}^{tt}\hat{\kappa}_{ij}^{ab}$, respectively.

Therefore, we write

$$Q_{ij}^{ab} = S_{ij}^{ab} - S_{ji}^{ab}. \tag{5.69}$$

In terms of ${}^{ss}\hat{\Sigma}_{ij}^{ab}$ and ${}^{tt}\hat{\Sigma}_{ij}^{ab}$, $\hat{\Sigma}_{ij}^{ab}$ is written as

$$\hat{\Sigma}_{ij}^{ab} = -\frac{\sqrt{3}}{2}\, {}^{ss}\hat{\Sigma}_{ij}^{ab} - \frac{1}{2}\, {}^{tt}\hat{\Sigma}_{ij}^{ab}. \tag{5.70}$$

For any $i \neq j$ and $a \neq b$, using Eq. (5.70) one can show that the terms in Eq. (5.17) and Eq. (5.66) pertinent to these indices are

$$S_{ij}^{ab}\,\hat{\Sigma}_{ij}^{ab} + S_{ji}^{ab}\,\hat{\Sigma}_{ji}^{ab} = -\frac{\sqrt{3}}{2}\left(S_{ij}^{ab} + S_{ji}^{ab}\right){}^{ss}\hat{\Sigma}_{ij}^{ab} - \frac{1}{2}\left(S_{ij}^{ab} - S_{ji}^{ab}\right){}^{tt}\hat{\Sigma}_{ij}^{ab} \tag{5.71}$$

$$= {}^{S}S_{ij}^{ab}\,{}^{ss}\hat{\Sigma}_{ij}^{ab} + {}^{A}S_{ij}^{ab}\,{}^{tt}\hat{\Sigma}_{ij}^{ab}, \tag{5.72}$$

which gives

$${}^{S}S_{ij}^{ab} = -\frac{\sqrt{3}}{2}\left(S_{ij}^{ab} + S_{ji}^{ab}\right), \tag{5.73}$$

$${}^{A}S_{ij}^{ab} = -\frac{1}{2}\left(S_{ij}^{ab} - S_{ji}^{ab}\right). \tag{5.74}$$

Comparing Eq. (5.74) and Eq. (5.69) proves Eq. (5.26).

Chapter 6

Open-Shell Coupled-Cluster Valence-Bond Theory Augmented with an Independent Amplitude Approximation for Three-Pair Correlations

6.1 Introduction

Low-order Møller-Plesset perturbation theory, based on the best possible independent particle model, qualitatively fails for systems with strong correlation (SC). Such failure is commonly observed in the bond dissociation of molecules. Upon dissociating bonds, all the electrons involved become perfectly localized and the different spin states become all degenerate. We define this particular type of strong correlation as strong spin-correlation (SSC).[128] SSC is often characterized by high energy costs for charge transfer excitations, versus very small energy costs for spin-flipping excitations that leave local charges unchanged. As a result SSC problems typically have wavefunctions in which the amplitudes for spin-flipping excitations are large and essential, while the amplitudes for charge transfer substitutions are small and of secondary importance.

There are a number of numerical techniques that can properly describe SSC and we mention some of the significant developments. We first mention density matrix renormalization group (DMRG) theory by White [34, 36, 404, 405] which was originally developed to simulate one-dimensional (1D) quantum lattice models.

DMRG correctly encodes the entanglement area law [36] for 1D gapped systems with local Hamiltonian, and this is the key to its success in solving 1D problems. This technique from the condensed matter physics community has been successfully applied to quantum chemical problems [40, 41, 514] although the scaling is still exponential in higher dimensions than 1D.

There are two promising quantum Monte Carlo (QMC) algorithms that work with Slater determinants. First, we mention Alavi and co-worker's full configuration interaction QMC (FCIQMC),[402] which is formally exponential scaling. It, however, has significantly pushed back the onset of the exponential wall to roughly 50 electrons. Sampling determinants stochastically, FCIQMC avoids the usual fixed-node approximations commonly used in diffusion MC. It has been applied to various molecular systems along with solid-state applications.[42, 410]

Another alternative is auxiliary field QMC (AFQMC).[515] AFQMC utilizes the Hubbard-Stratonovich transformation to elegantly cast an interacting many-body problem to non-interacting problems with a set of random auxiliary fields. Sampling an infinite number of auxiliary fields in principle converges to the exact answer. However, employing either a constrained-path or phaseless approximation is almost necessary in practice to control the sign problem in large systems at the expense of introducing bias.[516, 517] Its application to chemical systems has been somewhat limited although preliminary results are promising.[518–523]

From the quantum chemistry community, there are numerous brute-force approaches based on configuration interaction (CI) methods.[58] Most of them are in general exponential scaling using configuration selection with second-order perturbation theory to reduce the prefactor relative to full CI. [216, 365, 391, 524–535] A recently introduced, exponential-scaling heat-bath CI (HCI) also belongs to this category, [365, 391, 534, 535] and this method is used for the benchmark purpose in this paper. To best of our knowledge, none of the methods in this category can exactly dissociate multiple bonds with only a polynomial amount of work with respect to the number of bonds.

Other quantum chemistry methods are mainly based on coupled-cluster (CC) approaches. It is a particularly promising direction as those methods generally involve only a polynomial number of wavefunction parameters to describe an exponential of number of configurations through the non-linear wavefunction ansatz. There are numerous approaches in this category,[76, 92, 111, 128, 140, 141, 280, 281, 411, 412, 422, 425, 442, 447, 448, 451, 462, 505, 536–545] and our method discussed below also falls into this. Interested readers are referred to Introduction of ref. 142 and the references therein.

Our group has been developing a powerful polynomial-scaling approach to bond-breaking based on CC valence bond (CCVB).[128, 140–142, 280, 281] It encodes

strong spin-correlations by excitations from a generalized valence bond perfect pairing (GVB-PP) reference [362, 546] and involves only a quadratic number of wavefunction parameters associated with two-pair (2P) substitutions. Furthermore, it yields a spin-pure, size-extensive wavefunction and its cost is dominated by integral transformation as long as the amplitude equation is solved by a computationally inexpensive way. The CCVB ansatz generalizes spin-projected unrestricted Hartree-Fock (SPUHF) [481, 547–550] to a size-extensive wavefunction at the expense of orbital-invariance and variationality. It can reach the correct asymptote when breaking bonds as long as UHF can properly dissociate. Moreover, in some cases CCVB can break bonds when UHF cannot reach the correct asymptote such as a triplet O_2 dissociation to two triplet oxygens.

CCVB can be understood from various different perspectives. One of them is to look at CCVB from a VB perspective. The spin-coupled VB (SCVB) approach [492, 551–553] can describe bond-breaking exactly within a given active space at an exponential-scaling cost. Applying a modified CC expansion with double excitations along with strong orthogonality between pairs, we obtain CCVB that is polynomial-scaling and practically identical to SCVB at dissociation limits.

Another viewpoint is to start from CCVB with singles and doubles (CCVB-SD) [141, 142] which is a full singles and doubles model like restricted CC singles and doubles (RCCSD) and parametrizes connected quadruples in a different way than RCCSD. Replacing singles with orbital optimization and applying the pairing active space constraint and the local approximation (i.e., sparsifying T-amplitudes), we obtain CCVB with an RHF reference. One could then write the same wavefunction with a GVB-PP reference by converting the GVB-PP amplitudes to GVB-PP polarization angles. This allows for writing the CCVB ansatz in the originally proposed form.

The goal of this paper is to demonstrate the failure of the original CCVB model for open-shell spin-frustrated systems and the necessity to incorporate 3-pair (3P) substitutions in such systems. We also introduce an improved wavefunction where the number of independent wavefunction parameters scales still quadratically with system size, but it includes the influence of 3P substitutions within the independent amplitude approximation (IAA). We denote this new model as CCVB+i3 and we will present full details later in the paper.

This paper is organized as follows: we first review CCVB and then discuss the full 3P extension of this model, CCVB-3. We formally analyze CCVB-3 and discuss a subtle issue regarding the size-consistency of the model. We then introduce a new model, CCVB+i3 which is an attempt to include the 3P substitutions in a simpler, size-consistent manner. Lastly, we discuss interesting spin-frustrated model systems along with models of two chemically relevant, realistic systems. Therein, we show

promising results of CCVB+i3 compared to HCI.

6.2 Theory

6.2.1 Notation

In this paper we use $K, L, M, P, Q, R, \cdots$ to denote closed-shell (CS) pairs, $\mu, \nu, \lambda, \cdots$ to denote singly occupied orbitals, and $a, b, c, \cdots$ to denote either of them. More precisely, this means

$$1 \leq K, L, M, P, Q, R, \cdots \leq n_\beta \tag{6.1}$$
$$n_\beta < \mu, \nu, \lambda, \cdots \leq n_\alpha \tag{6.2}$$
$$1 \leq a, b, c, \cdots \leq n_\alpha \tag{6.3}$$

where n_α and n_β denote the number of α and β electrons, respectively.

We also establish a notation for several quantities which will be used throughout this paper. The GVB-PP (or PP for short) reference is defined as

$$|\psi_0\rangle = \prod_\mu \hat{a}^\dagger_{\mu_\alpha} \prod_K \hat{g}^\dagger_{s,K} |0\rangle \tag{6.4}$$

where we used $|0\rangle$ to denote the vacuum state, $\hat{a}^\dagger_{\mu_\alpha}$ is the fermionic creation operator, and the singlet pair (or geminal) K creation operator $\hat{g}^\dagger_{s,K}$ is defined as

$$\hat{g}^\dagger_{s,K} = \frac{1}{\sqrt{2\left(1+\cos^2\theta_K\right)}} \left(2\cos\theta_K \hat{a}^\dagger_{K_\alpha}\hat{a}^\dagger_{K_\beta} - \sin\theta_K \hat{a}^\dagger_{K_\alpha}\hat{a}^\dagger_{\hat{K}_\beta} - \sin\theta_K \hat{a}^\dagger_{\hat{K}_\alpha}\hat{a}^\dagger_{K_\beta}\right) \tag{6.5}$$

where θ_K is the polarization angle for a pair K and K_α, K_β, $\hat{K}_\alpha$, and $\hat{K}_\beta$ denote the four spin-orbitals associated with the pair. $\theta_K = \pi/2$ corresponds to a fully polarized pair (i.e., a perfect diradical). Those pairs are strongly orthogonal which simplifies the calculation of matrix elements discussed later.

In CCVB, other configurations in addition to the PP reference are defined with excitations from the reference. The 2P substitutions include a CS-CS substitution (δ_{s2}),

$$\left|\psi_{(KL)}\right\rangle = \hat{d}^\dagger_{s2,KL}\hat{g}_{s,K}\hat{g}_{s,L}\left|\psi_0\right\rangle, \tag{6.6}$$

and a CS-OS substitution (δ_{d2}),

$$\left|\psi_{(K\mu)}\right\rangle = \hat{d}^\dagger_{d2,K\mu}\hat{a}_{\mu_\alpha}\hat{g}_{s,K}\left|\psi_0\right\rangle \tag{6.7}$$

where

$$\hat{d}^{\dagger}_{s2,KL} = \frac{1}{\sqrt{3}}\left(\hat{g}^{\dagger}_{t1,K}\hat{g}^{\dagger}_{t1,L} - \hat{g}^{\dagger}_{t2,K}\hat{g}^{\dagger}_{t3,L} - \hat{g}^{\dagger}_{t3,K}\hat{g}^{\dagger}_{t2,L}\right), \tag{6.8}$$

and

$$\hat{d}^{\dagger}_{d2,K\mu} = \frac{1}{\sqrt{3}}\left(\hat{g}^{\dagger}_{t_1,K}\hat{a}^{\dagger}_{\mu_\alpha} + \sqrt{2}\hat{g}^{\dagger}_{t_2,K}\hat{a}^{\dagger}_{\mu_\beta}\right) \tag{6.9}$$

with the triplet pair creation operators,

$$\hat{g}^{\dagger}_{t1,K} = \frac{1}{\sqrt{2}}\left(-\hat{a}^{\dagger}_{K_\alpha}\hat{a}^{\dagger}_{\hat{K}_\beta} + \hat{a}^{\dagger}_{\hat{K}_\alpha}\hat{a}^{\dagger}_{K_\beta}\right), \tag{6.10}$$

$$\hat{g}^{\dagger}_{t2,K} = \hat{a}^{\dagger}_{K_\alpha}\hat{a}^{\dagger}_{\hat{K}_\alpha}, \tag{6.11}$$

$$\hat{g}^{\dagger}_{t3,K} = \hat{a}^{\dagger}_{K_\beta}\hat{a}^{\dagger}_{\hat{K}_\beta}. \tag{6.12}$$

In a simpler term, δ_{s2} represents a substitution of a product of two singlet pairs with two triplet pairs coupled into a four-electron singlet configuration. Similarly, δ_{d2} is a substitution of a product of a singlet geminal with an alpha electron with a triplet pair and a unpaired electron coupled into a three-electron doublet configuration.

The 3P substitutions include a CS-CS-CS substitution (ϵ_{s5}),

$$\left|\psi_{(KLM)}\right\rangle = \hat{e}^{\dagger}_{s5,KLM}\hat{g}_{s,K}\hat{g}_{s,L}\hat{g}_{s,M}\left|\psi_0\right\rangle \tag{6.13}$$

and a CS-CS-OS substitution (ϵ_{d5}),

$$\left|\psi_{(KL\mu)}\right\rangle = \hat{e}^{\dagger}_{d5,KL\mu}\,\hat{g}_{s,K}\hat{g}_{s,L}\hat{a}_{\mu_\alpha}\left|\psi_0\right\rangle \tag{6.14}$$

where

$$\begin{aligned}\hat{e}^{\dagger}_{s5,KLM} = \frac{1}{\sqrt{6}}(&\hat{g}^{\dagger}_{t1,K}\hat{g}^{\dagger}_{t2,L}\hat{g}^{\dagger}_{t3,M} - \hat{g}^{\dagger}_{t1,K}\hat{g}^{\dagger}_{t3,L}\hat{g}^{\dagger}_{t2,M} - \hat{g}^{\dagger}_{t2,K}\hat{g}^{\dagger}_{t1,L}\hat{g}^{\dagger}_{t3,M}\\ &+ \hat{g}^{\dagger}_{t2,K}\hat{g}^{\dagger}_{t3,L}\hat{g}^{\dagger}_{t1,M} + \hat{g}^{\dagger}_{t3,K}\hat{g}^{\dagger}_{t1,L}\hat{g}^{\dagger}_{t2,M} - \hat{g}^{\dagger}_{t3,K}\hat{g}^{\dagger}_{t2,L}\hat{g}^{\dagger}_{t1,M}),\end{aligned} \tag{6.15}$$

and

$$\hat{e}^{\dagger}_{d5,KL\mu} = \frac{1}{\sqrt{6}}\left(-\sqrt{2}\left(\hat{g}^{\dagger}_{t1,K}\hat{g}^{\dagger}_{t2,L} - \hat{g}^{\dagger}_{t2,K}\hat{g}^{\dagger}_{t1,L}\right)\hat{a}^{\dagger}_{\mu_\beta} + \left(\hat{g}^{\dagger}_{t2,K}\hat{g}^{\dagger}_{t3,L} - \hat{g}^{\dagger}_{t3,K}\hat{g}^{\dagger}_{t2,L}\right)\hat{a}^{\dagger}_{\mu_\alpha}\right). \tag{6.16}$$

Similarly to the 2P substitutions, ϵ_{s5} denotes a substitution of a product of three singlet pairs with a product of three triplet pairs coupled to an overall singlet and ϵ_{d5} represents a substitution of a product of two singlet pairs and an alpha electron with a product of two triplet pairs and a unpaired electron coupled to an overall doublet.

The higher-order substitutions are trivially defined with the definitions above by the virtue of a CC expansion. For instance, we have

$$\left|\psi_{(K\mu)(LMN)}\right\rangle = \hat{d}^{\dagger}_{d2,K\mu}\hat{a}_{\mu_\alpha}\hat{g}_{s,K}\left|\psi_{(LMN)}\right\rangle = \hat{d}^{\dagger}_{d2,K\mu}\hat{a}_{\mu_\alpha}\hat{g}_{s,K}\hat{e}^{\dagger}_{s5,LMN}\hat{g}_{s,L}\hat{g}_{s,M}\hat{g}_{s,N}\left|\psi_0\right\rangle . \tag{6.17}$$

Those substitutions are not necessarily orthogonal and generally linearly dependent for a given excitation level. We introduce a dual frame to $\{|\psi_i\rangle\}$, which we shall write $\{|\phi_i\rangle\}$. In particular, we define $\{|\phi_i\rangle\}$ to be the *canonical* dual frame of $\{|\psi_i\rangle\}$,

$$|\phi_i\rangle = \sum_j \left(\mathbf{S}^{+}\right)_{ij}|\psi_j\rangle \tag{6.18}$$

where $S_{ij} = \langle\psi_i|\psi_j\rangle$ and $\mathbf{S}^{+}$ is the pseudoinverse of $\mathbf{S}$. Forming $\mathbf{S}^{+}$ can be done quite cheaply exploiting the block structure of $\mathbf{S}$. Moreover, in some special cases we have $|\phi_i\rangle = |\psi_i\rangle$ as the relevant block in $\mathbf{S}$ forms an identity block. These include $|\phi_0\rangle = |\psi_0\rangle$, $|\phi_{(KL)}\rangle = |\psi_{(KL)}\rangle$, and $|\phi_{(KLM)}\rangle = |\psi_{(KLM)}\rangle$. Other than those three special cases, $|\phi_i\rangle$ is expected to be different from $|\psi_i\rangle$.

6.2.2 Review of CCVB

We review the CCVB wavefunction ansatz that includes only 2P substitutions (i.e., (KL), $(K\mu)$) and disconnected higher-order substitutions arising from those. The pertinent CC expansion in terms of $\{|\phi_i\rangle\}$ reads

$$\begin{aligned}
|\psi_{2\mathrm{P}}\rangle = |\phi_0\rangle &+ \sum_{\substack{KL\\K<L}} t_{KL}\left|\phi_{(KL)}\right\rangle + \sum_{K\mu} t_{K\mu}\left|\phi_{(K\mu)}\right\rangle \\
&+ \sum_{\substack{KLMN\\K<L<M<N}} \left(t_{KL}t_{MN}\left|\phi_{(KL)(MN)}\right\rangle + t_{KM}t_{LN}\left|\phi_{(KM)(LN)}\right\rangle + t_{KN}t_{LM}\left|\phi_{(KN)(LM)}\right\rangle\right) \\
&+ \sum_{\substack{KLM\mu\\K<L<M}} \left(t_{KL}t_{M\mu}\left|\phi_{(KL)(M\mu)}\right\rangle + t_{KM}t_{L\mu}\left|\phi_{(KM)(L\mu)}\right\rangle + t_{K\mu}t_{LM}\left|\phi_{(K\mu)(LM)}\right\rangle\right) \\
&+ \sum_{\substack{KL\mu\lambda\\K<L\\\mu<\lambda}} \left(t_{K\mu}t_{L\lambda}\left|\phi_{(K\mu)(L\lambda)}\right\rangle + t_{K\lambda}t_{L\mu}\left|\phi_{(K\lambda)(L\mu)}\right\rangle\right) + \cdots,
\end{aligned} \tag{6.19}$$

where we listed only those terms that are necessary to solve the CCVB 2P amplitude equation. The CCVB energy and the 2P amplitudes are computed via projection equations similar to those of regular CC methods:

$$E \equiv \langle\psi_0|\,\hat{\mathcal{H}}\,|\psi_{2\mathrm{P}}\rangle \tag{6.20}$$

$$Et_{Ka} = \left\langle\psi_{(Ka)}\right|\hat{\mathcal{H}}\left|\psi_{2\mathrm{P}}\right\rangle . \tag{6.21}$$

The 2P amplitude residual of CCVB reads

$$R_{Ka} = \left\langle \psi_{(Ka)} \right| \hat{\mathcal{H}} \left| \psi_{\mathrm{2P}} \right\rangle - E t_{Ka}. \tag{6.22}$$

When solving $R_{K\mu} = 0$, a complication arises as $\left\langle \psi_{(K\mu)} \middle| \psi_{(K\lambda)} \right\rangle \neq \delta_{\mu\lambda}$ and $\left\langle \psi_{(KL)} \middle| \psi_{(K\mu)(L\lambda)} \right\rangle \neq 0$. In other words, we need to compute the pseudoinverse of a block in $\mathbf{S}$ that is not as small as that of the CS case. In particular, the size of the block of $\mathbf{S}$ that we need to pseudo-invert is now system-dependent.

To circumvent this complication, Small and Head-Gordon employed a supersystem approach which adds fictitious β electrons to a high-spin original system to make it overall a CS system.[281] In this approach, each OS α electron is coupled with a fictitious β electron and they behave as a CS pair together in $|\Psi_0\rangle$. We refer to this pair composed of an original system electron and a fictitious electron as an "OS" pair. Note that we are using $|\Psi_0\rangle$ to denote the closed-shell supersystem in contrast to $|\psi_0\rangle$ which we used to denote the original system. We work with a CCVB wavefunction of this fictitious supersystem whose complete set of spin configurations (which include all 3P substitutions as well) contain those of the original CCVB configurations. Solving the modified 2P amplitude equation of the supersystem with some constraints is equivalent to solving the original CCVB amplitude equation.

We seek t_{Ka} that satisfies $\Omega_{Ka} = 0$ where

$$\Omega_{KL} = R_{KL}, \tag{6.23}$$

$$\Omega_{K\mu} = R_{K\mu} + \sum_{\lambda \neq \mu} \kappa_{K\mu;\lambda} t_{K\mu\lambda}, \tag{6.24}$$

where

$$\kappa_{ab;c} \equiv \left\langle \Psi_{(ab)} \right| \hat{\mathcal{H}} \left| \Psi_{(abc)} \right\rangle. \tag{6.25}$$

The constraints on the supersystem amplitudes are

$$t_{\mu\lambda} = \frac{1}{\sqrt{3}} \tag{6.26}$$

and

$$t_{K\mu\lambda} = \frac{-1}{\sqrt{2}} \left(t_{K\mu} - t_{K\lambda} \right) \tag{6.27}$$

We emphasize that those amplitudes, t_{Ka} and t_{KLa}, are equivalent to the amplitudes for the original system. Interested readers are referred to ref. 281 for the detailed derivation of this supersystem approach.

As shown in ref. 140, CCVB is capable of reaching the correct dissociation limit as long as UHF can. Its energy becomes exact in that limit as its energy

is merely the sum of the restricted open-shell HF (ROHF) energy of each high-spin fragment. The strengths of CCVB are its size-consistency, spin-purity, and polynomial-scaling cost (which is dominated by integral transformation). One would expect CCVB to fail for systems where UHF fails to reach a proper dissociation limit and only generalized HF (GHF) can reach the correct asymptote among available single-determinant wavefunctions. We shall see such examples later in the paper and we will also show that the scope of CCVB for OS systems turns out to be much broader than that of UHF.

6.2.3 Primer: The OS PP+i2 Ansatz

As mentioned in ref. 143, a simple way to go beyond CCVB for closed-shell systems is to remove all the terms that contain amplitudes other than t_{KL} when solving $R_{KL} = 0$ in Eq. (6.22). We refer to this as the independent amplitude approximation (IAA) approach. This modified amplitude equation leads to a model called PP+i2. Unlike CCVB, PP+i2 is quite often variationally unstable (i.e., the resulting PP+i2 energy is too low). However, it can often reach correct asymptotes when CCVB cannot. Due to its simplicity, we tried to extend the PP+i2 ansatz to the open-shell systems and shall explain subtle difficulties involved in pursuing it below. However, we do not report any results associated with this model in this work.

The CS PP+i2 amplitude equation follows

$$ {}^{(2)}R_{KL} \equiv \langle \psi_{(KL)} | \hat{\mathcal{H}} | \xi_{(KL)} \rangle - t_{KL} \langle \psi_0 | \hat{\mathcal{H}} | \xi_{(KL)} \rangle \tag{6.28} $$

where

$$ |\xi_{(KL)}\rangle = |\psi_0\rangle + t_{KL} |\phi_{(KL)}\rangle \tag{6.29} $$

Solving ${}^{(2)}R_{KL} = 0$ leads to a simple quadratic equation in t_{KL} and different amplitudes are decoupled from each other. The solution to this quadratic equation might not exist and we observed this quite frequently near its variational breakdown. When the solution exists, we chose the one out of two solutions that gives a lower CCVB total energy. This approach was inspired by independent electron-pair approximations in coupled-cluster theory.[554–565]

The natural inclination towards OS PP+i2 would be to solve (employing the supersystem approach) ${}^{(2)}\Omega_{Ka} = 0$ where we define

$$ {}^{(2)}\Omega_{KL} = {}^{(2)}R_{KL} \tag{6.30} $$

$$ {}^{(2)}\Omega_{K\mu} = \langle \Psi_{(K\mu)} | \hat{\mathcal{H}} | \Xi_{(K\mu)} \rangle - t_{K\mu} \langle \Psi_0 | \hat{\mathcal{H}} | \Xi_{(K\mu)} \rangle + \sum_{\lambda \neq \mu} \kappa_{K\mu;\lambda} t_{K\mu\lambda} \tag{6.31} $$

where

$$|\Xi_{(K\mu)}\rangle = |\Psi_0\rangle + t_{K\mu}|\Phi_{(K\mu)}\rangle \tag{6.32}$$

One may impose the constraints in Eq. (6.26) and Eq. (6.27) so that the supersystem amplitudes represent the original system amplitudes. This is what we initially tried and it worked reasonably well.

Alternatively to this approach, one may attempt to apply the IAA approach to the original system amplitude equation and then apply the supersystem transformation. This is not as simple as what is described above as $\left|\psi_{(K\mu)}\right\rangle$ and $\left|\psi_{(K\lambda)}\right\rangle$ (or the corresponding vectors in the dual frame) are not necessarily orthogonal even when $\mu \neq \lambda$. With this in mind, we tried to allow $t_{K\mu}$ to depend on $t_{K\lambda}$ in the supersystem amplitude equation. This then leads to a modified CS-OS residual:

$${}^{(2)}\tilde{\Omega}_{K\mu} = \langle\Psi_{(K\mu)}|\hat{\mathcal{H}}|\tilde{\Xi}_K\rangle - t_{K\mu}\langle\Psi_0|\hat{\mathcal{H}}|\tilde{\Xi}_K\rangle + \sum_{\lambda\neq\mu}\kappa_{K\mu;\lambda}t_{K\mu\lambda} \tag{6.33}$$

where

$$|\tilde{\Xi}_K\rangle = |\Psi_0\rangle + \sum_{\lambda} t_{K\lambda}|\Phi_{(K\lambda)}\rangle \tag{6.34}$$

Solving ${}^{(2)}\tilde{\Omega}_{K\mu} = 0$ under the constraints in Eq. (6.26) and Eq. (6.27) for $t_{K\mu}$ involves still a quadratic equation in $t_{K\mu}$ and one may employ an iterative approach to solve the residual equation until we have a self-consistent set of $\{t_{K\mu}\}$. This version of OS PP+i2 was found a little more variationally stable than the one described above, but it is still generally not recommended due to its instability. We use this OS PP+i2 to obtain a set of initial amplitudes for the subsequent CCVB calculations.

In the case of CS fragments, size-consistency means that the energy of non-interacting *closed-shell* molecules is merely the sum of individual CCVB energy of each molecule. This is satisfied if every intermolecular amplitude is zero at the well-separated limit. Evidently, Eq. (6.28) is size-consistent. In the case of OS fragments, we define the size-consistency as follows: the energy of non-interacting molecules (either *closed-shell* or *open-shell*) is the sum of their individual CCVB energies assuming that fragments are not spin-coupled into a lower spin manifold. Based on this definition, we conclude that both Eq. (6.31) and Eq. (6.33) ensure the size-consistency of PP+i2.

6.2.4 The OS CCVB-3 Ansatz

Extending the CCVB wavefunction might seem relatively straightforward; we augment the cluster expansion of CCVB with missing 3P substitutions. The first

inclination might be to try the following CC expansion,

$$
\begin{aligned}
|\psi_{3\mathrm{P}}\rangle = |\psi_{2\mathrm{P}}\rangle &+ \sum_{\substack{KLM \\ K<L<M}} t_{KLM} \left|\phi_{(KLM)}\right\rangle + \sum_{\substack{KL\mu \\ K<L}} t_{KL\mu} \left|\phi_{(KL\mu)}\right\rangle \\
&+ \sum_{\substack{KLPQR \\ K<L<P<Q<R}} \left(t_{KL} t_{PQR} \left|\phi_{(KL)(PQR)}\right\rangle + \{\text{nine other permutations}\}\right) \\
&+ \sum_{\substack{KLMN\mu \\ K<L<M<N}} \left(t_{KL} t_{MN\mu} \left|\phi_{(KL)(MN\mu)}\right\rangle + \{\text{five other permutations}\}\right) \\
&+ \sum_{\substack{KLMN\mu \\ K<L<M<N}} \left(t_{K\mu} t_{LMN} \left|\phi_{(K\mu)(LMN)}\right\rangle + \{\text{three other permutations}\}\right) \\
&+ \sum_{\substack{KLM\mu\lambda \\ K<L<M \\ \mu<\lambda}} \left(t_{K\mu} t_{LM\lambda} \left|\phi_{(K\mu)(LM\lambda)}\right\rangle + t_{L\mu} t_{KM\lambda} \left|\phi_{(L\mu)(KM\lambda)}\right\rangle + t_{M\mu} t_{KL\lambda} \left|\phi_{(M\mu)(KL\lambda)}\right\rangle \right. \\
&\left. + \{\text{3 terms from } (\mu \leftrightarrow \lambda)\}\right) + \cdots .
\end{aligned} \tag{6.35}
$$

We note that CCVB-3 includes all possible spin configurations through the cluster expansion. In other words, it is complete in the sense that the cluster expansion includes the same number of spin configurations as that of SCVB for a given active space. The remaining difference between SCVB and CCVB-3 is then largely from strong orthogonality between pairs assuming the CC approximation to the spin-coupling vector is reasonable.

Following the previous supersystem strategies, we first define the CCVB-3 energy as

$$E \equiv \langle \Psi_0 | \hat{\mathcal{H}} | \Psi_{3\mathrm{P}} \rangle \tag{6.36}$$

We then write the supersystem CS-CS 2P residual in the following manner:

$${}^{3\mathrm{p}}\Omega_{KL} = R_{KL} + \sum_{a \notin \{K,L\}} t_{KLa} \kappa_{KL;a} \tag{6.37}$$

The CS-OS 2P residual can also be similarly defined:

$${}^{3\mathrm{p}}\Omega_{K\mu} = R_{K\mu} + \sum_{a \notin \{K,\mu\}} t_{K\mu a} \kappa_{K\mu;a} \tag{6.38}$$

Up to the 2P amplitude equation, the model is evidently size-consistent.

We further proceed to the 3P amplitude residual equation:

$$
\begin{aligned}
{}^{3\mathrm{p}}\Omega_{KLa} &= \left\langle \Psi_{(KLa)} \right| \hat{\mathcal{H}} \left| \Psi_{3\mathrm{P}} \right\rangle - E t_{KLa} \\
&= t_{KL} \left\langle \Psi_{(KLa)} \right| \hat{\mathcal{H}} \left| \Phi_{(KL)} \right\rangle + t_{Ka} \left\langle \Psi_{(KLa)} \right| \hat{\mathcal{H}} \left| \Phi_{(Ka)} \right\rangle + t_{La} \left\langle \Psi_{(KLa)} \right| \hat{\mathcal{H}} \left| \Phi_{(La)} \right\rangle \\
&+ \sum_{b \notin \{K,L,a\}} \Bigg(t_{KLb} \left\langle \Psi_{(KLa)} \right| \hat{\mathcal{H}} \left| \Phi_{(KLb)} \right\rangle + t_{Kab} \left\langle \Psi_{(KLa)} \right| \hat{\mathcal{H}} \left| \Phi_{(Kab)} \right\rangle \\
&+ t_{Lab} \left\langle \Psi_{(KLa)} \right| \hat{\mathcal{H}} \left| \Phi_{(Lab)} \right\rangle \Bigg) \\
&+ \sum_{b \notin \{K,L,a\}} \Big(t_{Ka} t_{Lb} \langle \Psi_{(KLa)} | \hat{\mathcal{H}} | \Phi_{(Ka)(Lb)} \rangle + t_{Kb} t_{La} \langle \Psi_{(KLa)} | \hat{\mathcal{H}} | \Phi_{(Kb)(La)} \rangle \\
&+ t_{KL} t_{ab} \langle \Psi_{(KLa)} | \hat{\mathcal{H}} | \Phi_{(KL)(ab)} \rangle \Big) \\
&+ \sum_{b,c \notin \{K,L,a\}} \Big(t_{bc} t_{KLa} \langle \Psi_{(KLa)} | \hat{\mathcal{H}} | \Phi_{(bc)(KLa)} \rangle + \{9 \text{ other permutations}\} \Big) \\
&+ t_{KLa} \Big(\left\langle \Psi_{(KLa)} \right| \hat{\mathcal{H}} \left| \Phi_{(KLa)} \right\rangle - E \Big)
\end{aligned}
\tag{6.39}
$$

We now show that this residual equation may not yield a size-consistent model due to the contributions from the 5P substitutions.

We first assume that every amplitude that contains pairs associated with more than one fragment is all zero. We additionally assume that K is well separated from L and a in Eq. (6.39). Our goal is to check whether the residual equation in Eq. (6.39) is trivially zero under these assumptions. It is easy to see that the contributions from the 2P and 3P substitutions are zero either because the pertinent amplitude is zero or the hamiltonian matrix element is zero. Moreover, the last term in Eq. (6.39) is zero as $t_{KLa} = 0$.

The 4P contribution is not as trivial to see that it is zero, so we discuss more details. Among three terms listed in the summation of the 4P terms, only the second term may survive as $t_{Ka} = t_{KL} = 0$. We now claim that

$$
t_{Kb} t_{La} \langle \Psi_{(KLa)} | \hat{\mathcal{H}} | \Phi_{(Kb)(La)} \rangle = 0 \tag{6.40}
$$

for any b. If b is not on the same fragment as K, $t_{Kb} = 0$ and thus the entire 4P terms are zero. If b is on the same fragment as K, the matrix element, $\langle \Psi_{(KLa)} | \hat{\mathcal{H}} | \Phi_{(Kb)(La)} \rangle$, is zero. We provide more details on how to show that this matrix element is zero in the Appendix.

We turn our focus to the 5P contribution. We again assume that K is well separated form L and a. There are only three terms in the summation that are not

trivially zero:

$$\sum_{b,c\notin\{K,L,a\}}\Big(t_{Kb}t_{Lac}\langle\Psi_{(KLa)}|\hat{\mathcal{H}}|\Phi_{(Kb)(Lac)}\rangle + t_{Kc}t_{Lab}\langle\Psi_{(KLa)}|\hat{\mathcal{H}}|\Phi_{(Kc)(Lab)}\rangle + t_{La}t_{Kbc}\langle\Psi_{(KLa)}|\hat{\mathcal{H}}|\Phi_{(La)(Kbc)}\rangle\Big) \tag{6.41}$$

The overlap matrix and its pseudoinverse that defines the transformation between Φ-set and Ψ-set are given in Appendix. First, we consider the case where b and c both are on a different fragment from that of K. In this case, all the associated amplitudes vanish so the corresponding contribution to Eq. (6.41) is zero. Next, we consider the case where b and c both are on the same fragment as K. This automatically zeroes out the first two terms in Eq. (6.41) as $t_{Lac} = t_{Lab} = 0$. As the associated amplitudes are not zero for the third term, we must examine whether the integral vanishes. After some algebra, one can show that the third term does not vanish in general. Similarly, in the case where only one of b and c is on the same fragment as K and the other one is on the same fragment as L and a, the pertinent integral does not vanish in general. Therefore, we conclude that CCVB-3 is not size-consistent in general.

6.2.5 The OS CCVB+i3 Ansatz

In the previous section, we proved that CCVB-3 is in general not size-consistent due to the 5P contributions in the amplitude equation. It is quite tempting to ignore those 5P contributions and build a model based on other terms up to the 4P contributions. Though this is an interesting model to try, an even simpler model can be formulated by applying the same strategy as that of OS PP+i2. Namely, $\langle\Psi_{(KLa)}|$ couples only with configurations containing exactly (KLa) or its subset. We call this model along with the full treatment of 2P configurations (i.e., Eq. (6.37) and Eq. (6.38)), CCVB+i3.

The supersystem OS CCVB+i3 amplitude residual then reads

$${}^{(3)}\Omega_{KLa} = \langle\Psi_{(KLa)}|\hat{\mathcal{H}}|\Xi_{(KLa)}\rangle - t_{KLa}\langle\Psi_0|\hat{\mathcal{H}}|\Xi_{(KLa)}\rangle \tag{6.42}$$

where

$$|\Xi_{(KLa)}\rangle = |\Psi_0\rangle + t_{KL}|\Phi_{(KL)}\rangle + t_{Ka}|\Phi_{(Ka)}\rangle + t_{La}|\Phi_{(La)}\rangle + t_{KLa}|\Phi_{(KLa)}\rangle. \tag{6.43}$$

Solving ${}^{(3)}\Omega_{KLa} = 0$ for t_{KLa} is quite straightforward as it is a simple linear equation in t_{KLa}. The solution follows

$$t_{KLa} = \frac{t_{KL}\kappa_{KL;a} - t_{Ka}\kappa_{Ka;L} + t_{La}\kappa_{La;K}}{(t_{KL}\mu_{KL} + t_{Ka}\mu_{Ka} + t_{La}\mu_{La}) - \omega_{KLa}} \tag{6.44}$$

where

$$\omega_{KLa} = \left\langle \Psi_{(KLa)} \right| \hat{\mathcal{H}} \left| \Phi_{(KLa)} \right\rangle - \left\langle \Psi_0 \right| \hat{\mathcal{H}} \left| \Psi_0 \right\rangle \tag{6.45}$$

and

$$\mu_{Ka} = \left\langle \Psi_0 \right| \hat{\mathcal{H}} \left| \Phi_{(Ka)} \right\rangle . \tag{6.46}$$

$\kappa_{Ka;b}$, μ_{Ka}, and ω_{KLa} are expressed in terms of readily computable quantities given in Appendix. We note that $t_{KLa} = -t_{KaL} = t_{LaK} = -t_{LKa} = t_{aKL} = -t_{aLK}$ in constrast to $t_{Ka} = t_{aK}$.

Similarly to OS PP+i2, there may be more than one way to choose $|\Xi_{KL\mu}\rangle$ due to the fact that configurations involving an OS electron are not orthogonal configurations involving different OS electrons or even of different substitution levels. For instance, we have $\left\langle \psi_{(KL\mu)} \right| \left. \psi_{(KL\lambda)} \right\rangle \neq 0$ when $\mu \neq \lambda$. One may apply the IAA approach to the original system amplitude equation and then transform to the supersystem configurations. In this case, the amplitudes associated with $\left|\psi_{(KL\mu)}\right\rangle$ shall involve contributions from $\left|\psi_{(KL\lambda)}\right\rangle$ as they overlap. This leads to a different choice of $|\Xi_{KL\mu}\rangle$,

$$|\tilde{\Xi}_{(KL\mu)}\rangle = |\Psi_0\rangle + t_{KL}|\Phi_{(KL)}\rangle + \sum_{\lambda} \left(t_{K\lambda}|\Phi_{(K\lambda)}\rangle + t_{L\lambda}|\Phi_{(L\lambda)}\rangle + t_{KL\lambda}|\Phi_{(KL\lambda)}\rangle \right) \tag{6.47}$$

While this is certainly an interesting alternative, in this paper we focus on the CCVB+i3 model with Eq. (6.42).

In CCVB+i3, we work with only t_{Ka} as independent variables and t_{KLa} is directly parametrized by t_{Ka}. t_{KLa} can be viewed as an attempt to incorporate the 3P influence using only 2P amplitudes. One may argue that t_{KLa} should still be considered independent wavefunction parameters. Our viewpoint, however, is that t_{KLa} in CCVB+i3 is not considered independent as it does not increase the computational scaling of CCVB. Hence, we claim that we have not effectively increased the number of independent wavefunction parameters going from CCVB to CCVB+i3. This contrasts with other wavefunction methods such as the second-order Møller-Plesset perturbation theory (MP2) and CC singles and doubles with a perturbative triples (CCSD(T)). In MP2, the doubles amplitudes are directly parametrized by HF orbitals. It, however, has a steeper computational scaling compared to HF. Similarly, in CCSD(T), the perturbative triples amplitudes are directly parametrized by singles and doubles amplitudes with an increase in the computational scaling.

The scope of CCVB+i3 is not yet clear to us even though we have not yet found a system where CCVB+i3 fails to dissociate properly. Mathematical proofs related to this and a more complicated and improved CCVB model will be investigated in the future.

6.2.6 CCVB+i3 Lagrangian and Orbital Optimization

We establish the Lagrangian of CCVB+i3 for the orbital optimization. The Lagrangian follows

$$\mathcal{L} = E + \sum_{K<a} \lambda_{Ka} \left(R_{Ka} + \sum_{b \notin \{K,a\}} t_{Kab} \kappa_{Ka;b} \right) + \sum_{K<L<a} \lambda_{KLa} {}^{(3)}\Omega_{KLa} \tag{6.48}$$

where λ_{Ka} and λ_{KLa} represent the L-amplitudes. As we know t_{KLa} as a function of t_{KL}, t_{Ka}, and t_{La}, one may avoid using λ_{KLa} and directly substitute the result to t_{Kab} above. However, we chose to work with λ_{KLa} as a matter of convenience. In Eq. (6.48), we left out $\lambda_{\mu\nu}$ and $\lambda_{K\mu\nu}$ as their T-amplitudes are constrained; we incorporate $t_{\mu\nu}$ and $t_{K\mu\nu}$ through explicit substitutions to the Lagrangian using Eq. (6.26) and Eq. (6.27). Evidently, we have

$$\frac{\partial \mathcal{L}}{\partial \lambda_{Ka}} = 0 = \Omega_{Ka} \tag{6.49}$$

and

$$\frac{\partial \mathcal{L}}{\partial \lambda_{KLa}} = 0 = {}^{(3)}\Omega_{KLa} \tag{6.50}$$

From

$$\frac{\partial \mathcal{L}}{\partial t_{Ka}} = 0, \tag{6.51}$$

we obtain

$$0 = \frac{\partial E}{\partial t_{Ka}} + \sum_{M<b} \lambda_{Mb} \frac{\partial \Omega_{Mb}}{\partial t_{Ka}} + \sum_{b \notin \{K,a\}} \lambda_{Kab} \frac{\partial^{(3)} \Omega_{Kab}}{\partial t_{Ka}} \tag{6.52}$$

where in the last sum we have $\lambda_{K\mu\lambda} = 0$ as discussed before. Those derivatives in Eq. (6.52) are provided in terms of computable quantities in the Appendix. We obtain λ_{KLa} from

$$\frac{\partial \mathcal{L}}{\partial t_{KLa}} = 0, \tag{6.53}$$

which yields

$$\lambda_{KLa} = \frac{\lambda_{KL}\kappa_{KL;a} - \lambda_{Ka}\kappa_{Ka;L} + \lambda_{La}\kappa_{La;K}}{t_{KL}\mu_{KL} + t_{Ka}\mu_{Ka} + t_{La}\mu_{La} - \omega_{KLa}} \tag{6.54}$$

We note that λ_{KLa} is antisymmetric under permuting two indices as in t_{KLa}. We substitute λ_{KLa} in Eq. (6.52) using Eq. (6.54). The resulting equation is only linear in λ_{Ka} and therefore λ_{Ka} can be uniquely determined as long as Eq. (6.52) is not ill-defined.

Having solved the L-amplitude and T-amplitude equations, the subsequent orbital optimization is relatively straightforward. We parametrize orbital rotations with a unitary exponential matrix,

$$\mathbf{C} = \mathbf{C}_0 \exp\left(\Delta - \Delta^\dagger\right) \tag{6.55}$$

and the pertinent orbital gradient and Hessian are obtained taking derivatives of the Lagrangian in Eq. (6.48). The orbital gradient reads

$$L^{\Delta}_{pq} = \frac{\partial \mathcal{L}}{\partial \Delta_{pq}} \tag{6.56}$$

and the Hessian reads

$$H^{\Delta\Delta}_{pq,rs} = \frac{\partial \mathcal{L}}{\partial \Delta_{pq} \partial \Delta_{rs}} \tag{6.57}$$

We also need the gradient and the hessian of $\mathcal{L}$ with respect to the polarization angle θ_K (i.e., $\mathbf{L}^\theta$ and $\mathbf{H}^{\theta\theta}$) and those can be obtained in the exactly same fashion. We treat Δ_{pq} and θ_K as independent variables and optimize the Lagrangian over those parameters. These are enough to establish any first-order convergence techniques and the optimizer we employed in this work is the geometry direct minimization (GDM) [240, 251, 566] which needs an orbital gradient and the diagonal elements of Hessian. Most of the relevant terms in $\mathbf{L}^\Delta$, $\mathbf{H}^{\Delta\Delta}$, $\mathbf{L}^\theta$, and $\mathbf{H}^{\theta\theta}$ are available in ref. 280. We discuss the CCVB+i3 specific terms in Appendix.

6.2.7 Amplitude Solvers

We found solving the CCVB+i3 amplitude equations quite challenging for some systems presented below. This may be understood by observing that there are many low-lying states nearly degenerate for strongly correlated systems and this implies that there is more than one set of cluster amplitudes that can represent the state of our interest. Unlike linear wavefunctions, this poses a great challenge to CC wavefunctions as amplitude solvers may get easily lost during iterations and amplitude equations may become nearly ill-conditioned. Therefore, we had to try several different solvers discussed below.

For CCVB calculations, the recommended T-amplitude and L-amplitude solver is Gauss-Seidel combined with Pulay's direct inversion of the iterative space (GS-DIIS).[496, 567] The GS step solves a quadratic equation in Eq. (6.23) and Eq. (6.24) for t_{Ka} while keeping all other amplitudes fixed. It solves a linear equation in the case of λ_{Ka}. The GS step scales cubically with the number of pairs. One may consider using GS-DIIS for CCVB+i3 when solving Eq. (6.37) and Eq. (6.38). It

becomes a cubic equation in t_{Ka} once one multiplies both sides by the denominator of Eq. (6.44). It is still a linear equation in the case of λ_{Ka}. The computational cost scales still cubically with the system size.

When GS-DIIS fails to find a solution, we employ the Gauss-Newton method with line-search (GN-LS). This was done by defining a cost function f as a squared sum of amplitude equations. In other words, the cost function reads

$$f = \frac{1}{2} \sum_{K<a} |\Omega_{Ka}|^2 \tag{6.58}$$

The line-search guarantees a descent direction that decreases the value of f. The GN-LS method requires the evaluation of Jacobian $\mathbf{J}$ and the inverse of it. The Jacobian of CCVB and CCVB+i3 are given in Appendix. As the length of $\mathbf{J}$ scales quadratically with the number of pairs, n_p, it requires $\mathcal{O}(n_p^4)$ amount of work to evaluate it and $\mathcal{O}(n_p^6)$ to invert it. While this is not an ideal solver for CCVB due to the steep scaling, for the systems studied in this paper, the time for solving amplitudes with GN-LS is negligible compared to that of integral transformation.

Some systems exhibited serious numerical issues with GN-LS because $\mathbf{J}$ was nearly singular (i.e., the smallest singular value is roughly $1e^{-6}$–$1e^{-7}$). In such cases, we found it more effective to use preconditioned limited-memory Broydon-Fletcher-Goldfarb-Shanno (L-BFGS) with line-search (L-BFGS-LS) where we used the inverse of the diagonal elements of $\mathbf{J}\mathbf{J}^T$ as the preconditioner. The evaluation of $\mathbf{J}$ is the bottleneck in this case which scales $\mathcal{O}(n_p^4)$. With this solver, the overall cost of CCVB methods is still dominated by integral transformation.

In this work, we used L-BFGS-LS for the numbers reported and GN-LS for testing purposes. L-BFGS-LS has been adequate for most systems described here, but when $\mathbf{J}$ is nearly singular its convergence becomes extremely slow. In fact, there is no bulletproof method when $\mathbf{J}$ is nearly singular; this is an interesting open question in applied mathematics.[568]

6.2.8 Computational Cost

The computational cost of CCVB is dominated by integral transformation and the rest of the computations scale cubically with the system size if the amplitude equation is solved via GS-DIIS. [140] The cost of evaluating t_{KLa} in Eq. (6.44) is dominated by the computation of ω_{KLa}. A naive way to evaluate ω_{KLa} would scale quartically due to the summation involved in Eq. (S18). However, if we precompute $\sum_a (\sigma_{Ka;t_1t_1;ss} - \sigma_{Ka;ss;ss})$ (quantities defined in Appendix) and store this for every CS pair K, we can evaluate ω_{KLa} with a cubic amount of work. Thus, CCVB+i3, in

principle, scales the same as CCVB as long as the underlying amplitude solver takes an equal or less amount of work.

6.3 Computational Details

All CCVB, CCVB+i3, GVB-PP, spin-flip complete active space (SF-CAS),[343, 569] HF, and self-consistent field molecular interaction (SCF-MI) [570, 571] calculations were performed with the development version of `Q-Chem`.[236] CASSCF calculations were performed using `Orca` [572] and `PySCF`. [573] Heat-bath CI (HCI) [365] and HCISCF [391] calculations were carried out with `Dice`[574] interfaced with `PySCF`. We also used `GAMESS`,[575] and `Psi4` [576] to crosscheck some of the CASSCF numbers presented below.

For all CCVB calculations but those for the $[Cr_9]$ molecular magnet, we used a tolerance of 10^{-12} for the amplitudes solver, which tests the root-mean-square (RMS) of $\mathbf{J}\Omega$, and a tolerance of $1e^{-5}$ for the orbital optimizer, which tests the RMS of orbital gradients and the step size. These were enough to get energy converged up to 0.1-1 μH. Due to numerical challenges we faced in studying $[Cr_9]$, we used looser convergence criteria for $[Cr_9]$; 10^{-8}-10^{-10} for T-amplitudes. These were enough to converge energies up to 0.1-0.01 kcal/mol. The CASSCF calculations were converged up to at least 0.1 μH. All plots were generated with `Matplotlib`. [283] All molecular figures were generated with `Chemcraft`.[284]

We mention how we obtain an initial set of orbitals to perform CCVB calculations. Like most other pairing methods, the CCVB energy is not orbital-invariant and CCVB exhibits multiple local minima in orbital optimization. Therefore, obtaining physically correct initial orbitals and pairing them properly in the beginning are often crucial to properly run CCVB calculations. The procedure of obtaining an initial guess used in this work and running "spin-ladder" calculations is as follows:

1. We perform an SCF-MI calculation of the lowest spin state that UHF can describe for a given active space. For the examples discussed below, this state is always $M_S = 3/2$.

2. We then perform a GVB-PP calculation of $S = 3/2$ using the orbitals from the SCF-MI calculation. Orbitals from this GVB-PP calculation are well localized.

3. We use chemical intuition, usually based on sensible Lewis dot structures, to pair localized orbitals properly for $S = 1/2$. This is the most non-trivial step when running CCVB.

4. We run GVB-PP to optimize the new pairing for the lowest spin-state, in our case $S = 1/2$.

5. We run CCVB for $S = 1/2$ using GVB-PP orbitals from Step 4.

6. From the solution of $S = 1/2$, we unpair most polarized pairs based on their polarization angles to obtain initial orbitals for higher spin states. We found this "spin-ladder" calculation quite robust. This approach was also used in ref. 281.

For those systems discussed below, this procedure always produced a sensible solution. Due to the ambiguity involved in Step 3, one may try multiple possible Lewis dot structures in general.

6.4 Results and Discussions

Spin-frustrated systems often exhibit a UHF to GHF instability, so one may expect CCVB to fail qualitatively for those. In the following, we consider a total of five spin-frustrated systems. Those systems are spin-frustrated based on the Kahn's definition[577]; they are open-shell, involve an odd number of sites, and are geometrically symmetric. We consider systems with three unpaired electrons per site which correspond to the S-$\frac{3}{2}$ Heisenberg model. This choice was made based on observations from S-$\frac{1}{2}$ frustrated systems such as a hydrogen lattice where UHF can dissociate the lowest spin-state correctly. Consistent with the success of UHF, we did not observe any significant differences between CCVB and CCVB+i3 in this case.

Studying S-$\frac{3}{2}$ systems, we uncover that 3P configurations are necessary for a qualitatively correct description of the lowest spin state (i.e., doublet) and even higher spin states in some cases. We emphasize the role of ϵ_{s5} and ϵ_{d5}, which are missing in CCVB. In terms of the original system configurations, ϵ_{d5} is generated by annihilating two singlet pairs and an α electron and creating two triplet pairs coupled to a triplet which is then recoupled with the remaining unpaired electron to form an overall doublet. This configuration is captured by the corresponding supersystem configuration. The detailed discussion on the role of the ϵ_{s5} configurations in CS systems is given by two of us.[143]

6.4.1 N_3 (D_{3h}) – Spin-frustration involving p orbitals

Triangular N_3 is perhaps the simplest system that satisfies our criteria described above. It has three unpaired electrons per site and is strictly spin-frustrated due to

symmetry. We consider its dissociation to three nitrogens (^{4}S) within the cc-pVTZ basis set.[237] The active space we consider is (9e, 9o) and it is small enough to perform exact CASSCF calculations. For the $S = 9/2$ state, ROHF is exact within the active space and thus CCVB is also exact. There are no $|\Phi_{(KLa)}\rangle$ configurations in the $S = 7/2$ state. Hence, CCVB and CCVB+i3 are exactly identical in the case of $S = 7/2$. UHF can properly dissociate $M_S = 3/2$ and $M_S = 9/2$.

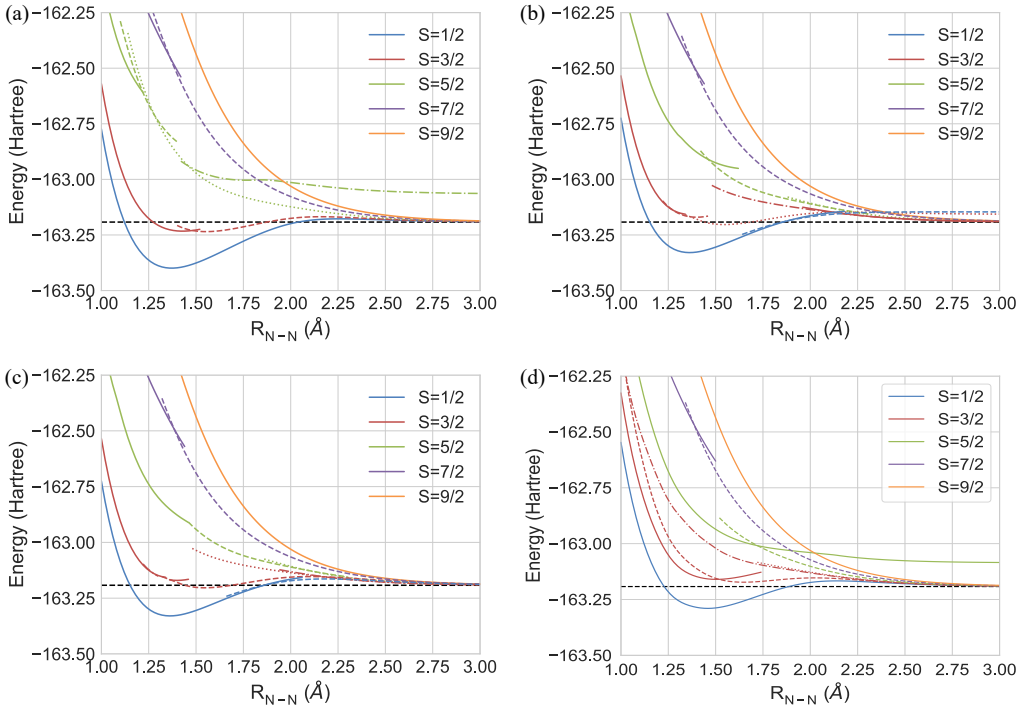

Figure 6.1: Potential energy curves of N_3 from (a) CASSCF (9e, 9o), (b) CCVB, (c) CCVB+i3, and (d) SF-CAS. The black dotted line indicates the asymptotic energy of three N(^{4}S), $E = -163.1920735\,E_h$. Different line styles for each spin state represent different local minima.

We first discuss potential energy curves (PECs) of CASSCF(9e,9o) calculations for each spin state as illustrated in Figure 6.1. Only $S = 1/2$ and $S = 3/2$ are bound states with a small hump towards the dissociation limit. The $S = 3/2$, $S = 5/2$, and $S = 7/2$ states exhibit multiple solutions, which may indicate an inadequate choice of active space. Moreover, those CASSCF solutions break the spatial symmetry. One could employ a larger active space to see whether it resolves these issues, but we focus on only pairing active spaces of the form of (ne, no) for the purpose of

this work. We note that we observed multiple solutions even from CASSCF(15e, 12o) calculations, which are full valence active space calculations. This indicates that those solutions may actually be physical and there may exist state crossings. However, this larger active space CASSCF still breaks spatial symmetry except for $S = 9/2$ (ROHF limit).

Two CASSCF solutions in $S = 3/2$ show small differences in converged orbitals. We employed Knizia's intrinsic bond orbital (IBO) localization scheme [578] to characterize two solutions at $R = 1.4$ Å. As we localized only the active space orbitals, this procedure does not change the CASSCF energy. The solid line solution has one bond-like orbital whereas the dotted line solution shows only localized orbitals. This is quite sensible given that the dotted line solution is connected to the dissociation limit where localized orbitals are most sensible. There is a third solution that appears between 2.42 Å and 3.00 Å. This solution is almost identical to the dotted line and the energy difference between those two is less than 1 mE_h. We did not include this solution for simplicity.

For $S = 5/2$, there are a total of five CASSCF solutions found. Interestingly, one of them does not dissociate properly. This solution involves a delocalized orbital even after the IBO localization. Its natural orbital occupation number indicates that there is a doubly occupied orbital and an empty orbital in the active space at $R = 3.0$ Å. One may suggest that this solution is dissociating to one N (^{2}D) and two N (^{4}S)'s, but its energy is about 16 kcal/mol higher than this limit at $R = 3.0$ Å. We suspect that it is an unphysical solution that comes from the delocalized orbital.

Lastly, there are two solutions observed in the $S = 7/2$ state. We compared orbitals of two solutions at $R = 1.2$ Å and the IBO localization analysis reveals more localized character in the higher energy solution (dotted) than in the lower energy solution (solid). Also, there is an almost doubly occupied orbital in the solid line based on natural orbital occupation numbers whereas the dotted line exhibits no such strong double occupation. It is sensible that the dashed line solutions are indeed lower in energy when approaching the dissociation limit.

Both CCVB and CCVB+i3 in Figure 6.1 successfully capture qualitative features of CASSCF solutions. Perhaps, the most interesting finding of two panels, (b) and (c), is that CCVB+i3 reaches the exact dissociation limit for every spin state while CCVB cannot reach the correct asymptote for $S = 1/2$ and has some solutions for $S = 3/2$ that cannot dissociate properly. This observation will be elaborated in greater detail later.

Lastly, we present SF-CAS results in Figure 6.1 (d). Since it is based on spatially symmetric high-spin $S = 9/2$ orbitals, these CAS wavefunctions are spatially symmetric. The low-spin solutions are lacking in orbital relaxation so these results are upper-bounds for symmetry-adapted CASSCF solutions. Other than $S = 1/2$,

there are numerous solutions crossing and these are very similar to broken symmetry CASSCF, CCVB, and CCVB+i3 solutions.

Both CCVB methods involve two solutions in the $S = 1/2$ state. We inspected the orbitals from two solutions at $R = 2.0$ Å. There are a pair of orbitals and a singly occupied orbital that are of very different character in each solution. The solid line, which is higher in energy at this geometry, has more delocalized orbitals while the dotted line exhibit more localized orbitals. There are more solutions than CASSCF in the case of $S = 3/2$ and two of those solutions resemble those of CASSCF. The rest of solutions exhibit a purely repulsive curve which are likely unphysical. Reading those repulsive solutions into CASSCF, we confirmed that they are not close to any stable stationary points and they all collapse to the other solutions we have. The solutions for $S = 5/2$ and $S = 7/2$ can be easily compared to their CASSCF counterparts. In passing, we note that those that appear in CCVB but not in CASSCF can be tentatively attributed to the pairwise nonorthogonality limitation of CCVB rather than the spin-coupling limitation. Therefore they are likely to disappear if we use its orbital-invariant generalization, CCVB-SD.[141, 142]

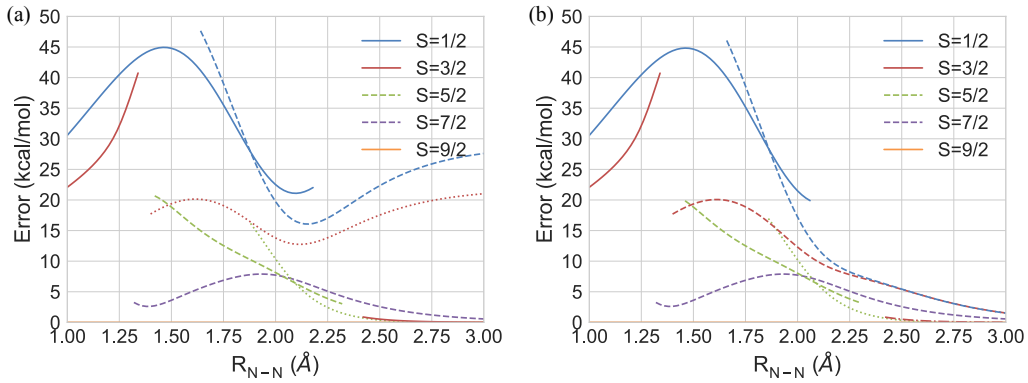

Figure 6.2: Errors in absolute energy relative to CASSCF of N_3 for (a) CCVB and (b) CCVB+i3. The line style of each line is consistent with that of Figure 6.1, and we omitted solutions that we could not find the counterpart in CASSCF.

We present a more precise error analysis of two CCVB models against CASSCF results in Figure 6.2. Near the equilibrium distance of $S = 1/2$, all the states exhibit quite substantial CCVB errors and this is a manifestation of the lack of ionic configurations relevant to dynamic correlations. However, as mentioned earlier, it should be emphasized that CCVB+i3 can dissociate all the spin states exactly in this example. CCVB shows two distinct solutions for $S = 1/2$ and $S = 3/2$ that

do not dissociate properly. This is indeed the hallmark of 3P substitutions that are necessary to describe the spin frustration.

We also note that there are $S = 5/2$ solutions in both CCVB and CCVB+i3, which exhibit a slight non-variationality (about 0.05 kcal/mol) at $R = 3.0$ Å. This is the first time for us to observe non-variationality of CCVB, and we further confirmed this by reading CCVB orbitals into a CASSCF calculation and observing higher energy in the final CASSCF energy. As the extent to which CCVB manifests this non-variationality is almost negligible, we did not find it very concerning.

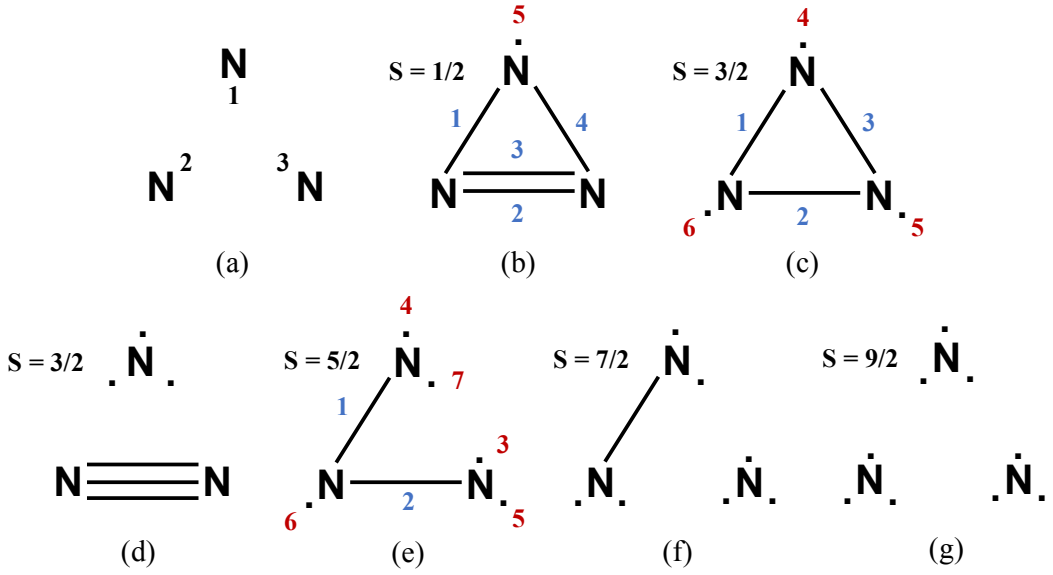

Figure 6.3: Panel (a) shows how we label the three nitrogens. The remaining panels illustrate possible Lewis structures of N_3 for each spin state: (b) $S = 1/2$, (c) $S = 3/2$, (d) $S = 3/2$, (e) $S = 5/2$, (f) $S = 7/2$, and (g) $S = 9/2$. The number next to each bond or unpaired electron is used to label a CS (blue) or OS (red) pair. (c) and (d) represent two possible Lewis structures of N_3 when $S = 3/2$. Every N-N bond consists of p-orbitals and each N atom has three p-orbitals which yields an active space of (9e, 9o).

It is interesting to discuss what the significant 3P substitutions are when dissociating this molecule. As CCVB+i3 does not make significant differences near equilibrium bond lengths, CCVB and CCVB+i3 energies are very similar. However, t_{KLa} becomes quite significant as one stretches bonds.

In Table 6.1, we present the 2P and 3P amplitudes of the $S = 1/2$ CCVB+i3 solution at $R = 3.0$ Å. Orbitals are strongly localized, so each CS or OS pair cor-

K	a	t_{Ka}
2	3	0.56500
4	5	-0.55826
1	5	-0.55825
3	4	-0.55449
1	3	0.55448
2	4	-0.53524
1	2	0.53523
1	4	0.53192
3	5	-0.00028
2	5	-0.00026

K	L	a	t_{KLa}
1	3	4	0.74396
1	2	4	0.71019
3	4	5	-0.38253
1	3	5	-0.38213
2	4	5	-0.36031
1	2	5	-0.35995
2	3	4	0.00260
1	2	3	0.00260
2	3	5	0.00015
1	4	5	0.00000

Table 6.1: The CCVB+i3 2-pair and 3-pair amplitudes of N_3 ($S = 1/2$) at $R = 3.0$ Å. 1–4 are CS pairs and 5 is an OS pair. Pair labels are consistent with those in Figure 6.3 (b).

responds to bonds and an unpaired electron in the Lewis structures in Figure 6.3. Most of the t_{Ka} amplitudes have values close to $\pm 1/\sqrt{3}$, but there are two amplitudes that are nearly zero. Those two correspond to the $t_{K\mu}$ type amplitudes, where the CS pair $K = 2, 3$ is not connected to the radical center, N(1) (See Figure 6.3 (a) and (b)). $t_{K\mu}$ involving a CS pair connecting N(1) and others all exhibit quite large values. All the t_{KL} amplitudes are large.

The two largest 3P amplitudes are of the t_{KLM} type. Those CS pairs form a perfect triangle and this is typical of large t_{KLM}. Those involving three CS pairs that do not form a triangle are almost negligible as shown in Table 6.1. There are a total of four significant $t_{KL\mu}$ amplitudes. The basic observation is that they all involve one CS pair that connects N(1) with N(2) or N(3) and the second CS pair should connect N(2) and N(3). All the other $t_{KL\mu}$ amplitudes that do not satisfy this condition are all negligible.

The $S = 3/2$ state involves two reasonable Lewis dot structures, Figure 6.3 (c) and (d). Using the PP references that represent those Lewis dot structures yields different CCVB solutions. The (c) orbitals give a reasonable description near equilibrium, but CCVB cannot dissociate this solution to the right limit (neither can UHF). (c) involves a triangle and three pair substitutions become crucial to correctly dissociate. There is no triangle involved in the bonding network of (d), so the 3P amplitudes are expected to be negligible and CCVB (and UHF) can properly dissociate. Therefore, CCVB can dissociate $S = 3/2$ exactly with orbitals from (d), but it gives a purely repulsive potential energy. Table 6.2 presents t_{Ka} and t_{KLa} for

K	a	t_{Ka}
1	6	0.55779
1	4	-0.55779
3	4	0.55779
2	6	-0.55779
2	5	0.55779
3	5	-0.55779
1	3	-0.53284
1	2	-0.53284
2	3	-0.53284
2	4	-0.00001
3	6	0.00001
1	5	0.00000

K	L	a	t_{KLa}
1	2	3	0.70949
1	2	4	0.36038
1	3	6	0.36038
1	2	5	-0.36038
1	3	5	-0.36038
2	3	6	0.36037
2	3	4	-0.36037
1	3	4	-0.00000
2	3	5	0.00000
1	2	6	0.00000

Table 6.2: The CCVB+i3 2-pair and 3-pair amplitudes of N_3 ($S = 3/2$) at $R = 3.0$ Å. The solution here is well represented by the Lewis structure in Figure 6.3 (c). 1–3 are CS pairs and 4–6 are OS pairs. Pair labels are consistent with those in Figure 6.3 (c).

CCVB+i3 calculation using the (c) orbitals. The observation here is consistent with what is discussed above in the case of $S = 1/2$.

The $S = 5/2$ state does not exhibit any notable 3P contributions as shown in Table 6.3. This is particularly interesting because it contains t_{125} and t_{124} that are significant in describing the dissociation of $S = 3/2$. The initial guess orbitals are from $S = 1/2$ orbitals and we unpair two most polarized electron pairs to obtain the Lewis structure in Figure 6.3 (e). The effect of orbital optimization is very small at this distance. However, once those localized initial orbitals are optimized, they become delocalized. The converged orbitals show almost no 3P contributions. Surprisingly, even the localized initial orbitals do not exhibit significant 3P contributions. Since the energy difference between those two orbitals is only 1 mE_h, the amplitudes in Table 6.3 are evaluated with those localized guess orbitals as a matter of convenience.

Furthermore, the amplitudes presented in Table 6.3 show differences relative to our previous observations from $S = 1/2$ and $S = 3/2$. All the t_{Ka} amplitudes are close to $\pm 1/\sqrt{3}$, which include amplitudes involving an OS pair centered on N(1) and a CS pair connecting the other two nitrogens. Moreover, this change in t_{Ka} essentially nullifies every t_{KLa}. For instance, we have non-negligible t_{125} in $S = 3/2$, but it is very small in $S = 5/2$. We compared every parameter involved in evaluating t_{125}

K	a	t_{Ka}
2	5	-0.56231
2	3	-0.56201
1	7	-0.56021
1	4	-0.55980
2	6	0.55930
1	6	0.55754
1	2	0.55043
2	7	-0.54007
2	4	-0.53817
1	3	-0.52954
1	5	-0.52867

K	L	a	t_{KLa}
1	2	5	0.01945
1	2	3	0.01861
1	2	4	-0.01249
1	2	7	-0.01122
1	2	6	-0.00010

Table 6.3: The CCVB+i3 2-pair and 3-pair amplitudes of N_3 ($S = 5/2$) at $R = 3.0$ Å. The orbitals used here are well represented by the Lewis structure in Figure 6.3 (e). 1 and 2 are CS pairs and 3–7 are OS pairs. Pair labels are consistent with those in Figure 6.3 (e).

through Eq. (6.44), and the only significant difference is that t_{15} is zero in $S = 3/2$, but is large in $S = 5/2$. The same applies to t_{124}. We believe that those large $t_{K\mu}$ amplitudes may be relevant to the broader applicability of CCVB than that of UHF for OS systems, but we do not have a clear way to understand the limit of its applicability yet. By contrast, it should be clear that UHF cannot dissociate $S = 5/2$.

6.4.2 V_3O_3 (D_{3h}) – Spin-frustration involving s and d orbitals

Vanadium oxides have drawn a lot of attention from the solid state physics community and they are often strongly correlated. In particular, VO_2 has been used to study metal-to-insulator transitions.[579, 580] In this section, we study a symmetric bond dissociation of a molecular vanadium oxide, V_3O_3, which is spin-frustrated under D_{3h} symmetry. It is probably not relevant to the strong correlations of VO_2 in bulk, but we found this molecule interesting enough to study. Each V(II) in a VO unit has an electron configuration of d^2s^1 as opposed to the more commonly seen d^3 and the VO molecule has a X $^4\Sigma^-$ ground state.[581] This is not an artifact from approximate quantum chemistry models and was confirmed experimentally before.[582] We used a fixed VO bond length of 1.547431 Å throughout and obtained the PECs

within the def2-SVP basis set [254] by varying the distance between V and the center of the triangle. The asymptote corresponds to three VO(X $^4\Sigma^-$).

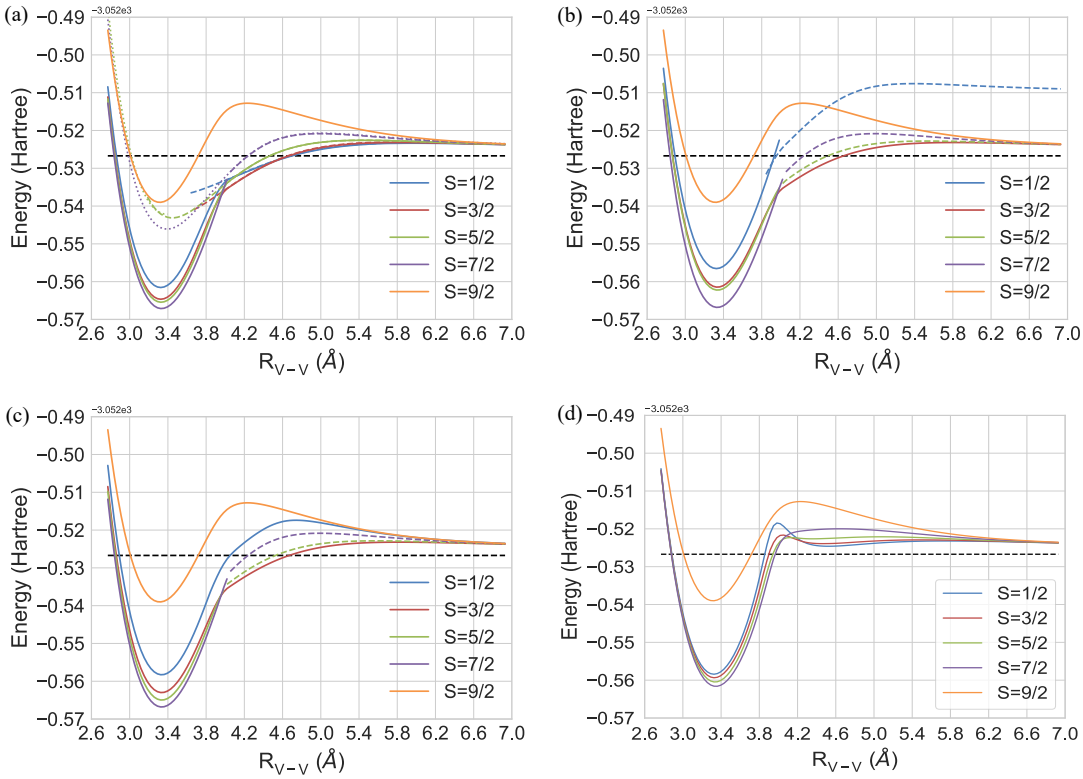

Figure 6.4: Potential energy curves of a symmetric dissociation of V_3O_3 from (a) CASSCF (9e, 9o), (b) CCVB, (c) CCVB+i3, and (d) SF-CAS. The black dotted line indicates the asymptotic energy of three VO(X $^4\Sigma$), $E = -3052.5267114\ E_h$. Different line styles for each spin state represent different local minima.

Based on the CASSCF(9e, 9o) results, the ground state is ferromagnetic with $S = 7/2$ within the active space. However, the CASSCF solutions other than that of $S = 9/2$ all break spatial symmetry (D_{3h}) to some extent and this artificial symmetry breaking indicates that the size of active space may not be fully appropriate with CASSCF orbital optimization. This spatial symmetry breaking may also be the reason that the energy of $S = 9/2$ is apparently too high compared to the rest. Moreover, the appearance of multiple solutions also indicates the same. This particular choice of the active space is made for the purpose of benchmarking like before, and it would be interesting to relax this pairing active space constraint in CASSCF and compare against CCVB-SD in the future.

As for lower spin states of other ferromagnetic systems, commonly used determinant based CI methods suffer from spin-contamination, so we employed the configuration state function (CSF) based CASSCF method in `Orca`. Some of the CASSCF results presented below started from CCVB or CCVB+i3 orbitals which are in general a very good guess. With determinant based CI methods, CASSCF can be very prone to high spin-contamination and often just collapses to an unwanted spin-state. This is commonly obeserved when trying to obtain a low-spin state when the ground state is a high-spin state. We observed this quite frequently when starting from CCVB orbitals and therefore for those which used CCVB orbitals as a guess we added a penalty function to the electronic Hamiltonian to penalize the contaminants as implemented in `PySCF`, which is to add $\lambda(\langle\hat{S}^2\rangle - S_z(S_z+1))^2$ where λ is a level-shift parameter.

The CASSCF solutions in Figure 6.4 (a) show quite interesting results. Near the minimum ($\sim$ 3.36 Å), the $S = 1/2 - 7/2$ states are very close in energy. Those states are all within a 7 kcal/mol energy window of each other, and this is indeed the hallmark of SSC. Electrons are well localized and flipping one of the spins costs only a small energy penalty. We note that the system exhibits a strikingly slow convergence to the asymptote as the bond length increases. This slow algebraic decay is due to the fact that each X $^4\Sigma^-$ VO is polar (roughly V^+O^-[581]), and therefore the system exhibits multipolar interactions at long range. This has been verified by a log-log plot of energy-distance.

As is evident from Figure 6.4 (b), CCVB solutions capture all the qualitative features of their CASSCF counterparts except for the $S = 1/2$ state at the dissociation limit. Similar to N_3, to describe the dissociation of the $S = 1/2$ state one needs 3P substitutions. We observed multiple solutions in the case of the $S = 3/2$ state similar to those obtained for N_3. Each of them corresponds to one of the Lewis structures of $S = 3/2$ described in Figure 6.3 (b) and (c), replacing N's with VO's. However, we only present the solution that dissociates properly. This solution is quite delocalized at $R = 4.0$ Å unlike the localized solution we found in N_3. The CCVB+i3 in Figure 6.4 (c) shows only one solution in $S = 1/2$ and it dissociates properly. The other states are more or less the same as those in CCVB. Both CCVB and CCVB+i3 correctly predict the relative energy ordering of different spin states near equilibrium.

SF-CAS results are presented in Figure 6.4 (d). These results are based on spatially symmetric wavefunctions. All the curves in Figure 6.4 (d) are smooth unlike those obtained from CASSCF and CCVB methods. CASSCF, CCVB, and CCVB+i3 do not capture a small hump in $S = 1/2$ present in SF-CAS. Instead, they exhibit a first-order derivative discontinuity due to the coexistence of two low-lying solutions. We believe that the discontinuity is closely related to the existence of

the hump in the $S = 1/2$ state of SF-CAS. The SF-CAS relative energy ordering of different spin states near equilibrium agrees with other methods. It will be interesting to study these spin gaps in conjunction with dynamic correlation treatments to draw quantitative conclusions.

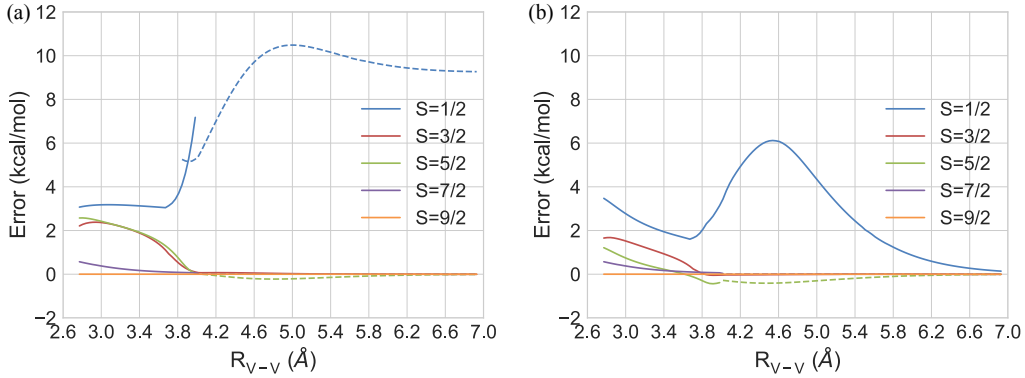

Figure 6.5: Errors in absolute energy relative to CASSCF of a symmetric dissociation of V_3O_3 for (a) CCVB and (b) CCVB+i3. The line style of each line is consistent with that of Figure 6.4.

The errors in absolute energy relative to CASSCF are shown in Figure 6.5 for both CCVB and CCVB+i3. All the errors are much smaller than those for N_3, which suggests that the bonding in V_3O_3 involves much smaller dynamic correlations compared to N_3 within the active space. Clearly, CCVB+i3 shows improved results compared to CCVB, and the key improvement is the exact bond dissociation of $S = 1/2$. It improves the $S = 3/2$ and $S = 5/2$ states by 1–2 kcal/mol. We also note that both CCVB and CCVB+i3 exhibit a slight non-variationality ($\leq$0.50 kcal/mol) in $S = 5/2$. The CASSCF calculations starting from those orbitals converged to higher values. As it is not significant in magnitude, we do not find it very concerning.

The CCVB+i3 amplitudes of the $S = 1/2$ state at $R = 4.0$ Å are shown in Table 6.4. There are several qualitatively different features compared to the N_3 results. The 2P amplitudes involving an OS pair localized on VO(1) and a CS pair connecting two other VO's are much larger. This is opposite to what was observed in N_3. Usually, when 2P amplitudes are much larger than $1/\sqrt{3}$ in magnitude, it is often possible to identify a different PP reference. In this case, it is not obvious to us if there exists a better reference. The 3P amplitudes show two $t_{KL\mu}$ amplitudes that are larger than the largest t_{KLM} amplitudes. In the case of N_3, the largest $t_{KL\mu}$ amplitudes were smaller than the largest t_{KLM} amplitudes. However, we confirm that the condition we found for having significant t_{KLa} still holds.

K	a	t_{Ka}
2	5	-1.32106
3	5	-1.31987
4	5	0.57741
2	3	0.57734
3	4	0.57708
2	4	0.57661
1	5	-0.57650
1	3	0.57425
1	2	0.57323
1	4	-0.57174

K	L	a	t_{KLa}
2	4	5	1.34229
3	4	5	1.34158
1	3	4	-0.80939
1	2	4	-0.80723
1	2	5	0.52392
1	3	5	0.52209
1	4	5	0.00045
1	2	3	-0.00045
2	3	5	-0.00026
2	3	4	-0.00015

Table 6.4: The CCVB+i3 2-pair and 3-pair amplitudes of V_3O_3 ($S = 1/2$) at $R = 4.0$ Å. 1–4 are CS pairs and 5 is an OS pair. The CS pair 1 consists of two s-like orbitals, the CS pair 2 consists of a d-like orbital and a s-like orbital, and the rest contains only d-like orbitals. Pair labels are consistent with those in Figure 6.3 (a) where each N is replaced by a VO.

When the $S = 5/2$ state at $R = 4.0$ Å is evaluated with localized orbitals (from the $S = 1/2$ state and unpairing polarized pairs), the 3P amplitudes are significant. The same analysis for N_3 revealed that the 3P amplitudes are negligible, so this result in V_3O_3 is quite different although the geometry setup is the same. We suspect that this is because in V_3O_3 there may be more than one way to spin-couple high-spin fragments to correctly reach the asymptote and some of them do not need the 3P substitutions and some do. If the former is the case, it is not too surprising that the energy difference between CCVB and CCVB+i3 is about 0.01 kcal/mol. It is, however, possible that some higher-body correlations functions beyond two-body correlators (or 4-point correlators) will show larger differences between different spin-couplings (i.e., those that involve 3P substitutions and those that do not). Those higher-body correlation functions such as three-body Green's functions are often studied in nuclear physics.[583, 584] After orbital optimization, the $S = 5/2$ CCVB orbitals become delocalized and the 3P amplitudes become negligible.

6.4.3 The $[CaMn_3O_4]$ Subunit of Oxygen-Evolving Complex

The cubane subunit, $[CaMn_3O_4]$, in the oxygen-evolving complex (OEC) has attracted a lot of interest in both experimental and theoretical chemistry.[40, 393, 394,

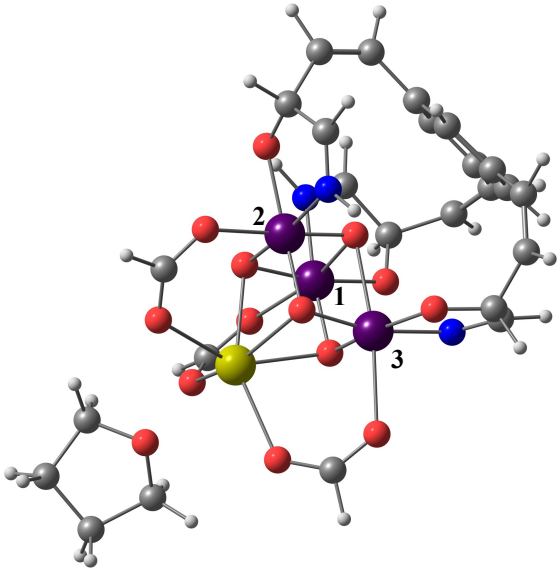

Figure 6.6: The molecular structure of a simplified synthetic model of the cubane subunit of OEC. The color code we used is as follows: grey: C, white: H, red: O, blue: N, purple: Mn, and yellow: Ca. The numbers indicate the labels for Mn atoms. The distances between Mn atoms are as follow: Mn(1)-Mn(2) = 2.83 Å, Mn(2)-Mn(3) = 2.90 Å, and Mn(3)-Mn(1) = 2.95 Å.

585–592] From a theoretical chemistry point of view, this is a very challenging system because it requires a balanced treatment of both static and dynamic correlations and there is no readily usable quantum chemistry model which can achieve this. Moreover, understanding electron correlations in this molecule may assist in the rational design of synthetic OECs, which is also of much interest.[588, 590, 593]

Most recent studies have focused on studying the complete complex including the fourth "dangling" Mn atom. The presence of the fourth Mn reduces the effect of 3P amplitudes significantly in the ground state, and hence CCVB appears to be well-suited for the full complex. For a more demanding test of CCVB+i3, we therefore considered the cubane subunit without the dangling Mn, which shows significant 3P contributions as we shall see.

The geometry shown in Figure 6.6 was taken from ref. 592, which is a simplified cubane subunit of the synthetic model reported by Agapie and co-workers.[588] The

structure is very similar to what Agapie and co-workers used in their theoretical study [591] and the corresponding molecule in ref. 591 was neutral with $[CaMn_3^{IV}O_4]$. However, the oxidation state studied in ref. 592 is $[CaMn_2^{III}Mn^{IV}O_4]$ with overall -2 charge. Since we are interested in maximizing spin-frustration, we chose to study $[CaMn_3^{IV}O_4]$ with charge neutrality. The natural active space is (9e, 9o) which includes all the d-electrons in 3 Mn^{IV} (d^3). This active space is small enough that exact CASSCF can easily be performed. This active space may be too small to describe the system properly, but it includes every d-orbital with strong open-shell character which are the primary source of strong correlation.

An interesting feature of this molecule is that the three Mn atoms form a nearly perfect triangle and thus 3P configurations ought to play a crucial role as we learned from the isoelectronic model systems above. We used the def2-SVP basis set [254] for hydrogen and carbon atoms and the def2-TZVP basis set [254] for everything else. We also employed the density-fitting approximation to the two-electron integrals with the corresponding density-fitting bases.[255]

We employed several computational approaches to compute spin gaps and compared against exact CASSCF as shown in Table 6.5. The CASSCF results show a monotonic increase in the spin gap as we go from the high-spin state to the low-spin state, indicating that the complex is ferromagnetic within the active space employed here. Remarkably, all the spin states lie within 1 kcal/mol and this is again a signature of SSC.

SF-CAS energies are also computed with the $S = 9/2$ reference, and it should be the upper bound to the CASSCF energies for each spin state as both methods are variational. The SF-CAS energies show the same trend as CASSCF and it is qualitatively accurate for this system. As orbitals are very well localized, the effect of orbital optimization is expected to be small, and this is consistent with the observation here. The perturbative correction to the SF-CAS states (SF-CAS(h,p)$_1$) [343], which attempts to incorporate orbital relaxation, fails quite significantly, and it yields negative spin gaps. This suggests that orbital relaxation is not negligible and one may try to regularize the energy denominators.[269]

CCVB and CCVB+i3 predict the relative spin gaps of $S = 3/2$ and $S = 5/2$ wrong, but essentially the errors are all within 1 kcal/mol for those states. These incorrect orderings may well be fixed by a full CC model which generalizes these CCVB models. Such a full CC model incorporates ionic excitations and thus will provide more accurate energies within this active space. CCVB fails catastrophically to describe the $S = 1/2$ state yielding a spin gap of roughly 29 kcal/mol! In contrast, CCVB+i3 yields a quantitatively accurate result. This highlights the role of 3P substitutions in spin-frustrated systems.

Turning to the 2P and 3P amplitudes of CCVB+i3 of $S = 1/2$ in Table 6.6, we

S	CASSCF	SF-CAS	SF-CAS(h,p)$_1$	CCVB	CCVB+i3
1/2	0.853	1.074	N/A	29.816	1.412
3/2	0.662	0.884	-0.012	0.791	0.796
5/2	0.535	0.672	-0.011	0.889	0.889
7/2	0.327	0.377	-0.006	0.588	0.588
9/2	0.000	0.000	0.000	0.000	0.000

Table 6.5: Relative energies (kcal/mol) of different spin states from different methods. N/A means "not available" due to the limited computational resource.

K	a	t_{Ka}
1	5	0.57570
4	5	0.57564
3	2	0.57497
1	4	0.57201
3	1	0.57116
2	1	0.57102
2	4	-0.57029
3	4	-0.56979
2	5	-0.13906
3	5	-0.13819

K	L	a	t_{KLa}
1	3	4	0.80176
1	2	4	0.80114
1	2	5	0.50033
1	3	5	0.49939
3	4	5	-0.30389
2	4	5	-0.30333
2	3	4	-0.00029
2	3	5	-0.00023
1	2	3	-0.00019
1	4	5	-0.00011

Table 6.6: The CCVB+i3 2-pair and 3-pair amplitudes of the cubane subunit for $S = 1/2$. 1–4 are CS pairs and 5 is an OS pair. Pair labels are consistent with those in Figure 6.3 (a) where each N is replaced by a Mn atom.

observe qualitatively similar results to those for N_3. Most of the 2P amplitudes are close to $1/\sqrt{3}$ in magnitude and only those types of $t_{K\mu}$ that were small in Table 6.1 are negligible here.

The natural orbital occupation numbers (NOONs) from CASSCF show strong open-shell characters in all 9 orbitals regardless of the spin state (i.e., they are all near 1.0). Both CCVB and CCVB+i3 successfully capture this (i.e., NOONs are all near 1.0). It is interesting that the NOONs of the $S = 1/2$ state in CCVB are almost the same as those of CASSCF even though its energy is 29 kcal/mol higher. In this particular case, orbital relaxation upon going from CCVB orbitals to CCVB+i3 orbitals is negligible, which indicates that including the proper 3P spin-coupling vectors is crucial to obtain an accurate energy. Reading CCVB orbitals into CCVB+i3 yields an energy that is higher only by 1 mH than the optimized energy.

S	CCVB	CCVB+i3	HCI-SCF ($\epsilon_1 = 10^{-3}$)	HCI-SCF ($\epsilon_1 = 10^{-4}$)	HCI-SCF ($\epsilon_1 = 10^{-5}$)	HCI-SCF ($\epsilon_1 = 10^{-6}$)
1/2	7.14 (7.14)	-3.22	173.50	-4.78	-5.35	-5.37
3/2	5.92 (5.92)	-2.98	85.54	-4.52	-5.04	-5.05
5/2	4.59 (4.59)	-2.68	131.31	-4.01	-4.60	-4.60
7/2	10.92 (-3.85)	-3.85	-0.89	-3.39	-3.95	-3.96
9/2	-2.18 (-2.18)	-2.20	-1.24	-2.70	-3.18	-3.18
11/2	-1.00 (-1.79)	-1.79	-1.35	-2.20	-2.26	-2.26
13/2	-0.48 (-0.48)	-0.48	-0.99	-1.19	-1.20	-1.20
15/2	0.00 (0.00)	0.00	0.00	0.00	0.00	0.00

Table 6.7: The relative energies (kcal/mol) of different spin states of P_5. The CCVB energies in parentheses are from the CCVB solutions where converged CCVB+i3 orbitals were used as an initial guess. For $S = 15/2$, every method presented here is exact since ROHF is exact for that state. The corresponding $S = 15/2$ ROHF energy is -1702.98131 E_h. These spin-gaps are directly comparable across different methods as they are measured with respect to this same energy.

6.4.4 P_5 (D_{5h}) – Spin-frustration in a pentagon

Clusters of phosphorus have been studied theoretically and experimentally by many researchers.[594–602] Here, we studied P_5 and fixed its geometry to D_{5h} so that the molecule is forced to be spin-frustrated. It is an interesting spin-frustrated model system that is beyond the triangular geometric frustrations that have been discussed in this work so far. UHF can dissociate properly to quartet P atoms only when $M_S = 3/2, 9/2, 15/2$.

The natural choice of an active space is (15e, 15o) for which exact CASSCF is demanding so we used the recently developed selected CI method, heat-bath CI (HCI) with orbital optimization (HCISCF) [391] for the reference benchmark data. We compare variational HCISCF energies and CCVB energies. In HCISCF, we test different values of ϵ_1 which controls the number of determinants included in the variational space. The smaller ϵ_1 value yields the larger variational space and thus the result becomes more accurate. As our focus is the strong correlation in this system, we chose a relatively stretched geometry, $R_{\text{P-P}} = 4.1145$ Å. This stretched geometry makes CCVB methodologies particularly well-suited since ionic excitations are negligible. The only important excitations are of the spin-flip type. We employed the def2-SVP basis set throughout.[254]

S	CCVB+i3	HCISCF ($\epsilon_1 = 10^{-3}$)	HCISCF ($\epsilon_1 = 10^{-4}$)	HCISCF ($\epsilon_1 = 10^{-5}$)	HCISCF ($\epsilon_1 = 10^{-6}$)
1/2	35	942	5331	145087	488263
3/2	39	885	6324	143864	465000
5/2	40	552	4946	96852	237935
7/2	38	2650	32849	158377	330978
9/2	33	772	4383	19184	35882
11/2	25	68	1181	2743	3538
13/2	14	31	87	122	122
15/2	0	0	0	0	0

Table 6.8: The number of independent wavefunction parameters used in each method in P_5. For CCVB+i3, this number is the same as for CCVB: 2-pair amplitudes t_{Ka} plus the number of polarization angles θ_K. For HCISCF, this is the number of determinants minus one due to the wavefunction normalization.

There can be more than one solution for each spin state as we saw in the previous examples. Here, we focus on CCVB solutions from the "spin-ladder guess" procedure described before. In other words, all the CCVB and CCVB+i3 calculations are performed using the orbitals from $S = 1/2$ as a guess. For HCISCF calculations, the CCVB+i3 converged orbitals were used as an initial guess.

In Table 6.7, we present the spin gaps of CCVB and CCVB+i3 along with the HCISCF spin gaps as a reference. Comparing the CCVB and CCVB+i3 energies, significant energy differences are observed for $S = 1/2, 3/2, 5/2, 7/2$. As UHF can dissociate $M_S = 3/2$ properly, there must be a CCVB solution for $S = 3/2$ that is lower in energy than what we found here. However, we discuss only those obtained from an $S = 1/2$ initial guess for the purpose of demonstration. For $S = 7/2$, CCVB yields a localized solution with a quite high energy while CCVB+i3 yields a delocalized solution with a lower energy and no significant 3P amplitudes. By reading the CCVB+i3 orbitals into CCVB, we were able to obtain a CCVB solution that reaches the correct asymptote. HCISCF energies are converged at around the ϵ_1 value of 10^{-5} and HCISCF of $\epsilon_1 = 10^{-3}$ shows very unconverged energies. In terms of energies, CCVB+i3 lies between HCISCF of $\epsilon_1 = 10^{-3}$ and $\epsilon_1 = 10^{-4}$, although the nature of the errors is quite different.

In Table 6.8, we present the number of independent wavefunction parameters used in each method. An advantage of CC methods is the ability to describe chemical systems with a much more compact representation through a cluster expansion, which linear CI wavefunctions do not offer. Table 6.8 shows that the number of parameters in the CCVB wavefunction is much smaller than in HCISCF. Comparing

CCVB and HCISCF of $\epsilon_1 = 10^{-3}$ or $\epsilon_1 = 10^{-4}$ which are similar in accuracy, we see that CCVB has 20-150 times fewer parameters than HCISCF for $S = 1/2$. Remarkably, for $S = 7/2$ CCVB is more accurate than HCISCF of $\epsilon_1 = 10^{-4}$ while involving roughly 860 times fewer parameters.

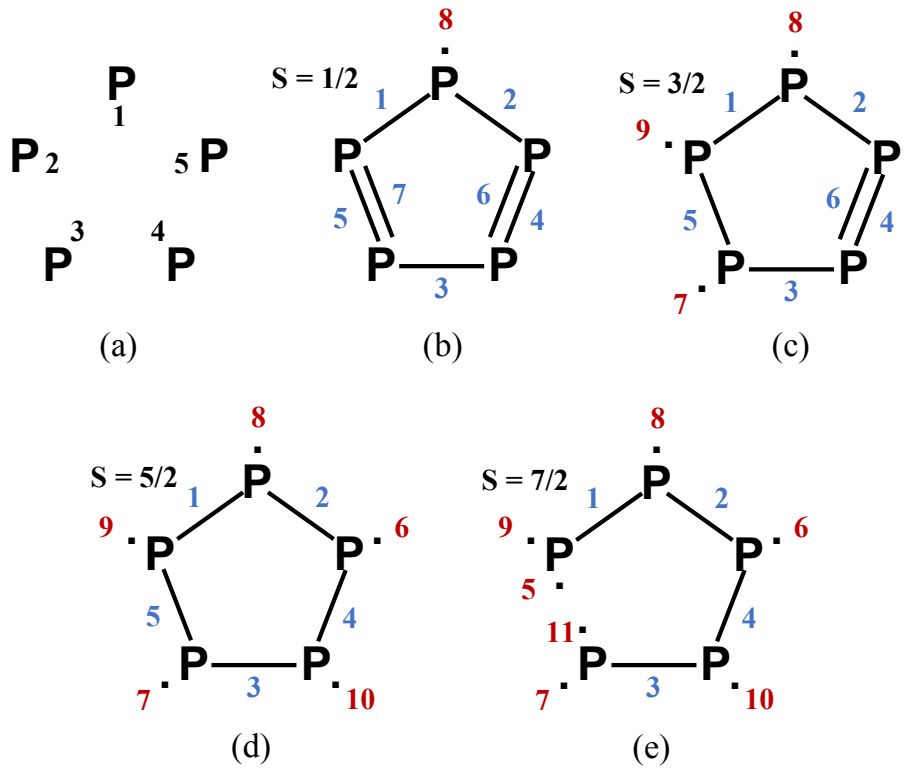

Figure 6.7: Panel (a) shows how we label five phosphorus atoms. The rest of panels illustrate represent possible Lewis structures of P_5 for each spin state: (b) $S = 1/2$, (c) $S = 3/2$, (d) $S = 5/2$, and (e) $S = 7/2$. The number next to each bond or unpaired electron is used to label a CS (blue) or OS (red) pair. Both of CCVB methods yield localized solutions for (b) to (d), and only CCVB yields a localized solution for (e). Every P-P bond consists of p-orbitals and each P atom has three p-orbitals which yields an active space of (15e, 15o).

Lastly, we discuss 3-pair (3P) amplitudes along with corresponding Lewis structures shown in Figure 6.7. In the previous examples (D_{3h}), we made empirical observations on significant 3P amplitudes. We will see how those transfer to this 15-electron D_{5h} case. Because there are quite a few 3P amplitudes, we will visualize a subset of those amplitudes as opposed to presenting every one of them. One way

to visualize 3P amplitudes is to fix one of the three indices and look at the matrix indexed by the other two indices. We will discuss such matrices below.

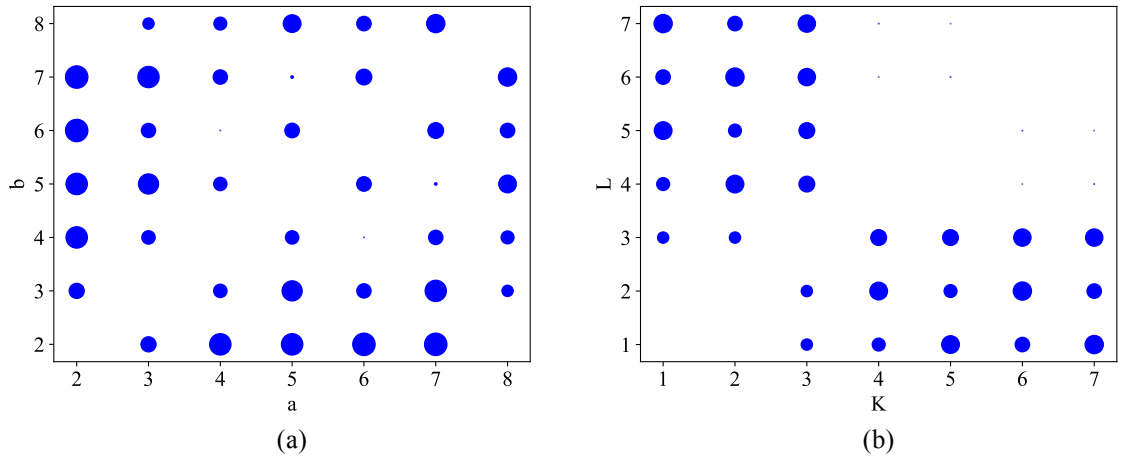

Figure 6.8: The 3P amplitudes of the $S = 1/2$ state of P_5. (a) t_{Kab} when $K = 1$, (b) $t_{KL\lambda}$ when $\lambda = 8$. The labeling here is consistent with the localized orbitals and labels in Figure 6.7 (b). Pairs 1-7 are CS and pair 8 is OS. The circle of largest area represents an amplitude of magnitude 0.18533 in (a) and an amplitude of magnitude 0.27933 in (b).

Figure 6.8 shows the 3P amplitudes of $S = 1/2$. Panel (a) and (b) fix a CS pair and an OS pair, respectively. As is clearly shown, involving an OS index yields sparser 3P amplitudes. There are many significant t_{KLM}'s that involve pair 1 and 2. Basically, t_{12M} for any CS pair M is non-negligible. As seen in Figure 6.7 (b), those pairs form incomplete triangles. All of them involve more than three P atoms. Obviously, this could not be observed in the D_{3h} examples since there are only three sites. Panel (b) shows negligible t_{KL8} when both K and L belong to $\{4, 5, 6, 7\}$. Non-negligible amplitudes involve either pair 1, 2 or 3. Involving pair 1 or 2 is consistent with what we found in the D_{3h} examples. Having more spin-frustrated sites gives a more rich spectrum of non-negligible 3P amplitudes and this is a manifestation of complex overall spin-coupling vectors whose total underlying dimension scales formally exponentially with the number of electrons.

Figure 6.9 illustrates the 3P amplitudes of the $S = 3/2$ state. Panel (b) may be easy to understand because it is basically the same as a subblock of panel (b) in Figure 6.8. Unpairing a pair in $S = 1/2$ basically results in removing a CS pair column and row in $t_{KL\lambda}$ for a given λ. At this stretched geometry, orbitals barely

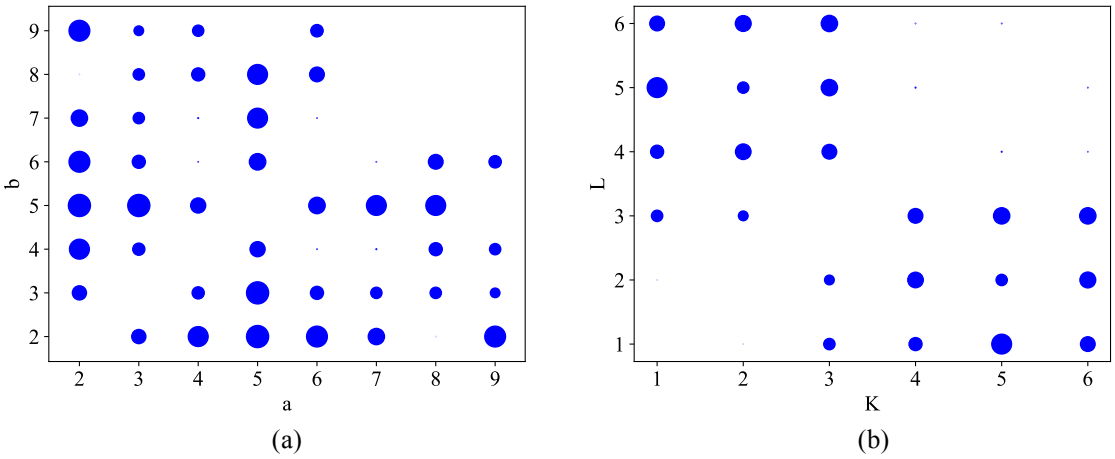

Figure 6.9: The 3P amplitudes of the $S = 3/2$ state of P_5. (a) t_{Kab} when $K = 1$, (b) $t_{KL\lambda}$ when $\lambda = 8$. The labeling here is consistent with the localized orbitals and labels in Figure 6.7 (c). Pairs 1-6 are CS and pairs 7-9 are OS. The circle of largest area represents an amplitude of magnitude 0.27484 in (a) and an amplitude of magnitude 0.21984 in (b).

change, and hence it is not surprising to see this similarity in $t_{KL\lambda}$ across different spin states. Panel (a) exhibits a similar result in that its subblock (2 to 6) is very similar to that of $S = 1/2$. The additional OS pairs 7 and 9 have non-negligible $t_{1L\mu}$. The other spin states, $S = 5/2, 7/2$, which correspond to (d) and (e) in Figure 6.7, show more or less the same result.

In summary, we have seen that P_5 exhibits a much more complex spin-coupling pattern compared to those of the D_{3h} examples. Namely, P_5 shows many non-negligible t_{KLa} amplitudes that are relevant in reaching the correct asymptote. Compared to HCISCF, it involves far fewer parameters, and yet their energies are comparable.

6.4.5 The [Cr_9] Single Molecular Magnet

Single molecular magnets (SMMs) have received a lot of interest lately since they can play a role of magnetic memory and potentially be used to build a quantum computer.[603, 604] A lot of theoretical studies on multinuclear complexes have been focused on broken-symmetry density functional theory (BS-DFT) often combined with the Heisenberg model to obtain a spin-spin coupling, J, between neighboring

sites.[262, 605–608]

Along this line, Mayhall and Head-Gordon devised a simple and useful scheme that utilizes a single spin-flip wavefunction, maps the wavefunction to the Heisenberg model, and computes spin-spin couplings between sites.[325, 609] As long as the Heisenberg model is valid, their scheme is also valid. However, in practice it is hard to know whether the Heisenberg model is valid for a given system. Besides this method does not yield ab-initio wavefunctions for each spin state. This is a good motivation to try other alternatives. When the Heisenberg model is valid, CCVB methodologies become very powerful because there is no need for ionic excitations. It also targets each spin state in a state-specific way with orbital optimizations and yields spin-pure wavefunctions.

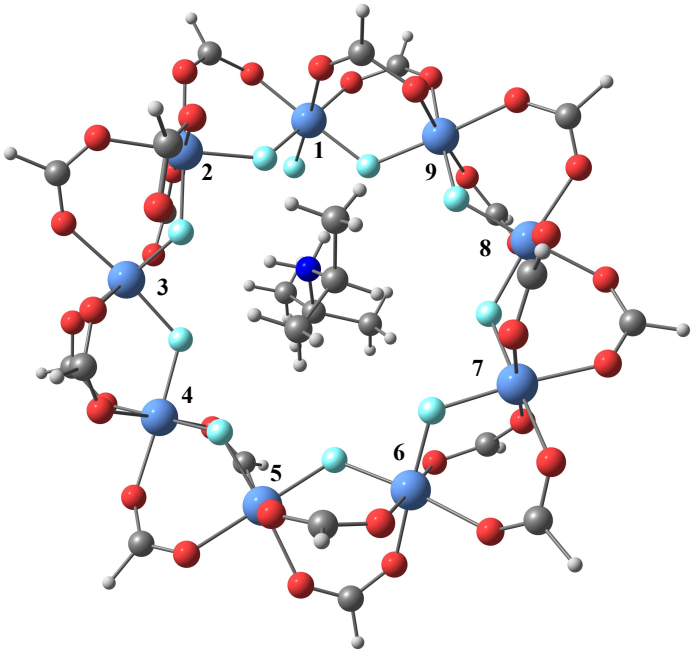

Figure 6.10: The molecular structure of the [Cr_9] SMM. The color code we used is as follows: grey: C, white: H, red: O, blue: N, light blue: F, and grey blue: Cr. The numbers next to Cr's indicate the label for each Cr. The molecule at the center is necessary to keep the system overall neutral and also found in the experimental crystal structure.

In what follows, we discuss the electron correlation in the [Cr_9] SMM. The geometry shown in Figure 6.10 is taken from the crystal structure reported in ref. 608 (denoted as structure 4 therein), and all acetates are replaced with formates for the

sake of computational simplicity. The C−H bond length in the formates was adjusted to be 1.09 Å. The neighboring Cr−Cr distances range from 3.50 Å to 3.90 Å. The diisopropyl-ammonium ion in the center keeps the system overall neutral. This [Cr_9] SMM exhibits spin-frustation at equilibrium. All the chromiums are Cr(III) and have a d^3 electron configuration. Therefore, the natural choice of an active space in this system is (27e, 27o). This is currently beyond the scope of exact CASSCF.

Hence, we benchmarked CCVB against HCI. HCI is not orbital-invariant, so choosing the right set of orbitals is quite crucial. We took converged CCVB orbitals and ran HCI with those orbitals. Ideally, optimizing orbitals with HCI should produce the best benchmark numbers. Using CCVB orbitals as an initial orbital, we attempted orbital optimization with various values of ϵ_1 in HCI. The orbital optimization exhibited an energy fluctuation of 10 μH, and we were not able to converge tightly. Therefore, we do not report those numbers and focus on the HCI results performed with CCVB orbitals (denoted as HCI//CCVB) for the following discussion. We used the def2-TZVP basis set [254] on Cr and the def2-SVP basis set [254] on all the other atoms along with the corresponding density-fitting bases.[255] In passing, we note that the value of using CCVB or PP orbitals for a subsequent HCI calculation has recently been pointed out by Zimmerman in the context of iFCI.[610]

The amplitude equation of CCVB+i3 becomes somewhat ill-defined in this case. In other words, the Jacobian in Eq. (6.58) becomes nearly singular and thus finding solutions becomes extremely challenging. As mentioned earlier in Computational Details, we loosened the convergence threshold of the t-amplitudes to $10^{-8}-10^{-10}$ and did not perform orbital optimization for CCVB+i3. Instead, we performed CCVB+i3 calculations on converged CCVB orbitals. We denote this as CCVB+i3//CCVB in the following discussion.

It is interesting that the Cr atoms in the molecule are nearly in D_{9h} symmetry. For $S = 1/2$, this particular geometry leaves 9 different choices of the location of a unpaired electron. We tried a couple of different Lewis structures (or PP references) that have a unpaired electron on different Cr's, and CCVB methodologies all yielded very similar energies. Therefore, we picked Cr(1) (see Figure 6.10 for the label) to be the radical site for simplicity. We tried two different pairing schemes in CCVB. One of them is simply alternating single and double bonds for $S = 1/2$ as shown in Figure 6.11 (a). The other one forms a triangle among Cr(1), Cr(2), and Cr(9) while having triple-bonded Cr_2 for the rest as in Figure 6.11 (b).

The UHF (or BS-DFT) approach can correctly separate on $M_S = 3/2$, 9/2, 15/2, 21/2, 27/2, while states with other than those M_S values will yield erroneously high energies. To obtain reasonable energies from UHF, we need to keep three electrons on each Cr to be the same spin. As we have seen from the previous examples, CCVB can be applied to a much broader range of problems than UHF, and CCVB+i3 can

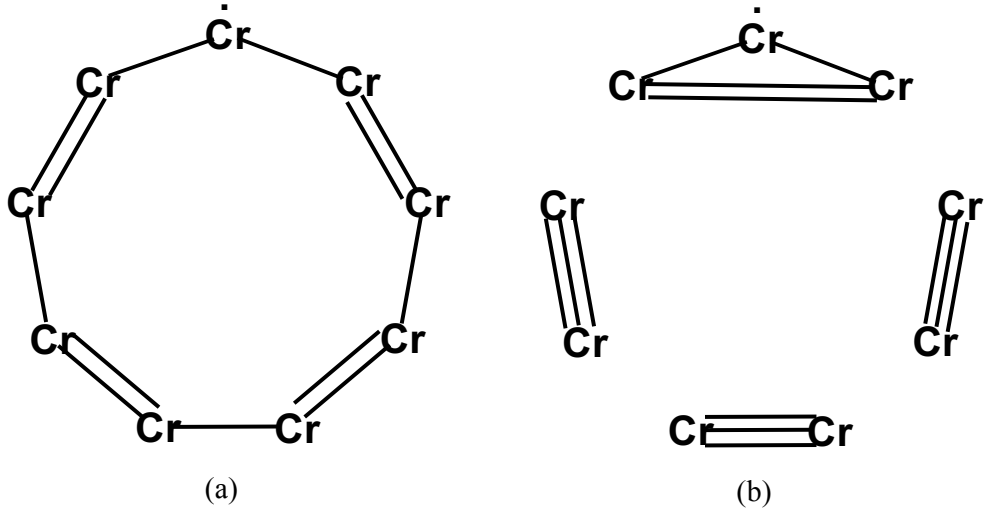

Figure 6.11: Possible Lewis structures for the $S = 1/2$ state of the $[Cr_9]$ SMM. Every Cr-Cr bond consists of d-orbitals and each Cr atom has three d-orbitals which yields an active space of (27e, 27o).

be applied to even broader of strong correlation problems with SSC.

In Table 6.9, we see that HCI provides almost converged energies with $\epsilon_1 = 10^{-4}$. The HCI energies indicate that different spin states lie within 1 kcal/mol, which is the signature of SSC. Converging absolute energies up to the usual chemical accuracy, namely 1 kcal/mol, may not be appropriate to resolve the energy scale of strongly spin-correlated systems like this SMM system. CCVB and CCVB+i3 show more or less the same results except for the $S = 1/2$ state. For the doublet state, there is a roughly 44 kcal/mol energy lowering going from 2P to 3P. This shows the significance of 3P substitutions when describing low-spin states of spin-frustrated systems. As the CCVB+i3//CCVB results are all above the converged HCI//CCVB energies, CCVB+i3//CCVB is *practically* variational.

Increasing the value of ϵ_1 to 5×10^{-4} results in catastrophic HCI failures for low-spin states, $S = 1/2 - 9/2$. These energies are considered qualitatively wrong as the relevant energy scale is less than a kcal/mol in this system. In passing we note that the quality of CCVB orbitals for $S = 1/2$ may be poor compared to other states given that there is a 0.60 kcal/mol energy jump going from $S = 3/2$ to $S = 1/2$ in HCI//CCVB. The unconverged HCISCF calculations indicate that spin-gaps are of the order of 0.01 kcal/mol for all states.

Table 6.10 presents the solutions obtained using the PP reference in Figure 6.11

S	CCVB	CCVB+i3// CCVB	HCI// CCVB ($\epsilon_1 = 5\times 10^{-4}$)	HCI// CCVB ($\epsilon_1 = 10^{-4}$)	HCI// CCVB ($\epsilon_1 = 10^{-5}$)	HCI// CCVB ($\epsilon_1 = 10^{-6}$)
1/2	45.82	1.05	63.81	0.67	0.65	0.64
3/2	0.36	0.34	517.42	0.07	0.07	0.06
5/2	0.33	0.31	530.89	0.06	0.05	0.05
7/2	0.32	0.31	63.20	0.05	0.06	0.05
9/2	0.31	0.28	505.25	0.06	0.05	0.05
11/2	0.31	0.28	0.16	0.06	0.05	0.04
13/2	0.29	0.25	0.13	0.04	0.04	0.04
15/2	0.28	0.22	0.09	0.04	0.05	0.04
17/2	0.25	0.23	0.08	0.04	0.04	0.03
19/2	0.17	0.13	0.05	0.04	0.06	0.04
21/2	0.13	0.12	0.03	0.02	0.02	0.02
23/2	0.05	0.05	0.02	0.01	0.01	0.01
25/2	0.07	0.07	0.01	0.00	0.00	0.00
27/2	0.00	0.00	0.00	0.00	0.00	0.00

Table 6.9: The relative energies (kcal/mol) of different spin states of Cr_9. The PP reference used for CCVB calculations corresponds to Figure 6.11 (a). CCVB+i3//CCVB denotes the CCVB+i3 energies evaluated with converged CCVB orbitals. HCI//CCVB denotes the HCI energies evaluated with converged CCVB orbitals. For $S = 27/2$, every method is exact since ROHF is exact for that state. The corresponding $S = 27/2$ energy is -14101.38880 E_h. These spin-gaps are directly comparable across different methods as they are measured with respect to this same energy.

(b). As CCVB energies are not invariant to the choice of a PP reference, we obtain different results. CCVB has a strong dependence on the PP reference because with this new reference the $S = 1/2$ energy is 18 kcal/mol lower and the $S = 3/2$ energy is 20 kcal/mol higher compared to the previous case. The qualitative failure of CCVB for $S = 1/2$ and $S = 3/2$ can be understood similarly to the D_{3h} cases discussed above as we have a localized triangle in the PP reference. HCI//CCVB exhibits a catastrophic behavior for large ϵ_1 values, but is adquately converged with $\epsilon_1 = 10^{-5}$. In the case of $\epsilon_1 = 5\times 10^{-4}$, HCI//CCVB fails for all spin states lower than $S = 15/2$ but $S = 3/2$.

Based on the results discussed in Table 6.9 and Table 6.10, we conclude that CCVB+i3 is less sensitive to the underlying PP reference and its accuracy lies some-

S	CCVB	CCVB+i3// CCVB	HCI// CCVB ($\epsilon_1 = 5\times 10^{-4}$)	HCI// CCVB ($\epsilon_1 = 10^{-4}$)	HCI// CCVB ($\epsilon_1 = 10^{-5}$)	HCI// CCVB ($\epsilon_1 = 10^{-6}$)
1/2	27.62	0.57	316.40	0.28	0.26	0.23
3/2	20.95	0.46	0.22	0.20	0.19	0.17
5/2	0.39	0.37	646.84	0.06	0.06	0.05
7/2	0.26	0.25	538.96	63.37	0.04	0.03
9/2	0.43	0.41	189.54	63.06	0.05	0.05
11/2	0.22	0.20	584.93	0.06	0.04	0.03
13/2	0.21	0.16	189.34	0.09	0.04	0.02
15/2	0.26	0.25	63.44	63.05	0.04	0.04
17/2	0.18	0.14	0.14	0.04	0.04	0.02
19/2	0.16	0.16	0.10	0.03	0.03	0.02
21/2	0.07	0.07	0.05	0.02	0.02	0.01
23/2	0.11	0.10	0.03	0.02	0.01	0.01
25/2	0.06	0.06	0.01	0.00	0.00	0.00
27/2	0.00	0.00	0.00	0.00	0.00	0.00

Table 6.10: Same as Table 6.9 except that the PP reference used here corresponds to Figure 6.11 (b).

where in between HCI of $\epsilon_1 = 10^{-4}$ and $\epsilon_1 = 5 \times 10^{-5}$. We further compare those two methodologies in terms of the number of independent wavefunction parameters and we emphasize the compactness of the CCVB+i3 wavefunction as shown in Table 6.11. Due to the larger system, the difference in the number of parameters is larger in $[Cr_9]$ than in P_5 (shown in Table 6.8). CCVB+i3 has a 300-500 times smaller number of parameters than HCI ($\epsilon_1 = 10^{-4}$) for $S = 1/2$ in $[Cr_9]$ whereas in P_5 it was only 150 times smaller compared to HCISCF ($\epsilon_1 = 10^{-4}$). One may think that orbital optimization must help reduce the number of determinants in HCI in the case of $[Cr_9]$. However, as the effect of orbital optimization is very small in this system we believe that the conclusion here will not be altered.

The situation will become only more favorable to CCVB when studying larger molecules or bulk materials as there will be too many determinants to include for HCISCF even to just achieve a similar accuracy as CCVB. The strength of CCVB is at the use of a CC-type expansion to avoid including an exponential number of wavefunction parameters while being able to describe strong spin correlation and yielding a size-consistent, spin-pure energy and wavefunction.

Lastly, we note that the singular Jacobian problem we faced in this system is not

S	CCVB+i3	HCI// CCVB(a) ($\epsilon_1 = 5 \times 10^{-4}$)	HCI// CCVB(a) ($\epsilon_1 = 10^{-4}$)	HCI// CCVB(b) ($\epsilon_1 = 5 \times 10^{-4}$)	HCI// CCVB(b) ($\epsilon_1 = 10^{-4}$)
1/2	104	8361	53061	17446	32707
3/2	114	9557	31082	12661	42455
5/2	121	5793	14178	12291	36431
7/2	125	6678	23750	9217	49014
9/2	126	4828	15764	7936	35872
11/2	124	2797	10107	4266	28343
13/2	119	1768	6029	6851	30096
15/2	111	1287	4743	2149	13229
17/2	100	912	3039	2320	8682
19/2	86	484	1218	1418	5804
21/2	69	310	781	860	1715
23/2	49	98	212	186	371
25/2	26	52	87	56	76
27/2	0	0	0	0	0

Table 6.11: The number of independent wavefunction parameters used in each method in the $[Cr_9]$ SMM. CCVB(a) and CCVB(b) denote the CCVB orbitals with the PP references in Figure 6.11 (a) and (b), respectively.

necessarily an indication of redundant wavefunction parameters. When evaluated with a solution to CC amplitude equations, a CC Jacobian is often interpreted as an equation-of-motion (EOM) CC Hamiltonian. Eigenvalues of the CC Jacobian are excitation gaps. We checked the first 5 roots of each spin state from HCI//CCVB and observed that the first 5 roots are all within 10 μH. This is consistent with the singular values of Jacobian we observed in CCVB+i3. Strongly spin-correlated systems have a dense spectrum of low-lying excited states which would necessarily imply (nearly) singular CC Jacobians. It is thus important to develop a better amplitude solver to tackle strongly correlated systems with non-linear CC wavefunctions. In passing we note that this may indicate that the EOM treatment to CCVB can yield quite accurate excitation gaps for strongly correlated systems. This will be further investigated along with EOM-CCVB-SD in future work.

6.5 Conclusions and Outlook

In this paper, we tested the CCVB ansatz on spin-frustrated systems with SSC. Those systems include N_3, V_3O_3, the cubane subunit of oxygen-evolving complex, P_5, and the $[Cr_9]$ single molecular magnet. We showed that the model catastrophically fails to describe the lowest-spin states of such systems. As an attempt to fix this problem, we introduced an improved electron correlation model, CCVB+i3, which includes 3-pair correlations that are missing in CCVB. Our working hypothesis is that the new model can in principle reach any bond dissociation limits exactly within an active space, and we numerically showed that it provides a qualitatively correct description of those spin-frustrated systems when CCVB fails. It was also emphasized that the new model involves the same number of independent wavefunction parameters as CCVB and scales the same.

We compared CCVB+i3 against an exponential-scaling heat-bath CI (HCI) method for P_5 and $[Cr_9]$. For those systems, HCI was able to converge the energy below 0.1 kcal/mol with a reasonable amount of computational work. CCVB+i3 energies are 1-2 kcal/mol and 0.5 kcal/mol above those of HCI in the case of P_5 and $[Cr_9]$, respectively. We emphasized the promise of CCVB+i3 by comparing the number of independent wavefunction parameters against HCI. To achieve a similar accuracy, HCI involves roughly a 300-500 times larger number of parameters than CCVB+i3 in $[Cr_9]$. Towards the application to large molecules and bulk strongly correlated systems, this scaling will become only more favorable to CCVB.

There are many promising future developments of CCVB and CCVB+i3. The most interesting extension is perhaps to incorporate missing dynamic correlations not only within the active space but also outside the active space. This could be achieved either using density functional theory, [30, 611, 612] perturbation theory,[112, 113, 216, 269, 613–619] or extended random phase approximations.[620, 621] Another interesting extension is to implement nuclear gradients and other properties of CCVB. In particular, nuclear gradients will be particularly useful as CCVB equilibrium geometries are quite close to CASSCF at least in small molecular systems that have been studied. Those two developments will help to put CCVB among the set of routinely applicable electron correlation models.

Other theoretical questions of CCVB include whether it is necessary to go beyond the IAA treatment of the 3P substitutions. The scope of CCVB+i3 remains unclear although the numerical results so far indicate that it is capable of dissociating any number of bonds. We are investigating its relation to the spin-projected generalized Hartree-Fock (SGHF) wavefunction to learn more about its scope. The full CCVB-3 model is not size-consistent as shown in this work. The next level of a size-consistent CCVB method would then be the one that includes everything up to the 4-pair

contributions in the 3-pair amplitude equation. This will be an interesting model to explore although the overall cost will no longer be the same as CCVB.

Another question is then whether we can take either CCVB+i3 or more sophisticated wavefunctions and generalize them to a full CC model with singles, doubles and triples. Given the promising initial success of CCVB-SD which generalizes CCVB, it will be interesting to generalize a variant of the 3-pair model to a full CC model as well. The main strength of CCVB+i3, as well as CCVB, is for systems where the strong correlations are primarily strong spin correlations. Systems where strong charge fluctuations are also important (e.g. mixed valence metal ions) require ionic excitations that are excluded in CCVB and CCVB+i3. They are restored in full CC model such as CCVB-SD. As mentioned in the main text, we are also investigating excited states of CCVB and CCVB-SD within the equation of motion framework.

6.6 Appendix

6.6.1 Definitions

We begin by defining some fundamental quantities that will be used to compute matrix elements and other relevant quantities discussed in the main text. Many of definitions below are already given in ref. 280, but it is our intention to keep this paper as self-contained as possible. Interested readers shall refer to 280 although it is not necessary unless otherwise noted.

We define a set of spin orbitals S_a for a pair a,

$$S_a = \{a_\alpha, a_\beta, \hat{a}_\alpha, \hat{a}_\beta\} \tag{6.59}$$

We define the density matrix of a closed-shell pair K,

$$P_{K;wx;pr} = \langle 0 | \, g_{w,K} a_p^\dagger a_r g_{x,K}^\dagger \, | 0 \rangle \tag{6.60}$$

where w and x denote the spin states of the pair either s, t_1, t_2, or t_3 and p and r denotes the spin-orbital indices in the set S_K. For a singly occupied orbital (or an open-shell pair) μ, only $P_{\mu;ss;\mu_\alpha\mu_\alpha} = 1$ and all the other elements are zero as they include the fictitious orbital. These are used to define the following quantities: the one-body contribution reads

$$\eta_{a;wx} = \sum_{pr \in S_a} h_{pr} P_{K;wx;pr}, \tag{6.61}$$

and the intrageminal Coulomb contribution follows

$$\rho_{a;w;x} = \sum_{prqs \in S_a} \langle pq || rs \rangle \, f_{a;w;pq} f_{a;x;rs}, \tag{6.62}$$

and the intergeminal Coulomb contribution reads

$$\sigma_{ab;wx;yz} = \sum_{pr\in S_a}\sum_{qs\in S_b} \langle pq||rs\rangle\, P_{a;wx;pr}P_{b;yz;qs}, \tag{6.63}$$

where

$$f_{K;s;K_\alpha K_\beta} = \frac{2\cos(\theta_K)}{\sqrt{2(1+\cos^2(\theta_K))}}, \tag{6.64}$$

$$f_{K;s;K_\alpha \hat{K}_\beta} = f_{K;s;\hat{K}_\alpha K_\beta} = \frac{-\sin(\theta_K)}{\sqrt{2(1+\cos^2(\theta_K))}} \tag{6.65}$$

$$f_{K;t_1;K_\alpha \hat{K}_\beta} = -f_{K;t_1;\hat{K}_\alpha K_\beta} = -f_{K;t_2;K_\alpha \hat{K}_\alpha} = -f_{K;t_2;K_\beta \hat{K}_\beta} = -\frac{1}{\sqrt{2}} \tag{6.66}$$

and all the other f's are zero. Obviously, we have $\rho_{\mu;w;x} = 0$.

6.6.2 Proof of Eq. (6.40)

In the main text, we proved that if b is not on the same fragment as K then the size-consistency claim is satisfied as $t_{Kb} = 0$. The rest of the proof is then showing that the following matrix element is zero when b is on the same fragment as K:

$$\begin{aligned}\langle\Psi_{(KLa)}|\hat{\mathcal{H}}|\Phi_{(Kb)(La)}\rangle = &-\frac{3}{10}\langle\Psi_{(KLa)}|\hat{\mathcal{H}}|\Psi_{(KL)(ab)}\rangle - \frac{3}{10}\langle\Psi_{(KLa)}|\hat{\mathcal{H}}|\Psi_{(Ka)(Lb)}\rangle \\ &+ \frac{6}{5}\langle\Psi_{(KLa)}|\hat{\mathcal{H}}|\Psi_{(Kb)(La)}\rangle\end{aligned} \tag{6.67}$$

where we wrote $|\Phi_{(Kb)(La)}\rangle$ in terms of $|\Psi_{(KL)(ab)}\rangle$, $|\Psi_{(Ka)(Lb)}\rangle$, and $|\Psi_{(Kb)(La)}\rangle$ using the relevant $\mathbf{S}^+$ in this 8-electron singlet subspace (see ref. 140 for details). After some algebra, one can show that

$$\langle\Psi_{(KLa)}|\hat{\mathcal{H}}|\Phi_{(Kb)(La)}\rangle = \frac{3\sqrt{6}}{10}\left(\sigma_{Kb;t_1t_3;st_2} + \sigma_{Kb;t_1t_2;st_3}\right) + \frac{2}{5}\langle\Psi_{[K]_1[L]_2[a]_3}|\hat{\mathcal{H}}|\Psi_{[K]_1[b]_1[L]_2[a]_3}\rangle = 0 \tag{6.68}$$

The first term is zero because $\sigma_{Kb;t_1t_3;st_2} = -\sigma_{Kb;t_1t_2;st_3}$ and it can be shown that the second term is also zero after little more algebra. Therefore, we proved Eq. (6.40).

6.6.3 S and $\mathbf{S}^+$ within the five-pair substitutions

The overlap matrix among vectors in the dual frame within the five-pair (5P) substitutions is

$$\mathbf{S}_{5\mathrm{P}} = \begin{bmatrix} 1 & \frac{1}{3} & -\frac{1}{3} & \frac{1}{3} & \frac{1}{3} & -\frac{1}{3} & \frac{1}{3} & 0 & 0 & 0 \\ \frac{1}{3} & 1 & 0 & 0 & -\frac{1}{3} & \frac{1}{3} & 1 & 0 & \frac{1}{3} & -\frac{1}{3} \\ -\frac{1}{3} & 0 & 1 & \frac{1}{3} & 0 & \frac{1}{3} & 0 & -\frac{1}{3} & 0 & \frac{1}{3} \\ \frac{1}{3} & 0 & \frac{1}{3} & 1 & \frac{1}{3} & 0 & 0 & -\frac{1}{3} & \frac{1}{3} & 0 \\ \frac{1}{3} & -\frac{1}{3} & 0 & \frac{1}{3} & 1 & \frac{1}{3} & -\frac{1}{3} & \frac{1}{3} & -\frac{1}{3} & 0 \\ -\frac{1}{3} & \frac{1}{3} & \frac{1}{3} & 0 & \frac{1}{3} & 1 & \frac{1}{3} & \frac{1}{3} & 0 & -\frac{1}{3} \\ \frac{1}{3} & 1 & 0 & 0 & -\frac{1}{3} & \frac{1}{3} & 1 & 0 & \frac{1}{3} & -\frac{1}{3} \\ 0 & 0 & -\frac{1}{3} & -\frac{1}{3} & \frac{1}{3} & \frac{1}{3} & 0 & 1 & \frac{1}{3} & \frac{1}{3} \\ 0 & \frac{1}{3} & 0 & \frac{1}{3} & -\frac{1}{3} & 0 & \frac{1}{3} & \frac{1}{3} & 1 & \frac{1}{3} \\ 0 & -\frac{1}{3} & \frac{1}{3} & 0 & 0 & -\frac{1}{3} & -\frac{1}{3} & \frac{1}{3} & \frac{1}{3} & 1 \end{bmatrix} \tag{6.69}$$

where we ordered columns and rows as $|\Psi_{(bc)(KLa)}\rangle$, $|\Psi_{(ab)(KLc)}\rangle$,$|\Psi_{(Lb)(Kac)}\rangle$, $|\Psi_{(Kb)(Lac)}\rangle$, $|\Psi_{(Kc)(Lab)}\rangle$, $|\Psi_{(Lc)(Kab)}\rangle$, $|\Psi_{(ac)(KLb)}\rangle$, $|\Psi_{(KL)(abc)}\rangle$, $|\Psi_{(Ka)(Lbc)}\rangle$, and $|\Psi_{(La)(Kbc)}\rangle$. As we expect only six orthogonal singlet configurations in this 12-electron singlet space, these 10 vectors are necessarily linearly-dependent. Indeed, there are 4 zero singular values along with 6 non-zero singular values, $\frac{1}{3}(5 \pm 2\sqrt{2})$ and four $\frac{5}{3}$'s. The corresponding pseudoinverse is then

$$\mathbf{S}_{5\mathrm{P}}^{+} = \begin{bmatrix} \frac{681}{1445} & \frac{39}{289} & \frac{57}{1445} & \frac{-57}{1445} & \frac{243}{1445} & \frac{-243}{1445} & \frac{39}{289} & 0 & \frac{-60}{289} & \frac{60}{289} \\ \frac{39}{289} & \frac{57}{289} & \frac{30}{289} & \frac{-30}{289} & \frac{-9}{289} & \frac{9}{289} & \frac{57}{289} & 0 & \frac{-21}{289} & \frac{21}{289} \\ \frac{57}{1445} & \frac{30}{289} & \frac{3954}{7225} & \frac{-486}{7225} & \frac{201}{7225} & \frac{666}{7225} & \frac{30}{289} & \frac{-3}{25} & \frac{-1554}{7225} & \frac{2421}{7225} \\ \frac{-57}{1445} & \frac{-30}{289} & \frac{-486}{7225} & \frac{3954}{7225} & \frac{666}{7225} & \frac{201}{7225} & \frac{-30}{289} & \frac{-3}{25} & \frac{2421}{7225} & \frac{-1554}{7225} \\ \frac{243}{1445} & \frac{-9}{289} & \frac{201}{7225} & \frac{666}{7225} & \frac{2454}{7225} & \frac{1014}{7225} & \frac{-9}{289} & \frac{3}{25} & \frac{-921}{7225} & \frac{54}{7225} \\ \frac{-243}{1445} & \frac{9}{289} & \frac{666}{7225} & \frac{201}{7225} & \frac{1014}{7225} & \frac{2454}{7225} & \frac{9}{289} & \frac{3}{25} & \frac{54}{7225} & \frac{-921}{7225} \\ \frac{39}{289} & \frac{57}{289} & \frac{30}{289} & \frac{-30}{289} & \frac{-9}{289} & \frac{9}{289} & \frac{57}{289} & 0 & \frac{-21}{289} & \frac{21}{289} \\ 0 & 0 & \frac{-3}{25} & \frac{-3}{25} & \frac{3}{25} & \frac{3}{25} & 0 & \frac{9}{25} & \frac{3}{25} & \frac{3}{25} \\ \frac{-60}{289} & \frac{-21}{289} & \frac{-1554}{7225} & \frac{2421}{7225} & \frac{-921}{7225} & \frac{54}{7225} & \frac{-21}{289} & \frac{3}{25} & \frac{4209}{7225} & \frac{-741}{7225} \\ \frac{60}{289} & \frac{21}{289} & \frac{2421}{7225} & \frac{-1554}{7225} & \frac{54}{7225} & \frac{-921}{7225} & \frac{21}{289} & \frac{3}{25} & \frac{-741}{7225} & \frac{4209}{7225} \end{bmatrix} \tag{6.70}$$

6.6.4 Eq. (6.44) In Terms of Computable Quantities

We express the matrix elements pertinent to evaluating Eq. (6.44) in terms of readily computable quantities. We write the following matrix elements,

$$\mu_{ab} = \langle \Psi_0 | \, \hat{\mathcal{H}} \, | \Phi_{(ab)} \rangle = -\sqrt{3}\sigma_{ab;st_2;st_3}, \tag{6.71}$$

and

$$\kappa_{Ka;b} = \sqrt{6} \left\langle \Psi_{[K]_1[a]_2[b]_3} \right| \hat{\mathcal{H}} \left| \Phi_{(Ka)} \right\rangle = \sqrt{2} \left(\sigma_{ab;t_2t_1;t_3s} - \sigma_{Kb;t_1t_3;t_3s} \right) \tag{6.72}$$

where we used the fact that Hamiltonian commutes with a singlet-projection operator and both bra and ket states are singlets and

$$\left\langle \Psi_{[K]_1[a]_2[b]_3} \right| \hat{\mathcal{H}} \left| \Phi_{(Ka)} \right\rangle = \langle 0| \hat{g}_{t_1,K} \hat{g}_{t_2,a} \hat{g}_{t_3,b} \hat{\mathcal{H}} \hat{d}^\dagger_{s2,Ka} \hat{g}^\dagger_{s,b} |0\rangle = \frac{1}{\sqrt{3}} \left(\sigma_{ab;t_2t_1;t_3s} - \sigma_{Kb;t_1t_3;t_3s} \right). \tag{6.73}$$

Similarly,

$$\left\langle \Psi_{(KLa)} \right| \hat{\mathcal{H}} \left| \Psi_{(KLa)} \right\rangle = \sqrt{6} \left\langle \Psi_{(KLa)} \right| \hat{\mathcal{H}} \left| \Psi_{[K]_1[L]_2[a]_3} \right\rangle \tag{6.74}$$

$$= -\sigma_{KL;t_2t_1;t_1t_2} - \sigma_{Ka;t_3t_1;t_1t_3} + \left\langle \Psi_{[K]_1[L]_2[a]_3} \right| \hat{\mathcal{H}} \left| \Psi_{[K]_1[L]_2[a]_3} \right\rangle \tag{6.75}$$

Using this, we write ω_{KLa} in terms of computable quantities:

$$\begin{aligned}
\omega_{KLa} &= \left\langle \Psi_{(KLa)} \right| \hat{\mathcal{H}} \left| \Psi_{(KLa)} \right\rangle - \langle \Psi_0| \hat{\mathcal{H}} |\Psi_0\rangle \\
&= -\sigma_{KL;t_2t_1;t_1t_2} - \sigma_{Ka;t_3t_1;t_1t_3} \\
&+ \eta_{K;t_1t_1} + \eta_{L;t_2t_2} + \eta_{a;t_3t_3} - \eta_{K;ss} - \eta_{L;ss} - \eta_{a;ss} \\
&+ \rho_{K;t_1;t_1} + \rho_{L;t_2;t_2} + \rho_{a;t_3;t_3} - \rho_{K;s;s} - \rho_{L;s;s} - \rho_{a;s;s} \\
&+ \sigma_{KL;t_1t_1;t_2t_2} + \sigma_{Ka;t_1t_1;t_3t_3} + \sigma_{La;t_2t_2;t_3t_3} - \sigma_{KL;ss;ss} - \sigma_{Ka;ss;ss} - \sigma_{La;ss;ss} \\
&+ \sum_{b \notin \{K,L,a\}} \left(\sigma_{Kb;t_1t_1;ss} + \sigma_{Lb;t_2t_2;ss} + \sigma_{ab;t_3t_3;ss} - \sigma_{Kb;ss;ss} - \sigma_{Lb;ss;ss} - \sigma_{ab;ss;ss} \right)
\end{aligned} \tag{6.76}$$

6.6.5 CCVB+i3 Jacobian

We derive the CCVB+i3 Jacobian which is used in amplitude solvers. The Jacobian reads

$$(J)_{Ka,Mc} = \frac{\partial \Omega_{Ka}}{\partial t_{Mc}} = \frac{\partial R_{Ka}}{\partial t_{Mc}} + \sum_{b \notin \{K,a\}} \frac{\partial t_{Kab}}{\partial t_{Mc}} \kappa_{Ka;b} \tag{6.77}$$

where

$$\begin{aligned}
\frac{\partial R_{Ka}}{\partial t_{Mc}} &= \left[\omega_{Ka} - 2 t_{Ka} \mu_{Ka} - \sum_{b \notin \{K,a\}} \left(t_{Kb} \mu_{Kb} + t_{ab} \mu_{ab} \right) \right] \delta_{Ka,Mc} \\
&+ \sum_{b \notin \{K,a\}} \left[(\kappa_{Kb} - t_{Ka} \mu_{ab}) \delta_{ab,Mc} + (\kappa_{ab} - t_{Ka} \mu_{Kb}) \delta_{Kb,Mc} \right]
\end{aligned} \tag{6.78}$$

and using Eq. (6.44) we obtain

$$\frac{\partial t_{Kab}}{\partial t_{Mc}} = \delta_{Ka,Mc}\left[\frac{\kappa_{Ka;b}}{\Delta_{Kab}} - \frac{\mu_{Ka}}{\Delta_{Kab}}t_{Kab}\right] + \delta_{Kb,Mc}\left[-\frac{\kappa_{Kb;a}}{\Delta_{Kab}} - \frac{\mu_{Ka}}{\Delta_{Kab}}t_{Kab}\right] + \delta_{Lb,Mc}\left[\frac{\kappa_{ab;K}}{\Delta_{Kab}} - \frac{\mu_{ab}}{\Delta_{Kab}}t_{Kab}\right] \tag{6.79}$$

where

$$\Delta_{Kab} = (t_{Ka}\mu_{Ka} + t_{Kb}\mu_{Kb} + t_{ab}\mu_{ab}) - \omega_{Kab} \tag{6.80}$$

6.6.6 CCVB+i3 Lagrangian and Its Derivatives

We derive derivatives of the CCVB+i3 Lagrangian defined in Eq. (6.48) and write them in terms of computable quantities. From

$$\frac{\partial \mathcal{L}}{\partial t_{Ka}} = 0, \tag{6.81}$$

we obtain

$$0 = \frac{\partial E}{\partial t_{Ka}} + \sum_{M<b} \lambda_{Mb}\frac{\partial R_{Mb}}{\partial t_{Ka}} + \sum_{b\notin\{K,a\}} \lambda_{Kab}\left(\kappa_{Ka;b} - t_{Kab}\mu_{Ka}\right). \tag{6.82}$$

We already have $\frac{\partial R_{Mb}}{\partial t_{Ka}}$ from Eq. (6.78) and we have

$$\frac{\partial E}{\partial t_{Ka}} = \mu_{Ka} \tag{6.83}$$

For the gradient of $\mathcal{L}$ with respect to some parameters $\mathbf{X}$ (either Θ or Δ), most terms are already discussed in ref. 280 and we discuss the 3P specific terms. First, consider

$$\frac{\partial}{\partial \mathbf{X}}\sum_{K<a}\sum_{b\notin\{K,a\}} t_{Kab}\kappa_{Ka;b} = \sqrt{2}\sum_{K<a}\sum_{b\notin\{K,a\}} t_{Kab}\frac{\partial}{\partial \mathbf{X}}\left(\sigma_{ab;t_2t_1;t_3s} - \sigma_{Kb;t_1t_3;t_3s}\right) \tag{6.84}$$

$$= \sqrt{2}\sum_{K<a}\sum_{b\notin\{K,a\}} t_{Kab}\left(\sigma^{\mathbf{X}}_{ab;t_2t_1;t_3s} - \sigma^{\mathbf{X}}_{Kb;t_1t_3;t_3s}\right) \tag{6.85}$$

Here, we learned that

$$\kappa^{\mathbf{X}}_{Ka;b} = \sqrt{2}\left(\sigma^{\mathbf{X}}_{ab;t_2t_1;t_3s} - \sigma^{\mathbf{X}}_{Kb;t_1t_3;t_3s}\right) \tag{6.86}$$

The derivatives of σ's with respect to Θ and Δ are available in ref. 280. The same applies to the diagonal elements of Hessian. Similarly, the last term in Eq. (6.48) follows

$$\sum_{K<L<a} \lambda_{KLa} \frac{\partial^{(3)} \Omega_{KLa}}{\partial \mathbf{X}} = \sum_{K<L<a} \lambda_{KLa} (t_{KL} \kappa^{\mathbf{X}}_{KL;a} - t_{Ka} \kappa^{\mathbf{X}}_{Ka;L} + t_{La} \kappa^{\mathbf{X}}_{La;K} - t_{KLa}(-\omega^{\mathbf{X}}_{KLa} + t_{KL} \mu^{\mathbf{X}}_{KL} + t_{Ka} \mu^{\mathbf{X}}_{Ka} + t_{La} \mu^{\mathbf{X}}_{La})) \tag{6.87}$$

Based on Eq. (6.76), we can compute $\omega^{\mathbf{X}}_{KLa}$ in terms of other more fundamental quantities discussed in ref. 280. For κ derivatives, we apply Eq. 6.86. μ derivatives are available in ref. 280. The same applies to the diagonal elements of Hessian. From

$$\frac{\partial \mathcal{L}}{\partial t_{KLM}} = 0, \tag{6.88}$$

we obtain

$$\lambda_{KLM} = \frac{\lambda_{KL} \kappa_{KL;M} - \lambda_{KM} \kappa_{KM;L} + \lambda_{LM} \kappa_{LM;K}}{t_{KL} \mu_{KL} + t_{KM} \mu_{KM} + t_{LM} \mu_{LM} - \omega_{KLM}} \tag{6.89}$$

$$\tag{6.90}$$

Chapter 7

Conclusions

"You have to know how to
accept rejection and
reject acceptance."
– Ray Bradbury

The work presented in this dissertation addresses two challenges in the electron correlation problem. Various challenges in different aspects of modern quantum chemistry methods are addressed during the author's Ph.D. study and two representative examples are presented in this dissertation.

First, we addressed the challenge of distinguishing weak and strong correlation between electrons. Distinguishing these two is necessary for choosing an appropriate electron correlation model for systems of our interest. Namely, one could use a perturbation theory for weakly correlated systems, whereas one must use much more computationally demanding (if not impossible) approaches for strongly correlated systems. Traditionally, symmetry breaking (SB) of a single determinant (SD) at the Hartree-Fock (HF) level has been used as a probe to distinguish these two. One concludes that a system is strongly correlated if the underlying HF SD is symmetry-broken. This general wisdom has been challenged by numerous examples that exhibit "artificial" SB. It is artificial because the SB in these cases is driven by the lack of weak correlation in HF, not by the lack of strong correlation. There is a need for a method that obtains an SD with only "essential" SB. It is essential in the sense that the underlying wavefunction is ill-behaved without SB due to strong correlation such as failing to dissociate bonds correctly.

To address this challenge, we developed a well-behaved perturbation theory (PT) called regularized orbital-optimized second-order Møller-Plesset theory (κ-OOMP2) whose energy no longer diverges even for strongly correlated systems, unlike other

PT approaches. κ-OOMP2 includes weak correlation while attenuating strong correlation. As such, it yields an SD with only "essential" SB. κ-OOMP2 has been shown to be quantitatively accurate for a broad range of benchmark data sets and applied to some "artificial" SB examples. For instance, Scuseria and co-workers [272] concluded that C_{60} (buckminsterfullerene) is polyradicaloid (or strongly correlated) based on the SB found in an HF solution. As C_{60} is a stable closed-shell molecule in experiments, this claim was met with doubts and led to a controversy. As the κ-OOMP2 orbitals exhibit no SB in C_{60}, we concluded that C_{60} is not strongly correlated and exhibits only "artificial" SB. This part of the dissertation provides a new way to distinguish strong and weak correlation and redefines the common wisdom in modern quantum chemistry.

The second challenge we addressed is due to the curse of dimensionality when treating strong spin correlation (SSC). When there are many spatially separated open-shell electrons, a spin-flip of an electron does not cost much energy. This is the defining property of SSC. For a given spin quantum number, in general the dimension of the corresponding spin space scales exponentially with the number of electrons. A general belief in modern valence bond (VB) theory is that one needs to include all possible ways to spin-couple open-shell electrons to describe SSC exactly, which leads to an exponential cost for describing such systems.

We developed an approach called coupled-cluster VB (CCVB) and showed that it is possible to incorporate all essential spin-couplings while maintaining a polynomial-scaling cost, unlike the general belief in modern VB theory. We extended CCVB to open-shell formalisms as well as a more black-box approach CCVB with singles and doubles (CCVB-SD). This method has been applied to metalloenzymes and single molecular magnets. The remaining challenge in strong correlation is then how we incorporate "charge" strong correlation excluded from CCVB. As such, this part of the dissertation sets new challenges for the future methodology development.

References

(1) Szabo, A.; Ostlund, N. S., *Modern quantum chemistry: introduction to advanced electronic structure theory*; Courier Corporation: 2012.

(2) Born, M.; Oppenheimer, R. Zur quantentheorie der molekeln. *Ann. Phys.* **1927**, *389*, 457–484.

(3) Foulkes, W.; Mitas, L.; Needs, R.; Rajagopal, G. Quantum Monte Carlo simulations of solids. *Rev. Mod. Phys.* **2001**, *73*, 33.

(4) Ruedenberg, K.; Raffenetti, R.; Bardo, R. Energy, structure and reactivity, Proceedings of the 1972 Boulder conference on theoretical chemistry., 1973.

(5) Pople, J. A. Nobel lecture: Quantum chemical models. *Rev. Mod. Phys.* **1999**, *71*, 1267.

(6) Pople, J. A.; Binkley, J. S.; Seeger, R. Theoretical models incorporating electron correlation. *Int. J. Quantum Chem.* **1976**, *10*, 1–19.

(7) Pople, J.; Krishnan, R.; Schlegel, H.; Binkley, J. Electron correlation theories and their application to the study of simple reaction potential surfaces. *Int. J. Quantum Chem.* **1978**, *14*, 545–560.

(8) Krishnan, R.; Frisch, M.; Pople, J. Contribution of triple substitutions to the electron correlation energy in fourth order perturbation theory. *J. Chem. Phys.* **1980**, *72*, 4244–4245.

(9) Pople, J. A.; Frisch, M. J.; Luke, B. T.; Binkley, J. S. A moller–plesset study of the energies of AHn molecules (A= Li to F). *Int. J. Quantum Chem.* **1983**, *24*, 307–320.

(10) Nobes, R. H.; Pople, J. A.; Radom, L.; Handy, N. C.; Knowles, P. J. Slow convergence of the møller-plesset perturbation series: the dissociation energy of hydrogen cyanide and the electron affinity of the cyano radical. *Chem. Phys. Lett.* **1987**, *138*, 481–485.

(11) Knowles, P. J.; Andrews, J. S.; Amos, R. D.; Handy, N. C.; Pople, J. A. Restricted Møller-Plesset theory for open-shell molecules. *Chem. Phys. Lett.* **1991**, *186*, 130–136.

(12) Pople, J. A.; Head-Gordon, M.; Raghavachari, K. Quadratic configuration interaction. A general technique for determining electron correlation energies. *J. Chem. Phys.* **1987**, *87*, 5968–5975.

(13) Bartlett, R. J. Many-body perturbation theory and coupled cluster theory for electron correlation in molecules. *Annu. Rev. Phys. Chem.* **1981**, *32*, 359–401.

(14) Raghavachari, K.; Trucks, G. W.; Pople, J. A.; Head-Gordon, M. A fifth-order perturbation comparison of electron correlation theories. *Chem. Phys. Lett.* **1989**, *157*, 479–483.

(15) Curtiss, L. A.; Raghavachari, K.; Redfern, P. C.; Baboul, A. G.; Pople, J. A. Gaussian-3 theory using coupled cluster energies. *Chem. Phys. Lett.* **1999**, *314*, 101–107.

(16) Pople, J. A.; Gill, P. M.; Johnson, B. G. KohnSham density-functional theory within a finite basis set. *Chem. Phys. Lett.* **1992**, *199*, 557–560.

(17) Gill, P. M.; Johnson, B. G.; Pople, J. A.; Frisch, M. J. The performance of the BeckeLeeYangParr (BLYP) density functional theory with various basis sets. *Chem. Phys. Lett.* **1992**, *197*, 499–505.

(18) Johnson, B. G.; Gill, P. M.; Pople, J. A. The performance of a family of density functional methods. *J. Chem. Phys.* **1993**, *98*, 5612–5626.

(19) Curtiss, L. A.; Raghavachari, K.; Redfern, P. C.; Pople, J. A. Assessment of Gaussian-2 and density functional theories for the computation of enthalpies of formation. *J. Chem. Phys.* **1997**, *106*, 1063–1079.

(20) Curtiss, L. A.; Redfern, P. C.; Raghavachari, K.; Pople, J. A. Assessment of Gaussian-2 and density functional theories for the computation of ionization potentials and electron affinities. *J. Chem. Phys.* **1998**, *109*, 42–55.

(21) Curtiss, L. A.; Raghavachari, K.; Redfern, P. C.; Pople, J. A. Assessment of Gaussian-3 and density functional theories for a larger experimental test set. *J. Chem. Phys.* **2000**, *112*, 7374–7383.

(22) Cohen, A. J.; Mori-Snchez, P.; Yang, W. Challenges for Density Functional Theory. *Chem. Rev.* **2012**, *112*, 289–320.

(23) Perdew, J. P.; Zunger, A. Self-interaction correction to density-functional approximations for many-electron systems. *Phys. Rev. B* **1981**, *23*, 5048–5079.

(24) Polo, V.; Kraka, E.; Cremer, D. Electron correlation and the self-interaction error of density functional theory. *Mol. Phys.* **2002**, *100*, 1771–1790.

(25) Mori-Sánchez, P.; Cohen, A. J.; Yang, W. Many-electron self-interaction error in approximate density functionals. *J. Chem. Phys.* **2006**, *125*, 201102.

(26) Zhang, Y.; Yang, W. A challenge for density functionals: Self-interaction error increases for systems with a noninteger number of electrons. *J. Chem. Phys.* **1998**, *109*, 2604–2608.

(27) Gräfenstein, J.; Kraka, E.; Cremer, D. The impact of the self-interaction error on the density functional theory description of dissociating radical cations: Ionic and covalent dissociation limits. *J. Chem. Phys.* **2004**, *120*, 524–539.

(28) Miehlich, B.; Stoll, H.; Savin, A. A correlation-energy density functional for multideterminantal wavefunctions. *Mol. Phys.* **1997**, *91*, 527–536.

(29) Gräfenstein, J.; Kraka, E.; Cremer, D. Density functional theory for open-shell singlet biradicals. *Chem. Phys. Lett.* **1998**, *288*, 593–602.

(30) Kurzweil, Y.; Lawler, K. V.; Head-Gordon, M. Analysis of multi-configuration density functional theory methods: theory and model application to bond-breaking. *Mol. Phys.* **2009**, *107*, 2103–2110.

(31) Gusarov, S.; Malmqvist, P.-Å.; Lindh, R. Using on-top pair density for construction of correlation functionals for multideterminant wave functions. *Mol. Phys.* **2004**, *102*, 2207–2216.

(32) Khait, Y. G.; Hoffmann, M. R. Multireference spin-adapted variant of density functional theory. *J. Chem. Phys.* **2004**, *120*, 5005–5016.

(33) Li Manni, G.; Carlson, R. K.; Luo, S.; Ma, D.; Olsen, J.; Truhlar, D. G.; Gagliardi, L. Multiconfiguration Pair-Density Functional Theory. *J. Chem. Theory Comput.* **2014**, *10*, 3669–3680.

(34) White, S. R. Density matrix formulation for quantum renormalization groups. *Phys. Rev. Lett.* **1992**, *69*, 2863–2866.

(35) Schollwöck, U. The density-matrix renormalization group: a short introduction. *Phil. Trans. R. Soc. A.* **2011**, *369*, 2643–61.

(36) Schollwöck, U. The density-matrix renormalization group in the age of matrix product states. *Ann. Phys.* **2011**, *326*, 96–192.

(37) Chan, G. K.-L.; Head-Gordon, M. Highly correlated calculations with a polynomial cost algorithm: A study of the density matrix renormalization group. *J. Chem. Phys.* **2002**, *116*, 4462.

(38) Hachmann, J.; Dorando, J. J.; Avils, M.; Chan, G. K.-L. The radical character of the acenes: A density matrix renormalization group study. *J. Chem. Phys.* **2007**, *127*, 134309.

(39) Mizukami, W.; Kurashige, Y.; Yanai, T. More π Electrons Make a Difference: Emergence of Many Radicals on Graphene Nanoribbons Studied by Ab Initio DMRG Theory. *J. Chem. Theory Comput.* **2013**, *9*, 401–407.

(40) Kurashige, Y.; Chan, G. K.-L.; Yanai, T. Entangled quantum electronic wavefunctions of the Mn_4CaO_5 cluster in photosystem II. *Nat. Chem.* **2013**, *5*, 660–6.

(41) Sharma, S.; Sivalingam, K.; Neese, F.; Chan, G. K.-L. Low-energy spectrum of iron-sulfur clusters directly from many-particle quantum mechanics. *Nat. Chem.* **2014**, *6*, 927–33.

(42) Booth, G. H.; Grüneis, A.; Kresse, G.; Alavi, A. Towards an exact description of electronic wavefunctions in real solids. *Nature* **2013**, *493*, 365–70.

(43) Hirata, S.; Podeszwa, R.; Tobita, M.; Bartlett, R. J. Coupled-cluster singles and doubles for extended systems. *J. Chem. Phys.* **2004**, *120*, 2581–2592.

(44) Grüneis, A. A coupled cluster and Møller-Plesset perturbation theory study of the pressure induced phase transition in the LiH crystal. *J. Chem. Phys.* **2015**, *143*, 102817.

(45) McClain, J.; Sun, Q.; Chan, G. K.-L.; Berkelbach, T. C. Gaussian-based coupled-cluster theory for the ground-state and band structure of solids. *J. Chem. Theory Comput.* **2017**, *13*, 1209–1218.

(46) Gruber, T.; Liao, K.; Tsatsoulis, T.; Hummel, F.; Grüneis, A. Applying the coupled-cluster ansatz to solids and surfaces in the thermodynamic limit. *Phys. Rev. X* **2018**, *8*, 021043.

(47) Lin, C.; Zong, F. H.; Ceperley, D. M. Twist-averaged boundary conditions in continuum quantum Monte Carlo algorithms. *Phys. Rev. E* **2001**, *64*, 016702.

(48) Kwee, H.; Zhang, S.; Krakauer, H. Finite-Size Correction in Many-Body Electronic Structure Calculations. *Phys. Rev. Lett.* **2008**, *100*, 126404.

(49) Gruber, T.; Grüneis, A. Ab initio calculations of carbon and boron nitride allotropes and their structural phase transitions using periodic coupled cluster theory. *Phys. Rev. B* **2018**, *98*, 134108.

(50) Ruggeri, M.; Ríos, P. L.; Alavi, A. Correlation energies of the high-density spin-polarized electron gas to meV accuracy. *Phys. Rev. B* **2018**, *98*, 161105.

(51) Cheung, L. M.; Sundberg, K. R.; Ruedenberg, K. Dimerization of carbene to ethylene. *J. Am. Chem. Soc.* **1978**, *100*, 8024–8025.

(52) Roos, B. O.; Taylor, P. R.; Si, P. E., et al. A complete active space SCF method (CASSCF) using a density matrix formulated super-CI approach. *Chem. Phys.* **1980**, *48*, 157–173.

(53) Ruedenberg, K.; Schmidt, M. W.; Gilbert, M. M.; Elbert, S. Are atoms intrinsic to molecular electronic wavefunctions? I. The FORS model. *Chem. Phys.* **1982**, *71*, 41–49.

(54) McWeeny, R.; Sutcliffe, B. T. Fundamentals of Self-Consistent-Field (SCF), Hartree-Fock (HF), Multi-Configuration (MC) SCF and Configuration Interaction (CI) schemes. *Comput. Phys. Rep.* **1985**, *2*, 219–278.

(55) Shepard, R. The multiconfiguration self-consistent field method. *Adv. Chem. Phys.* **1987**, *69*, 63–200.

(56) Olsen, J.; Roos, B. O.; Jørgensen, P.; Jensen, H. J. A. Determinant based configuration interaction algorithms for complete and restricted configuration interaction spaces. *J. Chem. Phys.* **1988**, *89*, 2185–2192.

(57) Malmqvist, P.-Å.; Rendell, A.; Roos, B. O. The restricted active space self-consistent-field method, implemented with a split graph unitary group approach. *J. Phys. Chem.* **1990**, *94*, 5477–5482.

(58) Szalay, P. G.; Müller, T.; Gidofalvi, G.; Lischka, H.; Shepard, R. Multiconfiguration Self-Consistent Field and Multireference Configuration Interaction Methods and Applications. *Chem. Rev.* **2012**, *112*, 108–181.

(59) Liu, B. Ab initio potential energy surface for linear H3. *J. Chem. Phys.* **1973**, *58*, 1925–1937.

(60) Siegbahn, P. E. M. Generalizations of the direct CI method based on the graphical unitary group approach. II. Single and double replacements from any set of reference configurations. *J. Chem. Phys.* **1980**, *72*, 1647–1656.

(61) Saebø, S.; Pulay, P. Local treatment of electron correlation. *Annu. Rev. Phys. Chem.* **1993**, *44*, 213–236.

(62) Neese, F.; Hansen, A.; Liakos, D. G. Efficient and accurate approximations to the local coupled cluster singles doubles method using a truncated pair natural orbital basis. *J. Chem. Phys.* **2009**, *131*, 064103.

(63) Yang, J.; Chan, G. K.-L.; Manby, F. R.; Schütz, M.; Werner, H.-J. The orbital-specific-virtual local coupled cluster singles and doubles method. *J. Chem. Phys.* **2012**, *136*, 144105.

(64) Sparta, M.; Neese, F. Chemical applications carried out by local pair natural orbital based coupled-cluster methods. *Chem. Soc. Rev.* **2014**, *43*, 5032–5041.

(65) Yang, J.; Hu, W.; Usvyat, D.; Matthews, D.; Schütz, M.; Chan, G. K.-L. Ab initio determination of the crystalline benzene lattice energy to sub-kilojoule/mole accuracy. *Science* **2014**, *345*, 640–643.

(66) Liakos, D. G.; Sparta, M.; Kesharwani, M. K.; Martin, J. M.; Neese, F. Exploring the accuracy limits of local pair natural orbital coupled-cluster theory. *J. Chem. Theory Comput.* **2015**, *11*, 1525–1539.

(67) Werner, H.-J.; Koppl, C.; Ma, Q.; Schwilk, M., *Explicitly correlated local electron correlation methods*; John Wiley & Sons: 2017, p 1.

(68) Bender, C. F.; Davidson, E. R. Studies in configuration interaction: The first-row diatomic hydrides. *Phys. Rev.* **1969**, *183*, 23.

(69) Buenker, R. J.; Peyerimhoff, S. D. Individualized configuration selection in CI calculations with subsequent energy extrapolation. *Theor. Chim. Acta* **1974**, *35*, 33–58.

(70) Buenker, R. J.; Peyerimhoff, S. D.; Butscher, W. Applicability of the multi-reference double-excitation CI (MRD-CI) method to the calculation of electronic wavefunctions and comparison with related techniques. *Mol. Phys.* **1978**, *35*, 771–791.

(71) Knowles, P. J.; Werner, H.-J. An efficient method for the evaluation of coupling coefficients in configuration interaction calculations. *Chem. Phys. Lett.* **1988**, *145*, 514–522.

(72) Werner, H.-J.; Knowles, P. J. An efficient internally contracted multiconfiguration–reference configuration interaction method. *J. Chem. Phys.* **1988**, *89*, 5803–5814.

(73) Jeziorski, B.; Monkhorst, H. J. Coupled-cluster method for multideterminantal reference states. *Phys. Rev. A* **1981**, *24*, 1668–1681.

(74) Balková, A.; Kucharski, S. A.; Meissner, L.; Bartlett, R. J. A Hilbert space multi-reference coupled-cluster study of the H4 model system. *Theor. Chim. Acta* **1991**, *80*, 335–348.

(75) Kucharski, S. A.; Balkov, A.; Szalay, P. G.; Bartlett, R. J. Hilbert space multireference coupled-cluster methods. II. A model study on H8. *J. Chem. Phys.* **1992**, *97*, 4289.

(76) Piecuch, P.; Paldus, J. Orthogonally spin-adapted multi-reference Hilbert space coupled-cluster formalism: diagrammatic formulation. *Theor. Chim. Acta* **1992**, *83*, 69–103.

(77) Evangelista, F. A.; Allen, W. D.; Schaefer, H. F. High-order excitations in state-universal and state-specific multireference coupled cluster theories: Model systems. *J. Chem. Phys.* **2006**, *125*, 154113.

(78) Datta, D.; Mukherjee, D. An explicitly spin-free compact open-shell coupled cluster theory using a multireference combinatoric exponential ansatz: Formal development and pilot applications. *J. Chem. Phys.* **2009**, *131*, 044124.

(79) Lindgren, I.; Mukherjee, D. On the connectivity criteria in the open-shell coupled-cluster theory for general model spaces. *Phys. Rep.* **1987**, *151*, 93–127.

(80) Lindgren, I. Linked-Diagram and Coupled-Cluster Expansions for Multi-Configurational, Complete and Incomplete Model Spaces. *Phys. Scripta* **1985**, *32*, 291–302.

(81) Mukherjee, D.; Moitra, R. K.; Mukhopadhyay, A. Applications of a non-perturbative many-body formalism to general open-shell atomic and molecular problems: calculation of the ground and the lowest π-π^* singlet and triplet energies and the first ionization potential of trans-butadiene. *Mol. Phys.* **1977**, *33*, 955–969.

(82) Stolarczyk, L. Z.; Monkhorst, H. J. Coupled-cluster method with optimized reference state. *Int. J. Quantum Chem.* **1984**, *26*, 267–291.

(83) Stolarczyk, L. Z.; Monkhorst, H. J. Coupled-cluster method in Fock space. I. General formalism. *Phys. Rev. A* **1985**, *32*, 725–742.

(84) Stolarczyk, L. Z.; Monkhorst, H. J. Coupled-cluster method in Fock space. II. Brueckner-Hartree-Fock method. *Phys. Rev. A* **1985**, *32*, 743–747.

(85) Stolarczyk, L. Z.; Monkhorst, H. J. Coupled-cluster method in Fock space. III. On similarity transformation of operators in Fock space. *Phys. Rev. A* **1988**, *37*, 1908–1925.

(86) Stolarczyk, L. Z.; Monkhorst, H. J. Coupled-cluster method in Fock space. IV. Calculation of expectation values and transition moments. *Phys. Rev. A* **1988**, *37*, 1926–1933.

(87) Stolarczyk, L. Z.; Monkhorst, H. J. Quasiparticle Fock-space coupled-cluster theory. *Mol. Phys.* **2010**, *108*, 3067–3089.

(88) Fang, T.; Shen, J.; Li, S. Block correlated coupled cluster method with a complete-active-space self-consistent-field reference function: The formula for general active spaces and its applications for multibond breaking systems. *J. Chem. Phys.* **2008**, *128*, 224107.

(89) Datta, D.; Kong, L.; Nooijen, M. A state-specific partially internally contracted multireference coupled cluster approach. *J. Chem. Phys.* **2011**, *134*, 214116.

(90) Fang, T.; Li, S. Block correlated coupled cluster theory with a complete active-space self-consistent-field reference function: The formulation and test applications for single bond breaking. *J. Chem. Phys.* **2007**, *127*, 204108.

(91) Hanauer, M.; Köhn, A. Pilot applications of internally contracted multireference coupled cluster theory, and how to choose the cluster operator properly. *J. Chem. Phys.* **2011**, *134*, 204111.

(92) Evangelista, F. A.; Gauss, J. An orbital-invariant internally contracted multireference coupled cluster approach. *J. Chem. Phys.* **2011**, *134*, 114102.

(93) Kinoshita, T.; Hino, O.; Bartlett, R. J. Coupled-cluster method tailored by configuration interaction. *J. Chem. Phys.* **2005**, *123*, 074106.

(94) Lyakh, D. I.; Ivanov, V. V.; Adamowicz, L. Automated generation of coupled-cluster diagrams: Implementation in the multireference state-specific coupled-cluster approach with the complete-active-space reference. *J. Chem. Phys.* **2005**, *122*, 024108.

(95) Hanrath, M. An exponential multireference wave-function Ansatz. *J. Chem. Phys.* **2005**, *123*, 084102.

(96) Pittner, J.; Šmydke, J.; Čársky, P.; Hubač, I. State-specific Brillouin-Wigner multireference coupled cluster study of the F_2 molecule: assessment of the a posteriori size-extensivity correction. *J. Mol. Struc.-THEOCHEM* **2001**, *547*, 239–244.

(97) Hubač, I.; Wilson, S. On the use of Brillouin-Wigner perturbation theory for many-body systems. *J. Phys. B: At., Mol. Opt. Phys.* **2000**, *33*, 365–374.

(98) Hubač, I.; Pittner, J.; Čársky, P. Size-extensivity correction for the state-specific multireference Brillouin-Wigner coupled-cluster theory. *J. Chem. Phys.* **2000**, *112*, 8779.

(99) Pittner, J.; Nachtigall, P.; Čársky, P.; Hubač, I. State-Specific Brillouin-Wigner Multireference Coupled Cluster Study of the Singlet-Triplet Separation in the Tetramethyleneethane Diradical. *J. Phys. Chem. A* **2001**, *105*, 1354–1356.

(100) Chattopadhyay, S.; Mahapatra, U. S.; Mukherjee, D. Development of a linear response theory based on a state-specific multireference coupled cluster formalism. *J. Chem. Phys.* **2000**, *112*, 7939.

(101) Kong, L. Connection between a few Jeziorski-Monkhorst ansatz-based methods. *Int. J. Quantum Chem.* **2009**, *109*, 441–447.

(102) Chattopadhyay, S.; Mahapatra, U. S.; Mukherjee, D. Property calculations using perturbed orbitals via state-specific multireference coupled-cluster and perturbation theories. *J. Chem. Phys.* **1999**, *111*, 3820.

(103) Pittner, J. Continuous transition between Brillouin-Wigner and Rayleigh-Schrödinger perturbation theory, generalized Bloch equation, and Hilbert space multireference coupled cluster. *J. Chem. Phys.* **2003**, *118*, 10876.

(104) Mahapatra, U. S.; Datta, B.; Mukherjee, D. A size-consistent state-specific multireference coupled cluster theory: Formal developments and molecular applications. *J. Chem. Phys.* **1999**, *110*, 6171.

(105) Mahapatra, U. S.; Datta, B.; Mukherjee, D. A state-specific multi-reference coupled cluster formalism with molecular applications. *Mol. Phys.* **2010**.

(106) Mášik, J.; Hubač, I.; Mach, P. Single-root multireference Brillouin-Wigner coupled-cluster theory: Applicability to the F_2 molecule. *J. Chem. Phys.* **1998**, *108*, 6571.

(107) Mášik, J.; Hubač, I. Comparison of the Brillouin-Wigner Coupled Cluster Theory with the Standard Coupled Cluster Theory. Cancellation of Disconnected Terms in the Brillouin-Wigner Coupled Cluster Theory. *Collect. Czech. Chem. Commun.* **1997**, *62*, 829–842.

(108) Hubač, I.; Neogrády, P. Size-consistent Brillouin-Wigner perturbation theory with an exponentially parametrized wave function: Brillouin-Wigner coupled-cluster theory. *Phys. Rev. A* **1994**, *50*, 4558–4564.

(109) Adamowicz, L.; Malrieu, J.-P.; Ivanov, V. V. New approach to the state-specific multireference coupled-cluster formalism. *J. Chem. Phys.* **2000**, *112*, 10075.

(110) Kállay, M.; Szalay, P. G.; Surján, P. R. A general state-selective multireference coupled-cluster algorithm. *J. Chem. Phys.* **2002**, *117*, 980.

(111) Piecuch, P.; Kowalski, K. The State-Universal Multi-Reference Coupled-Cluster Theory: An Overview of Some Recent Advances. *Int. J. Mol. Sci.* **2002**, *3*, 676–709.

(112) Andersson, K.; Malmqvist, P. A.; Roos, B. O.; Sadlej, A. J.; Wolinski, K. Second-order perturbation theory with a CASSCF reference function. *J. Phys. Chem.* **1990**, *94*, 5483–5488.

(113) Hirao, K. Multireference Møller-Plesset method. *Chem. Phys. Lett.* **1992**, *190*, 374–380.

(114) Hirao, K. Multireference Møller-Plesset perturbation theory for high-spin open-shell systems. *Chem. Phys. Lett.* **1992**, *196*, 397–403.

(115) Werner, H.-J. Third-order multireference perturbation theory The CASPT3 method. *Mol. Phys.* **1996**, *89*, 645–661.

(116) Grimme, S.; Waletzke, M. Multi-reference Møller–Plesset theory: computational strategies for large molecules. *Phys. Chem. Chem. Phys.* **2000**, *2*, 2075–2081.

(117) Celani, P.; Werner, H.-J. Multireference perturbation theory for large restricted and selected active space reference wave functions. *J. Chem. Phys.* **2000**, *112*, 5546–5557.

(118) Angeli, C.; Cimiraglia, R.; Evangelisti, S.; Leininger, T.; Malrieu, J.-P. Introduction of n-electron valence states for multireference perturbation theory. *J. Chem. Phys.* **2001**, *114*, 10252–10264.

(119) Angeli, C.; Bories, B.; Cavallini, A.; Cimiraglia, R. Third-order multireference perturbation theory: The n-electron valence state perturbation-theory approach. *J. Chem. Phys.* **2006**, *124*, 054108.

(120) Jackels, C. F.; Davidson, E. R. The two lowest energy 2A' states of NO_2. *J. Chem. Phys.* **1976**, *64*, 2908–2917.

(121) Davidson, E. R.; Borden, W. T. Symmetry breaking in polyatomic molecules: real and artifactual. *J. Phys. Chem.* **1983**, *87*, 4783–4790.

(122) Andrews, J. S.; Jayatilaka, D.; Bone, R. G.; Handy, N. C.; Amos, R. D. Spin contamination in single-determinant wavefunctions. *Chem. Phys. Lett.* **1991**, *183*, 423–431.

(123) Ayala, P. Y.; Schlegel, H. B. A nonorthogonal CI treatment of symmetry breaking in sigma formyloxyl radical. *J. Chem. Phys.* **1998**, *108*, 7560.

(124) McLean, A. D.; Lengsfield, B. H.; Pacansky, J.; Ellinger, Y. Symmetry breaking in molecular calculations and the reliable prediction of equilibrium geometries. The formyloxyl radical as an example. *J. Chem. Phys.* **1985**, *83*, 3567–3576.

(125) Sherrill, C.; Lee, M. S.; Head-Gordon, M. On the performance of density functional theory for symmetry-breaking problems. *Chem. Phys. Lett.* **1999**, *302*, 425–430.

(126) Crawford, T. D.; Stanton, J. F. Some surprising failures of Brueckner coupled cluster theory. *J. Chem. Phys.* **2000**, *112*, 7873.

(127) Paldus, J.; Thiamová, G. Approximate symmetry-breaking in the independent particle model of monocyclic completely conjugated polyenes. *J. Math. Chem.* **2007**, *44*, 88–120.

(128) Small, D. W.; Head-Gordon, M. Post-modern valence bond theory for strongly correlated electron spins. *Phys. Chem. Chem. Phys.* **2011**, *13*, 19285–97.

(129) Yachandra, V. K.; Sauer, K.; Klein, M. P. Manganese Cluster in Photosynthesis: Where Plants Oxidize Water to Dioxygen. *Chem. Rev.* **1996**, *96*, 2927–2950.

(130) Yamaguchi, K.; Shoji, M.; Saito, T.; Isobe, H.; Nishihara, S.; Koizumi, K.; Yamada, S.; Kawakami, T.; Kitagawa, Y.; Yamanaka, S.; Okumura, M. Theory of chemical bonds in metalloenzymes. XV. Local singlet and triplet diradical mechanisms for radical coupling reactions in the oxygen evolution complex. *Int. J. Quantum Chem.* **2010**, *110*, 3101–3128.

(131) Yson, R. L.; Gilgor, J. L.; Guberman, B. A.; Varganov, S. A. Protein induced singlettriplet quasidegeneracy in the active site of [NiFe]-hydrogenase. *Chem. Phys. Lett.* **2013**, *577*, 138–141.

(132) Rod, T. H.; Nørskov, J. K. Modeling the nitrogenase FeMo cofactor. *J. Am. Chem. Soc.* **2000**, *122*, 12751–12763.

(133) Schimpl, J.; Petrilli, H. M.; Blöchl, P. E. Nitrogen binding to the FeMo-cofactor of nitrogenase. *J. Am. Chem. Soc.* **2003**, *125*, 15772–15778.

(134) Lancaster, K. M.; Roemelt, M.; Ettenhuber, P.; Hu, Y.; Ribbe, M. W.; Neese, F.; Bergmann, U.; DeBeer, S. X-ray emission spectroscopy evidences a central carbon in the nitrogenase iron-molybdenum cofactor. *Science* **2011**, *334*, 974–977.

(135) Bjornsson, R.; Neese, F.; DeBeer, S. Revisiting the Mossbauer Isomer Shifts of the FeMoco Cluster of Nitrogenase and the Cofactor Charge. *Inorg. Chem.* **2017**, *56*, 1470–1477.

(136) Pauncz, R., *Spin eigenfunctions: construction and use*; Springer Science & Business Media: 2012.

(137) Cooper, D.; Gerratt, J.; Raimondi, M. Modern valence bond theory. *Advances in Chemical Physics: Ab Initio Methods in Quantum Chemistry Part 2* **1987**, *69*, 319–397.

(138) Cooper, D.; Gerratt, J. a.; Raimondi, M. Spin-coupled valence bond theory. *International Reviews in Physical Chemistry* **1988**, *7*, 59–80.

(139) Cooper, D. L.; Gerratt, J.; Raimondi, M. Applications of spin-coupled valence bond theory. *Chem. Rev.* **1991**, *91*, 929–964.

(140) Small, D. W.; Head-Gordon, M. Tractable spin-pure methods for bond breaking: Local many-electron spin-vector sets and an approximate valence bond model. *J. Chem. Phys.* **2009**, *130*, 084103.

(141) Small, D. W.; Head-Gordon, M. A fusion of the closed-shell coupled cluster singles and doubles method and valence-bond theory for bond breaking. *J. Chem. Phys.* **2012**, *137*, 114103.

(142) Lee, J.; Small, D. W.; Epifanovsky, E.; Head-Gordon, M. Coupled-Cluster Valence-Bond Singles and Doubles for Strongly Correlated Systems: Block-Tensor Based Implementation and Application to Oligoacenes. *J. Chem. Theory Comput.* **2017**, *13*, 602–615.

(143) Small, D. W.; Head-Gordon, M. Independent amplitude approximations in coupled cluster valence bond theory: Incorporation of 3-electron-pair correlation and application to spin frustration in the low-lying excited states of a ferredoxin-type tetrametallic iron-sulfur cluster. *J. Chem. Phys.* **2018**, *149*, 144103.

(144) Lee, J.; Small, D. W.; Head-Gordon, M. Open-shell coupled-cluster valence-bond theory augmented with an independent amplitude approximation for three-pair correlations: Application to a model oxygen-evolving complex and single molecular magnet. *J. Chem. Phys.* **2018**, *149*, 244121.

(145) Lee, J.; Bertels, L. W.; Head-Gordon, M. Kohn-Sham Density Functional Theory with Complex, Spin-Restricted Orbitals: Accessing a New Class of Densities without the Symmetry Dilemma. **2019**, arXiv:1904.08093.

(146) Hohenstein, E. G.; Parrish, R. M.; Martínez, T. J. Tensor hypercontraction density fitting. I. Quartic scaling second- and third-order Møller-Plesset perturbation theory. *J. Chem. Phys.* **2012**, *137*, 1085.

(147) Hohenstein, E. G.; Parrish, R. M.; Sherrill, C. D.; Martínez, T. J. Communication: Tensor hypercontraction. III. Least-squares tensor hypercontraction for the determination of correlated wavefunctions. *J. Chem. Phys.* **2012**, *137*, 221101.

(148) Parrish, R. M.; Hohenstein, E. G.; Martínez, T. J.; Sherrill, C. D. Tensor hypercontraction. II. Least-squares renormalization. *J. Chem. Phys.* **2012**, *137*, 224106.

(149) Hohenstein, E. G.; Kokkila, S. I.; Parrish, R. M.; Martínez, T. J. Tensor hypercontraction equation-of-motion second-order approximate coupled cluster: Electronic excitation energies in O (N^4) time. *Journal of Physical Chemistry B* **2013**, *117*, 12972–12978.

(150) Hohenstein, E. G.; Kokkila, S. I.; Parrish, R. M.; Martínez, T. J. Quartic scaling second-order approximate coupled cluster singles and doubles via tensor hypercontraction: THC-CC2. *J. Chem. Phys.* **2013**, *138*, 124111.

(151) Parrish, R. M.; Hohenstein, E. G.; Schunck, N. F.; Sherrill, C. D.; Martínez, T. J. Exact Tensor Hypercontraction: A Universal Technique for the Resolution of Matrix Elements of Local Finite-Range N -Body Potentials in Many-Body Quantum Problems. *Phys. Rev. Letters* **2013**, *111*, 132505.

(152) Parrish, R. M.; Hohenstein, E. G.; Martínez, T. J.; Sherrill, C. D. Discrete variable representation in electronic structure theory: Quadrature grids for least-squares tensor hypercontraction. *J. Chem. Phys.* **2013**, *138*, 194107.

(153) Parrish, R. M.; Sherrill, C. D.; Hohenstein, E. G.; Kokkila, S. I. L.; Martínez, T. J. Communication: Acceleration of coupled cluster singles and doubles via orbital-weighted least-squares tensor hypercontraction. *J. Chem. Phys.* **2014**, *140*, 181102.

(154) Kokkila Schumacher, S. I. L.; Hohenstein, E. G.; Parrish, R. M.; Wang, L.-P.; Martínez, T. J. Tensor Hypercontraction Second-Order MøllerPlesset Perturbation Theory: Grid Optimization and Reaction Energies. *J. Chem. Theory Comput.* **2015**, *11*, 3042–3052.

(155) Song, C.; Martínez, T. J. Atomic orbital-based SOS-MP2 with tensor hypercontraction. I. GPU-based tensor construction and exploiting sparsity. *J. Chem. Phys.* **2016**, *144*, 174111.

(156) Song, C.; Martínez, T. J. Atomic orbital-based SOS-MP2 with tensor hypercontraction. II. Local tensor hypercontraction. *J. Chem. Phys.* **2017**, *146*, 034104.

(157) Song, C.; Martínez, T. J. Analytical gradients for tensor hyper-contracted MP2 and SOS-MP2 on graphical processing units. *J. Chem. Phys.* **2017**, *147*, 161723.

(158) Lu, J.; Ying, L. Compression of the electron repulsion integral tensor in tensor hypercontraction format with cubic scaling cost. *J. Comput. Phys.* **2015**, *302*, 329–335.

(159) Lu, J.; Thicke, K. Cubic scaling algorithms for RPA correlation using interpolative separable density fitting. *J. Comput. Phys.* **2017**, *351*, 187–202.

(160) Hu, W.; Lin, L.; Yang, C. Interpolative Separable Density Fitting Decomposition for Accelerating Hybrid Density Functional Calculations with Applications to Defects in Silicon. *J. Chem. Theory Comput.* **2017**, *13*, 5420–5431.

(161) Hu, W.; Shao, M.; Cepellotti, A.; da Jornada, F. H.; Lin, L.; Thicke, K.; Yang, C.; Louie, S. G. In *Lecture Notes in Computer Science (including subseries Lecture Notes in Artificial Intelligence and Lecture Notes in Bioinformatics)*, Springer, Cham: 2018; Vol. 10861 LNCS, pp 604–617.

(162) Dong, K.; Hu, W.; Lin, L. Interpolative Separable Density Fitting through Centroidal Voronoi Tessellation with Applications to Hybrid Functional Electronic Structure Calculations. *J. Chem. Theory Comput.* **2018**, *14*, 1311–1320.

(163) Lee, J.; Malone, F. D.; Morales, M. A. An Auxiliary-Field Quantum Monte Carlo Perspective on the Ground State of the Uniform Electron Gas: An Investigation with Spin-Restricted Hartree-Fock Trial Wavefunctions. **2019**, arXiv:1905.04361.

(164) Peruzzo, A.; McClean, J.; Shadbolt, P.; Yung, M.-H.; Zhou, X.-Q.; Love, P. J.; Aspuru-Guzik, A.; O'Brien, J. L. A variational eigenvalue solver on a photonic quantum processor. *Nat. Comm.* **2014**, *5*, 4213.

(165) Lee, J.; Huggins, W. J.; Head-Gordon, M.; Whaley, K. B. Generalized Unitary Coupled Cluster Wave functions for Quantum Computation. *J. Chem. Theory Comput.* **2018**, *15*, 311–324.

(166) Feyereisen, M.; Fitzgerald, G.; Komornicki, A. Use of approximate integrals in ab initio theory. An application in MP2 energy calculations. *Chem. Phys. Lett.* **1993**, *208*, 359–363.

(167) Bernholdt, D. E.; Harrison, R. J. Large-scale correlated electronic structure calculations: the RI-MP2 method on parallel computers. *Chem. Phys. Lett.* **1996**, *250*, 477–484.

(168) Jordan, K. D.; Wang, F. Theory of Dipole-Bound Anions. *Annu. Rev. Phys. Chem.* **2003**, *54*, 367–396.

(169) Morgan, J. D.; Simon, B. The calculation of molecular resonances by complex scaling. *J. Phys. B* **1981**, *14*, L167–L171.

(170) Grimme, S. Improved second-order Møller-Plesset perturbation theory by separate scaling of parallel- and antiparallel-spin pair correlation energies. *J. Chem. Phys.* **2003**, *118*, 9095–9102.

(171) Jung, Y.; Lochan, R. C.; Dutoi, A. D.; Head-Gordon, M. Scaled opposite-spin second order moller-plesset correlation energy: An economical electronic structure method. *J. Chem. Phys.* **2004**, *121*, 9793–9802.

(172) Grimme, S. Accurate Calculation of the Heats of Formation for Large Main Group Compounds with Spin-Component Scaled MP2 Methods. *J. Phys. Chem. A* **2005**, *109*, 3067–3077.

(173) Lochan, R. C.; Jung, Y.; Head-Gordon, M. Scaled opposite spin second order Møller-Plesset theory with improved physical description of long-range dispersion interactions. *J. Phys. Chem. A* **2005**, *109*, 7598–7605.

(174) Distasio, R. A.; Head-Gordon, M. Optimized spin-component scaled second-order Møller-Plesset perturbation theory for intermolecular interaction energies. *Mol. Phys.* **2007**, *105*, 1073–1083.

(175) Lochan, R. C.; Shao, Y.; Head-Gordon, M. Quartic-Scaling Analytical Energy Gradient of Scaled Opposite-Spin Second-Order Møller-Plesset Perturbation Theory. *J. Chem. Theory Comput.* **2007**, *3*, 988–1003.

(176) Lochan, R. C.; Head-Gordon, M. Orbital-optimized opposite-spin scaled second-order correlation: an economical method to improve the description of open-shell molecules. *J. Chem. Phys.* **2007**, *126*, 164101.

(177) Neese, F.; Schwabe, T.; Kossmann, S.; Schirmer, B.; Grimme, S. Assessment of Orbital-Optimized, Spin-Component Scaled Second-Order Many-Body Perturbation Theory for Thermochemistry and Kinetics. *J. Chem. Theory Comput.* **2009**, *5*, 3060–73.

(178) Bozkaya, U.; Turney, J. M.; Yamaguchi, Y.; Schaefer, H. F.; Sherrill, C. D. Quadratically convergent algorithm for orbital optimization in the orbital-optimized coupled-cluster doubles method and in orbital-optimized second-order Mller-Plesset perturbation theory. *The Journal of Chemical Physics* **2011**, *135*, 104103.

(179) Grimme, S. Semiempirical hybrid density functional with perturbative second-order correlation. *J. Chem. Phys.* **2006**, *124*, 034108.

(180) Chai, J.-D.; Head-Gordon, M. Long-range corrected double-hybrid density functionals. *J. Chem. Phys.* **2009**, *131*, 174105.

(181) Kozuch, S.; Martin, J. M. L. DSD-PBEP86: in search of the best double-hybrid DFT with spin-component scaled MP2 and dispersion corrections. *Phys. Chem. Chem. Phys.* **2011**, *13*, 20104.

(182) Mardirossian, N.; Head-Gordon, M. Survival of the most transferable at the top of Jacob's ladder: Defining and testing the ωB97M(2) double hybrid density functional. *J. Chem. Phys.* **2018**, *148*, 241736.

(183) Goldey, M.; Head-Gordon, M. Attenuating Away the Errors in Inter- and Intramolecular Interactions from Second-Order Møller-Plesset Calculations in the Small Aug-cc-pVDZ Basis Set. *J. Phys. Chem. Lett.* **2012**, *3*, 3592–3598.

(184) Goldey, M.; Dutoi, A.; Head-Gordon, M. Attenuated second-order Møller-Plesset perturbation theory: performance within the aug-cc-pVTZ basis. *Phys. Chem. Chem. Phys.* **2013**, *15*, 15869.

(185) Goldey, M. B.; Head-Gordon, M. Convergence of attenuated second order Møller-Plesset perturbation theory towards the complete basis set limit. *Chem. Phys. Lett.* **2014**, *608*, 249–254.

(186) Goldey, M. B.; Belzunces, B.; Head-Gordon, M. Attenuated MP2 with a Long-Range Dispersion Correction for Treating Nonbonded Interactions. *J. Chem. Theory Comput.* **2015**, *11*, 4159–4168.

(187) Farnell, L.; Pople, J. A.; Radom, L. Structural predictions for open-shell systems: a comparative assessment of ab initio procedures. *J. Phys. Chem.* **1983**, *87*, 79–82.

(188) Nobes, R. H.; Pople, J. A.; Radom, L.; Handy, N. C.; Knowles, P. J. Slow convergence of the møller-plesset perturbation series: the dissociation energy of hydrogen cyanide and the electron affinity of the cyano radical. *Chem. Phys. Lett.* **1987**, *138*, 481–485.

(189) Gill, P. M. W.; Pople, J. A.; Radom, L.; Nobes, R. H. Why does unrestricted Møller-Plesset perturbation theory converge so slowly for spin-contaminated wave functions? *J. Chem. Phys.* **1988**, *89*, 7307–7314.

(190) Jensen, F. A remarkable large effect of spin contamination on calculated vibrational frequencies. *Chem. Phys. Lett.* **1990**, *169*, 519–528.

(191) Dykstra, C. E. An examination of the Brueckner condition for the selection of molecular orbitals in correlated wavefunctions. *Chem. Phys. Lett.* **1977**, *45*, 466–469.

(192) Handy, N. C.; Pople, J. A.; Head-Gordon, M.; Raghavachari, K.; Trucks, G. W. Size-consistent Brueckner theory limited to double substitutions. *Chem. Phys. Lett.* **1989**, *164*, 185–192.

(193) Soydaş, E.; Bozkaya, U. Assessment of Orbital-Optimized MP2.5 for Thermochemistry and Kinetics: Dramatic Failures of Standard Perturbation Theory Approaches for Aromatic Bond Dissociation Energies and Barrier Heights of Radical Reactions. *J. Chem. Theory Comput.* **2015**, *11*, 1564–1573.

(194) Kurlancheek, W.; Head-Gordon, M. Violations of N-representability from spin-unrestricted orbitals in Møller-Plesset perturbation theory and related double-hybrid density functional theory. *Mol. Phys.* **2009**, *107*, 1223–1232.

(195) Stück, D.; Baker, T. A.; Zimmerman, P.; Kurlancheek, W.; Head-Gordon, M. On the nature of electron correlation in C_{60}. *J. Chem. Phys.* **2011**, *135*, 194306.

(196) Kurlancheek, W.; Lochan, R.; Lawler, K.; Head-Gordon, M. Exploring the competition between localization and delocalization of the neutral soliton defect in polyenyl chains with the orbital optimized second order opposite spin method. *J. Chem. Phys.* **2012**, *136*, 054113.

(197) Soydaş, E.; Bozkaya, U. Assessment of Orbital-Optimized Third-Order Møller-Plesset Perturbation Theory and Its Spin-Component and Spin-Opposite Scaled Variants for Thermochemistry and Kinetics. *J. Chem. Theory Comput.* **2013**, *9*, 1452–1460.

(198) Bozkaya, U.; Sherrill, C. D. Orbital-optimized coupled-electron pair theory and its analytic gradients: Accurate equilibrium geometries, harmonic vibrational frequencies, and hydrogen transfer reactions. *J. Chem. Phys.* **2013**, *139*, 054104.

(199) Stück, D.; Head-Gordon, M. Regularized orbital-optimized second-order perturbation theory. *J. Chem. Phys.* **2013**, *139*, 244109.

(200) Peverati, R.; Head-Gordon, M. Orbital optimized double-hybrid density functionals. *J. Chem. Phys.* **2013**, *139*, 024110.

(201) Sancho-García, J. C.; Pérez-Jiménez, A. J.; Savarese, M.; Brémond, E.; Adamo, C. Importance of Orbital Optimization for Double-Hybrid Density Functionals: Application of the OO-PBE-QIDH Model for Closed- and Open-Shell Systems. *J. Phys. Chem. A* **2016**, *120*, 1756–1762.

(202) Bozkaya, U. Orbital-optimized linearized coupled-cluster doubles with density-fitting and Cholesky decomposition approximations: an efficient implementation. *Phys. Chem. Chem. Phys.* **2016**, *18*, 11362–11373.

(203) Razban, R. M.; Stück, D.; Head-Gordon, M. Addressing first derivative discontinuities in orbital-optimised opposite-spin scaled second-order perturbation theory with regularisation. *Mol. Phys.* **2017**, *115*, 2102–2109.

(204) Najibi, A.; Goerigk, L. A Comprehensive Assessment of the Effectiveness of Orbital Optimization in Double-Hybrid Density Functionals in the Treatment of Thermochemistry, Kinetics, and Noncovalent Interactions. *J. Phys. Chem. A* **2018**, *122*, 5610–5624.

(205) Bozkaya, U. Orbital-optimized third-order Mller-Plesset perturbation theory and its spin-component and spin-opposite scaled variants: Application to symmetry breaking problems. *The Journal of Chemical Physics* **2011**, *135*, 224103.

(206) Bozkaya, U.; Sherrill, C. D. Orbital-optimized MP2.5 and its analytic gradients: Approaching CCSD(T) quality for noncovalent interactions. *J. Chem. Phys.* **2014**, *141*, 204105.

(207) Bozkaya, U. Orbital-Optimized MP3 and MP2.5 with Density-Fitting and Cholesky Decomposition Approximations. *Journal of Chemical Theory and Computation* **2016**, *12*, 1179–1188.

(208) Bozkaya, U.; Sherrill, C. D. Analytic energy gradients for the orbital-optimized second-order Møller-Plesset perturbation theory. *J. Chem. Phys.* **2013**, *138*, 184103.

(209) Bozkaya, U. Analytic Energy Gradients and Spin Multiplicities for Orbital-Optimized Second-Order Perturbation Theory with Density-Fitting Approximation: An Efficient Implementation. *J. Chem. Theory Comput.* **2014**, *10*, 4389–4399.

(210) Bozkaya, U. Orbital-Optimized Second-Order Perturbation Theory with Density-Fitting and Cholesky Decomposition Approximations: An Efficient Implementation. *Journal of Chemical Theory and Computation* **2014**, *10*, 2371–2378.

(211) Bach, V.; Lieb, E. H.; Loss, M.; Solovej, J. P. There are no unfilled shells in unrestricted Hartree-Fock theory. *Phys. Rev. Lett.* **1994**, *72*, 2981–2983.

(212) Sharada, S. M.; Stück, D.; Sundstrom, E. J.; Bell, A. T.; Head-Gordon, M. Wavefunction stability analysis without analytical electronic Hessians: application to orbital-optimised second-order Møller-Plesset theory and VV10-containing density functionals. *Mol. Phys.* **2015**, *113*, 1802–1808.

(213) Coulson, C.; Fischer, I. XXXIV. Notes on the molecular orbital treatment of the hydrogen molecule. *Philos. Mag.* **1949**, *40*, 386–393.

(214) Roos, B. O.; Andersson, K. Multiconfigurational perturbation theory with level shift – the Cr_2 potential revisited. *Chem. Phys. Lett.* **1995**, *245*, 215–223.

(215) Ohnishi, Y.-y.; Ishimura, K.; Ten-no, S. Interaction Energy of Large Molecules from Restrained Denominator MP2-F12. *J. Chem. Theory Comput.* **2014**, *10*, 4857–4861.

(216) Evangelista, F. A. A driven similarity renormalization group approach to quantum many-body problems. *J. Chem. Phys.* **2014**, *141*, 054109.

(217) Eshuis, H.; Yarkony, J.; Furche, F. Fast computation of molecular random phase approximation correlation energies using resolution of the identity and imaginary frequency integration. *J. Chem. Phys.* **2010**, *132*, 234114.

(218) Assfeld, X.; Almlöf, J. E.; Truhlar, D. G. Degeneracy-corrected perturbation theory for electronic structure calculations. *Chem. Phys. Lett.* **1995**, *241*, 438–444.

(219) Lawler, K. V.; Parkhill, J. A.; Head-Gordon, M. Penalty functions for combining coupled-cluster and perturbation amplitudes in local correlation methods with optimized orbitals. *Mol. Phys.* **2008**, *106*, 2309–2324.

(220) Chen, G. P.; Voora, V. K.; Agee, M. M.; Balasubramani, S. G.; Furche, F. Random-Phase Approximation Methods. *Annu. Rev. Phys. Chem.* **2017**, *68*, 421–445.

(221) Bartlett, R. J.; Purvis, G. D. Many-body perturbation theory, coupled-pair many-electron theory, and the importance of quadruple excitations for the correlation problem. *Int. J. Quantum Chem.* **1978**, *14*, 561–581.

(222) Karton, A.; Daon, S.; Martin, J. M. W4-11: A high-confidence benchmark dataset for computational thermochemistry derived from first-principles W4 data. *Chem. Phys. Lett.* **2011**, *510*, 165–178.

(223) Goerigk, L.; Hansen, A.; Bauer, C.; Ehrlich, S.; Najibi, A.; Grimme, S. A look at the density functional theory zoo with the advanced GMTKN55 database for general main group thermochemistry, kinetics and noncovalent interactions. *Phys. Chem. Chem. Phys.* **2017**, *19*, 32184–32215.

(224) Zipse, H. In *Radicals in Synthesis I*, Gansäuer, A., Ed.; Springer Berlin Heidelberg: Berlin, Heidelberg, 2006, pp 163–189.

(225) Tentscher, P. R.; Arey, J. S. Binding in Radical-Solvent Binary Complexes: Benchmark Energies and Performance of Approximate Methods. *J. Chem. Theory Comput.* **2013**, *9*, 1568–1579.

(226) Hu, P.; Lee, S.; Herng, T. S.; Aratani, N.; Gonçalves, T. P.; Qi, Q.; Shi, X.; Yamada, H.; Huang, K.-W.; Ding, J.; Kim, D.; Wu, J. Towards Tetraradicaloid: The Effect of Fusion Mode on Radical Character and Chemical Reactivity. *J. Am. Chem. Soc.* **2015**, *138*, 1065.

(227) Kobayashi, Y.; Okajima, H.; Sotome, H.; Yanai, T.; Mutoh, K.; Yoneda, Y.; Shigeta, Y.; Sakamoto, A.; Miyasaka, H.; Abe, J. Direct Observation of the Ultrafast Evolution of Open-Shell Biradical in Photochromic Radical Dimer. *J. Am. Chem. Soc.* **2017**, *139*, 6382–6389.

(228) Shavitt, I.; Bartlett, R. J., *Many-Body Methods in Chemistry and Physics: MBPT and Coupled-Cluster Theory*; Cambridge University Press: 2009, p 67.

(229) Hillier, I. H.; Saunders, V. R. A new SCF procedure and its applications toab initio calculations of the states of the fluorosulphate radical. *Int. J. Quantum Chem.* **1970**, *4*, 503–518.

(230) Hillier, I. H.; Saunders, V. R. Ab initio Molecular Orbital Calculations of the Ground and Excited States of the Permanganate and Chromate Ions. *Proc. Royal Soc. Lond. A* **1970**, *320*, 161–173.

(231) Sorber, L.; Barel, M. V.; Lathauwer, L. D. Unconstrained Optimization of Real Functions in Complex Variables. *SIAM J. Optimiz.* **2012**, *22*, 879–898.

(232) Distasio, R. A.; Steele, R. P.; Rhee, Y. M.; Shao, Y.; Head-Gordon, M. An improved algorithm for analytical gradient evaluation in resolution-of-the-identity second-order Møller-Plesset perturbation theory: application to alanine tetrapeptide conformational analysis. *J. Comput. Chem.* **2007**, *28*, 839–56.

(233) Almlöf, J. Elimination of energy denominators in Møller-Plesset perturbation theory by a Laplace transform approach. *Chem. Phys. Lett.* **1991**, *181*, 319–320.

(234) Häser, M.; Almlöf, J. Laplace transform techniques in Møller-Plesset perturbation theory. *J. Chem. Phys.* **1992**, *96*, 489.

(235) Häser, M. Møller-Plesset (MP2) perturbation theory for large molecules. *Theor. Chim. Acta* **1993**, *87*, 147–173.

(236) Shao, Y. et al. Advances in molecular quantum chemistry contained in the Q-Chem 4 program package. *Mol. Phys.* **2015**, *113*, 184–215.

(237) Dunning, T. H. Gaussian basis sets for use in correlated molecular calculations. I. The atoms boron through neon and hydrogen. *J. Chem. Phys.* **1989**, *90*, 1007–1023.

(238) Weigend, F.; Köhn, A.; Hättig, C. Efficient use of the correlation consistent basis sets in resolution of the identity MP2 calculations. *J. Chem. Phys.* **2002**, *116*, 3175–3183.

(239) Davidson, E. R. The iterative calculation of a few of the lowest eigenvalues and corresponding eigenvectors of large real-symmetric matrices. *J. Comput. Phys.* **1975**, *17*, 87–94.

(240) Van Voorhis, T.; Head-Gordon, M. A geometric approach to direct minimization. *Mol. Phys.* **2002**, *100*, 1713–1721.

(241) Helgaker, T.; Klopper, W.; Koch, H.; Noga, J. Basis-set convergence of correlated calculations on water. *J. Chem. Phys.* **1998**, *106*, 9639.

(242) Mardirossian, N.; Head-Gordon, M. Thirty years of density functional theory in computational chemistry: an overview and extensive assessment of 200 density functionals. *Mol. Phys.* **2017**, *115*, 2315–2372.

(243) Halkier, A.; Klopper, W.; Helgaker, T.; Jørgensen, P.; Taylor, P. R. Basis set convergence of the interaction energy of hydrogen-bonded complexes. *J. Chem. Phys.* **1999**, *111*, 9157.

(244) Jung, Y.; Head-Gordon, M. How Diradicaloid Is a Stable Diradical? *ChemPhysChem* **2003**, *4*, 522–525.

(245) Abe, M. Diradicals. *Chem. Rev.* **2013**, *113*, 7011–7088.

(246) Yamaguchi, K.; Jensen, F.; Dorigo, A.; Houk, K. A spin correction procedure for unrestricted Hartree-Fock and Møller-Plesset wavefunctions for singlet diradicals and polyradicals. *Chem. Phys. Lett.* **1988**, *149*, 537–542.

(247) Yamaguchi, K.; Takahara, Y.; Fueno, T.; Houk, K. N. Extended Hartree-Fock (EHF) theory of chemical reactions. *Theor. Chim. Acta* **1988**, *73*, 337–364.

(248) Coulaud, E.; Guihéry, N.; Malrieu, J.-P.; Hagebaum-Reignier, D.; Siri, D.; Ferré, N. Analysis of the physical contributions to magnetic couplings in broken symmetry density functional theory approach. *J. Chem. Phys.* **2012**, *137*, 114106.

(249) Coulaud, E.; Malrieu, J.-P.; Guihéry, N.; Ferré, N. Additive Decomposition of the Physical Components of the Magnetic Coupling from Broken Symmetry Density Functional Theory Calculations. *J. Chem. Theory Comput.* **2013**, *9*, 3429–3436.

(250) Ferré, N.; Guihéry, N.; Malrieu, J.-P. Spin decontamination of broken-symmetry density functional theory calculations: deeper insight and new formulations. *Phys. Chem. Chem. Phys.* **2015**, *17*, 14375–14382.

(251) Lawler, K. V.; Small, D. W.; Head-Gordon, M. Orbitals That Are Unrestricted in Active Pairs for Generalized Valence Bond Coupled Cluster Methods. *J. Phys. Chem. A* **2010**, *114*, 2930–2938.

(252) Yanai, T.; Tew, D. P.; Handy, N. C. A new hybrid exchange-correlation functional using the Coulomb-attenuating method (CAM-B3LYP). *Chem. Phys. Lett.* **2004**, *393*, 51–57.

(253) Shiozaki, T.; Györffy, W.; Celani, P.; Werner, H.-J. Communication: Extended multi-state complete active space second-order perturbation theory: Energy and nuclear gradients. *J. Chem. Phys.* **2011**, *135*, 081106.

(254) Weigend, F.; Ahlrichs, R. Balanced basis sets of split valence, triple zeta valence and quadruple zeta valence quality for H to Rn: Design and assessment of accuracy. *Phys. Chem. Chem. Phys.* **2005**, *7*, 3297.

(255) Hättig, C. Optimization of auxiliary basis sets for RI-MP2 and RI-CC2 calculations: Core-valence and quintuple-ζ basis sets for H to Ar and QZVPP basis sets for Li to Kr. *Phys. Chem. Chem. Phys.* **2005**, *7*, 59–66.

(256) Krylov, A. I.; Sherrill, C. D.; Byrd, E. F. C.; Head-Gordon, M. Size-consistent wave functions for nondynamical correlation energy: The valence active space optimized orbital coupled-cluster doubles model. *J. Chem. Phys.* **1998**, *109*, 10669–10678.

(257) Pulay, P.; Hamilton, T. P. UHF natural orbitals for defining and starting MC-SCF calculations. *J. Chem. Phys.* **1988**, *88*, 4926–4933.

(258) Bofill, J. M.; Pulay, P. The unrestricted natural orbital-complete active space (UNO-CAS) method: An inexpensive alternative to the complete active space-self-consistent-field (CAS-SCF) method. *J. Chem. Phys.* **1989**, *90*, 3637–3646.

(259) Small, D.; Zaitsev, V.; Jung, Y.; Rosokha, S. V.; Head-Gordon, M.; Kochi, J. K. Intermolecular π-to-π Bonding between Stacked Aromatic Dyads. Experimental and Theoretical Binding Energies and Near-IR Optical Transitions for Phenalenyl Radical/Radical versus Radical/Cation Dimerizations. *J. Am. Chem. Soc.* **2004**, *126*, 13850–13858.

(260) Small, D.; Rosokha, S. V.; Kochi, J. K.; Head-Gordon, M. Characterizing the Dimerizations of Phenalenyl Radicals by ab Initio Calculations and Spectroscopy:σ-Bond Formation versus Resonance π-Stabilization. *J. Phys. Chem. A* **2005**, *109*, 11261–11267.

(261) Lykos, P.; Pratt, G. W. Discussion on The Hartree-Fock Approximation. *Rev. Mod. Phys.* **1963**, *35*, 496–501.

(262) Yamanaka, S.; Okumura, M.; Nakano, M.; Yamaguchi, K. EHF theory of chemical reactions Part 4. UNO CASSCF, UNO CASPT2 and R(U)HF coupled-cluster (CC) wavefunctions. *J. Mol. Struct.* **1994**, *310*, 205–218.

(263) Meyer, W. Theory of self-consistent electron pairs. An iterative method for correlated many-electron wavefunctions. *J. Chem. Phys.* **1976**, *64*, 2901–2907.

(264) Shavitt, I.; Rosenberg, B. J.; Palalikit, S. Comparison of configuration interaction expansions based on different orbital transformations. *Int. J. Quantum Chem.* **1976**, *10*, 33–46.

(265) Brueckner, K. A. Nuclear Saturation and Two-Body Forces. II. Tensor Forces. *Phys. Rev.* **1954**, *96*, 508–516.

(266) Nesbet, R. K. Brueckner's Theory and the Method of Superposition of Configurations. *Phys. Rev.* **1958**, *109*, 1632–1638.

(267) Sherrill, C. D.; Krylov, A. I.; Byrd, E. F. C.; Head-Gordon, M. Energies and analytic gradients for a coupled-cluster doubles model using variational Brueckner orbitals: Application to symmetry breaking in $O_4{}^+$. *J. Chem. Phys.* **1998**, *109*, 4171–4181.

(268) Kossmann, S.; Neese, F. Correlated ab Initio Spin Densities for Larger Molecules: Orbital-Optimized Spin-Component-Scaled MP2 Method. *J. Phys. Chem. A* **2010**, *114*, 11768–11781.

(269) Lee, J.; Head-Gordon, M. Regularized Orbital-Optimized Second-Order Møller-Plesset Perturbation Theory: A Reliable Fifth-Order-Scaling Electron Correlation Model with Orbital Energy Dependent Regularizers. *J. Chem. Theory Comput.* **2018**, *14*, 5203–5219.

(270) Fowler, P. W.; Manolopoulos, D. E., *An Atlas of Fullerenes (Dover Books on Chemistry)*; Dover Publications: 2007.

(271) Prinzbach, H.; Weiler, A.; Landenberger, P.; Wahl, F.; Wörth, J.; Scott, L. T.; Gelmont, M.; Olevano, D.; v. Issendorff, B. Gas-phase production and photoelectron spectroscopy of the smallest fullerene, C_{20}. *Nature* **2000**, *407*, 60–63.

(272) Jiménez-Hoyos, C. A.; Rodríguez-Guzmán, R.; Scuseria, G. E. Polyradical character and spin frustration in fullerene molecules: an ab initio non-collinear Hartree-Fock study. *J. Phys. Chem.. A* **2014**, *118*, 9925–40.

(273) Fukutome, H. Unrestricted Hartree-Fock theory and its applications to molecules and chemical reactions. *Int. J. Quantum Chem.* **1981**, *20*, 955–1065.

(274) Stuber, J. L.; Paldus, J. In, Brändas, E. J., Kryachko, E. S., Eds.; Springer: 2003; Vol. 1, pp 67–139.

(275) Yamaki, D.; Shigeta, Y.; Yamanaka, S.; Nagao, H.; Yamaguchi, K. MP2, Tamm-Dancoff, and RPA methods based on the generalized HF solution. *Int. J. Quantum Chem.* **2000**, *80*, 701–707.

(276) Jiménez-Hoyos, C. A.; Henderson, T. M.; Scuseria, G. E. Generalized Hartree-Fock Description of Molecular Dissociation. *J. Chem. Theory Comput.* **2011**, *7*, 2667–2674.

(277) Small, D. W.; Sundstrom, E. J.; Head-Gordon, M. A simple way to test for collinearity in spin symmetry broken wave functions: general theory and application to generalized Hartree Fock. *J. Chem. Phys.* **2015**, *142*, 094112.

(278) Cassam-Chenaï, P. Spin contamination and noncollinearity in general complex Hartree-Fock wave functions. *Theor. Chem. Acc.* **2015**, *134*, 125.

(279) Small, D. W.; Sundstrom, E. J.; Head-Gordon, M. Restricted Hartree Fock using complex-valued orbitals: a long-known but neglected tool in electronic structure theory. *J. Chem. Phys.* **2015**, *142*, 024104.

(280) Small, D. W.; Lawler, K. V.; Head-Gordon, M. Coupled Cluster Valence Bond Method: Efficient Computer Implementation and Application to Multiple Bond Dissociations and Strong Correlations in the Acenes. *J. Chem. Theory Comput.* **2014**, *10*, 2027–2040.

(281) Small, D. W.; Head-Gordon, M. Coupled cluster valence bond theory for open-shell systems with application to very long range strong correlation in a polycarbene dimer. *J. Chem. Phys.* **2017**, *147*, 024107.

(282) Head-Gordon, M. Characterizing unpaired electrons from the one-particle density matrix. *Chem. Phys. Lett.* **2003**, *372*, 508–511.

(283) Hunter, J. D. Matplotlib: A 2D Graphics Environment. *Comput. Sci. Eng.* **2007**, *9*, 90–95.

(284) `Chemcraft`., `https://www.chemcraftprog.com`, Accessed: 2017-10-31.

(285) Paul, P.; Kim, K.-C.; Sun, D.; Boyd, P. D. W.; Reed, C. A. Artifacts in the Electron Paramagnetic Resonance Spectra of C60Fullerene Ions: Inevitable C120O Impurity. *J. Am. Chem. Soc.* **2002**, *124*, 4394–4401.

(286) Tomita, S.; Andersen, J.; Hansen, K.; Hvelplund, P. Stability of Buckminsterfullerene, C_{60}. *Chem. Phys. Lett.* **2003**, *382*, 120–125.

(287) Hehre, W. J.; Stewart, R. F.; Pople, J. A. Self-Consistent Molecular-Orbital Methods. I. Use of Gaussian Expansions of Slater-Type Atomic Orbitals. *J. Chem. Phys.* **1969**, *51*, 2657–2664.

(288) Sassara, A.; Zerza, G.; Chergui, M. Phosphorescence of C_{60} in rare gas matrices. *Chem. Phys. Lett.* **1996**, *261*, 213–220.

(289) Varganov, S. A.; Avramov, P. V.; Ovchinnikov, S. G.; Gordon, M. S. A study of the isomers of C_{36} fullerene using single and multireference MP2 perturbation theory. *Chem. Phys. Lett.* **2002**, *362*, 380–386.

(290) Piskoti, C.; Yarger, J.; Zettl, A. C_{36}, a new carbon solid. *Nature* **1998**, *393*, 771–774.

(291) Fowler, P.; Heine, T.; Rogers, K.; Sandall, J.; Seifert, G.; Zerbetto, F. C_{36}, a hexavalent building block for fullerene compounds and solids. *Chem. Phys. Lett.* **1999**, *300*, 369–378.

(292) Fowler, P. W.; Mitchell, D.; Zerbetto, F. C_{36}: The Best Fullerene for Covalent Bonding. *Journal of the American Chemical Society* **1999**, *121*, 3218–3219.

(293) Jagadeesh, M. N.; Chandrasekhar, J. Computational studies on C_{36} and its dimer. *Chem. Phys. Lett.* **1999**, *305*, 298–302.

(294) Ito, A.; Monobe, T.; Yoshii, T.; Tanaka, K. Do C_{36} and $C_{36}H_6$ molecules have [36-D_{6h}]fullerene structure? *Chem. Phys. Lett.* **2000**, *328*, 32–38.

(295) Slanina, Z.; Uhlík, F.; Zhao, X.; Ōsawa, E. Enthalpy-entropy interplay for C_{36} cages: B3LYP/6-31G* calculations. *J. Chem. Phys.* **2000**, *113*, 4933.

(296) Yuan, L.-F.; Yang, J.; Deng, K.; Zhu, Q.-S. A First-Principles Study on the Structural and Electronic Properties of C36Molecules. *J. Phys. Chem. A* **2000**, *104*, 6666–6671.

(297) Paulus, B. Electronic and structural properties of the cage-like molecules C_{20} to C_{36}. *Phys. Chem. Chem. Phys.* **2003**, *5*, 3364.

(298) Becke, A. D. Density-functional exchange-energy approximation with correct asymptotic behavior. *Phys. Rev. A* **1988**, *38*, 3098–3100.

(299) Lee, C.; Yang, W.; Parr, R. G. Development of the Colle-Salvetti correlation-energy formula into a functional of the electron density. *Phys. Rev. B* **1988**, *37*, 785–789.

(300) Hariharan, P. C.; Pople, J. A. The influence of polarization functions on molecular orbital hydrogenation energies. *Theor. Chim. Acta.* **1973**, *28*, 213–222.

(301) Hehre, W. J.; Ditchfield, R.; Pople, J. A. Self—Consistent Molecular Orbital Methods. XII. Further Extensions of Gaussian—Type Basis Sets for Use in Molecular Orbital Studies of Organic Molecules. *J. Chem. Phys.* **1972**, *56*, 2257–2261.

(302) Schwerdtfeger, P.; Wirz, L. N.; Avery, J. The topology of fullerenes. *WIRES: Comput. Mol. Sci.* **2015**, *5*, 96–145.

(303) Parasuk, V.; Almlöf, J. C_{20}: the smallest fullerene? *Chem. Phys. Lett.* **1991**, *184*, 187–190.

(304) Feyereisen, M.; Gutowski, M.; Simons, J.; Almlöf, J. Relative stabilities of fullerene, cumulene, and polyacetylene structures for C_n: n=1860. *J. Chem. Phys.* **1992**, *96*, 2926–2932.

(305) Raghavachari, K.; Strout, D.; Odom, G.; Scuseria, G.; Pople, J.; Johnson, B.; Gill, P. Isomers of C_{20}. Dramatic effect of gradient corrections in density functional theory. *Chem. Phys. Lett.* **1993**, *214*, 357–361.

(306) Von Helden, G.; Hsu, M.; Gotts, N.; Kemper, P.; Bowers, M. Do small fullerenes exist only on the computer? Experimental results on ${C_{20}}^{+/-}$ and ${C_{24}}^{+/-}$. *Chem. Phys. Lett.* **1993**, *204*, 15–22.

(307) Bylaska, E. J.; Taylor, P. R.; Kawai, R.; Weare, J. H. LDA Predictions of C_{20} Isomerizations: Neutral and Charged Species. *J. Phys. Chem.* **1996**, *100*, 6966–6972.

(308) Martin, J. M.; El-Yazal, J.; François, J.-P. On the structure and vibrational frequencies of C_{20}. *Chem. Phys. Lett.* **1996**, *248*, 345–352.

(309) Jones, R. O.; Seifert, G. Structure and Bonding in Carbon Clusters C_{14} to C_{24}: Chains, Rings, Bowls, Plates, and Cages. *Phys. Rev. Lett.* **1997**, *79*, 443–446.

(310) Kietzmann, H.; Rochow, R.; Ganteför, G.; Eberhardt, W.; Vietze, K.; Seifert, G.; Fowler, P. W. Electronic Structure of Small Fullerenes: Evidence for the High Stability of C_{32}. *Phys. Rev. Lett.* **1998**, *81*, 5378–5381.

(311) Sokolova, S.; Lüchow, A.; Anderson, J. B. Energetics of carbon clusters C_{20} from all-electron quantum Monte Carlo calculations. *Chem. Phys. Lett.* **2000**, *323*, 229–233.

(312) Grimme, S.; Mück-Lichtenfeld, C. Structural isomers of C_{20} revisited: The cage and bowl are almost isoenergetic. *ChemPhysChem* **2002**, *3*, 207–209.

(313) Lu, J.; Re, S.; Choe, Y.-k.; Nagase, S.; Zhou, Y.; Han, R.; Peng, L.; Zhang, X.; Zhao, X. Theoretical identification of C_{20} carbon clusters: Prevalence of the monocyclic isomer and existence of the smallest fullerene and bowl isomer. *Phys. Rev. B* **2003**, *67*, 125415.

(314) An, W.; Gao, Y.; Bulusu, S.; Zeng, X. C. Ab initio calculation of bowl, cage, and ring isomers of C_{20} and C_{20}^{-}. *J. Chem. Phys.* **2005**, *122*, 204109.

(315) Jin, Y.; Perera, A.; Lotrich, V. F.; Bartlett, R. J. Coupled cluster geometries and energies of C_{20} carbon cluster isomers - A new benchmark study. *Chem. Phys. Lett.* **2015**, *629*, 76–80.

(316) Manna, D.; Martin, J. M. L. What Are the Ground State Structures of C_{20} and C_{24}? An Explicitly Correlated Ab Initio Approach. *J. Phys. Chem. A* **2016**, *120*, 153–160.

(317) Adams, G. B.; Sankey, O. F.; Page, J. B.; O'Keeffe, M. Jahn-Teller distortions in solid C_{20} and other fullerene structures. *Chem. Phys.* **1993**, *176*, 61–66.

(318) Krylov, A. I. Size-consistent wave functions for bond-breaking: the equation-of-motion spin-flip model. *Chem. Phys. Lett.* **2001**, *338*, 375–384.

(319) Fan, M.-F.; Lin, Z.; Yang, S. Closed-shell electronic requirements for small fullerene cage structures. *J. Mol. Struc-THEOCHEM* **1995**, *337*, 231–240.

(320) Prinzbach, H.; Wahl, F.; Weiler, A.; Landenberger, P.; Wörth, J.; Scott, L. T.; Gelmont, M.; Olevano, D.; Sommer, F.; von Issendorff, B. C_{20} Carbon Clusters: Fullerene-Boat-Sheet Generation, Mass Selection, Photoelectron Characterization. *Chem.-Eur. J.* **2006**, *12*, 6268–6280.

(321) Handy, N. C.; Cohen, A. J. Left-right correlation energy. *Mol. Phys.* **2001**, *99*, 403–412.

(322) Hollett, J. W.; Gill, P. M. W. The two faces of static correlation. *J. Chem. Phys.* **2011**, *134*, 114111.

(323) Hollett, J. W.; McKemmish, L. K.; Gill, P. M. W. The nature of electron correlation in a dissociating bond. *J. Chem. Phys.* **2011**, *134*, 224103.

(324) Atanasov, M.; Aravena, D.; Suturina, E.; Bill, E.; Maganas, D.; Neese, F. First principles approach to the electronic structure, magnetic anisotropy and spin relaxation in mononuclear 3d-transition metal single molecule magnets. *Coord. Chem. Rev.* **2015**, *289-290*, 177–214.

(325) Mayhall, N. J.; Head-Gordon, M. Computational Quantum Chemistry for Multiple-Site Heisenberg Spin Couplings Made Simple: Still Only One Spin-Flip Required. *J. Phys. Chem. Lett.* **2015**, *6*, 1982–1988.

(326) Ungur, L.; Chibotaru, L. F. Strategies toward High-Temperature Lanthanide-Based Single-Molecule Magnets. *Inorg. Chem.* **2016**, *55*, 10043–10056.

(327) Frost, J. M.; Harriman, K. L. M.; Murugesu, M. The rise of 3-d single-ion magnets in molecular magnetism: towards materials from molecules? *Chem. Sci.* **2016**, *7*, 2470–2491.

(328) Ward, M. D.; McCleverty, J. A. Non-innocent behaviour in mononuclear and polynuclear complexes: consequences for redox and electronic spectroscopic properties. *Dalton Trans.* **2002**, 275–288.

(329) Butschke, B.; Fillman, K. L.; Bendikov, T.; Shimon, L. J. W.; Diskin-Posner, Y.; Leitus, G.; Gorelsky, S. I.; Neidig, M. L.; Milstein, D. How Innocent are Potentially Redox Non-Innocent Ligands? Electronic Structure and Metal Oxidation States in Iron-PNN Complexes as a Representative Case Study. *Inorg. Chem.* **2015**, *54*, 4909–4926.

(330) Bendikov, M.; Duong, H. M.; Starkey, K.; Houk, K. N.; Carter, E. A.; Wudl, F. Oligoacenes: Theoretical Prediction of Open-Shell Singlet Diradical Ground States. *J. Am. Chem. Soc.* **2004**, *126*, 7416–7417.

(331) Schriber, J. B.; Hannon, K. P.; Li, C.; Evangelista, F. A. A Combined Selected Configuration Interaction and Many-Body Treatment of Static and Dynamical Correlation in Oligoacenes. *J. Chem. Theory Comput.* **2018**, *14*, 6295–6305.

(332) Mullinax, J. W.; Epifanovsky, E.; Gidofalvi, G.; DePrince, A. E. Analytic Energy Gradients for Variational Two-Electron Reduced-Density Matrix Methods within the Density Fitting Approximation. *J. Chem. Theory Comput.* **2019**, *15*, 276–289.

(333) Salem, L.; Rowland, C. The Electronic Properties of Diradicals. *Angew. Chem. Int. Ed. Engl.* **1972**, *11*, 92–111.

(334) Slipchenko, L. V.; Krylov, A. I. Singlet-triplet gaps in diradicals by the spin-flip approach: A benchmark study. *J. Chem. Phys.* **2002**, *117*, 4694–4708.

(335) Scheschkewitz, D.; Amii, H.; Gornitzka, H.; Schoeller, W. W.; Bourissou, D.; Bertrand, G. Singlet diradicals: From transition states to crystalline compounds. *Science* **2002**, *295*, 1880–1881.

(336) Bachler, V.; Olbrich, G.; Neese, F.; Wieghardt, K. Theoretical evidence for the singlet diradical character of square planar nickel complexes containing two o-semiquinonato type ligands. *Inorg. Chem.* **2002**, *41*, 4179–4193.

(337) Kamada, K.; Ohta, K.; Shimizu, A.; Kubo, T.; Kishi, R.; Takahashi, H.; Botek, E.; Champagne, B.; Nakano, M. Singlet diradical character from experiment. *J. Phys. Chem. Lett.* **2010**, *1*, 937–940.

(338) Roos, B. O.; Taylor, P. R.; Sigbahn, P. E. A complete active space SCF method (CASSCF) using a density matrix formulated super-CI approach. *Chem. Phys.* **1980**, *48*, 157–173.

(339) Ruedenberg, K.; Schmidt, M. W.; Gilbert, M. M.; Elbert, S. Are atoms intrinsic to molecular electronic wavefunctions? I. The FORS model. *Chem. Phys.* **1982**, *71*, 41–49.

(340) Nakano, H. Quasidegenerate perturbation theory with multiconfigurational selfconsistentfield reference functions. *J. Chem. Phys.* **1993**, *99*, 7983–7992.

(341) Krylov, A. I. Spin-flip configuration interaction: an electronic structure model that is both variational and size-consistent. *Chem. Phys. Lett.* **2001**, *350*, 522–530.

(342) Shao, Y.; Head-Gordon, M.; Krylov, A. I. The spinflip approach within time-dependent density functional theory: Theory and applications to diradicals. *J. Chem. Phys.* **2003**, *118*, 4807–4818.

(343) Mayhall, N. J.; Horn, P. R.; Sundstrom, E. J.; Head-Gordon, M. Spinflip non-orthogonal configuration interaction: a variational and almost black-box method for describing strongly correlated molecules. *Phys. Chem. Chem. Phys.* **2014**, *16*, 22694–22705.

(344) Mato, J.; Gordon, M. S. A general spin-complete spin-flip configuration interaction method. *Phys. Chem. Chem. Phys.* **2018**, *20*, 2615–2626.

(345) Krylov, A. I. Equation-of-Motion Coupled-Cluster Methods for Open-Shell and Electronically Excited Species: The Hitchhiker's Guide to Fock Space. *Ann. Rev. Phys. Chem.* **2008**, *59*, 433–462.

(346) Kitagawa, Y.; Saito, T.; Ito, M.; Shoji, M.; Koizumi, K.; Yamanaka, S.; Kawakami, T.; Okumura, M.; Yamaguchi, K. Approximately spin-projected geometry optimization method and its application to di-chromium systems. *Chem. Phys. Lett.* **2007**, *442*, 445–450.

(347) Saito, T.; Nishihara, S.; Kataoka, Y.; Nakanishi, Y.; Matsui, T.; Kitagawa, Y.; Kawakami, T.; Okumura, M.; Yamaguchi, K. Transition state optimization based on approximate spin-projection (AP) method. *Chem. Phys. Lett.* **2009**, *483*, 168–171.

(348) Nakano, M.; Minami, T.; Fukui, H.; Yoneda, K.; Shigeta, Y.; Kishi, R.; Champagne, B.; Botek, E. Approximate spin-projected spin-unrestricted density functional theory method: Application to the diradical character dependences of the (hyper)polarizabilities in p-quinodimethane models. *Chem. Phys. Lett.* **2010**, *501*, 140–145.

(349) Mak, A. M.; Lawler, K. V.; Head-Gordon, M. Approximate spin-projected broken symmetry energies from optimized orbitals that are unrestricted in active pairs. *Chem. Phys. Lett.* **2011**, *515*, 173–178.

(350) Saito, T.; Thiel, W. Analytical Gradients for Density Functional Calculations with Approximate Spin Projection. *J. Phys. Chem. A* **2012**, *116*, 10864–10869.

(351) Hratchian, H. P. Communication: An efficient analytic gradient theory for approximate spin projection methods. *J. Chem. Phys.* **2013**, *138*, 101101.

(352) Thompson, L. M.; Hratchian, H. P. Modeling the Photoelectron Spectra of $MoNbO_2^-$ Accounting for Spin Contamination in Density Functional Theory. *J. Phys. Chem. A* **2015**, *119*, 8744–8751.

(353) Radom, L.; Hariharan, P. C.; Pople, J. A.; Schleyer, P. V. R. Molecular orbital theory of the electronic structure of organic compounds. XIX. Geometries and energies of C_3H_5 cations. Energy relations among allyl, vinyl, and cyclopropyl cations. *J. Am. Chem. Soc.* **1973**, *95*, 6531–6544.

(354) Fukutome, H. The Unrestricted Hartree-Fock Theory of Chemical Reactions. III: Instability Conditions for Paramagnetic and Spin Density Wave States and Application to Internal Rotation of Ethylene. *Progr. Theor. Phys.* **1973**, *50*, 1433–1451.

(355) Haddon, R. C.; Poppinger, D.; Radom, L. Ab initio molecular orbital study of ethylenedione (O.dbd.C.dbd.C.dbd.O). *J. Am. Chem. Soc.* **1975**, *97*, 1645–1649.

(356) Dill, J. D.; Schleyer, P. v. R.; Pople, J. A. Molecular orbital theory of the electron structure of organic compounds. XXIV. Geometries and energies of small boron compounds. Comparisons with carbocations. *J. Am. Chem. Soc.* **1975**, *97*, 3402–3409.

(357) Böhm, M. C. On the non-validity of the hartree-fock picture in metallocenes. *Chem. Phys. Lett.* **1981**, *83*, 533–538.

(358) Böhm, M. C. Electron Correlation in Weakly Coupled Transition Metal Compounds: Poly-Decker Systems. *Ber. Bunsegenes. Phys. Chem.* **1981**, *85*, 755–768.

(359) Böhm, M. C. Symmetry breaking in the Hartree-Fock approximation for binuclear transition metal compounds-a theoretical investigation based on a variable model operator. *Int. J. Quantum Chem.* **1983**, *24*, 185–237.

(360) Krogh-Jespersen, K. Structural and energetic features of fully substituted silylenes, disilenes, and silylsilylenes (SiX_2, X_2SiSiX_2, and $XSiSiX_3$; X = Li, CH_3, and F). *J. Am. Chem. Soc.* **1985**, *107*, 537–543.

(361) Mains, G. J.; Bock, C. W.; Trachtman, M. Theoretical structures for boron-silicon fluorohydrides. *J. Phys. Chem.* **1990**, *94*, 5449–5454.

(362) Goddard, W. A.; Dunning, T. H.; Hunt, W. J.; Hay, P. J. Generalized Valence Bond Description of Bonding in Low-Lying States of Molecules. *Acc. Chem. Res.* **1973**, *6*, 368–376.

(363) Lee, J.; Head-Gordon, M. Distinguishing artificial and essential symmetry breaking in a single determinant: Approach and application to the C 60, C 36, and C 20 fullerenes. *Phys. Chem. Chem. Phys.* **2019**, *21*, 4763–4778.

(364) NIST Chemistry WebBook., `https://webbook.nist.gov/chemistry/`, Accessed: 2019-02-01.

(365) Holmes, A. A.; Tubman, N. M.; Umrigar, C. J. Heat-Bath Configuration Interaction: An Efficient Selected Configuration Interaction Algorithm Inspired by Heat-Bath Sampling. *J. Chem. Theory Comput.* **2016**, *12*, 3674–3680.

(366) Kendall, R. A.; Dunning, T. H.; Harrison, R. J. Electron affinities of the first-row atoms revisited. Systematic basis sets and wave functions. *J. Chem. Phys.* **1992**, *96*, 6796–6806.

(367) Ogilby, P. R. Singlet oxygen: there is indeed something new under the sun. *Chem. Soc. Rev.* **2010**, *39*, 3181.

(368) Davies, M. J. Reactive species formed on proteins exposed to singlet oxygen. *Photochem. Photobiol. Sci.* **2004**, *3*, 17.

(369) Mardirossian, N.; Head-Gordon, M. ωB97X-V: A 10-parameter, range-separated hybrid, generalized gradient approximation density functional with nonlocal correlation, designed by a survival-of-the-fittest strategy. *Phys. Chem. Chem. Phys.* **2014**, *16*, 9904.

(370) Mardirossian, N.; Head-Gordon, M. ωB97M-V: A combinatorially optimized, range-separated hybrid, meta-GGA density functional with VV10 nonlocal correlation. *J. Chem. Phys.* **2016**, *144*, 214110.

(371) Zhang, B. L.; Wang, C. Z.; Ho, K. M.; Xu, C. H.; Chan, C. T. The geometry of small fullerene cages: C_{20} to C_{70}. *J. Chem. Phys.* **1992**, *97*, 5007–5011.

(372) Mardirossian, N.; Head-Gordon, M. Mapping the genome of meta-generalized gradient approximation density functionals: The search for B97M-V. *J. Chem. Phys.* **2015**, *142*, 074111.

(373) Gallagher, N. M.; Bauer, J. J.; Pink, M.; Rajca, S.; Rajca, A. High-Spin Organic Diradical with Robust Stability. *J. Am. Chem. Soc.* **2016**, *138*, 9377–9380.

(374) Rajca, A. Organic Diradicals and Polyradicals: From Spin Coupling to Magnetism? *Chem. Rev.* **1994**, *94*, 871–893.

(375) Gallagher, N.; Zhang, H.; Junghoefer, T.; Giangrisostomi, E.; Ovsyannikov, R.; Pink, M.; Rajca, S.; Casu, M. B.; Rajca, A. Thermally and Magnetically Robust Triplet Ground State Diradical. *J. Am. Chem. Soc.* **2019**, jacs.9b00558.

(376) Haris, K.; Kramida, A. Critically Evaluated Spectral Data for Neutral Carbon. *Astrophys. J. Suppl. S.* **2017**, *233*, 16.

(377) Martin, W. C.; Zalubas, R. Energy levels of silicon, Si I through Si XIV. *J. Phys. Chem. Ref. Data* **1983**, *12*, 323–380.

(378) *Tables of Spectra of Hydrogen, Carbon, Nitrogen, and Oxygen Atoms and Ions (Evaluated Data in Atomic Physics)*; CRC Press: 1993.

(379) Martin, W. C.; Zalubas, R.; Musgrove, A. Energy Levels of Sulfur, S I through S XVI. *J. Phys. Chem. Ref. Data* **1990**, *19*, 821–880.

(380) Kardahakis, S.; Pittner, J.; Čársky, P.; Mavridis, A. Multireference configuration interaction and coupled-cluster calculations on the $X^3\Sigma^-$, $a^1\Delta$, and $b^1\Sigma+$ states of the NF molecule. *International Journal of Quantum Chemistry* **2005**, *104*, 458–467.

(381) Krishnamurty, G.; Narasimham, N. Predissociations in the d $^1\Sigma^+$-c$^1\Pi$ bands of NH. *J. Mol. Spectrosc.* **1969**, *29*, 410–414.

(382) Siegel, M. W.; Celotta, R. J.; Hall, J. L.; Levine, J.; Bennett, R. A. Molecular Photodetachment Spectrometry. I. The Electron Affinity of Nitric Oxide and the Molecular Constants of NO-. *Phys. Rev. A* **1972**, *6*, 607–631.

(383) Teillet-Billy, D.; Fiquet-Fayard, F. The NO^- $^3\Sigma^-$ and $^1\Delta$ resonances: theoretical analysis of electron scattering data. *J. Phys. B* **1977**, *10*, L111–L117.

(384) Krupenie, P. H. The Spectrum of Molecular Oxygen. *J. Phys. Chem. Ref. Data* **1972**, *1*, 423–534.

(385) Douglas, A. E.; Frackowiak, M. The Electronic Spectra of PF and PF^+. *Can. J. Phys.* **1962**, *40*, 832–849.

(386) Rostas, J.; Cossart, D.; Bastien, J. R. Rotational Analysis of the PH and PD $A^3\Pi i$–$X^3\Sigma^-$ Band Systems. *Can. J. Phys.* **1974**, *52*, 1274–1287.

(387) Balfour, W. J.; Douglas, A. E. The absorption spectrum of PH in the vacuum ultraviolet. *Can. J. Phys.* **1968**, *46*, 2277–2280.

(388) Swope, W. C.; Lee, Y.-P.; Schaefer, H. F. Diatomic sulfur: Low lying bound molecular electronic states of S_2. *J. Chem. Phys.* **1979**, *70*, 947.

(389) Clark, W. W.; Lucia, F. C. D. The microwave spectrum and rotational structure of the $^1\Delta$ and $^3\Sigma$ electronic states of sulfur monoxide. *J. Mol. Spectrosc.* **1976**, *60*, 332–342.

(390) Saito, S. Microwave Spectrum of the SO Radical in the First Electronically Excited State, $^1\Delta$. *J. Chem. Phys.* **1970**, *53*, 2544–2545.

(391) Smith, J. E.; Mussard, B.; Holmes, A. A.; Sharma, S. Cheap and near exact CASSCF with large active spaces. *J. Chem. Theory Comput.* **2017**, *13*, 5468–5478.

(392) Blomberg, M. R. A.; Borowski, T.; Himo, F.; Liao, R.-Z.; Siegbahn, P. E. M. Quantum Chemical Studies of Mechanisms for Metalloenzymes. *Chem. Rev.* **2014**, *114*, 3601–3658.

(393) McEvoy, J. P.; Brudvig, G. W. Water-Splitting Chemistry of Photosystem II. *Chem. Rev.* **2006**, *106*, 4455–4483.

(394) Mukhopadhyay, S.; Mandal, S. K.; Bhaduri, S.; Armstrong, W. H. Manganese Clusters with Relevance to Photosystem II. *Chem. Rev.* **2004**, *104*, 3981–4026.

(395) Savéant, J.-M. Electron transfer, bond breaking and bond formation. *Adv. Phys. Org. Chem.* **2000**, *35*, 117–192.

(396) Huang, R.; Phan, H.; Herng, T. S.; Hu, P.; Zeng, W.; Dong, S.-q.; Das, S.; Shen, Y.; Ding, J.; Casanova, D.; Wu, J. Higher Order π-Conjugated Polycyclic Hydrocarbons with Open-Shell Singlet Ground State: Nonazethrene versus Nonacene. *J. Am. Chem. Soc* **2016**, *138*, 10323–10330.

(397) Hinkel, F.; Freudenberg, J.; Bunz, U. H. A Stable π-Conjugated Singlet Biradical. *Angew. Chem. Int. Ed. Engl.* **2016**, *55*, 9830–9832.

(398) Trinquier, G.; Malrieu, J.-P. Kekulé versus Lewis: When Aromaticity Prevents Electron Pairing and Imposes Polyradical Character. *Chem. Eur. J* **2015**, *21*, 814–828.

(399) Sadowsky, D.; McNeill, K.; Cramer, C. J. Electronic structures of [n]-cyclacenes (n = 6-12) and short, hydrogen-capped, carbon nanotubes. *Farad. Discuss.* **2010**, *145*, 507–521.

(400) Dai, P. Antiferromagnetic order and spin dynamics in iron-based superconductors. *Rev. Mod. Phys.* **2015**, *87*, 855–896.

(401) Georges, A.; Kotliar, G.; Krauth, W.; Rozenberg, M. J. Dynamical mean-field theory of strongly correlated fermion systems and the limit of infinite dimensions. *Rev. Mod. Phys.* **1996**, *68*, 13–125.

(402) Booth, G. H.; Thom, A. J. W.; Alavi, A. Fermion Monte Carlo without fixed nodes: a game of life, death, and annihilation in Slater determinant space. *J. Chem. Phys.* **2009**, *131*, 054106.

(403) Cleland, D.; Booth, G. H.; Alavi, A. Communications: Survival of the fittest: accelerating convergence in full configuration-interaction quantum Monte Carlo. *J. Chem. Phys.* **2010**, *132*, 041103.

(404) White, S. R. Density-matrix algorithms for quantum renormalization groups. *Phys. Rev. B* **1993**, *48*, 10345–10356.

(405) White, S. R.; Martin, R. L. Ab initio quantum chemistry using the density matrix renormalization group. *J. Chem. Phys.* **1999**, *110*, 4127.

(406) Knowles, P.; Handy, N. A new determinant-based full configuration interaction method. *Chem. Phys. Lett.* **1984**, *111*, 315–321.

(407) Knowles, P. J.; Handy, N. C. A determinant based full configuration interaction program. *Comput. Phys. Commun.* **1989**, *54*, 75–83.

(408) Daday, C.; Smart, S.; Booth, G. H.; Alavi, A.; Filippi, C. Full Configuration Interaction Excitations of Ethene and Butadiene: Resolution of an Ancient Question. *J. Chem. Theory Comput.* **2012**, *8*, 4441–4451.

(409) Cleland, D.; Booth, G. H.; Overy, C.; Alavi, A. Taming the First-Row Diatomics: A Full Configuration Interaction Quantum Monte Carlo Study. *J. Chem. Theory Comput.* **2012**, *8*, 4138–4152.

(410) Thomas, R. E.; Booth, G. H.; Alavi, A. Accurate AbInitio Calculation of Ionization Potentials of the First-Row Transition Metals with the Configuration-Interaction Quantum MonteCarlo Technique. *Phys. Rev. Lett.* **2015**, *114*, 033001.

(411) Bartlett, R. J.; Musiał, M. Coupled-cluster theory in quantum chemistry. *Rev. Mod. Phys.* **2007**, *79*, 291–352.

(412) Lyakh, D. I.; Musiał, M.; Lotrich, V. F.; Bartlett, R. J. Multireference Nature of Chemistry: The Coupled-Cluster View. *Chem. Rev.* **2012**, *112*, 182–243.

(413) Köhn, A.; Hanauer, M.; Mück, L. A.; Jagau, T.-C.; Gauss, J. State-specific multireference coupled-cluster theory. *Wiley Interdiscip. Rev. Comput. Mol. Sci.* **2013**, *3*, 176–197.

(414) Schucan, T.; Weidenmüller, H. The effective interaction in nuclei and its perturbation expansion: An algebraic approach. *Ann. Phys.* **1972**, *73*, 108–135.

(415) Kaldor, U. Intruder states and incomplete model spaces in multireference coupled-cluster theory: The $2p^2$ states of Be. *Phys. Rev. A* **1988**, *38*, 6013–6016.

(416) Malrieu, J. P.; Durand, P.; Daudey, J. P. Intermediate Hamiltonians as a new class of effective Hamiltonians. *J. Phys. A: Math. Gen.* **1985**, *18*, 809–826.

(417) Jankowski, K.; Malinowski, P. A valence-universal coupled-cluster single- and double-excitations method for atoms. III. Solvability problems in the presence of intruder states. *J. Phys. B: At., Mol. Opt. Phys.* **1994**, *27*, 1287–1298.

(418) Raghavachari, K.; Trucks, G. W.; Pople, J. A.; Head-Gordon, M. A fifth-order perturbation comparison of electron correlation theories. *Chem. Phys. Lett.* **1989**, *157*, 479–483.

(419) Taube, A. G.; Bartlett, R. J. Improving upon CCSD(T): ΛCCSD(T). I. Potential energy surfaces. *J. Chem. Phys.* **2008**, *128*, 044110.

(420) Włoch, M.; Gour, J. R.; Piecuch, P. Extension of the Renormalized Coupled-Cluster Methods Exploiting Left Eigenstates of the Similarity-Transformed Hamiltonian to Open-Shell Systems:A Benchmark Study. *J. Phys. Chem. A* **2007**, *111*, 11359–11382.

(421) Kowalski, K.; Piecuch, P. A comparison of the renormalized and active-space coupled-cluster methods: Potential energy curves of BH and F_2. *Chem. Phys. Lett.* **2001**, *344*, 165–175.

(422) Piecuch, P.; Kowalski, K.; Pimienta, I. S. O.; Fan, P.-D.; Lodriguito, M.; McGuire, M. J.; Kucharski, S. A.; Kuś, T.; Musiał, M. Method of moments of coupled-cluster equations: a new formalism for designing accurate electronic structure methods for ground and excited states. *Theor. Chem. Acc.* **2004**, *112*, 349–393.

(423) Kowalski, K.; Piecuch, P. Renormalized CCSD(T) and CCSD(TQ) approaches: Dissociation of the N_2 triple bond. *J. Chem. Phys.* **2000**, *113*, 5644.

(424) Piecuch, P.; Kowalski, K.; Pimienta, I. S.; McGuire, M. J. Recent advances in electronic structure theory: Method of moments of coupled-cluster equations and renormalized coupled-cluster approaches. *Int. Rev. Phys. Chem.* **2002**, *21*, 527–655.

(425) Piecuch, P.; Włoch, M. Renormalized coupled-cluster methods exploiting left eigenstates of the similarity-transformed Hamiltonian. *J. Chem. Phys.* **2005**, *123*, 224105.

(426) Kowalski, K.; Piecuch, P. The method of moments of coupled-cluster equations and the renormalized CCSD[T], CCSD(T), CCSD(TQ), and CCSDT(Q) approaches. *J. Chem. Phys.* **2000**, *113*, 18.

(427) Piecuch, P.; Kucharski, S. A.; Kowalski, K.; Musiał, M. Efficient computer implementation of the renormalized coupled-cluster methods: The R-CCSD[T], R-CCSD(T), CR-CCSD[T], and CR-CCSD(T) approaches. *Comput. Phys. Commun.* **2002**, *149*, 71–96.

(428) Kowalski, K.; Piecuch, P. New coupled-cluster methods with singles, doubles, and noniterative triples for high accuracy calculations of excited electronic states. *J. Chem. Phys.* **2004**, *120*, 1715.

(429) Van Voorhis, T.; Head-Gordon, M. Benchmark variational coupled cluster doubles results. *J. Chem. Phys.* **2000**, *113*, 8873.

(430) Cooper, B.; Knowles, P. J. Benchmark studies of variational, unitary and extended coupled cluster methods. *J. Chem. Phys.* **2010**, *133*, 234102.

(431) Bartlett, R. J.; Noga, J. The expectation value coupled-cluster method and analytical energy derivatives. *Chem. Phys. Lett.* **1988**, *150*, 29–36.

(432) Hoffmann, M. R.; Simons, J. A unitary multiconfigurational coupled-cluster method: Theory and applications. *J. Chem. Phys.* **1988**, *88*, 993.

(433) Pal, S. Use of a unitary wavefunction in the calculation of static electronic properties. *Theor. Chim. Acta* **1984**, *66*, 207–215.

(434) Bartlett, R. J.; Kucharski, S. A.; Noga, J. Alternative coupled-cluster ansätze II. The unitary coupled-cluster method. *Chem. Phys. Lett.* **1989**, *155*, 133–140.

(435) Watts, J. D.; Trucks, G. W.; Bartlett, R. J. The unitary coupled-cluster approach and molecular properties. Applications of the UCC(4) method. *Chem. Phys. Lett.* **1989**, *157*, 359–366.

(436) Pal, S. Bivariational coupled-cluster approach for the study of static electronic properties. *Phys. Rev. A* **1986**, *34*, 2682–2686.

(437) Basu Kumar, A.; Vaval, N.; Pal, S. An extended coupled-cluster functional for molecular properties: study of an analytical and numerical approach. *Chem. Phys. Lett.* **1998**, *295*, 189–194.

(438) Manohar, P. U.; Vaval, N.; Pal, S. Extended coupled-cluster approach for magnetizabilities of small molecules. *Chem. Phys. Lett.* **2004**, *387*, 442–447.

(439) Fan, P.-D.; Kowalski, K.; Piecuch, P. Non-iterative corrections to extended coupled-cluster energies employing the generalized method of moments of coupled-cluster equations. *Mol. Phys.* **2005**, *103*, 2191–2213.

(440) Fan, P.-D.; Piecuch, P. The Usefulness of Exponential Wave Function Expansions Employing One- and Two-Body Cluster Operators in Electronic Structure Theory: The Extended and Generalized Coupled-Cluster Methods. *Adv. Quantum Chem.* **2006**, *51*, 1–57.

(441) Arponen, J. Variational principles and linked-cluster exp S expansions for static and dynamic many-body problems. *Ann. Phys.* **1983**, *151*, 311–382.

(442) Van Voorhis, T.; Head-Gordon, M. The quadratic coupled cluster doubles model. *Chem. Phys. Lett.* **2000**, *330*, 585–594.

(443) Byrd, E. F. C.; Van Voorhis, T.; Head-Gordon, M. Quadratic Coupled-Cluster Doubles: Implementation and Assessment of Perfect Pairing Optimized Geometries. *J. Phys. Chem. B* **2002**, *106*, 8070–8077.

(444) Gwaltney, S. R.; Byrd, E. F.; Van Voorhis, T.; Head-Gordon, M. A perturbative correction to the quadratic coupled-cluster doubles method for higher excitations. *Chem. Phys. Lett.* **2002**, *353*, 359–367.

(445) Noga, J.; Bartlett, R. J. The full CCSDT model for molecular electronic structure. *J. Chem. Phys.* **1987**, *86*, 7041.

(446) Oliphant, N.; Adamowicz, L. Coupled-cluster method truncated at quadruples. *J. Chem. Phys.* **1991**, *95*, 6645.

(447) Parkhill, J. A.; Lawler, K.; Head-Gordon, M. The perfect quadruples model for electron correlation in a valence active space. *J. Chem. Phys.* **2009**, *130*, 084101.

(448) Parkhill, J. A.; Head-Gordon, M. A tractable and accurate electronic structure method for static correlations: the perfect hextuples model. *J. Chem. Phys.* **2010**, *133*, 024103.

(449) Parkhill, J. A.; Azar, J.; Head-Gordon, M. The formulation and performance of a perturbative correction to the perfect quadruples model. *J. Chem. Phys.* **2011**, *134*, 154112.

(450) Lehtola, S.; Parkhill, J.; Head-Gordon, M. Cost-effective description of strong correlation: Efficient implementations of the perfect quadruples and perfect hextuples models. *J. Chem. Phys.* **2016**, *145*, 134110.

(451) Krylov, A. I. Spin-Flip Equation-of-Motion Coupled-Cluster Electronic Structure Method for a Description of Excited States, Bond Breaking, Diradicals, and Triradicals. *Acc. Chem. Res.* **2006**, *39*, 83–91.

(452) Paldus, J.; Čížek, J.; Takahashi, M. Approximate account of the connected quadruply excited clusters in the coupled-pair many-electron theory. *Phys. Rev. A* **1984**, *30*, 2193–2209.

(453) Paldus, J.; Takahashi, M.; Cho, R. W. H. Coupled-cluster approach to electron correlation in one dimension: Cyclic polyene model in delocalized basis. *Phys. Rev. B* **1984**, *30*, 4267–4291.

(454) Jankowski, K.; Paldus, J. Applicability of coupled-pair theories to quasidegenerate electronic states: A model study. *Int. J. Quantum Chem.* **1980**, *18*, 1243–1269.

(455) Adams, B. G.; Jankowski, K.; Paldus, J. Symmetry-adapted coupled-pair approach to the many-electron correlation problem. III. Approximate coupled-pair approaches for the Be atom. *Phys. Rev. A* **1981**, *24*, 2330–2338.

(456) Chiles, R. A.; Dykstra, C. E. An efficient and accurate approximation to double substitution coupled cluster wavefunctions. *Chem. Phys. Lett.* **1981**, *80*, 69–72.

(457) Dykstra, C. E.; Liu, S.-y.; Daskalakis, M. F.; Lucia, J. P.; Takahashi, M. Further tests of the approximate double substitution coupled-cluster method. *Chem. Phys. Lett.* **1987**, *137*, 266–272.

(458) Taube, A. G.; Bartlett, R. J. Rethinking linearized coupled-cluster theory. *J. Chem. Phys.* **2009**, *130*, 144112.

(459) Bartlett, R. J.; Musiał, M. Addition by subtraction in coupled-cluster theory: A reconsideration of the CC and CI interface and the nCC hierarchy. *J. Chem. Phys.* **2006**, *125*, 204105.

(460) Meyer, W. PNO-CI and CEPA studies of electron correlation effects. *Theor. Chim. Acta* **1974**, *35*, 277–292.

(461) Ahlrichs, R.; Lischka, H.; Staemmler, V.; Kutzelnigg, W. PNO-CI (pair natural orbital configuration interaction) and CEPA-PNO (coupled electron pair approximation with pair natural orbitals) calculations of molecular systems. I. Outline of the method for closed-shell states. *J. Chem. Phys.* **1975**, *62*, 1225.

(462) Kats, D.; Manby, F. R. Communication: The distinguishable cluster approximation. *J. Chem. Phys.* **2013**, *139*, 021102.

(463) Kats, D. The distinguishable cluster approach from a screened Coulomb formalism. *J. Chem. Phys.* **2016**, *144*, 044102.

(464) Kats, D. Communication: The distinguishable cluster approximation. II. The role of orbital relaxation. *J. Chem. Phys.* **2014**, *141*, 061101.

(465) Rishi, V.; Perera, A.; Bartlett, R. J. Assessing the distinguishable cluster approximation based on the triple bond-breaking in the nitrogen molecule. *J. Chem. Phys.* **2016**, *144*, 124117.

(466) Bulik, I. W.; Henderson, T. M.; Scuseria, G. E. Can Single-Reference Coupled Cluster Theory Describe Static Correlation? *J. Chem. Theory Comput.* **2015**, *11*, 3171–3179.

(467) Paldus, J. Correlation problems in atomic and molecular systems. V. Spin-adapted coupled cluster many-electron theory. *J. Chem. Phys.* **1977**, *67*, 303.

(468) Adams, B. G.; Paldus, J. Orthogonally-spin-adapted coupled-cluster theory for closed-shell systems including triexcited clusters. *Phys. Rev. A* **1979**, *20*, 1–17.

(469) Geertsen, J.; Oddershede, J. A coupled cluster polarization propagator method applied to CH^+. *J. Chem. Phys.* **1986**, *85*, 2112.

(470) Piecuch, P.; Paldus, J. Orthogonally spin-adapted coupled-cluster equations involving singly and doubly excited clusters. Comparison of different procedures for spin-adaptation. *Int. J. Quantum Chem.* **1989**, *36*, 429–453.

(471) This is confirmed with our in-house code. Once CCVB-SD is implemented, CCSD0 can be easily implemented by removing antisymmetric doubles terms in the CCVB-SD equation.

(472) Gomez, J. A.; Henderson, T. M.; Scuseria, G. E. Recoupling the singlet- and triplet-pairing channels in single-reference coupled cluster theory. *J. Chem. Phys.* **2016**, *145*, 134103.

(473) Paldus, J.; Li, X. Externally Corrected Coupled-Cluster Approaches: Energy versus Amplitude Corrected CCSD. *Collect. Czech. Chem. Commun.* **2003**, *68*, 554–586.

(474) Stolarczyk, L. Z. Complete active space coupled-cluster method. Extension of single-reference coupled-cluster method using the CASSCF wavefunction. *Chem. Phys. Lett.* **1994**, *217*, 1–6.

(475) Li, X.; Peris, G.; Planelles, J.; Rajadall, F.; Paldus, J. Externally corrected singles and doubles coupled cluster methods for open-shell systems. *J. Chem. Phys.* **1997**, *107*, 90.

(476) Paldus, J.; Planelles, J. Valence bond corrected single reference coupled cluster approach. *Theor. Chim. Acta* **1994**, *89*, 13–31.

(477) Planelles, J.; Paldus, J.; Li, X. Valence bond corrected single reference coupled cluster approach. *Theor. Chim. Acta* **1994**, *89*, 33–57.

(478) Planelles, J.; Paldus, J.; Li, X. Valence bond corrected single reference coupled cluster approach. *Theor. Chim. Acta* **1994**, *89*, 59–76.

(479) Piecuch, P.; Toboła, R.; Paldus, J. Coupled-Cluster approaches with an approximate account of triply and quadruply excited clusters: Implementation of the orthogonally spin-adapted CCD +ST(CCD),CCSD +T(CCSD), and ACPQ +ST(ACPQ) formalisms. *Int. J. Quantum Chem.* **1995**, *55*, 133–146.

(480) Piecuch, P.; Toboła, R.; Paldus, J. Approximate account of connected quadruply excited clusters in single-reference coupled-cluster theory via cluster analysis of the projected unrestricted Hartree-Fock wave function. *Phys. Rev. A* **1996**, *54*, 1210–1241.

(481) Löwdin, P.-O. Quantum Theory of Many-Particle Systems. III. Extension of the Hartree-Fock Scheme to Include Degenerate Systems and Correlation Effects. *Phys. Lett.* **1955**, *97*, 1509–1520.

(482) Qiu, Y.; Henderson, T. M.; Scuseria, G. E. Projected Hartree Fock Theory as a Polynomial Similarity Transformation Theory of Single Excitations. *J. Chem. Phys.* **2016**, *145*, 111102.

(483) Hajgat, B.; Szieberth, D.; Geerlings, P.; De Proft, F.; Deleuze, M. S. A benchmark theoretical study of the electronic ground state and of the singlet-triplet split of benzene and linear acenes. *J. Chem. Phys.* **2009**, *131*, 224321.

(484) Pelzer, K.; Greenman, L.; Gidofalvi, G.; Mazziotti, D. A. Strong Correlation in Acene Sheets from the Active-Space Variational Two-Electron Reduced Density Matrix Method: Effects of Symmetry and Size. *J. Phys. Chem. A* **2011**, *115*, 5632–5640.

(485) Fosso-Tande, J.; Nascimento, D. R.; DePrince, A. E. Accuracy of two-particle N-representability conditions for describing different spin states and the singlet-triplet gap in the linear acene series. *Mol. Phys.* **2015**, 1–8.

(486) Fosso-Tande, J.; Nguyen, T.-S.; Gidofalvi, G.; DePrince, A. E. Large-Scale Variational Two-Electron Reduced-Density-Matrix-Driven Complete Active Space Self-Consistent Field Methods. *J. Chem. Theory Comput.* **2016**, *12*, 2260–2271.

(487) Schriber, J. B.; Evangelista, F. A. Communication: An adaptive configuration interaction approach for strongly correlated electrons with tunable accuracy. *J. Chem. Phys.* **2016**, *144*, 161106.

(488) Bettinger, H. F.; Tönshoff, C.; Doerr, M.; Sanchez-Garcia, E. Electronically Excited States of Higher Acenes up to Nonacene: A Density Functional Theory/Multireference Configuration Interaction Study. *J. Chem. Theory Comput.* **2016**, *12*, 305–312.

(489) Chai, J.-D. Density functional theory with fractional orbital occupations. *J. Chem. Phys.* **2012**, *136*, 154104.

(490) Ess, D. H.; Johnson, E. R.; Hu, X.; Yang, W. Singlet-Triplet Energy Gaps for Diradicals from Fractional-Spin Density-Functional Theory. *J. Phys. Chem. A* **2011**, *115*, 76–83.

(491) Yang, Y.; Davidson, E. R.; Yang, W. Nature of ground and electronic excited states of higher acenes. *Proc. Natl. Acad. Sci. U.S.A.* **2016**, *113*, E5098–E5107.

(492) Gerratt, J.; Cooper, D. L.; Karadakov, P. B.; Raimondi, M. Modern valence bond theory. *Chem. Soc. Rev.* **1997**, *26*, 87.

(493) Goddard, W. A.; Harding, L. B. The Description of Chemical Bonding From AB Initio Calculations. *Ann. Rev. Phys. Chem.* **1978**, *29*, 363–396.

(494) Shavitt, I.; Bartlett, R. J., *Many-Body Methods in Chemistry and Physics: MBPT and Coupled-Cluster Theory*; Cambridge University Press: 2009, pp 347–405.

(495) Epifanovsky, E.; Wormit, M.; Kuś, T.; Landau, A.; Zuev, D.; Khistyaev, K.; Manohar, P.; Kaliman, I.; Dreuw, A.; Krylov, A. I. New implementation of high-level correlated methods using a general block tensor library for high-performance electronic structure calculations. *J. Comput. Chem* **2013**, *34*, 2293–2309.

(496) Pulay, P. Convergence acceleration of iterative sequences. the case of scf iteration. *Chem. Phys. Lett.* **1980**, *73*, 393–398.

(497) Plasser, F.; Pašalić, H.; Gerzabek, M. H.; Libisch, F.; Reiter, R.; Burgdörfer, J.; Müller, T.; Shepard, R.; Lischka, H. The Multiradical Character of One- and Two-Dimensional Graphene Nanoribbons. *Angew. Chem. Int. Ed. Engl.* **2013**, *52*, 2581–2584.

(498) Horn, S.; Plasser, F.; Müller, T.; Libisch, F.; Burgdörfer, J.; Lischka, H. A comparison of singlet and triplet states for one- and two-dimensional graphene nanoribbons using multireference theory. *Theor. Chem. Acc.* **2014**, *133*, 1511.

(499) Deleuze, M. S.; Claes, L.; Kryachko, E. S.; Franois, J.-P. Benchmark theoretical study of the ionization threshold of benzene and oligoacenes. *J. Chem. Phys.* **2003**, *119*, 3106.

(500) Rangel, T.; Hamed, S. M.; Bruneval, F.; Neaton, J. B. Evaluating the GW Approximation with CCSD(T) for Charged Excitations Across the Oligoacenes. *J. Chem. Theory Comput.* **2016**, *12*, 2834–2842.

(501) We used an exponential fit $[a + b\exp[cn]]$ for CCVB-SD whereas the DMRG study in ref.39 employed a different fit $[2 - a(1 + \tanh[c(n - b)])]$ for HONO and LUNO is constructed by $2 - n_{\mathrm{HONO}}$. Moreover, when fitting CCVB-SD data we took only points with n $>$ 5. We prefer using the exponential fit because it yields asymptotes closer to 1 than the longest acene's HONO and LUNO occupation numbers whilst the hyperbolic tangent fit does not.

(502) Gwaltney, S. R.; Head-Gordon, M. A second-order correction to singles and doubles coupled-cluster methods based on a perturbative expansion of a similarity-transformed Hamiltonian. *Chem. Phys. Lett.* **2000**, *323*, 21–28.

(503) Piecuch, P.; Zarrabian, S.; Paldus, J.; Čižek, J. Coupled-cluster approaches with an approximate account of triexcitations and the optimized-inner-projection technique. III. Lower bounds to the ground-state correlation energy of cyclic-polyene model systems. *Phys. Rev. A* **1990**, *42*, 5155–5167.

(504) Piecuch, P.; Zarrabian, S.; Paldus, J.; Čížek, J. Coupled-cluster approaches with an approximate account of triexcitations and the optimized-inner-projection technique. II. Coupled-cluster results for cyclic-polyene model systems. *Phys. Rev. B* **1990**, *42*, 3351–3379.

(505) Piecuch, P.; Paldus, J. Coupled cluster approaches with an approximate account of triexcitations and the optimized inner projection technique. *Theor. Chim. Acta* **1990**, *78*, 65–128.

(506) Sekino, H.; Bartlett, R. J. A linear response, coupled-cluster theory for excitation energy. *Int. J. Quantum Chem.* **1984**, *26*, 255–265.

(507) Gwaltney, S. R.; Nooijen, M.; Bartlett, R. J. Simplified methods for equation-of-motion coupled-cluster excited state calculations. *Chem. Phys. Lett.* **1996**, *248*, 189–198.

(508) Henkelman, G.; Uberuaga, B. P.; Jónsson, H. A climbing image nudged elastic band method for finding saddle points and minimum energy paths. *J. Chem. Phys.* **2000**, *113*, 9901.

(509) Henkelman, G.; Jónsson, H. Improved tangent estimate in the nudged elastic band method for finding minimum energy paths and saddle points. *J. Chem. Phys.* **2000**, *113*, 9978.

(510) Peters, B.; Heyden, A.; Bell, A. T.; Chakraborty, A. A growing string method for determining transition states: Comparison to the nudged elastic band and string methods. *J. Chem. Phys.* **2004**, *120*, 7877.

(511) Goodrow, A.; Bell, A. T.; Head-Gordon, M. Transition state-finding strategies for use with the growing string method. *J. Chem. Phys.* **2009**, *130*, 244108.

(512) Goodrow, A.; Bell, A. T.; Head-Gordon, M. A strategy for obtaining a more accurate transition state estimate using the growing string method. *Chem. Phys. Lett.* **2010**, *484*, 392–398.

(513) Zimmerman, P. Reliable Transition State Searches Integrated with the Growing String Method. *J. Chem. Theory Comput.* **2013**, *9*, 3043–3050.

(514) Chan, G. K.-L.; Sharma, S. The Density Matrix Renormalization Group in Quantum Chemistry. *Ann. Rev. Phys. Chem.* **2011**, *62*, 465–481.

(515) Sugiyama, G.; Koonin, S. Auxiliary field Monte-Carlo for quantum many-body ground states. *Ann. Phys.* **1986**, *168*, 1–26.

(516) Zhang, S.; Carlson, J.; Gubernatis, J. E. Constrained path quantum Monte Carlo method for fermion ground states. *Phys. Rev. Lett.* **1995**, *74*, 3652–3655.

(517) Suewattana, M.; Purwanto, W.; Zhang, S.; Krakauer, H.; Walter, E. J. Phaseless auxiliary-field quantum Monte Carlo calculations with plane waves and pseudopotentials: Applications to atoms and molecules. *Phys. Rev. B* **2007**, *75*, 245123.

(518) Al-Saidi, W. A.; Zhang, S.; Krakauer, H. Bond breaking with auxiliary-field quantum Monte Carlo. *J. Chem. Phys.* **2007**, *127*, 144101.

(519) Purwanto, W.; Al-Saidi, W. A.; Krakauer, H.; Zhang, S. Eliminating spin contamination in auxiliary-field quantum Monte Carlo: Realistic potential energy curve of F2. *J. Chem. Phys.* **2008**, *128*, 114309.

(520) Purwanto, W.; Zhang, S.; Krakauer, H. Frozen-orbital and downfolding calculations with auxiliary-field quantum Monte Carlo. *J. Chem. Theory Comput.* **2013**, *9*, 4825–4833.

(521) Purwanto, W.; Zhang, S.; Krakauer, H. An auxiliary-field quantum Monte Carlo study of the chromium dimer. *J. Chem. Phys.* **2015**, *142*, 064302.

(522) Purwanto, W.; Zhang, S.; Krakauer, H. Auxiliary-field quantum Monte Carlo calculations of the molybdenum dimer. *J. Chem. Phys.* **2016**, *144*, 244306.

(523) Shee, J.; Zhang, S.; Reichman, D. R.; Friesner, R. A. Chemical Transformations Approaching Chemical Accuracy via Correlated Sampling in Auxiliary-Field Quantum Monte Carlo. *J. Chem. Theory Comput.* **2017**, *13*, 2667–2680.

(524) Bender, C. F.; Davidson, E. R. Studies in Configuration Interaction: The First-Row Diatomic Hydrides. *Phys. Rev.* **1969**, *183*, 23–30.

(525) Langhoff, S. R.; Elbert, S. T.; Davidson, E. R. A configuration interaction study of the spin dipole-dipole parameters for formaldehyde and methylene. *Int. J. Quantum Chem* **1973**, *7*, 999–1019.

(526) Huron, B.; Malrieu, J. P.; Rancurel, P. Iterative perturbation calculations of ground and excited state energies from multiconfigurational zeroth-order wavefunctions. *J. Chem. Phys.* **1973**, *58*, 5745–5759.

(527) Buenker, R. J.; Peyerimhoff, S. D. Individualized configuration selection in CI calculations with subsequent energy extrapolation. *Theor. Chim. Acta* **1974**, *35*, 33–58.

(528) Buenker, R. J.; Peyerimhoff, S. D.; Butscher, W. Applicability of the multi-reference double-excitation CI (MRD-CI) method to the calculation of electronic wavefunctions and comparison with related techniques. *Mol. Phys.* **1978**, *35*, 771–791.

(529) Evangelisti, S.; Daudey, J.-P.; Malrieu, J.-P. Convergence of an improved CIPSI algorithm. *Chem. Phys.* **1983**, *75*, 91–102.

(530) Harrison, R. J. Approximating full configuration interaction with selected configuration interaction and perturbation theory. *J. Chem. Phys.* **1991**, *94*, 5021–5031.

(531) Caballol, R.; Malrieu, J.-P. Direct selected configuration interaction using a hole-particle formalism. *Chem. Phys. Lett.* **1992**, *188*, 543–549.

(532) Giner, E.; Scemama, A.; Caffarel, M. Using perturbatively selected configuration interaction in quantum Monte Carlo calculations. *Can. J. Chem.* **2013**, *91*, 879–885.

(533) Tubman, N. M.; Lee, J.; Takeshita, T. Y.; Head-Gordon, M.; Whaley, K. B. A deterministic alternative to the full configuration interaction quantum Monte Carlo method. *J. Chem. Phys.* **2016**, *145*, 044112.

(534) Sharma, S.; Holmes, A. A.; Jeanmairet, G.; Alavi, A.; Umrigar, C. J. Semistochastic Heat-Bath Configuration Interaction Method: Selected Configuration Interaction with Semistochastic Perturbation Theory. *J. Chem. Theory Comput.* **2017**, *13*, 1595–1604.

(535) Holmes, A. A.; Umrigar, C. J.; Sharma, S. Excited states using semistochastic heat-bath configuration interaction. *J. Chem. Phys.* **2017**, *147*, 164111.

(536) Jankowski, K.; Paldus, J.; Piecuch, P. Method of moments approach and coupled cluster theory. *Theor. Chem. Acc* **1991**, *80*, 223–243.

(537) Piecuch, P.; Oliphant, N.; Adamowicz, L. A state-selective multireference coupled-cluster theory employing the single-reference formalism. *J. Chem. Phys.* **1993**, *99*, 1875.

(538) Li, S. Block-correlated coupled cluster theory: The general formulation and its application to the antiferromagnetic Heisenberg model. *J. Chem. Phys.* **2004**, *120*, 5017–5026.

(539) Piecuch, P. Active-space coupled-cluster methods. *Mol. Phys.* **2010**, *108*, 2987–3015.

(540) Huntington, L. M.; Nooijen, M. PCCSD: Parameterized coupled-cluster theory with single and double excitations. *J. Chem. Phys.* **2010**, *133*, 184109.

(541) Malrieu, J.-P.; Zhang, H.; Ma, J. Ability of a coupled electron pair approximation to treat single bond breakings. *Chem. Phys. Lett.* **2010**, *493*, 179–184.

(542) Lyakh, D. I.; Bartlett, R. J. An adaptive coupled-cluster theory: @CC approach. *J. Chem. Phys.* **2010**, *133*, 244112.

(543) Xu, E.; Kou, Z.; Li, S. A coupled cluster approach with excitations up to six orbital pairs: the formulation and test applications for bond breaking processes. *J. Chem. Phys.* **2011**, *134*, 234104.

(544) Robinson, J. B.; Knowles, P. J. Approximate variational coupled cluster theory. *J. Chem. Phys.* **2011**, *135*, 044113.

(545) Henderson, T. M.; Scuseria, G. E. Spin-projected generalized Hartree-Fock method as a polynomial of particle-hole excitations. *Phys. Rev. A* **2017**, *96*, 022506.

(546) Goddard, W. A.; Ladner, R. C. A Generalized Orbital Description of the Reactions of Small Molecules. *J. Am. Chem. Soc.* **1971**, *93*, 6750–6756.

(547) Mayer, I.; Ladik, J.; Biczó, G. Spin projected extended Hartree-Fock equations. *Int. J. Quantum Chem* **1973**, *7*, 583–608.

(548) Nakatsuji, H. On the orbital theories in the spin-correlation problems. II. Unrestricted and spin-extended Hartree-Fock theories. *J. Chem. Phys.* **1973**, *59*, 2586.

(549) Yamaguchi, K.; Yoshioka, Y.; Takatsuka, T.; Fueno, T. Extended Hartree-Fock (EHF) theory in chemical reactions - II. Symmetry properties of the EHF wavefunctions constructed by the magnetically ordered general spin orbitals. *Theor. Chem. Acc* **1978**, *48*, 185–206.

(550) Jiménez-Hoyos, C. A.; Henderson, T. M.; Tsuchimochi, T.; Scuseria, G. E. Projected Hartree-Fock theory. *J. Chem. Phys.* **2012**, *136*, 164109.

(551) Gerratt, J.; Raimondi, M. The Spin-Coupled Valence Bond Theory of Molecular Electronic Structure. I. Basic Theory and Application to the Formula States of BeH. *Proc. Royal Soc. A* **1980**, *371*, 525–552.

(552) Cooper, D. L.; Gerratt, J.; Raimondi, M. Applications of Spin-Coupled Valence Bond Theory. *Chem. Rev.* **1991**, *91*, 929–964.

(553) Hiberty, P. C.; Shaik, S. A survey of recent developments in ab initio valence bond theory. *J. Comput. Chem.* **2007**, *28*, 137–151.

(554) Sinanoğlu, O. Many-Electron Theory of Atoms and Molecules. I. Shells, Electron Pairs vs Many-Electron Correlations. *J. Chem. Phys.* **1962**, *36*, 706–717.

(555) Ahlrichs, R.; Kutzelnigg, W. Direct Calculation of Approximate Natural Orbitals and Natural Expansion Coefficients of Atomic and Molecular Electronic Wavefunctions. II. Decoupling of the Pair Equations and Calculation of the Pair Correlation Energies for the Be and LiH Ground States. *J. Chem. Phys.* **1968**, *48*, 1819–1832.

(556) Ahlrichs, R.; Kutzelnigg, W. Ab initio calculations on small hydrides including electron correlation - I. The BeH_2 molecule in its ground state. *Theor. Chim. Acta.* **1968**, *10*, 377–387.

(557) Ahlrichs, R.; Kutzelnigg, W. Ab-Initio Calculations of Small Hydrides including electron correlation. II. Preliminary results for the CH_4 ground state. *Chem. Phys. Lett.* **1968**, *1*, 651–654.

(558) Jungen, M.; Ahlrichs, R. Ab initio calculations on small hydrides including electron correlation - III. A study of the valence shell intrapair and interpair correlation energy of some first row hydrides. *Theor. Chim. Acta.* **1970**, *17*, 339–347.

(559) Ahlrichs, R. Ab initio calculations on small hydrides including Electron correlation - IV. A study of the molecules BeH_2, Be_2H_4 and Be_3H_{46}. *Theor. Chim. Acta.* **1970**, *17*, 348–361.

(560) Gélus, M.; Ahlrichs, R.; Staemmler, V.; Kutzelnigg, W. Ab initio calculations of small hydrides including electron correlation - VI. Study of the correlation energy of the BH ground state and its dependence on the internuclear distance. *Theor. Chim. Acta.* **1971**, *21*, 63–68.

(561) Gelus, M.; Kutzelnigg, W. Ab initio calculations of small hydrides including electron correlation - VIII. Equilibrium geometry and harmonic force constants of BH_3. *Theor. Chim. Acta.* **1973**, *28*, 103–110.

(562) Lischka, H. Ab initio calculations on small hydrides including electron correlation - IX. Equilibrium geometries and harmonic force constants of HF, OH^-, H_2F^+ and H_2O and proton affinities of F^-, OH^-, HF and H_2O. *Theor. Chim. Acta.* **1973**, *31*, 39–48.

(563) Staemmler, V. Ab initio calculations on small hydrides including electron correlation - X. Triplet-singlet energy separation and other properties of the CH_2 radical. *Theor. Chim. Acta.* **1973**, *31*, 49–61.

(564) Driessler, F.; Ahlrichs, R.; Staemmler, V.; Kutzelnigg, W. Ab-initio calculations on small hydrides including electron correlation - XI. Equilibrium geometries and other properties of CH_3, ${CH_3}^+$, and ${CH_3}^-$, and inversion barrier of ${CH_3}^-$. *Theor. Chim. Acta.* **1973**, *30*, 315–326.

(565) Dyczmons, V.; Kutzelnigg, W. Ab initio calculations of small hydrides including electron correlation - XII. the ions ${CH_5}^+$ and ${CH_5}^-$. *Theor. Chim. Acta.* **1974**, *33*, 239–247.

(566) Dunitez, B. D.; Van Voorhis, T.; Head-Gordon, M. Geometric Direct Minimization of Hartree-Fock Calculations Involving Open Shell Wavefunctions with Spin Restricted Orbitals. *J. Theor. Comput. Chem.* **2002**, *01*, 255–261.

(567) Pulay, P. Improved SCF convergence acceleration. *J. Comput. Chem* **1982**, *3*, 556–560.

(568) Nocedal, J.; Wright, S. J., *Numerical optimization*; Springer: 2006, pp 245–269.

(569) Mayhall, N. J.; Head-Gordon, M. Increasing spin-flips and decreasing cost: Perturbative corrections for external singles to the complete active space spin flip model for low-lying excited states and strong correlation. *J. Chem. Phys.* **2014**, *141*, 044112.

(570) Stoll, H.; Wagenblast, G.; Preuß, H. On the use of local basis sets for localized molecular orbitals. *Theor. Chem. Acc* **1980**, *57*, 169–178.

(571) Khaliullin, R. Z.; Head-Gordon, M.; Bell, A. T. An efficient self-consistent field method for large systems of weakly interacting components. *J. Chem. Phys.* **2006**, *124*, 204105.

(572) Neese, F. Software update: The ORCA program system, version 4.0. *Wiley Interdiscip. Rev.: Comput. Mol. Sci.* **2017**, e1327.

(573) Sun, Q.; Berkelbach, T. C.; Blunt, N. S.; Booth, G. H.; Guo, S.; Li, Z.; Liu, J.; McClain, J. D.; Sayfutyarova, E. R.; Sharma, S.; Wouters, S.; Chan, G. K.-L. PySCF: the Python-based simulations of chemistry framework. *Wiley Interdiscip. Rev.: Comput. Mol. Sci.* **2017**, e1340.

(574) `Dice.`, `https://sanshar.github.io/Dice/`, Accessed: 2017-10-31.

(575) Schmidt, M. W.; Baldridge, K. K.; Boatz, J. A.; Elbert, S. T.; Gordon, M. S.; Jensen, J. H.; Koseki, S.; Matsunaga, N.; Nguyen, K. A.; Su, S.; Windus, T. L.; Dupuis, M.; Montgomery, J. A. General atomic and molecular electronic structure system. *J. Comput. Chem.* **1993**, *14*, 1347–1363.

(576) Parrish, R. M. et al. Psi4 1.1: An Open-Source Electronic Structure Program Emphasizing Automation, Advanced Libraries, and Interoperability. *J. Chem. Theory Comput.* **2017**, *13*, 3185–3197.

(577) Kahn, O. Competing spin interactions and degenerate frustration for discrete molecular species. *Chem. Phys. Lett.* **1997**, *265*, 109–114.

(578) Knizia, G. Intrinsic Atomic Orbitals: An Unbiased Bridge between Quantum Theory and Chemical Concepts. *J. Chem. Theory Comput.* **2013**, *9*, 4834–4843.

(579) Dagotto, E. Mott Transition in VO2 Revealed by Infrared Spectroscopy and Nano-Imaging. *Science* **2007**, *318*, 1750.

(580) Zheng, H.; Wagner, L. K. Computation of the correlated metal-insulator transition in vanadium dioxide from first principles. *Phys. Rev. Lett.* **2015**, *114*, 176401.

(581) Miliordos, E.; Mavridis, A. Electronic Structure of Vanadium Oxide. Neutral and Charged Species, VO0, ±. *The Journal of Physical Chemistry A* **2007**, *111*, 1953–1965.

(582) Kasai, P. H. ESR of VO in argon matrix at 4K; establishment of its electronic ground state. *J. Chem. Phys.* **1968**, *49*, 4979–4984.

(583) Ethofer, S.; Schuck, P. An integral equation for the six-point green function and the many body problem. *Phys. Lett. A* **1969**, *29*, 223–224.

(584) Bender, C. M.; Milton, K. A.; Moshe, M.; Pinsky, S. S.; Simmons, L. M. Novel perturbative scheme in quantum field theory. *Phys. Rev. D* **1988**, *37*, 1472–1484.

(585) Lundberg, M.; Siegbahn, P. E. M. Theoretical investigations of structure and mechanism of the oxygen-evolving complex in PSII. *Phys. Chem. Chem. Phys.* **2004**, *6*, 4772.

(586) Fliegl, H.; Fink, K.; Klopper, W.; Anson, C. E.; Powell, A. K.; Clérac, R. Ab initio study of the magnetic exchange coupling constants of a structural model [$CaMn_3^{III}Mn^{II}$] of the oxygen evolving center in photosystem II. *Phys. Chem. Chem. Phys.* **2009**, *11*, 3900.

(587) Dismukes, G. C.; Brimblecombe, R.; Felton, G. A.; Pryadun, R. S.; Sheats, J. E.; Spiccia, L.; Swiegers, G. F. Development of bioinspired Mn_4O_4-cubane water oxidation catalysts: Lessons from photosynthesis. *Acc. Chem. Res.* **2009**, *42*, 1935–1943.

(588) Kanady, J. S.; Tsui, E. Y.; Day, M. W.; Agapie, T. A Synthetic Model of the Mn_3Ca Subsite of the Oxygen-Evolving Complex in Photosystem II. *Science* **2011**, *333*, 733–736.

(589) Ames, W.; Pantazis, D. A.; Krewald, V.; Cox, N.; Messinger, J.; Lubitz, W.; Neese, F. Theoretical evaluation of structural models of the S 2 state in the oxygen evolving complex of photosystem II: Protonation states and magnetic interactions. *J. Am. Chem. Soc.* **2011**, *133*, 19743–19757.

(590) Mukherjee, S.; Stull, J. A.; Yano, J.; Stamatatos, T. C.; Pringouri, K.; Stich, T. A.; Abboud, K. A.; Britt, R. D.; Yachandra, V. K.; Christou, G. Synthetic model of the asymmetric [Mn_3CaO_4] cubane core of the oxygen-evolving complex of photosystem II. *Proc. Natl. Acad. Sci.* **2012**, *109*, 2257–2262.

(591) Kanady, J. S.; Mendoza-Cortes, J. L.; Tsui, E. Y.; Nielsen, R. J.; Goddard, W. A.; Agapie, T. Oxygen atom transfer and oxidative water incorporation in cuboidal Mn_3MOn complexes based on synthetic, isotopic labeling, and computational studies. *J. Am. Chem. Soc.* **2013**, *135*, 1073–1082.

(592) Lee, C.; Aikens, C. M. Water Splitting Processes on Mn_4O_4 and $CaMn_3O_4$ Model Cubane Systems. *J. Phys. Chem. A* **2015**, *119*, 9325–9337.

(593) Zhang, C.; Chen, C.; Dong, H.; Shen, J.-R.; Dau, H.; Zhao, J. A synthetic Mn4Ca-cluster mimicking the oxygen-evolving center of photosynthesis. *Science* **2015**, *348*, 690–693.

(594) Jones, R. O.; Hohl, D. Structure of phosphorus clusters using simulated annealing-P_2 to P_8. *J. Chem. Phys.* **1990**, *92*, 6710.

(595) Häser, M.; Schneider, U.; Ahlrichs, R. Clusters of Phosphorus: A Theoretical Investigation. *J. Am. Chem. Soc.* **1992**, *114*, 9551–9559.

(596) Huang, R.; Li, H.; Lin, Z.; Yang, S. Experimental and Theoretical Studies of Small Homoatomic Phosphorus Clusters. *J. Phys. Chem.* **1995**, *99*, 1418–1423.

(597) Böcker, S.; Häser, M. Covalent Structures of Phosphorus: A Comprehensive Theoretical Study. *Z. Anorg. Allg. Chem.* **1995**, *621*, 258–286.

(598) Huang, R.; Li, H.; Lin, Z.; Yang, S. Phosphorus-Cluster Cations Produced By Laser Ablation of Red Phosphorus. *Surf. Rev. Lett.* **1996**, *03*, 167–169.

(599) Chen, M. D.; Li, J. T.; Huang, R. B.; Zheng, L. S.; Au, C. T. Structure prediction of large cationic phosphorus clusters. *Chem. Phys. Lett.* **1999**, *305*, 439–445.

(600) Chen, M.; Huang, R.; Zheng, L.; Au, C. The prediction of isomers for phosphorus clusters P_8 and P_9^+. *J. Mol. Struc. THEOCHEM* **2000**, *499*, 195–201.

(601) Chen, M. D.; Huang, R. B.; Zheng, L. S.; Zhang, Q. E.; Au, C. T. A theoretical study for the isomers of neutral, cationic and anionic phosphorus clusters P_5, P_7, P_9. *Chem. Phys. Lett.* **2000**, *325*, 22–28.

(602) Bulgakov, A.; Bobrenok, O.; Ozerov, I.; Marine, W.; Giorgio, S.; Lassesson, A.; Campbell, E. Phosphorus cluster production by laser ablation. *Appl. Phys. A* **2004**, *79*, 1369–1372.

(603) Tejada, J.; Chudnovsky, E. M.; del Barco, E.; Hernandez, J. M.; Spiller, T. P. Magnetic qubits as hardware for quantum computers. *Nanotechnology* **2001**, *12*, 181–186.

(604) Leuenberger, M. N.; Loss, D. Quantum computing in molecular magnets. *Nature* **2001**, *410*, 789–793.

(605) Yamaguchi, K.; Fukui, H.; Fueno, T. Molecular orbital (MO) theory for magnetically interacting organic compounds. Ab-initio MO calculations of the effective exchange integrals for cyclophane-type carbene dimers. *Chem. Lett* **1986**, *15*, 625–628.

(606) Noodleman, L.; Davidson, E. R. Ligand spin polarization and antiferromagnetic coupling in transition metal dimers. *Chem. Phys.* **1986**, *109*, 131–143.

(607) Noodleman, L.; Case, D. A., *Advances in Inorganic Chemistry*; Academic Press: 1992; Vol. 38, pp 423–470.

(608) Baker, M. L. et al. A classification of spin frustration in molecular magnets from a physical study of large odd-numbered-metal, odd electron rings. *Proc. Natl. Acad. Sci.* **2012**, *109*, 19113–8.

(609) Mayhall, N. J.; Head-Gordon, M. Computational quantum chemistry for single Heisenberg spin couplings made simple: Just one spin flip required. *J. Chem. Phys.* **2014**, *141*, 134111.

(610) Zimmerman, P. M. Singlet-Triplet Gaps through Incremental Full Configuration Interaction. *Journal of Physical Chemistry A* **2017**, *121*, 4712–4720.

(611) Grimme, S.; Waletzke, M. A combination of Kohn-Sham density functional theory and multi-reference configuration interaction methods. *J. Chem. Phys.* **1999**, *111*, 5645–5655.

(612) Gagliardi, L.; Truhlar, D. G.; Li Manni, G.; Carlson, R. K.; Hoyer, C. E.; Bao, J. L. Multiconfiguration Pair-Density Functional Theory: A New Way To Treat Strongly Correlated Systems. *Acc. Chem. Res.* **2017**, *50*, 66–73.

(613) Kucharski, S. A.; Bartlett, R. J. Multireference many-body perturbation theory. *Int. J. Quantum Chem* **1988**, *34*, 383–405.

(614) Wolinski, K.; Pulay, P. Generalized Møller-Plesset perturbation theory: Second order results for two-configuration, open-shell excited singlet, and doublet wave functions. *J. Chem. Phys.* **1989**, *90*, 3647–3659.

(615) Murphy, R. B.; Messmer, R. P. Generalized Møller-Plesset perturbation theory applied to general MCSCF reference wave functions. *Chem. Phys. Lett.* **1991**, *183*, 443–448.

(616) Dyall, K. G. The choice of a zeroth-order Hamiltonian for second-order perturbation theory with a complete active space self-consistent-field reference function. *J. Chem. Phys.* **1995**, *102*, 4909–4918.

(617) Beran, G. J. O.; Head-Gordon, M.; Gwaltney, S. R. Second-order correction to perfect pairing: An inexpensive electronic structure method for the treatment of strong electron-electron correlations. *J. Chem. Phys.* **2006**, *124*, 114107.

(618) Xu, E.; Li, S. Block correlated second order perturbation theory with a generalized valence bond reference function. *J. Chem. Phys.* **2013**, *139*, 174111.

(619) Li, C.; Evangelista, F. A. Multireference driven similarity renormalization group: A second-order perturbative analysis. *J. Chem. Theory Comput.* **2015**, *11*, 2097–2108.

(620) Pernal, K. Intergeminal correction to the antisymmetrized product of strongly orthogonal geminals derived from the extended random phase approximation. *J. Chem. Theory Comput.* **2014**, *10*, 4332–4341.

(621) Pastorczak, E.; Pernal, K. ERPA-APSG: a computationally efficient geminal-based method for accurate description of chemical systems. *Phys. Chem. Chem. Phys.* **2015**, *17*, 8622–8626.